"THE CHEMICAL CHARACTERISTICS OF VICTORIAN BROWN COAL"

G. J. Perry, D. J. Allardice and L. T. Kiss*

Victorian Brown Coal Council, 151 Flinders Street, Melbourne, 3000 Australia,
*State Electricity Commission of Victoria, Herman Research Laboratory, Howard Street, Richmond, 3121 Australia.

1. INTRODUCTION

Extensive deposits of soft brown coal exist in Tertiary age sediments in a number of areas in Victoria and the largest single deposit occurs in the Latrobe Valley, about 150 kilometers east of Melbourne. In this region the coal seams often exceed 150 metres in thickness, with an overburden to coal ratio usually better than 1:2 making the coal ideally suited for large-scale open-cut mining.

A recent study (1) has estimated the State's brown coal resources to be almost 200,000 million tonnes with approximately 52,000 million tonnes defined as usable reserves. About 85% of this coal is located in the Latrobe Valley.

Since 1920 Latrobe Valley brown coal has been developed for power generation. The State Electricity Commission of Victoria (SECV) wins coal from two major open cuts at Yallourn and Morwell and operates coal fired power stations which presently consume approximately 35 million tonnes per annum. In addition to power generation, small quantities of brown coal are used for briquette manufacture and char production.

Brown coal accounts for about 95% of Victoria's non-renewable energy reserves and it is now recognized that with suitable up-grading, primarily drying, it has the potential to become the basis of the supply of energy in a variety of forms. Currently various studies for major conversion projects proposed by Australian, Japanese and German interests are being undertaken with the co-operation of the Victorian Brown Coal Council, the most advanced project being a 50 tonne per day hydrogenation pilot plant currently under construction at Morwell funded by New Energy Development Organization (NEDO) of Japan.

The chemical characteristics of Latrobe Valley brown coals have been extensively studied over the last twenty-five years, primarily in relation to the effect of coal quality on combustion for power generation. More recently a research project was initiated with the objective of determining the characteristics and suitability of the State's brown coal resources for uses other than power generation, primarily conversion to liquid fuels.

This paper outlines the chemical characteristics of Victorian brown coal and discusses the variability of the coal both between fields and within a seam. The importance of chemical properties in relation to coal quality and the implications for utilization are also briefly addressed.

2. PROPERTIES OF VICTORIAN BROWN COAL

The development and adaptation of modern analytical techniques for analysis of Victorian brown coal was pioneered jointly in the 1960's by the Commonwealth Scientific and Industrial Research Organization and the State Electricity Commission of Victoria. As a result the total coal analysis time was halved and the determination of the ash forming constituents directly on the coal took one sixth of the time of conventional ash analysis. More importantly brown coal analysis was put onto a rational basis taking its unique properties into account; and providing more pertinent information concerning the genesis, occurrence and use of Victorian brown coal.

Moisture

One of the most important chemical measurements made on brown coal is the bed moisture content which is also a good measure of physical rank; the greater the degree of compaction of the coal and its degree of coalification, the lower is the moisture content. To obtain meaningful results the sampling and sample preparation have to be carried out quickly to avoid moisture loss. The choice of the method of determination is important as thermal decomposition of functional groups can result in loss of CO_2 as well as H_2O. The preferred methods therefore involve direct measurement of the water released either by azeotropic distillation or adsorption from an intert carrier gas rather than by weight loss of the coal.

It is important to realize that the bed moisture content of soft brown coals is significantly higher than the equilibrium moisture holding capacity, a parameter which is used to characterize higher ranks coals. This is illustrated in Table 1 for a range of Victorian brown coals.

In terms of moisture the economic value of high rank coals is best indicated by the moisture holding capacity because it reflects the condition of the coal for utilization. In the case of Victorian brown coal the bed moisture content is the critical value, since the coal is used directly from the open cut.

Mineral and Inorganic Content

Ash content has been traditionally used to assess the magnitude of combustion residue and to derive the so called "coal substance" by difference which allows meaningful comparisons of different coals. In this context the ash is used as an approximation of the mineral matter content. The tacit assumption made, of course, is that the ash is derived solely from coal minerals, and this is certainly not the case for Victorian brown coal where the bulk of the ash forming material occurs as inherent inorganic matter in the form of exchangeable cations, associated with oxygen containing functional groups. This is also the case with many other low rank coals.

Using a combination of X-Ray fluorescence (XRF) on coal pellets and Atomic absorption (AA) techniques on acid extracts, direct chemical analyses of the ash forming elements in Victorian brown coal has been performed. Arising from this, a method of expression of results has been developed (2) which is based on classifying the mineral matter in brown coal into mineral and inorganic matter fractions and expressing each in a way which reflects their occurrence in the coal.

The Inorganics are a group of exchangeable cations and water soluble salts, analysed by AA on dilute acid extracts from the coal and expressed in terms of chemical analysis on a coal basis as -

$$\text{Inorganics} = Na + Ca + Mg + Fe + (Al) + (Si) + NaCl$$

where Fe refers to the non-pyritic iron and (Al) and (Si) to the acid soluble aluminium and silicon respectively. This expression is complicated by the fact that some iron and aluminium can be present as acid soluble hydroxides, but these are not usually significant.

The group named Minerals, which occurs as discrete particles principally of quartz, kaolinite and pyrite/marcasite is expressed in terms of chemical analysis as -

$$\text{Minerals} = SiO_2 + Al_2O_3 + TiO_2 + K_2O + FeS_2$$

This expression ignores the water of constitution of clays which is usually of negligible magnitude for Victorian brown coals.

The total weight of Minerals and Inorganics expressed on a dry coal basis gives the best estimate corresponding to "mineral matter" in high rank coal technology. In the case of Latrobe Valley coals the Inorganics are far more important than Minerals both in quantity and from a utilization point of view.

From a knowledge of the chemical constitution of the mineral matter it is possible to calculate and predict the composition of the ash or inorganic residue remaining after most technological processes. Table 2 illustrates the comparison between mineral matter content and ash content and the successful calculation of ash content from mineral matter data for a number of typical Victorian brown coals. Table 3 illustrates the futility of predicting the quantities of ash produced in modern, pulverized fuel fired power stations from the empirical ash test results. It illustrates for Morwell and Yallourn coals the quantities of ash produced in a boiler as opposed to the ash test; and it compares the laboratory ash composition with the precipitator ash actually produced. The mineral matter composition is also given as a guide. Both the laboratory and precipitator ash compositions can be calculated from the composition of the mineral matter by allowing for the difference in the degree of sulphation of the Inorganics. By extending this approach it should also be possible to calculate the composition of the inorganic residue obtained in hydrogenation processes.

It should also be noted that oxygen can only be estimated by difference if the mineral matter is known; using the ash value will yield misleading results.

Oxygen Functional Groups

Oxygen is one of the major elements present in the organic substance of Victorian brown coal. For Latrobe Valley brown coals oxygen generally comprises over 25% on a dry mineral and inorganic free (dmif) basis and about half of this oxygen can be accounted for in the acidic functional groups -phenolic hydroxyl, free carboxylic acid and carboxylate. The 40-50% of the oxygen not accounted for as acidic oxygen is primarily contained in carbonyl groups, ether linkages and heterocyclic ring structures.

3. VARIATION OF CHEMICAL PROPERTIES WITHIN A SEAM

The variation of chemical properties in a brown coal seam is attributable to the influence of two independent variables, namely coal rank and coal type. Rank variations are due to the burial history of the coal, that is the time, temperature and pressure it has undergone since its deposition. However, type (or lithotype) variations also significantly influence brown coal properties. Lithotypes arise from variations in the prevailing botanical communities, in the depth and nature of the swamp water and in the conditions of decay and decomposition of plant material. In Victorian brown coal these lithotypes are macroscopically recognizable bands or layers within a coal seam which become readily apparent on partially dried and weathered faces of open cuts. The basic factors on which lithotypes are classified are colour and texture in air dried coal , with degree of gelification, weathering pattern and physical properties used as supplementary characteristics which varies from pale to dark brown. In the case of Latrobe Valley coals, the colour of the air dried coal as measured by its diffuse reflectance and expressed as a Colour Index gives a numerical value related to lithotype.

The variation in rank with depth in the Morwell Open Cut is illustrated by the yearly weighted averages for each operating level. The gradation in rank is clearly illustrated in Figure 1 by the increase in carbon content, and the associated increase in gross dry specific energy; the volatile matter also decreases slightly with depth. These samples were not selected on a lithotype basis and the gradual changes in these coal properties are presumed to arise primarily from the increase in rank with depth.

The variation of coal properties with lithotype has been examined within continuous sequences of samples taken from five Latrobe Valley coal fields (3). The results indicate that the coal properties related to the organic coal substance, eg: volatile matter, hydrogen, carbon, oxygen and specific energy vary with lithotype layers in the coal seam. The dependence of carbon and hydrogen on lithotype (as measured by colour index) is illustrated in Figure 2 for a typical bore. All the major constituents of the organic coal substance are lithotype dependent and their variation within a seam is a direct consequence of the changes in depositional environment which occurred during formation of the seam.

The occurrence of organic sulphur and organic nitrogen is independent of lithotype although the concentration of nitrogen is influenced by the presence of wood in the coal.

Generally speaking, the concentration of minerals in the coal is highest near the overburden and the interseam sediment layers. Because of the discrete nature of the minerals their sporadic distribution in a seam cannot be accurately assessed from a single traverse of sampling through the seam.

The concentration of inorganics, particularly sodium, magnesium, calcium and non-pyritic iron show no relationship to lithotype (Figure 2) although some depth related concentration gradients are apparent. Sodium and magnesium often show a concentration increase near the top of a bore whilst the aluminium concentration tends to increase near the bottom. This is believed to be due to diffusion of aluminium into the coal from the clay containing sediments below the coal seam. On the other hand calcium in the Morwell open cut has the highest concentration near the middle of the profile.

The lack of correlation between these inorganic species and lithotype indicates that the inorganics are probably post-depositional in origin. This is consistent with their diffusion through the water of the coal giving rise to concentration gradients.

4. VARIATION IN CHEMICAL PROPERTIES BETWEEN COALFIELDS

In addition to the variation of chemical properties within coal seams, significant variation also occurs between different coalfields in Victoria. An extensive research programme in which this variation was investigated has been conducted by the State Electricity Commission of Victoria on behalf of the Victorian Brown Coal Council.

In this Brown Coal Evaluation Programme a sampling philosophy was adopted that would highlight the natural variability of the coal and indicate the range of coal qualities which may be encountered during mining and utilization of the deposits.

The programme commenced in the Latrobe Valley coalfields by sampling open-cut faces and 220 mm diameter bore cores and was later extended to include major coal deposits in Victoria. Lithotype logs were prepared using quarter core sections laid out to dry, and selected lithotype samples from each core were analysed for a variety of chemical, physical and petrographic characteristics and utilization parameters; 144 parameters in all. To date, a total of 219 coal samples have been analysed from three open cut faces and twenty 220 mm diameter bore cores, representing 11 coalfields throughout Victoria. Coal samples from a further six bores are presently being characterized.

The data generated from these analyses and tests was evaluated by statistical methods and correlation coefficients have been determined between all pairs of variables. Analysis of this data has revealed significant differences in the chemical properties of the coal from different fields and enables the selection of coal with specific properties for particular applications. Table 4 illustrates

some of these differences by showing the range of values determined for selected coal properties from 219 samples (11 coalfields). Typical values from the two open cut mines currently operating in the Latrobe Valley are shown for comparison. These differences in chemical properties between the different coalfields are generally more significant than lateral variations within a particular field (ie: between different bores within a field) and they are primarily related to rank.

5. EFFECT OF CHEMICAL PROPERTIES ON UTILIZATION

As a result of the Brown Coal Evaluation Programme, the understanding of the variability of Victorian brown coals and its implications for utilization have improved substantially. It has become apparent that certain chemical properties can have important consequences for utilization of the coal for power generation, liquefaction and other applications.

A number of examples will be briefly described -

Carbonate Formation During Hydrogenation

The formation of carbonate minerals during hydrogenation of low rank coals can cause serious operational difficulties in the reactor systems. A good correlation has been found between the calcium content of a number of Victorian brown coals and the carbonate formed during hydrogenation. However, the results indicated that cations other than calcium were involved in the formation of carbonate.

XRD analysis has revealed the presence of several different types of carbonate minerals in residues from a number of coals. Minerals identified included vaterite and calcite (two polymorphs of $CaCO_3$) dolomite ($CaMg[CO_3]_2$) and in the residue from a high sulphur (2.26% db) coal anhydrite, ($CaSO_4$) was identified. The types of mineral deposits formed depend not only on the coal but also on the reaction conditions. Our data indicates that whilst vaterite forms at low temperatures (380°C) as the temperature increases the vaterite becomes progressively converted to calcite, the more stable form. After further increases in temperature, particularly at long reaction times, dolomite begins to form.

The reaction to form anhydrite, in the case of the high sulphur coal, must compete for calcium with the formation of calcium carbonate, and this may have a beneficial effect.

Clearly the types of inorganic precipitates which form during hydrogenation of Victorian brown coal are dependent on the nature of the exchangeable cations and to some extent the available coal sulphur.

Sodium and Boiler Fouling

The concentration of sodium in coal is regarded as the most significant factor in the formation of troublesome ash deposits during combustion. Although Victorian brown coals are generally low in ash forming constituents, coals with a high proportion of sodium can form ashes which contain of large amounts of low melting point, sodium sulphate compounds. These are formed during combustion from the inorganic sodium and organic sulphur in the coal.

The sodium sulphate condenses on the surface of boiler tubes and together with fly-ash particles forms sticky deposits, which can consolidate on heating and lead to extremely dense hard-to-remove deposits. The presence of high sodium sulphate content ash thus requires special consideration during the design and operation of boilers.

Aluminium and Precipitator Ash

In some Victorian brown coals significant quantities of acid soluble aluminium are found. This is believed to be present as aluminium hydroxide which is dispersed throughout the water phase of the coal. During combustion of this coal the refractory aluminium oxide formed takes the shape of the relics of the plant material present in the coal, thus forming an extremely low density ash (approximately 100 kg/m³). Whilst the collection of these particles by lectrostatic precipitation is possible, the problem of reentrainment on rapping has necessitated the use of larger sized units than would otherwise be required. It is therefore important to determine the acid soluble aluminium fraction in the coal to determine if precipitation of fly ash is likely to be a problem.

6. ACKNOWLEDGEMENTS

The authors wish to acknowledge the support of the State Electricity Commission of Victoria (SECV), the Victorian Brown Coal Council (VBCC), and the companies in the VBCC Industrial Participants Group. The associated drilling, logging and sampling activities were managed by the SECV's Geological and Exploration Division, and the analytical work was performed by the staff at the Herman Research Laboratory.

7. REFERENCES

1. Victorian Brown Coal Resource Development Study, Kinhill Pty Ltd. 9 Volumes. December 1982.

2. Kiss LT and King TN. Fuel 56, 340 (1977).

3. King TN, George AM, Hibbert WD and Kiss LT. Variation of Coal Properties with Lithotype Pt 2. SECV Report No. SO/83/55 (1983).

TABLE 1. **BED MOISTURE AND MOISTURE HOLDING CAPACITY FOR SELECTED VICTORIAN COALS**

Coal Field (Selected Values)	Bed Moisture (As Received)		Moisture Holding Capacity % (Equilibrium Moisture)*
	Kg/Kg Dry Coal	Weight Percent	
Yallourn-Maryvale	1.82	64.2	38.4
Morwell-Narracan	1.54	60.5	38.2
Loy Yang	1.63	61.9	42.1
Flynn	1.76	63.5	41.2
Yallourn North Ext	.98	49.5	41.2
Coolungoolun	1.19	54.4	35.0
Gormandale	1.27	56.0	39.0
Gelliondale	1.83	64.6	35.3
Stradbroke	1.41	58.4	37.1
Anglesea	.87	46.6	32.9
Bacchus Marsh	1.53	60.4	31.2

* Determined at 97% humidity and 30°C

TABLE 2. **COMPARISON OF ASH CONTENT AND MINERAL MATTER FOR SELECTED VICTORIAN BROWN COALS**

Coal Field (Selected Values)	% Ash, Coal Dry Basis		% Mineral Matter, Coal Dry Basis
	Determined	Calculated	
Yallourn-Maryvale	2.3	2.4	1.7
Morwell-Narracan	2.4	2.6	1.5
Loy Yang	1.0	1.1	0.8
Flynn	1.4	1.5	0.1
Yallourn North Ext	4.3	4.5	3.0
Coolungoolun	2.3	2.4	2.2
Gormandale	1.6	1.6	1.3
Gelliondale	5.8	5.8	3.4
Stradbroke	3.9	3.6	2.0
Anglesea	3.9	3.4	2.2
Bacchus Marsh	7.4	7.4	3.5

TABLE 3. **COAL-ASH CHEMISTRY : MORWELL OPEN CUT**

Coal % Dry Basis		Ash%	Laboratory	Boiler Precipitator
Minerals				
FeS_2	0.13	-	-	-
SiO_2	0.19	SiO_2	6.2	8.0
Al_2O_3	0.04	Al_2O_3	1.3	1.7
Inorganics				
Fe	0.32	Fe_2O_3	17.6	22.7
Ca	0.70	CaO	32.0	41.2
Mg	0.24	MgO	13.1	16.8
Na	0.08	Na_2O	3.6	4.6
Cl	0.04	-	-	-
Organic S	0.25	SO_3	26.1	5.0
Total Ash			3.1	2.6

TABLE 4. **VARIATION IN SELECTED CHEMICAL PROPERTIES BETWEEN VICTORIAN BROWN COALFIELDS**

Property	Yallourn Open Cut	Morwell Open Cut	Range of Values (219 Samples)
Moisture (wt %)	66.4	60.2	43.7 - 71.0
Net wet specific energy (MJ Kg^{-1})	6.87	8.95	5.24 - 13.87
Ash (wt %)	1.3	3.5	0.5 - 12.8
Minerals and Inorganics (wt %, db)	1.3	2.7	0.3 - 12.8
Volatile Matter (wt%, dmif)	52.1	49.2	43.3 - 67.8
H/C Atomic Ratio	0.86	0.86	0.77 - 1.16
Oxygen (wt%, dmif)	26.2	24.2	17.4 - 30.0
Nitrogen (wt%, dmif)	0.52	0.62	0.36 - 0.85
Sulphur (wt%, dmif)	0.27	0.34	0.14 - 5.36
SiO_2 (wt% db)	0.38	0.14	0.01 - 7.6
Calcium (wt% db)	0.04	0.74	0.01 - 2.07
Magnesium (wt% db)	0.18	0.23	0.02 - 0.85
Sodium (wt% db)	0.06	0.13	0.02 - 0.47
Iron - total (wt% db)	0.18	0.19	0.01 - 1.80
Phenolic - OH (meq/g)	3.72	3.70	1.91 - 4.44
-COOH (meq/g)	2.21	1.90	0.90 - 2.94
$-COO^-$ (meq/g)	0.49	0.59	0.03 - 1.66

dmif - dry, mineral and inorganic-free basis db - dry basis

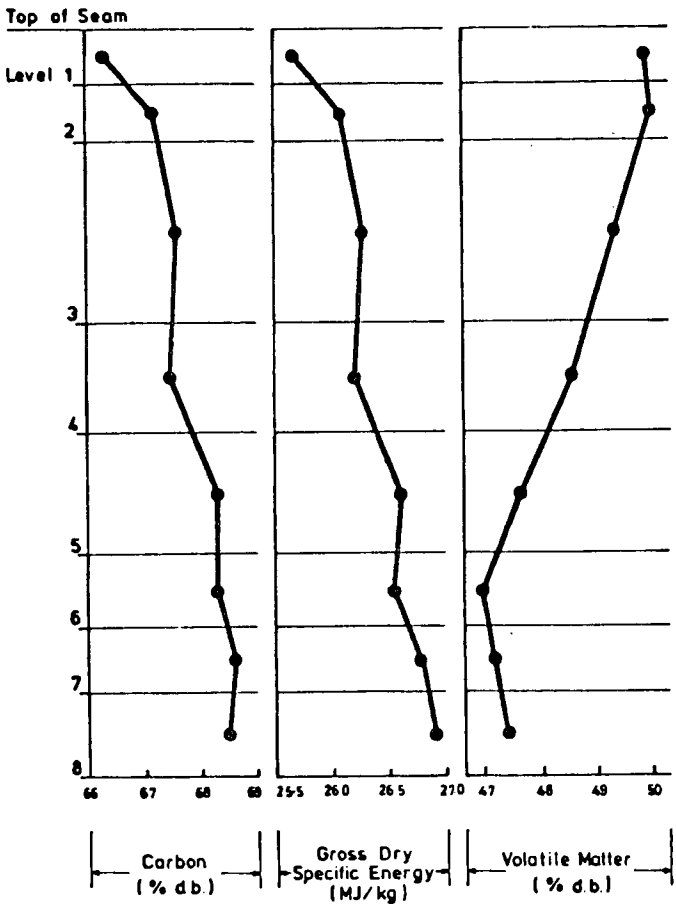

Fig. 1. Variation in selected coal properties with depth in the Morwell Open Cut.

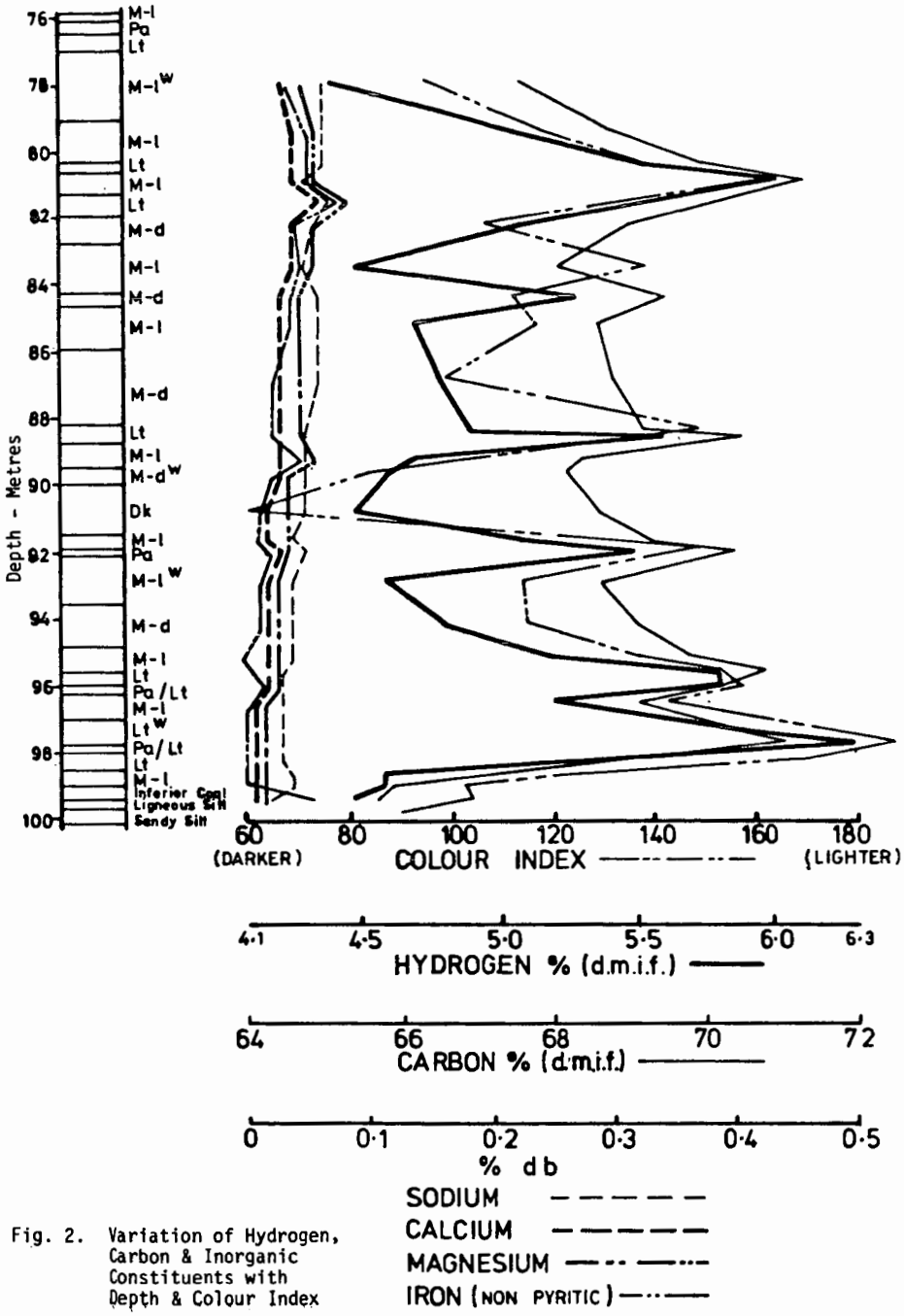

Fig. 2. Variation of Hydrogen, Carbon & Inorganic Constituents with Depth & Colour Index

Correlations between petrographical properties, chemical structure and technological behaviour of Rhenish brown coal

E. A. Wolfrum

Rheinische Braunkohlenwerke AG
Stüttgenweg 2
5000 Köln 41

Federal Republic of Germany

1. Introduction

The Brown coal reserves in the Federal Republic of Germany amount to approx. 56 billion metric tons, 55 billion metric tons of which are in the Rhenish brown coal district located west of Cologne (Fig. 1). About 35 billion metric tons of that reserve are considered to be technologically and economically mineable today what, in terms of energetics, equals the overall oil reserves of Iran (1).

Rhenish brown coal is mined in five opencast mines (Fig. 2) with an average depth of about 280 m. Modern mining equipment having a daily capacity of some 240,000 m^3 of brown coal and high-speed belt conveyor systems are used. About 119 million metric tons of brown coal were mined in 1981.

84.5 % of that output was used for power generation, 7.9 % for briquette production in 4 briquetting plants of the Rheinische Braunkohlenwerke and 4.2 % for powdered brown coal production in two grinding mills. A low portion, viz. 0.3 % was used in a Salem-Lurgi rotary hearth furnace to produce about 96,000 metric tons of fine coke in 1981. 2.7 % of the brown coal output was used for other purposes, inter alia in test plants for processes, like gasification and hydrogenation (Fig. 3).

Longt-term mining plans ensure that this source of energy will be available in sufficient quantities well beyond the turn of the millennium.

This calls for opening up the deep-seated seam horizons as it is being done for the first time with depths of 240 to 450 m at the Hambach mine which is now developed. Today's technology allows opencast mines with a maximum depth of 600 m to be operated.

Mining in greater depths leads to a change of the geotectonic conditions and hence a natural change in the brown coal quality characteristics.

This has varying and graduated effects on the individual refining processes (2).

The petrographical and chemical investigations presented in the following were carried out in order to describe the behaviour of the coal types characteristics of the Rhenish brown coal area during refining processes.

As an introduction, a short survey of the geological conditions of the Rhenish brown coal deposit is given.

2. Geological conditions in the Rhenish brown coal district

In geological terms, the deposit is part of the Lower Rhine Basin extending over about 2,500 km² which was formed by a subsidence in the Early Tertiary. Brown coal itself was formed about 15 to 20 million years ago in the Miocene; during millions of years it was repeatedly flooded with sea or river water and covered with sands, clays and gravels.

The geological profile from NE to SW across the southern part of the Lower Rhine Basin (Fig. 4) shows that the brown coal seams sank down to ever growing depths towards the southwest and then rose again from their deepest point below the Erft river towards the west. Tectonic events caused faults and fractures of several hundred meters.

Accounting these geological conditions, the opencast mines - following the seam - have to operate in ever growing depths.

Therefore selective mining for refining purposes is getting more and more expensive.

3. Structure and composition of Rhenish brown coal

Rhenish brown coal consists of a variety of lithotypes which are discernible in the coal seam already by brightness varations (Fig. 5).
Recent pollen analytical investigations proved that the bright and dark layers result mainly from changing conversion and decomposition conditions. The bog facies has only a limited influence.

The gradation from dark to bright layers reflects the degree of brown coal destruction (3.4).

Figures 6 to 8 show three different types of coal, viz. a bright unstratified coal, a medium-dark stratified coal and a dark heavily stratified coal. The high degree of decomposition of the lithotype represented in Figure 6 indicates an aerobic formation while the high-texture fibrous coal (Fig. 8) is an indicator of an anaerobic formation.

The discovered textures are above all gymnosperms represented by highly resistent coniferous woods which account for a quantity overproportionate to their share of the mainly anigospermous vegetation which formed brown coal.

Only a model can establish the complex, heterogeneous structure of brown coal.

Figure 9 shows a model that inter connects the various structural components, namely lignin, humic acid and

aromatic structural elements. High content of functional groups causes high reactivity. Figure 10 shows how oxygen-containing functional groups are distributed in the Rhenish brown coal.

3.1 Macropetrographical characterization

Based on macropetrographical criterias 15 brown coal lithotypes were selected for the investigations described in the following; they represent more than 90 % of the main seam.

Figure 11 shows these 15 brown coal lithotypes arranged according to stratification an texture.

The coal can be subdiveded into 3 groups depending on the mode of stratification: unstratified, slightly stratified and heavily stratified.

The brightness tends to abate from unstratified to heavily stratified coals.

3.2 Micropetrographical characterization

Micropetrography evaluates the coal components ascertainable by microscopy. Figure 12 shows an extract of the results obtained from the combination analysis of the 15 brown coal lithotypes.*

Obviously the investigated brown coal lithotypes differ in micropetrographic respect.

*We thank H.W. Hagemann, PhD., member of the faculty of geology, geochemistry and oil and coal deposits of the Aachen technical university for having carried out the investigations.

Based on the qualitative assignment of the individual coal components, rhenish brown coal can be divided into four groups having similar petrographical properties which, correspond with the macropetrographical features (principle of classification: stratification and texture). This classification into 4 groups differs only negligibly from the macropetrographical division into three main groups.

The classification into four main groups results in the correlations shown in the following Figures. Figure 13 shows the liptinite content as a function of the group classifications 1 to 4. With rising group number, corresponding to stronger stratification and texture, the liptinite content declines. Figure 14 which shows the huminite as a function of the group numbers indicates that the huminite content rises with increasing stratification and texture.

These two correlations stand for a variety of functions of technological relevance between brown coal maceral groups.

3.3 Chemical and physical composition

Subsequent to the petrographical coal analysis, both a chemical and a chemo-physical investigation were carried out. Figure 15 shows the chemical and physical properties of the investigated brown coal lithotypes.

Rhenish brown coal has an average ash content of about 4 % (wf), a volatile matter of about 52 % (waf) and a lower heating value of 11.000 Btu/lb of coal (waf). The final analysis of the coal under waf conditions shows the following average composition:

69 % carbon, 5 % hydrogen, 1 % nitrogen and approx. 25 % oxygen; the sulphur content amounts to about 0.35 % (waf) about 50 to 70 % of which is bound to the ash during the combustion process since approx. half of the mineral components of Rhenish brown coal consist of basic alkali and alkaline earth compounds - primarily those of calcium.

The following investigations were aimed at revealing correlations between the chemical and chemo-physical coal data and the petrographical analysis that may help assess the coal quality prior to its use as a feedstock in various refining processes.

4. Correlations between petrographical structure, chemical composition and refining behaviour of Rhenish brown coal

The correlations between the chemical brown coal data, petrographical parameters and the refining behaviour are described in the following complex regression calculations therefore were carried out. Statistic calculation methods were applied as an objective criterion to prove such correlations.

To nearly all brown coal refining processes is applicable that

- the quality of the desired refinement products
- the refining cost
- the quality of the raw material

have a direct correlation. Hence, it is indispensible for any refining operation to know and assess the composition of the raw material and its behaviour during the refining process.

The usability of the results obtained from the raw material characterization in everyday practice depends on

- the spacing of drillings usuable for quality assessment
- the level of geological knowledge of the coal forming conditions
- a representative sampling in the opencast mine, taking into account the cutting geometry of the excavator (position of the excavator cuts to the deposit), the fast mining advance and the high mass flow involved.

4.1 Correlations between chemical and petrographical parameters

4.1.1 Heating value

Figure 16 shows that the heating value declines with increasing coal stratification. A comparison of the heating value of coal and its hydrogen content in Figure 17 indicates that according to expectation the heating value of the coal rises parallel to an increase in its hydrogen content. This again is due to the portion of hydrogen-rich minerals, such as liptinite, declining in the said order - a correlation clearly evident in Figure 18. The heating value of the coal obviously rises in proportion to its liptinite share. The oxygen-rich lignitic coal components, such as huminite, have the opposite effect on the heating value: Figure 19 shows that the heating value of the coal is down sharply with an increase in the portion of this maceral group.

4.1.2 Volatile content

The individual coal constituents contribute different shares to the volatile matter of the coals (5). With increased stratification, the volatile matter decreases, caused by the respective distribution of the various maceral groups. Figure 20 gives an example how the content of volatile matters and that of the hydrogen-rich liptinite maceral correlate. It is obvious that this constituent contributes a lot to the volatile matters.

4.1.3 Hydrogen content

Figure 21 shows that also the hydrogen content is closely corresponding to the petrographical brown coal properties. Figure 22 shows the correlation between the hydrogen content and the Lipto-Humodetrite and/or the Humo-Telinite content of the investigated lithotypes. A higher amound of Lipto-Humodetrite leads to an increased hydrogen content. The content of the Humo-Telinite maceral, however, has a totally different effect: This component has a high portion of oxygen-rich molecular groups what causes the hydrogen content of the brown coal to drop.

4.2 Correlations between coal quality and refining behaviour

4.2.1 Briquetting and coking

There are many investigations and publications available on the briquetting behaviour of brown coals, both from the GDR and the Rhenish area (6 to 9).

In order to establish statistically usable data on the briquetting behaviour of Rhenish brown coals, the 15 brown coal lithotypes were briquetted under identical conditions with a laboratory press (water content, grain size distribution and mould pressure).

For assessing the briquettability of these coals, a number of briquetting parameters were correlated with the petrographical properties of the brown coal types. A statistic evaluation of these briquetting parameters and the micropetrographical composition of the coals reveal only a minimal degree of interdepence. Figure 23 clearly shows that the Humo-Telinite content stands for the height and volume expansion of the briquettes.

The briquetting expenditure is related to the Telo-Humocollite content. The definition factor (r^2) varies between 0.58 and 0.67, and is comparatively low. All the other correlations between the briquetting parameters (e.g. diametrical expansion) and the petrographical coal composition turned out to be rather insignificant so that they need not to be taken into consideration.

These investigations on correlations established between the raw material properties and briquettability of Rhenish brown coal led to the following results:

1. A macro- and micropetrographical analysis with a view to technological problems involved in the briquetting process allows at the most to judge the briquettability of Rhenish brown coal on the basis of trend data.

2. A correlation analysis of the chemo-physical parameters of Rhenish brown coal and its briquettability gives only trend data as well.

Therefore generaly an anticipated quality assessment of the briquettes is restricted to the following points:

1. Macropetrographical assessment of the coal seam and evaluation of the briquettability on the basis of values gained by experience.

2. Laboratory production of briquettes and determination of their pressure resistance.

3. Determination of the ash content as an essential factor for the assessment of brown coal briquettability. Ash contents exceeding 3 to 4 % result both in a reduction of the resistance to pressure and a high wear of the molds of the briquetting presses, and are not suited to be processed into briquettes.
   Gelled coals, unsuitable for briquetting purpose as well, are used as steam coal.

Coking

Numerous publications (10 to 12) have been made above all in the GDR on the required quality properties of brown coal and their influence on the quality characteristics of formed coke. Since the Rheinische Braunkohlenwerke AG does not consider formed coke production at present, raw material quality and coking behaviour are of interest only for the production of fine coke using the rotary hearth furnace principle (13, 14) (Fig. 24).

This technology is dependent only to a low extent on the specific raw material composition. The petrographical factors of the feedstock have an impact above all on grain size and grain size distribution. It is not the final coke strength that is crucial for this process but the grain spectrum caused by grain decomposition.

Correlations so far unkown may lie in the petrographical composition of brown coal (in connection with the mineral composition) and the reactivity of fine coke to oxygen. Therefore, an anticipated quality assessment of feed coals corresponds to that used for briquetting coal.

4.2.2 Gasification

Two gasification processes under development, namely gasification using oxygen (HTW) and hydrogasification, (HKV), helped to study the gasification behaviour of various brown coal lithotypes (15).

The reactivity of the residual char is the speed-controlling factor for brown coal hydrogasification (16). Laboratory-scale investigations on the gasification behaviour of various types of brown coal coke showed that the mode of pretreatment has a greater influence on the gasification process than the raw material properties. To give an example, helium flushing of the coke under gasification temmperature has a very favourable effect on gasification.

With one exception only, gasification rates close to 100 % were achieved.

Differences in gasifaction speeds are due to the heterogeneous pore structure and the inhomogeneous iron distribution in the coal matrix.

Irregularly localized iron groupings contained in cokes of the lithotypes 1 and 8 show a varying reactivity behaviour.

Cokes of the lithotypes 4, 5, 9, 11, 13 and 15 with similar gasification behaviours have a comparatively homogeneous distribution of all ash components (Fig. 25). No correlation was established between the maceral composition and the reactivity behaviour of the cokes (17).

As it was the case with the mentioned hydrogasification process, the results obtained with HTW gasification did not show any statistically significant correlations between the petrographical composition of the lithotypes and their gasification behaviour.

4.2.3 Liquefaction

To determine potential raw material impacts on brown coal hydroliquefaction, the 15 lithotypes were converted into liquid products using various techniques (18).

1. moderate indirect hydrogenation with tetralin as a hydrogen-transferring solvent

2. direct hydrogenation with hydrogen and different catalysts similar to operational conditions.

- Indirect hydrogenation with tetralin

Indirect hydrogenation using tetralin at a reaction temperature of 410 °C, a pressure of 400 bar and an overall reaction time of 2 h produced carbon conversion rates from 50 to 79 (%wt) and liquid product yields from 43 to 69 (%wt). Of the multitude of correlations established between the results of the hydrogenation tests and the micropetrographical composition of the coal types only a few examples are given.

Figure 26 shows the product yields of indirect brown coal hydrogenation with tetralin as a function of stratification and texture (lithotype number). It is obvious that with increasing stratification and texture, i.e. with rising lithotype number, the liquid product yield drops and the portion of hydrogenation residue increases. Regarding the fine structure of the coal the following correlations turn out:

Figure 27 represents the carbon conversion rate as a function of the liptinite and huminite maceral portions. It can be seen that an increase in the hydrogen-rich liptinite constituent improves carbon conversion while the oxygen-rich huminite reduces the carbon conversion rate. These trends also apply to the yield of liquid products. It should be pointed out again that it is only possible to give trend data. Quantitative assignments are impossible since the statistical certainty is insufficient.

- Direct hydrogenation with molecular hydrogen and catalyst

The influence of the raw material was expected to weaken using hydrogen and a catalyst under the conditions similar to those in the real hydroliquefaction process. An increase in the carbon conversion rate up to a maximum of 96 (%wt) shows that both brown coals with high or low carbon-to-hydrogen ratios achieve high product yields. Plain impacts of the raw material on the liquefaction results are no longer observed.

Resuming it can be said that the hydrogenation degree from indirect to direct hydrogenation rises parallel to an increase in carbon conversion. The result is that nearly all brown coal types mineable in the Rhenish area can be converted into liquid products with high yields. Hydrogenation process engineering, i.e. the optimization of the reaction conditions (temperature, pressure, residence time, catalyst type), is considered with priority over the raw material properties.

The investigations showed that in general practice no importance is attributed to a micropetrographical assessment of the coal types as a criterion for selecting specific brown coals from the Rhenish area. Tar content and/or low-temperature carbonization product yield and paraffin content suffice as parameters to assess the hydrogenatability of Rhenish brown coals. For exploratory drilling programmes, these parameters are determined separately. In general, brown coals from various areas that meet the quality parameters given in Figure 28 have satisfactory hydrogenation properties.

5. Summary

For the purpose of an assessement with a view to refining, the petrographical, chemical and physical properties of lithotypes of Rhenish brown coal were established and compared with one another.

The investigated coal typs cover more than 90 % of the coal types proved in the Rhenish deposit. A correlation of the results shows a describable, sometimes multidimension al dependancy.

A comparison of raw material properties and the results of the technical experiments quickly reveals the limits set to such an approach.

Out of all the refining processes subjected to investigation briquetting places the highest requirements on the raw material properties. The major part of the established parameters leads only to qualitative indications of the briquetting properties of the coals. Parameters of greater significance can hardly be utilized in pratice. What remains in the experience gained by coal technologists, is the determination of the classical coal properties and indications from laboratory briquetting.

For the gasification process no usuable quantitative relations were established between the petrographical coal properties and the gasification behaviour. It is possible without any material problems to convert nearly all the rhenish coal types into gaseous hydrocarbons or synthesis gas.

This statement applies without any restriction to coal liquefaction as well. Apart from a few comparatively rare coal types, all brown coals from the Rhenish area can be converted into liquid hydrocarbons with high product yields. Hence, hydrogenation process engineering, i.e. the optimization of the reaction conditions, has priority over the raw material properties.

Under the given conditions of the Rhenish brown coal deposit, an opencast mining operation, a high output and the large feed quantities required for future refining plants brown coal petrography is one out of many tesseraes for quality assessement.

The development of appropriate modes of determining the quality characteristics of raw brown coal is a task indispensable for the future.

6) References

1) P. Speich:
"Technische und wirtschaftliche Gesichtspunkte der Braunkohlenveredlung"
Brennstoff-Wärme-Kraft 32 (1980) Nr. 8, 307-312

2) E. Wolfrum, J. Wawrzinek:
"Beziehungen zwischen petrographischen und chemischen Eigenschaften Rheinischer Braunkohle"
Braunkohle Heft 11/81, 381-386

3) G. von der Brelie, M. Wolf:
"Zur Petrographie und Palynologie heller und dunkler Schichten im rheinischen Hauptbraunkohlenflöz"
- Fortschr. Geol. Rheinld. u. Westf. (1981) 29; 95-163

4) H. W. Hagemann, A. Hollerbach
"Relationship between the macropetrographic and organic geochemical composition of lignites"
- Advances in organic Geochemistry 1979,
A. G. Douglas, J. R. Maxwell (Editors)
Pergamon Press Oxford, New York, Frankfurt

5) R. Kurtz, E. Wolfrum, W. Assmann:
"Die Verkokungseigenschaften chemischer Stoffgruppen in einigen Braunkohlentypen des rheinischen Reviers"
Comm. Eur. Communities, Rep EUR 1977
EUR 6075, Round Table Meet. Chem. Phys. Valorication Coal, 125-150

6) E. Sontag, M. Süss:
"Beispiel petrologischer Untersuchungen zur Klärung rohstoffabhängiger verfahrenstechnischer Probleme der Braunkohlenveredlung"
Bergbautechnik 19 (1969) 5. 255-260:7. 376-381

7) R. Kurtz:
"Zusammenhang zwischen mikropetrographischem Aufbau der Weichbraunkohlen und ihrer Brikettierbarkeit"
Dissertation, RWTH Aachen, Fakultät für Bergbau und Hüttenwesen (1970)

8) E. Rammler:
"Zur Kenntnis der Brikettierbarkeit von Braunkohle"
Freiberger Forschungshefte A99 (1958), 81-104

9) H. Jakob:
"Neuere Ergebnisse der angewandten Braunkohlenpetrologie"
Berg- und Hüttenmännische Monatshefte 105, Heft 2 (1960), 21-29.

10) E. Rammler, G. Bilkenroth:
"Zur technischen Entwicklung der Braunkohlenkokerei"
Freiberger Forschungshefte A 184 (1961) 85 - 113

11) E. Rammler, W. Fischer, G. Hänseroth:
"Schrumpfverhalten von Braunkohlen Feinstkornbriketts bei der Verkokung bis 1000 °C"
Freiberger Forschungshefte A453 (1968), 121-145

12) W. März:
"Untersuchungen zum Verlauf der Verkokung von Braunkohlenbriketts, insbesondere bei der Spülgasverkokung"
Freiberger Forschungshefte A375 (1966), 79-99

13) R. Kurtz:
"Koksherstellung aus Braunkohle"
Braunkohle Heft 11, Nov. 1975, 352-356.

14) E. Scherrer:
"Herstellung von Braunkohlenkoks im Salem-Lurgi-Herdofen"
Braunkohle Heft 7, Juli 1981, 242-246.

15) H. Teggers, K.A. Theis, L. Schrader:
"Synthesegase und synthetisches Erdgas aus Braunkohle"
Erdöl und Kohle-Erdgas ver. mit Brennstoff-Chemie Bd.35, Heft 4, April 1982, 178-184

16) L. Schrader, H. Teggers, K.A. Theis:
"Hydrierende Vergasung von Kohle"
Chem.-Ing.-Tech. 52 (1980) Nr. 10, 794-802

17) M. Ghodsi, J.P. Lempereur, E. Wolfrum:
"Etude cinétique de l´hydrogénation directe des cokes de différents lithotypes de lignite"
Vortrag gehalten auf der Internationalen Kohlenwissenschaftlichen Tagung, Düsseldorf 07. - 09.09.81

18) E. Wolfrum, J. Wawrzinek, W. Dolkemeyer:
"Einfluß der Rohstoffeigenschaften auf die Verflüssigung Rheinischer Braunkohlen"
Vortrag gehalten auf der Internationalen Kohlenwissenschaftlichen Tagung, Düsseldorf 07.-09.09.81

Fig. 1 Rhenish Brown Coal District

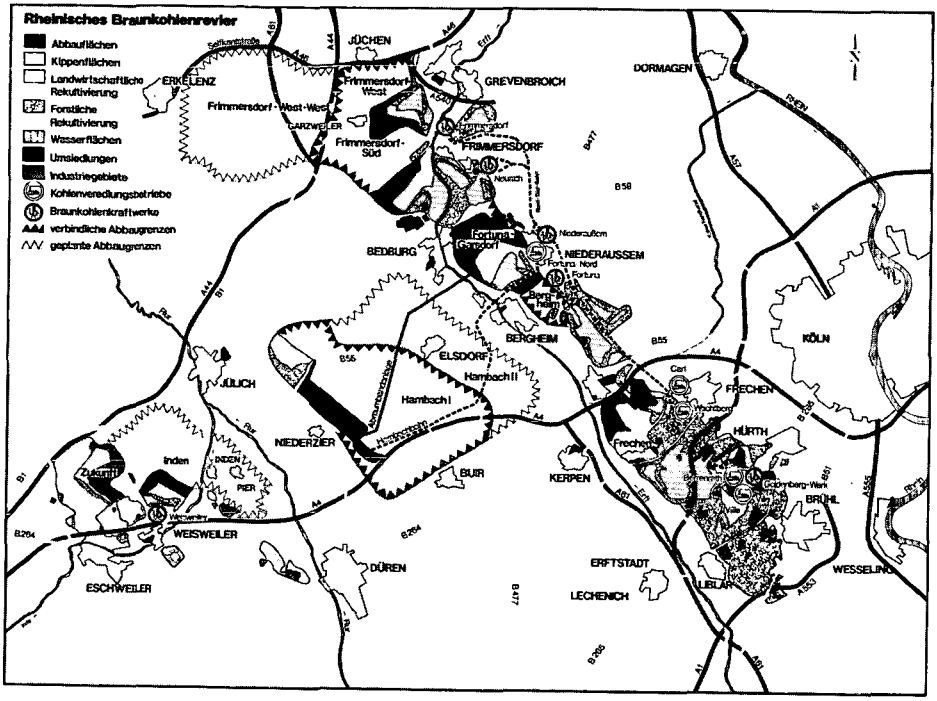

Rhenish brown coal district

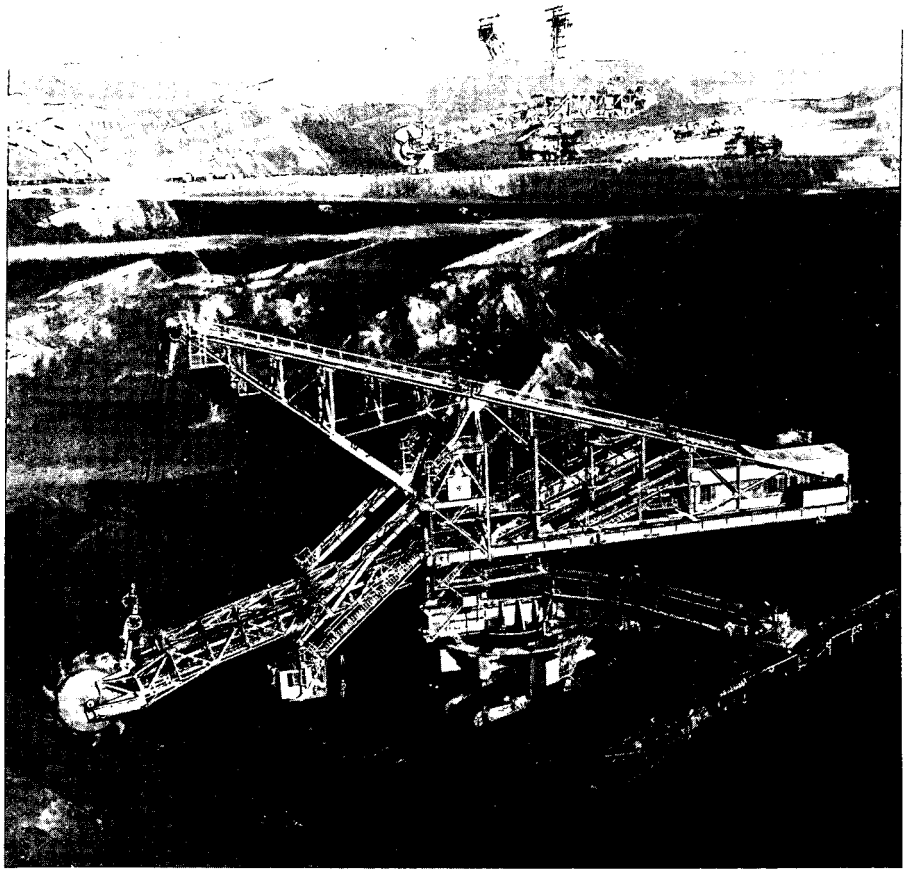

Fig.2 Excavator

Fig. 3

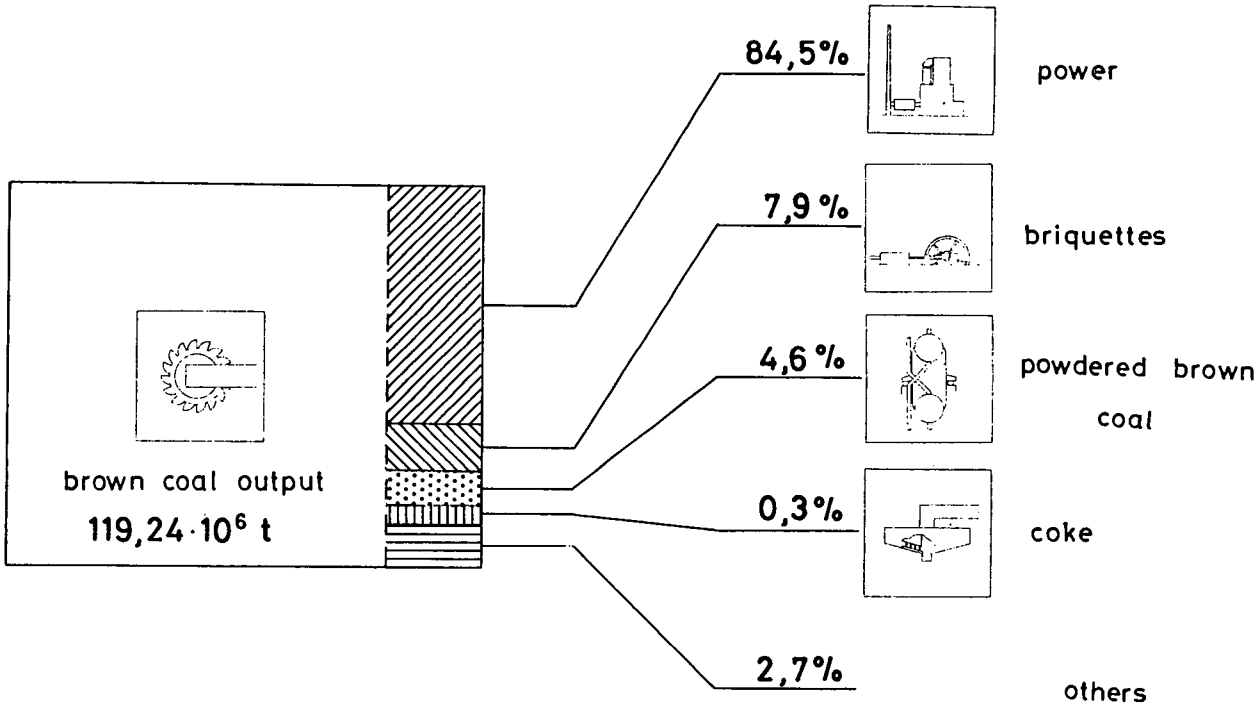

raw brown coal output and use
Rheinbraun 1981

RHEINBRAUN

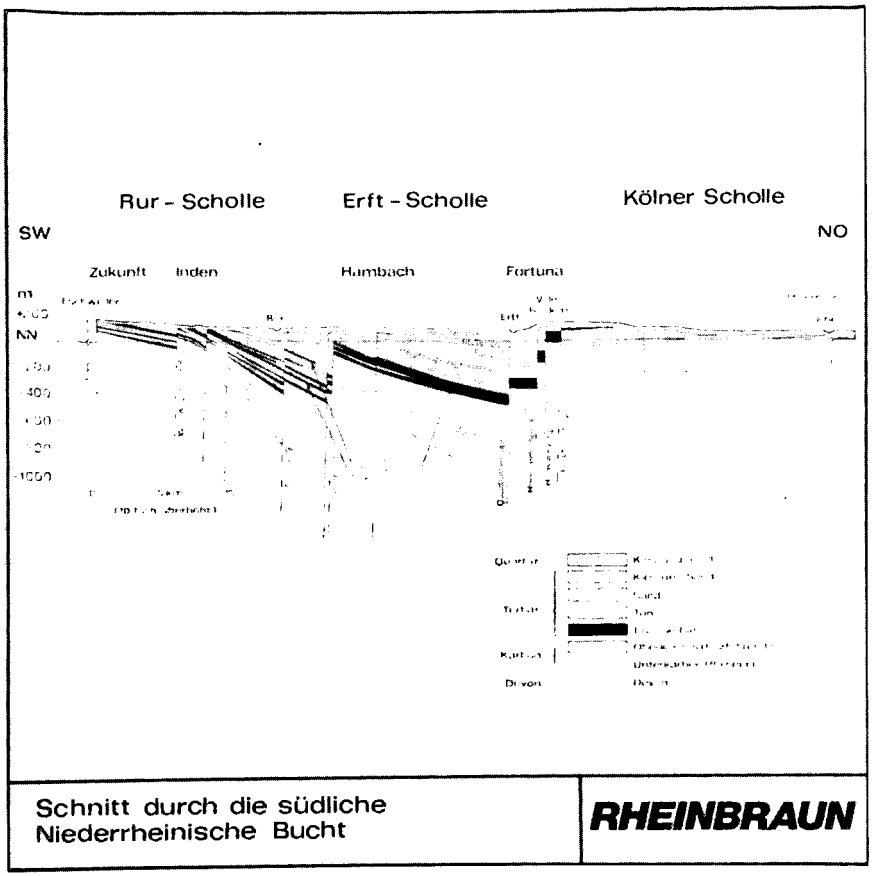

Fig.4 Geological profile

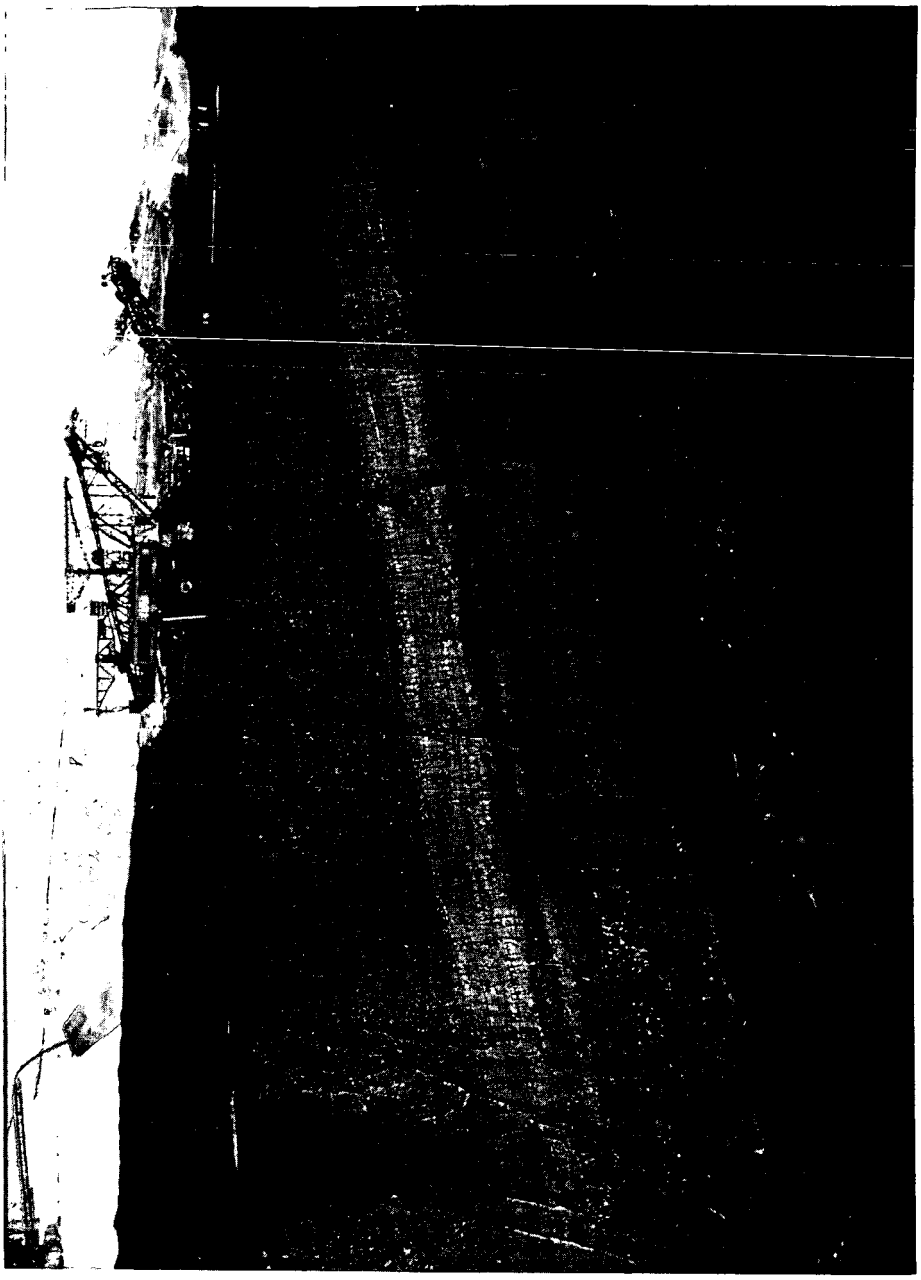

Fig.5 Brown coal seam

Fig. 6 Lithotype 1

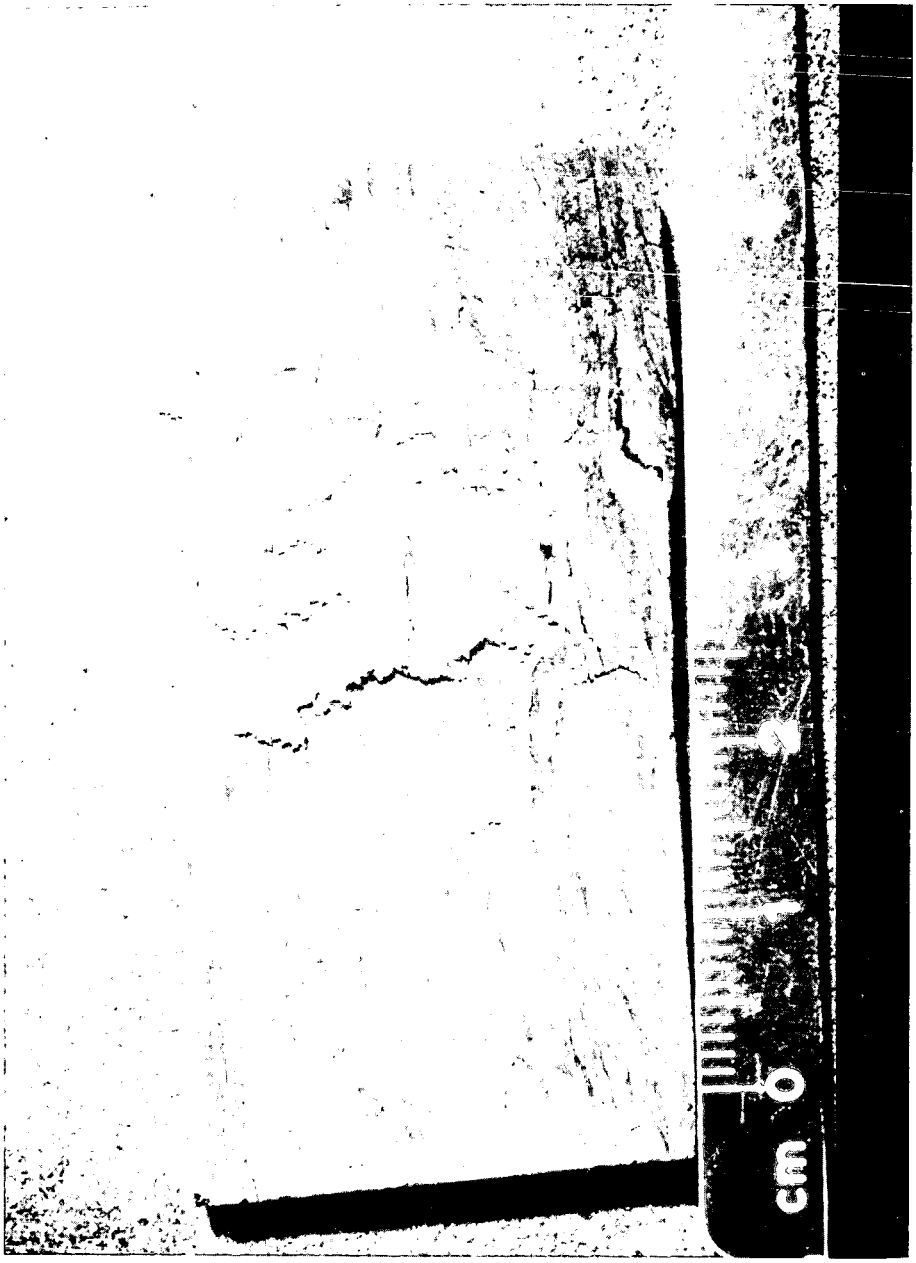

Fig. 7 Lithotype 9

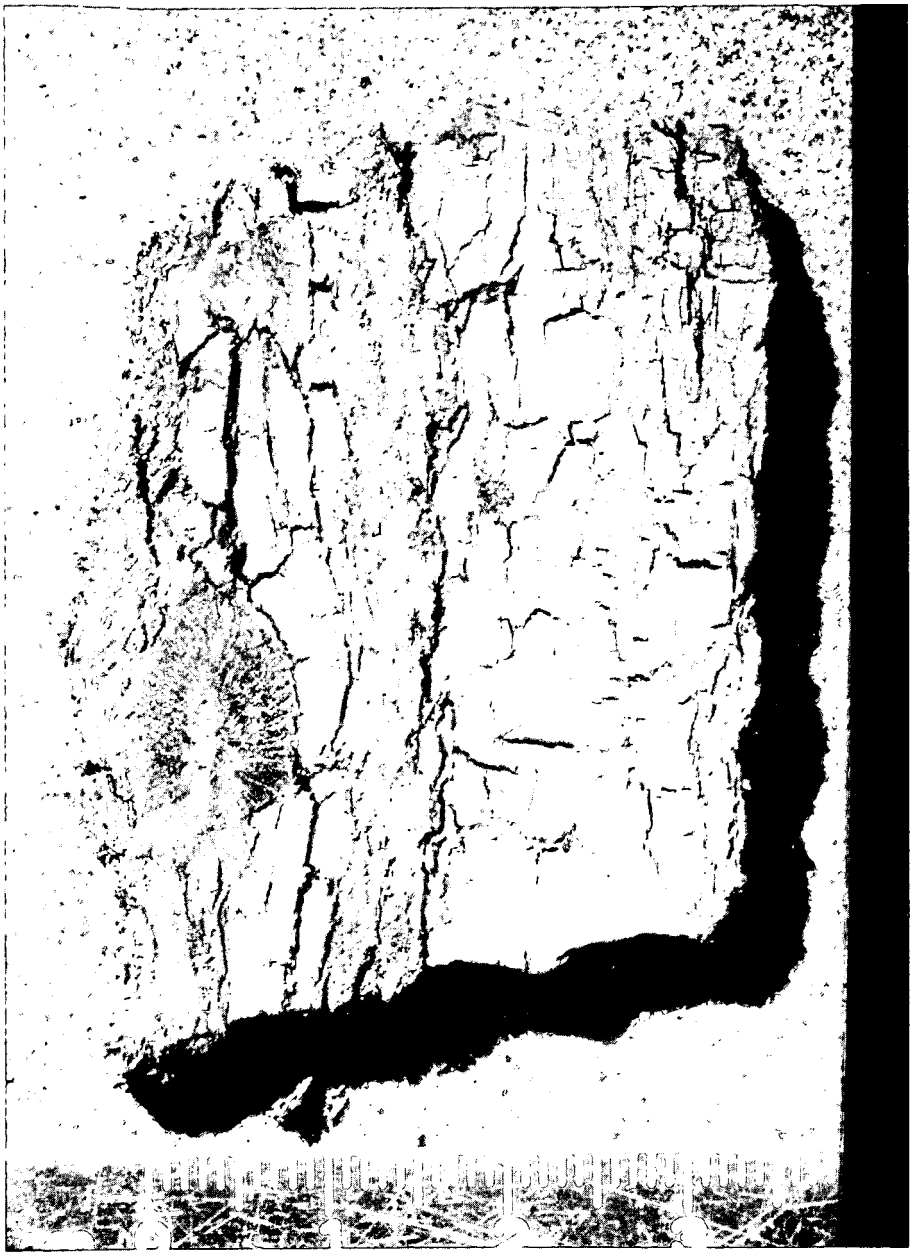

Fig. 8 Lithotyp 15

Fig. 9

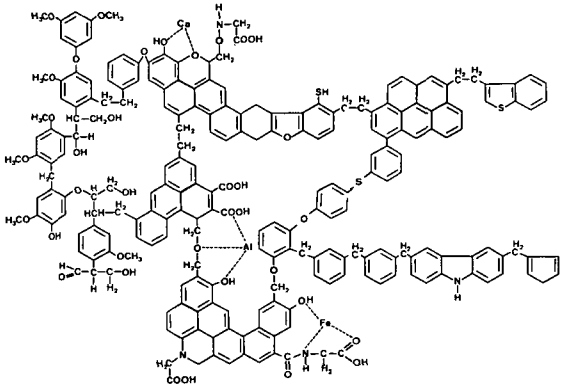

element	Rhenish brown coal (maf)
C	68,7
H	5,05
O	25,0
N	1,0
S(org.)	0,25

typical composition

lignin humic acids structural aromatic elements

Schematic composition of the brown coal structure elementary analysis

Fig. 10

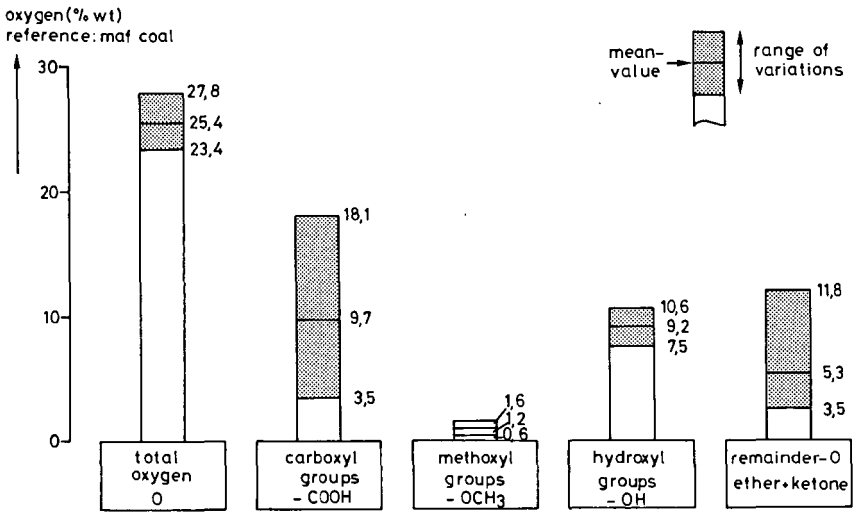

Distribution of the oxygen-containing functional groups in Rhenish brown coal

RHEINBRAUN

Fig. 11

percentage of a seam section	sample no.	structure matrix / texture	brightness and coluor	gelification rate accessory intercalations
4,2 %	1	unstratified coal	bright	xylite-and mineral-free, matrix
3,9 %	2	unstratified coal	dark	granular gelification nests, xylite
5,5 %	3	unstratified coal	medium-bright	xylite-containing
15,0 %	4	unstratified coal	medium-bright	slightly textured and xylite
12,8 %	5	unstratified coal	medium-dark	slightly textured,xylite,surface gel
7,8 %	6	unstratified coal	medium-bright	slightly textured,xylite-free
5,8 %	7	unstratified coal	dark	slightly textured,xylite,gel,fusite
18,5 %	8	slightly stratified coal	medium-bright	textured,xylite and resinous substance
9,2 %	9	slightly stratified coal	medium-dark	textured,xylite and bright texture
3,0 %	10	slightly stratified coal	dark	xylite and gelled,textured
5,7 %	11	slightly stratified coal	dark	textured,xylite and fusite nests
1,9 %	12	heavily stratified coal	medium-bright	sub. heavily textured,bright texture,resinous
2,5 %	13	heavily stratified coal	dark	heavily textured,xylite and fusite nests
2,2 %	14	heavily stratified coal	dark	heavily textured,xylite,gelled
2,0 %	15	fibrous coal	dark (black)	heavily textured,fusite texture

Macropetrographical classification of 15 brown coal lithotypes from the Rhenish area

RHEINBRAUN

Fig. 12

maceral, maceral subgroup, lithotype	group no.	1	2	3	4
	lith. no.	1,2	7,3,4,6	5,10,8	14,15,11 13,9,12
Liptinite	% vol.	26 - 28	20 - 26	6 - 11	3 - 12
Humo-Detrinite	% vol.	56 - 59	54 - 58	31 - 43	12 - 31
Humo-Telinite	% vol.	3 - 5	10 - 17	26 - 33	34 - 50
Humo-Collinite	% vol.	6 - 7	3 - 8	19 - 26	17 - 31
Huminite	% vol.	67 - 69	72 - 79	87 - 92	80 - 90
Inertinite	% vol.	5	1 - 3	1 - 4	2 - 17
Lipto-Humodetrite	% vol.	79 - 80	56 - 67	3 - 17	-
Telo-Humodetrite	% vol.	3	21 - 30	8 - 15	10 - 30
Telo-Humocollite	% vol.	-	-	9 - 15	3 - 17
Detro-Humocollite	% vol.	-	-	3 - 7	3
Gelo-Humotellite	% vol.	3	3	10 - 12	10 - 39

Micropetrographical classification of 15 lithotypes into 4 groups

RHEINBRAUN

Fig. 13

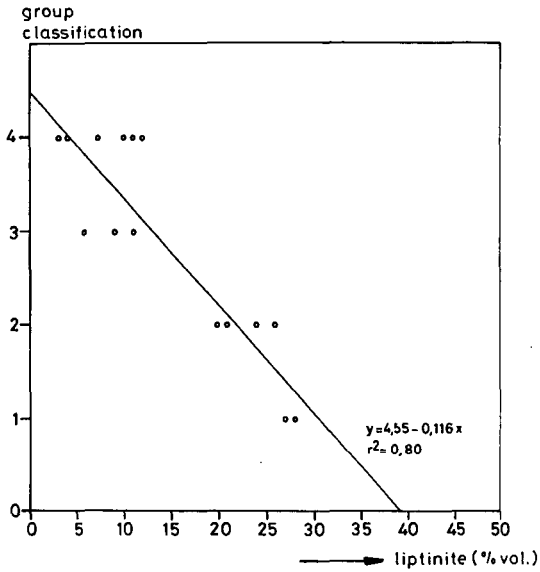

Liptinite content as a function of micropetrographical classification	RHEINBRAUN

Fig. 14

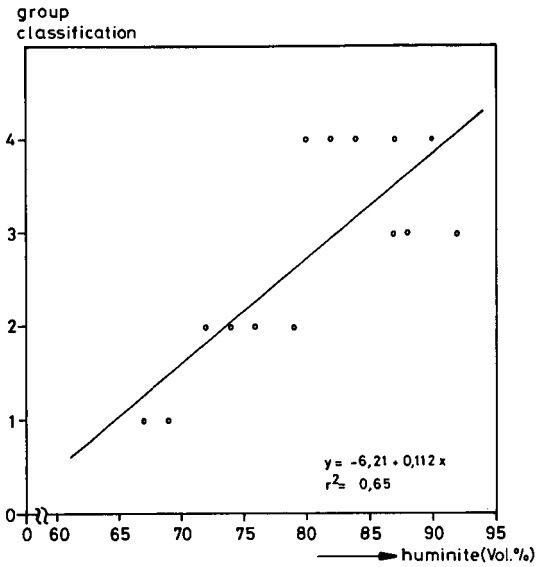

Huminite content as a function of micropetrographical classification	**RHEINBRAUN**

Fig. 15

lithotype no.			1	2	3	4	5	6	7	8	9	10	11	12	13	14	15
Short analysis																	
- brown coal (raw)	ar *	% wf	62,2	60,4	60,1	55,6	52,0	55,6	54,0	50,0	53,4	55,1	54,0	59,7	60,6	58,6	49,0
- ash content	mf	% wf	6,53	2,44	2,78	3,86	3,90	4,42	3,55	4,27	3,04	3,52	3,73	2,73	3,56	3,38	3,92
- volatiles	maf	% wf	59,68	58,25	55,11	54,70	52,42	52,09	51,91	52,98	49,65	49,76	48,36	53,72	51,74	51,77	48,79
- C-fix	maf	% wf	40,32	44,75	44,89	45,30	47,58	47,97	48,09	47,02	50,35	50,24	51,64	46,28	48,26	48,23	51,21
- heating value	maf	MJ/kg	27,99	25,67	25,69	26,69	25,85	25,97	26,30	25,27	25,55	25,43	25,31	24,96	25,43	25,36	24,99
Elementary analysis																	
- carbon	maf	% wf	69,6	67,5	67,8	68,9	68,2	69,3	69,6	65,7	68,5	68,4	68,9	67,4	66,3	67,4	69,5
- hydrogen	maf	% wf	5,89	5,60	5,24	5,56	5,19	5,21	5,25	4,71	5,10	4,92	4,69	4,91	4,79	4,86	4,51
Extraction analysis																	
- bitumen content	maf	% wf	12,87	12,25	10,96	12,04	8,79	7,43	8,96	7,29	7,10	5,40	9,18	7,20	9,65	5,11	7,31
- paraffin content	maf	% wf	10,19	9,46	9,00	10,00	4,53	6,53	7,46	6,00	5,77	3,93	5,90	5,93	8,20	4,19	3,10

* as received

Chemo-physical characterization of the brown coal lithotypes subjected to investigation

RHEINBRAUN

Fig. 16

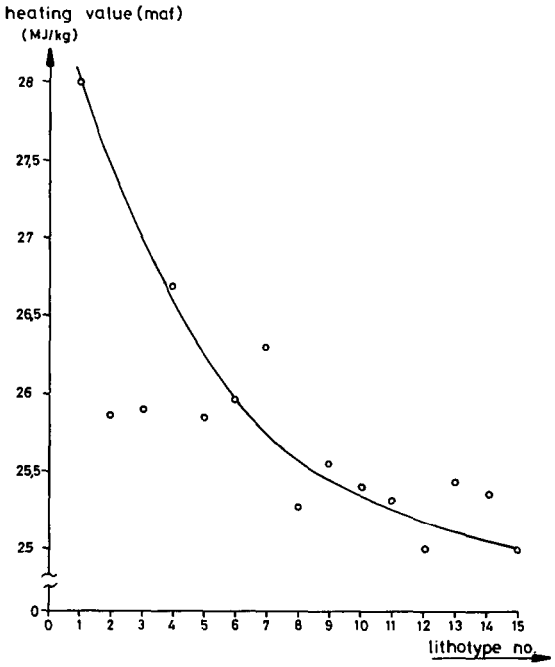

Heating value of the brown coal lithotypes as a function of macropetrographical classification	RHEINBRAUN

Fig. 17

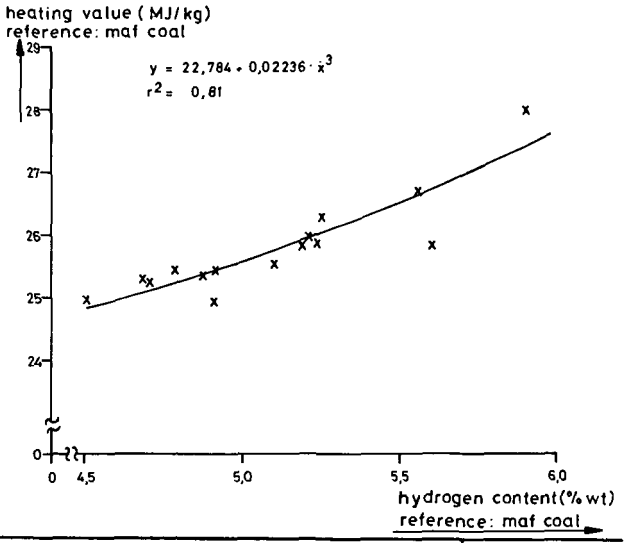

Correlation between the heating values and hydrogen contents of the 15 lithotypes investigated	RHEINBRAUN

Fig. 18

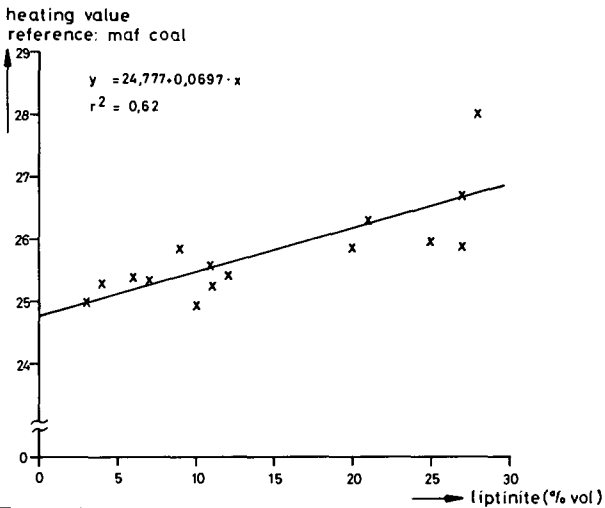

Heating value as a function of the liptinite content of the 15 lithotypes investigated

RHEINBRAUN

Fig. 19

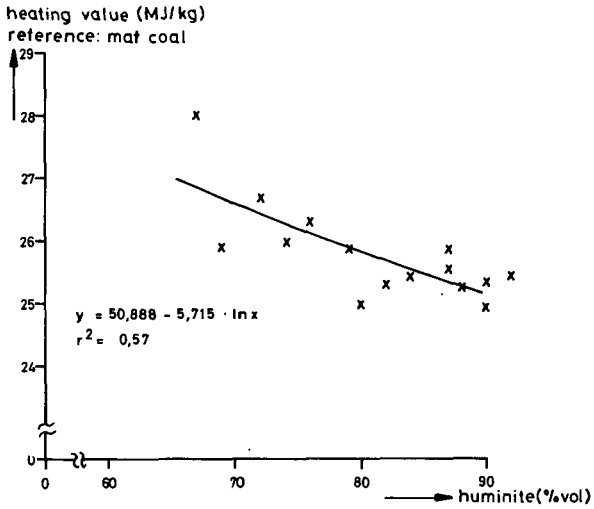

Correlation between heating values and huminite contents of the 15 lithotypes investigated	**RHEINBRAUN**

Fig. 20

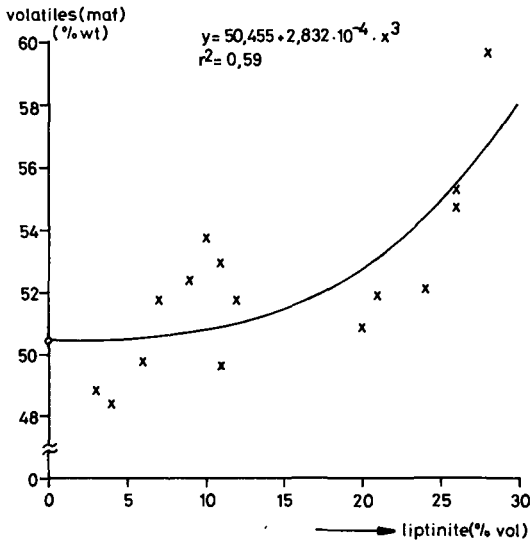

Volatile portion as a function of the liptinite content	RHEINBRAUN

Fig. 21

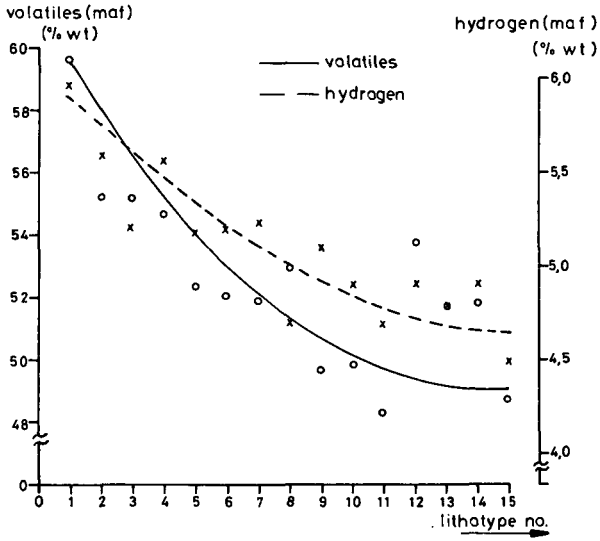

Correlation between volatile matters, hydrogen contents of the lithotypes and the macro-petrographical classification	RHEINBRAUN

Fig . 22

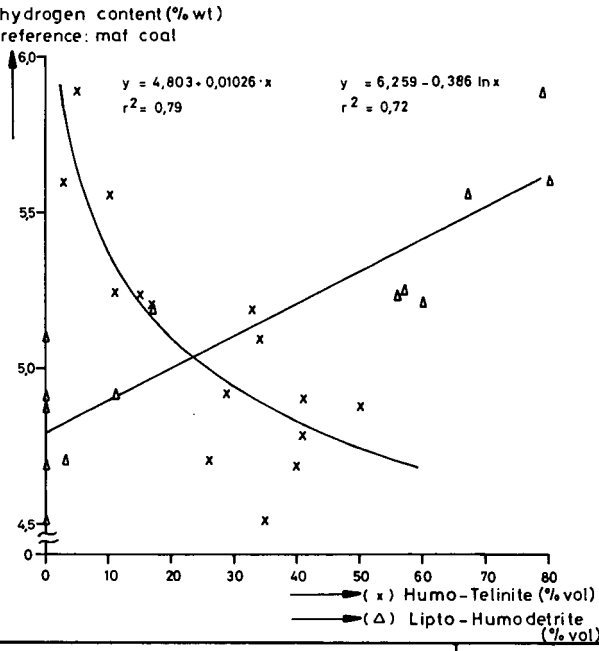

Correlation between hydrogen and Humo-Telinite and Lipto-Humodetrite portions

RHEINBRAUN

Fig. 23

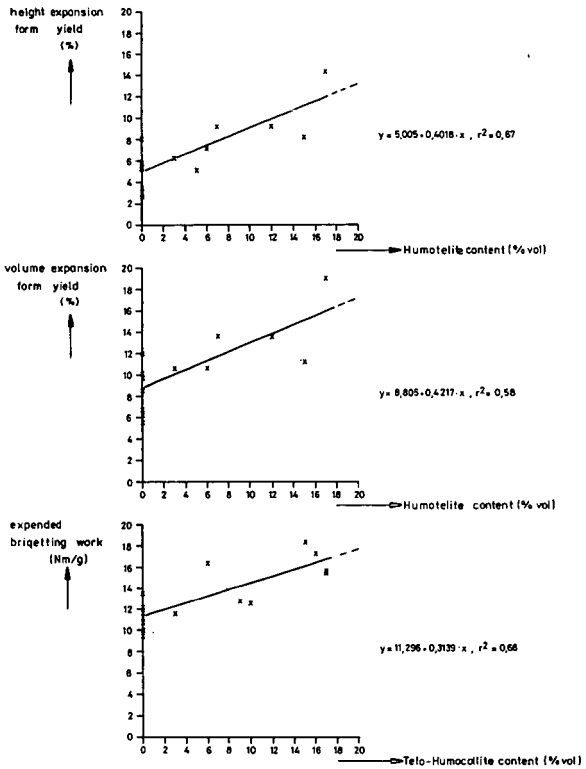

Correlation between the contents of various microlithotypes and for subgroups and various briquetting results

RHEINBRAUN

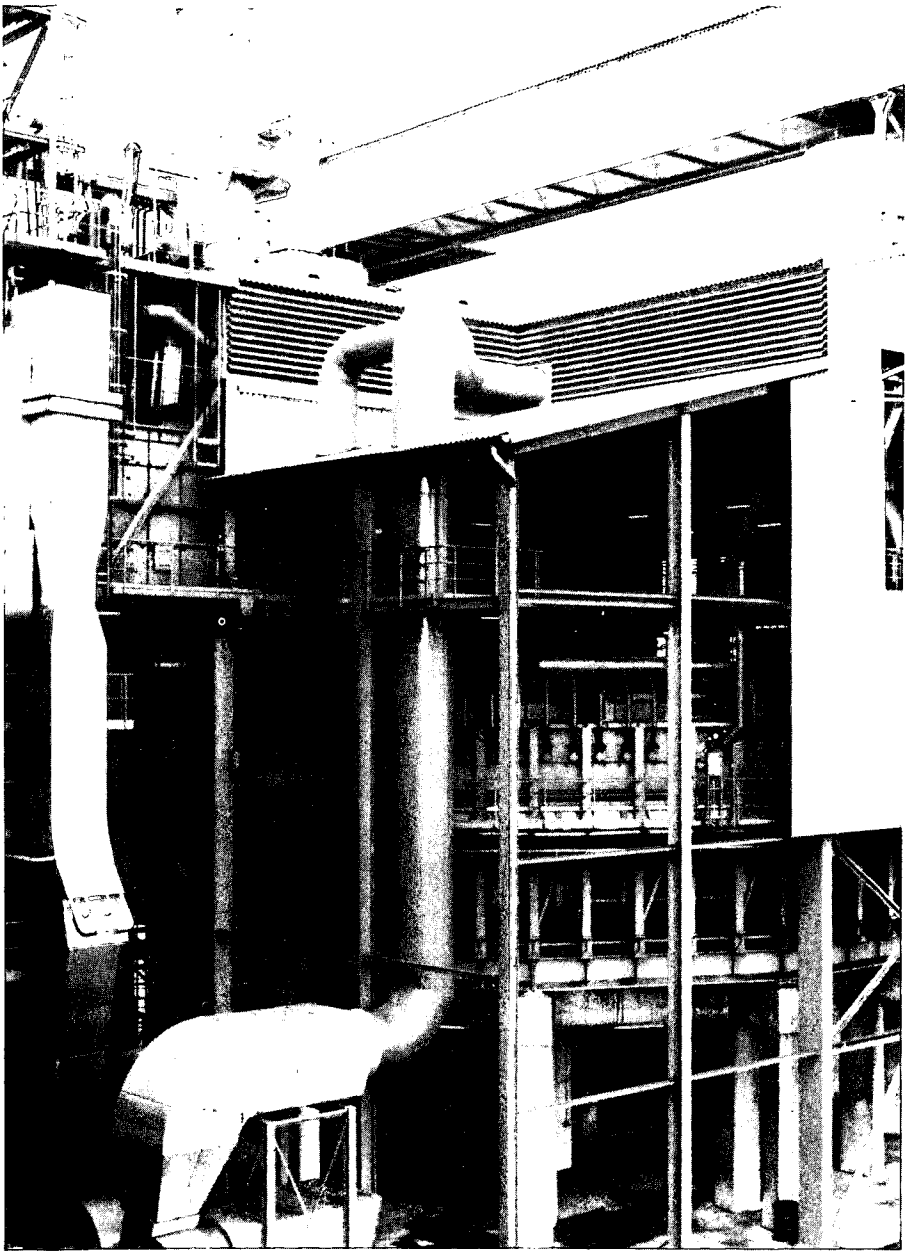

Fig. 24 rotary hearth furnace

Fig. 25

40 atm H_2 bei 900°C

Vorbehandlung: 1/2 h im Heliumstrom von 1 atm bei 900°C

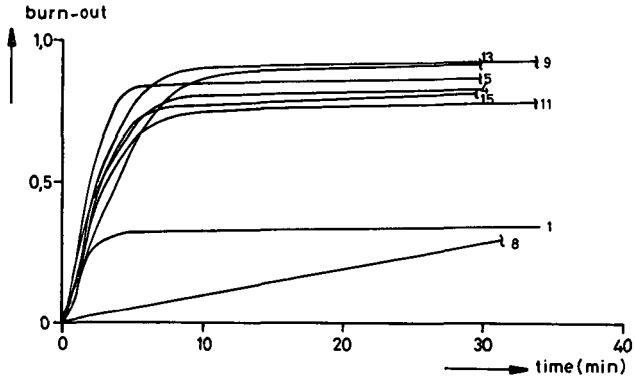

lith. no.	burn-out	time (min)
9	93,3	72
13	92,5	80
5	88,3	120
4	82,1	30
15	82,4	46
11	87	240
1	34,1	34
8	100	390

Conversion as a function of time with hydrogasification of brown coal cokes

RHEINBRAUN

Fig. 26

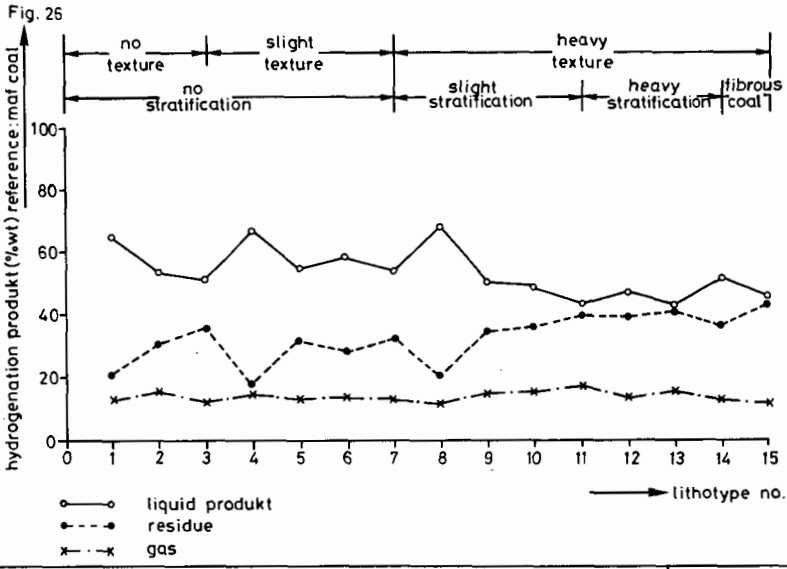

Produkt yields achieved through indirect hydrogenation with tetralin as a function of stratification and texture (lith. no.)

RHEINBRAUN

Fig. 27

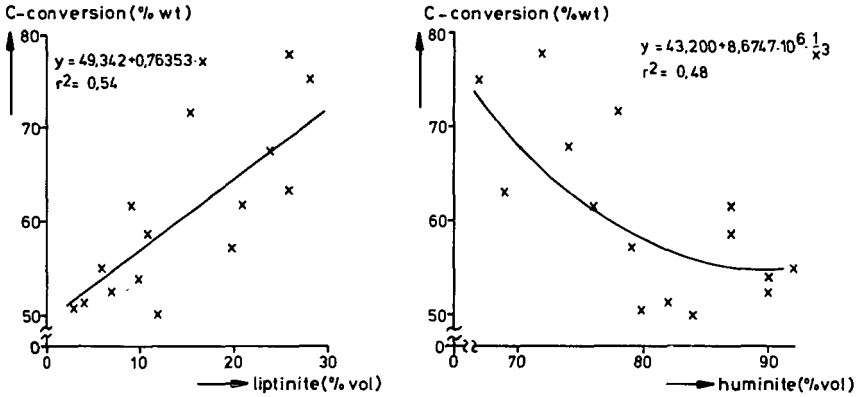

Carbon conversion achieved through indirect hydrogenation with tetralin as a function of the liptinite and huminite contents	RHEINBRAUN

Fig. 28

1. Petrographical properties

Liptinite content	>20 % vol
Lipto - Humodetrite content	>50 % vol
Humo - Detrinite content	>50 % vol
Inertinite content	< 3 % vol
Gelo - Humotelite content	< 6 % vol
Reflectance value	> 7 % vol

2. Chemical properties

Tar content	> 11 % wt (mf)
Paraffin content	> 7 % wt (maf)
Hydrogen content	> 5,3% wt (mf)
C/H ratio	< 1,1
Volatiles	> 53 % wt (maf)
Carbonization water	< 8,7% wt (mf)

Under the conditions stated above, the 5th and 6th seam of the Fortuna - Garsdorf mine contain approx. 78 %wt of good hydrogenation coals

Petrographical and chemical properties of good hydrogenation coals	RHEINBRAUN

SOME ASPECTS OF THE STRUCTURE AND REACTIONS OF NORTHERN GREAT PLAINS LIGNITES

W.R. Kube[1], H.H. Schobert[2], S.A. Benson[2], and F.R. Karner[2]

[1]Department of Chemical Engineering,
University of North Dakota, Grand Forks, North Dakota

[2]Grand Forks Energy Technology Center, USDOE, Grand Forks, North Dakota

The lignites of the Northern Great Plains are in the Fort Union Region, which contains the largest reserves of lignite of any coal basin in the world. The Fort Union Region encompasses areas of North Dakota, South Dakota, Montana, and Saskatchewan. The identified resources of lignite in this region amount to 422 Gt (465 billion short tons), of which 24 Gt (26 billion short tons) constitute the demonstrated reserve base (1).

Until about 1970, the utilization of lignite was limited, accounting for no more than 1-2% of the total annual U.S. coal production. In recent years the production of low-rank coals has increased dramatically, so that by 1980 production represented about 24% of the total national coal production. It has been estimated that in another ten years, low-rank coals could amount to half the total coal production (1).

It has long been recognized that lignites possess unusual properties which can have profound effects on utilization. Such properties include high moisture content, high quantities of oxygen functional groups in the carbon structure, an alkaline ash, and inorganic cations attached to carboxylic acid groups. The rapid expansion of lignite utilization in recent years has brought with it an increasing realization of the importance of developing a better understanding of the organic and inorganic structures in lignite and of how those structural features influence lignite reactivity or processing behavior. Here we present results from some current studies in progress in our laboratories on lignite structure and reactivity.

Comparison of Northern Great Plains Lignites with Bituminous Coals

The predominant position of bituminous coal in the total U.S. coal production has resulted, not unreasonably, in the properties of bituminous coals being more extensively studied and thus better known to the general coal research community than those of lignites.

The average proximate and ultimate analyses of Fort Union lignites are summarized in Table 1, together with average values for a Pittsburgh seam bituminous coal. The data in Table 1 were taken from references (2) and (3) for lignite and bituminous coal, respectively. The important points to note are the much higher moisture content, higher oxygen, and lower heating value of the lignite.

Usually, lignitic ash contains a much higher proportion of alkali and alkaline earth elements, and consequently lower proportions of acidic oxides such as silica and alumina, than does ash from bituminous coals. These differences are illustrated by the data in Table 2, as taken from reference (1). The data on spruce bark ash are taken from reference (4) and show the similarity of lignitic and woody ashes. Of interest are the contrasts between the lignite and bituminous averages first with regard to silica and alumina and, second, to lime, magnesia, and sodium oxide.

TABLE 1

AVERAGE ANALYSES OF NORTHERN GREAT PLAINS LIGNITE AND BITUMINOUS COAL SAMPLES, AS-RECEIVED BASIS

	Northern Great Plains Lignite	Pittsburgh Seam Bituminous
Proximate, %		
Moisture	37.2	2.3
Volatile Matter	26.3	36.5
Fixed Carbon	30.3	56.0
Ash	6.2	5.2
Ultimate, %		
Hydrogen	4.9	5.5
Carbon	71.9	78.4
Nitrogen	1.1	1.6
Oxygen	21.0	8.5
Sulfur	1.1	0.8
Heating Value, MJ/kg	15.9	32.6

TABLE 2

AVERAGE ASH COMPOSITIONS OF NORTHERN GREAT PLAINS LIGNITES AND BITUMINOUS COALS, SO_3 - FREE BASIS

	Spruce Bank	Lignite	Bituminous
Acidic Components:			
SiO_2	32.0	24.9	48.1
Al_2O_3	11.0	14.0	24.9
Fe_2O_3	6.4	11.5	14.9
TiO_2	0.8	0.5	1.1
P_2O_5	-	0.4	0.0
Basic Components:			
CaO	25.3	31.1	6.6
MgO	4.1	8.7	1.7
Na_2O	8.0	8.2	1.2
K_2O	2.4	0.5	1.5

Organic Structural Relationships

Lignite is an early stage in the coalification process and thus could be expected to retain some characteristics of wood. This relationship is illustrated by the electron micrographs shown as Figures 1 and 2. Pieces of plant debris, presumably twigs or rootlets, can be seen in Figure 1. Remains of the cellular structure are visible in Figure 2; the close similarity to the structure of softwood may be seen by comparing reference (5) for example.

On the molecular level, the distinguishing features of the organic structure of lignite are the lower aromaticity (or fraction of total carbon in aromatic structures), compared to bituminous coals; aromatic clusters containing only one or two rings; and the prevalence of oxygen-containing functional groups. A proposed structural representation, modified slightly from the original version (6), is given in Figure 3. We do not claim that this represents the structure of Northern Great Plains lignite, but rather use it as an illustration of major structural features.

The aromaticity has been studied by pressure differential scanning calorimetry (PDSC). The details of the experimental technique and of the methods for calculating aromaticity from a PDSC thermogram have been published elsewhere (7). Briefly, the PDSC experiment provides for controlled combustion of a 1-1.5 mg sample of -100 mesh coal in a 3.5 MPa atmosphere of oxygen. The sample is heated at 20°C/min in the range 150° to 600°C. The instrument response is a thermogram plotting heat flux, Δq, versus temperature, the integrated value thus being the heat of combustion. For most coals, and many organic compounds and polymers, the thermogram in this region consists of two peaks, which, from comparison to the behavior of model compounds, arise primarily from combustion of the aliphatic and aromatic portions of the sample. The aromaticity may be deduced from a comparison of peak heights.

The aromaticity for several samples of Northern Great Plains lignites, as measured on run-of-mine material, lies in the range of 0.61 to 0.66. For comparison, a sample of Australian brown coal available to us was found to have aromaticity of 0.56; a sample of Minnesota peat had an aromaticity of 0.50. Samples of vitrinite concentrates from the Northern Great Plains lignites were more aromatic, with values in the range of 0.72 to 0.74.

The temperature at which the maximum of the aromatic peak occurs has been shown to be a function of the extent of ring condensation (7), the maximum shifting to higher temperatures with increasing condensation. In support of the studies on coal structure, we have measured the PDSC behavior of over 30 organic compounds (most of which have been suggested as coal models or have been identified in the products of coal processing) and about 50 polymers. The maxima of the aromatic peaks in the thermograms of Northern Great Plains lignites generally fall into the same temperature range (375°-400°C) as those for compounds or polymers having benzene or naphthalene rings. One example is given in Figure 4, in which the PDSC thermograms of Gascoyne (N.D.) lignite and poly(4-methoxystyrene) are compared. We conclude that the aromatic ring systems therefore are mostly one- or two-ring systems.

Much less is known about the hydroaromatic structures or aliphatic bridges between ring systems. A methylene bridge is often suggested as a typical aliphatic bridging group, and was originally shown in the proposed structural representation (6). However, considerations based on thermochemical kinetics predict a half-life of 10^6 years for bond cleavage of diphenylmethane in tetralin at 400°C (8). Exhaustive analyses of the products from liquefaction of Northern Great Plains lignite at 400°C and higher in the presence of tetralin, (see (9) for example) have never identified diphenylmethane or related compounds. Absense of diphenylmethane constitutes strong circumstantial evidence for the relative unimportance of methylene linkages between aromatic clusters.

Oxygen is distributed among carboxylate, phenol, and ether functional groups. The carboxylate concentration has been measured by reaction of demineralized coal with calcium acetate following the precedure of van Krevelen and co-workers (10). A study of the carboxylate concentrations is still in progress; preliminary data for the Northern Great Plains lignites indicate carboxylate concentrations ranging from 1.75 to 1.93 meq/g on a dry basis. Concentrations of phenolic or ether functional groups have not yet been measured. Electron spectroscopy for chemical analysis (ESCA) provides a means for discriminating between carbon atoms incorporated in C=O and C-O structures by a Gaussian-Lorentzian decomposition of the carbon 1s spectrum (11). Figure 5 provides a comparison of the decomposed carbon 1s spectra of Beulah (N.D.) lignite and polyethylene terephthalate. At present, the ESCA data cannot be resolved into phenolic and etheric carbons. However, it can be shown that the ratio of carbon in carboxylate groups to that in (phenol plus ether) groups is about 0.62 (11). The presence of methoxy groups has been qualitatively confirmed; as-yet unpublished work by E.S. Olson and J.W. Diehl demonstrates the production of methanol from sodium periodate oxidation of Beulah lignite.

Little consideration has yet been given to the three-dimensional structure. A preliminary examination of lithotypes of Beulah lignite has been conducted by laser Raman spectroscopy (11). The lithotype having a higher concentration of carboxylic acid groups has a weaker band at 1600 cm^{-1}. If this band is assigned as a graphite mode (12), results suggest that the relatively bulky carboxylate groups, with their associated counterions, may disrupt, or preclude, three-dimensional ordering.

Distribution of Inorganic Constituents

In lignites the inorganic constituents are incorporated not only as discrete mineral phases, but also as relatively mobile ions, presumably associated with the carboxylic acid functional groups. The distribution of inorganic constituents has been studied principally by the chemical fractionation procedure developed by Miller and Given (13).

Extraction of the coal with 1M ammonium acetate removes those elements present on ion exchange sites, which are presumed to be carboxylic acid functional groups. Sodium and magnesium are incorporated almost exclusively as ion-exchangeable cations. For a suite of Northern Great Plains lignites tested, 84 to 100% of the sodium originally in the coal and 88 to 90% of the magnesium are removed by ammonium acetate extraction. Figure 6 is an electron micrograph showing an electron backscatter image due to the presence of sodium intimately associated with the organic material. Calcium is largely present in cationic form, 48 to 76% being extracted. Some potassium is also extracted in this step, in amounts ranging from 20 to 57%.

Further treatment with 1M hydrochloric acid then removes elements present as acid-soluble minerals or possibly as acid-decomposable coordination compounds. This acid extraction removes essentially all of the calcium and magnesium not removed by ammonium acetate. This finding is suggestive of the presence of calcite or dolomite minerals, which are known to be present in Northern Great Plains lignites (14). The hydrochloric acid extraction behavior of other major metallic elements is quite variable, which suggests significant differences in the mineralogy of the samples. Of those elements not extracted at all by ammonium acetate, some iron, aluminum, and titanium are removed by hydrochloric acid.

The portions of elements which are not removed by either reagent are considered to be incorporated in acid-insoluble minerals, particularly clays, pyrite, and quartz. This group includes all of the silicon, the remaining sodium and potassium, and the residual iron, aluminum and titanium. The acid-insoluble minerals are present as discrete phases. Frequently the mineral particles are quite small (see Figure 7, for example) and very highly dispersed through the carbonaceous material, to such

an extent that only about 15-30% of the discrete mineral matter is separable in a traditional float/sink experiment.

Effects of Structure on Reactivity

The small aromatic clusters, the high concentration of organic oxygen functional groups, and the presence of inorganic species as ion-exchangeable cations are unique features of low-rank coals. Each of these features should influence the reactivity of low-rank coals, thereby giving low-rank coals distinctly different reactions when compared to bituminous coals. The reactivity indeed has unique features. As yet, however, little has been done in a deliberate way to develop an understanding of the connections between structure and reactivity.

The carboxylic functional group is thermally labile and is driven off by heating to 450°C (15). Although the volatile matter content of lignite is higher than that of bituminous coals, much of the material released from lignite is carbon dioxide rather than hydrocarbon gases or tars. Thus only about 17% of the calorific yield occurs in volatile products from Northern Great Plains lignites at 500°C, compared with 30% for some bituminous coals (16). Since this thermal decomposition removes much of the oxygen from the coal, in a liquefaction reaction the removal of oxygen would require no net consumption of external hydrogen.

Oxygen functional groups can promote β-bond scission (8), which may be an important process in the degradation of the coal structure. The role of ether, carboxyl, and other groups in wood pyrolysis and combustion has been discussed (17); it seems reasonable to assume that analogous reactions would occur in low-rank coals. Other possible roles for oxygen functional groups include ether cleavage, cleavage of aliphatic bridges linked to aromatic rings bearing a phenolic group, and the enchancement of the ability of free radicals to form adducts with potential solvent or reactant molecules. The relationship of organic structure to reactivity should be a fertile field for research.

Sodium is the best-studied of the inorganic constituents of Northern Great Plains lignite. The combustion of the sodium carboxylates generates sodium-containing vapor species which can then be deposited on boiler tubes. The relationship of the sodium content of the coal to the formation of ash deposits on boiler tubes is well known. While the ash deposition problem can be severe and expensive for commercial installations (18), the mobility of cationic sodium holds out the promise for sodium removal or reduction by ion-exchange processes (19). The possible role of the ion-exchangeable sodium in the catalysis of liquefaction reactions has been studied by Given (20).

Acknowledgements

We thank Edwin Olson and John Diehl for the data on periodate oxidations, and George Montgomery for the ESCA spectrum. Thanks are due to several participants in Associated Western Universities' research participation programs, particularly David Kleesattel for separation of the lithotypes of Beulah lignite and for providing Figure 2, Kathleen Groon for the PDSC thermograms, and Paul Holm for chemical fractionation and carboxylate functional group data.

Literature Cited

1. Low-Rank Coal Study Volume 1 Executive Summary. U.S. Department of Energy Report DOE/FC/10066-T1 (Vol. 1), 1980.

2. Low-Rank Coal Study Volume 2 Resource Characterization. U.S. Department of Energy Report DOE/FC/10066-T1 (Vol. 2), 1980, p.40.

3. Banmeister, T. Standard Handbook for Mechanical Engineers, McGraw-Hill Book Co. Inc., New York, 1967, p. 7-4.

4. Tillman, D.A., Rossi, A.J., and Kitto, W.D. Wood Combustion, Academic Press, New York, 1981, p.42.

5. Went, F.W. The Plants, Time-Life Books, New York, 1963, p. 51.

6. Sondreal, E.A., Willson, W.G., Stenberg, V.I. Fuel, 1982, 61 925-38.

7. Benson, S.A., Schobert, H.H. In Technology and Use of Lignite, U.S. Department of Energy Report GFETC/1C-82/1, 1982, pp. 442-70.

8. Stein, S.E. In New Approaches in Coal Chemistry, American Chemical Society, Washington, 1981, p. 104.

9. Farnum, S.A., Farnum, B.W. Analytical Chemistry, 1982, 54 979-85.

10. Blom, L., Edelhausen, L., van Krevelen, D.W. Fuel, 1957, 36 135-53.

11. Schobert, H.H., Montgomery, G.G., Mitchell, M.J., Benson, S.A. Proc. 9th Int. Conf. Coal Sci. (In press, 1983).

12. Zerda, T.W., John, A., Chmura, K. Fuel, 1981, 60 375-8.

13. Miller, R.N., Given, P.H. In Ash Deposits and Corrosion Due to Impurities in Combustion Gases, Hemisphere Publishing Corp., Washington, 1977, pp. 39-50.

14. Schobert, H.H., Benson, S.A., Jones, M.L., Karner, F.R. Proc. 8th Int. Conf. Coal Sci., 1981, pp. 10-15.

15. Suuberg, E.M., Peter, W.A., Howard, J.B. Ind. Eng. Chem. Process Des. Devel. 1978, 17 37-46.

16. Goodman, J.B., Gomez, M., Parry, V.F., Landers, W.S. U.S. Bureau of Mines Bulletin 530, 1954.

17. Tillman, D.A., Rossi, A.J., Kitto, W.D. Wood Combustion, Academic Press, New York, 1981, Chapter 4.

18. Honea, F.I., Montgomery, G.G., Jones, M.L. In Technology and Use Of Lignite, U.S. Department of Energy Report GFETC/1C-82/1, 1982, pp. 504-45.

19. Paulson, L.E., Baria, D.N., Kube, W.R. In Technology and Use of Lignite, U.S. Department of Energy Report GFETC/1C-82/1, 1982, pp. 756-74.

20. Given, P.H., Cronauer, D.C., Spackman, W., Levell, H.L., Davis, A. and Biswas, B. Fuel 1975, 54 34-9.

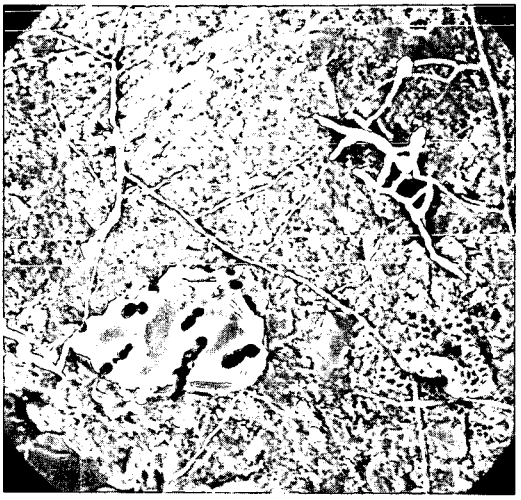

FIGURE 1. Electron micrograph of ion-etched Beulah lignite, showing rootlets or other plant debris. 7800x.

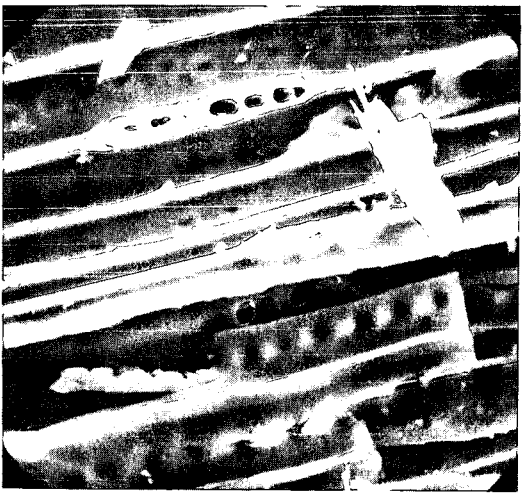

FIGURE 2. Electron micrograph of woody lithotype of Beulah lignite showing cellular structure. 390x. Compare softwood structure in reference (5).

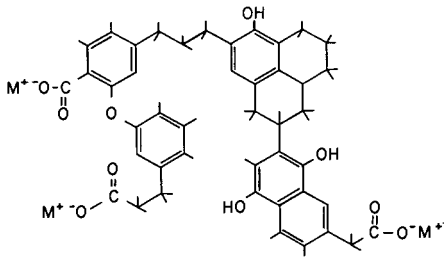

FIGURE 3. Proposed representation of structural features of lignite. Adapted with minor modification from reference (6).

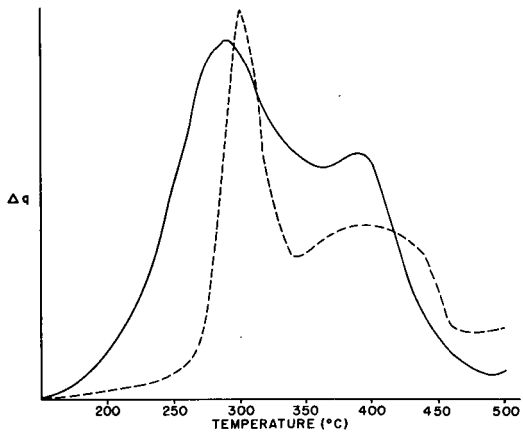

FIGURE 4. PDSC thermograms of Gascoyne lignite (solid line) and poly(4-methoxystyrene) (dashed line). Plot is of heat flux in arbitrary units versus temperature, °C.

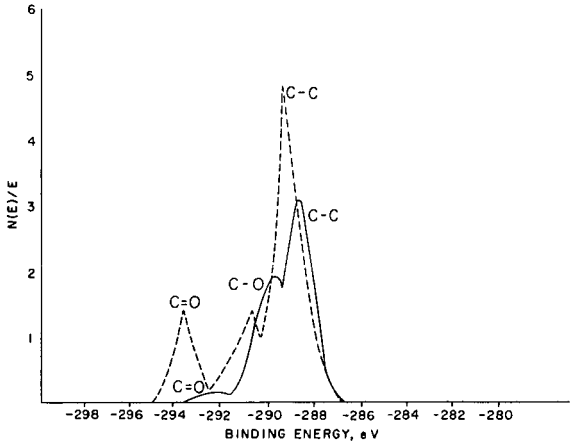

FIGURE 5. Decomposed ESCA carbon 1s spectra of Beulah lignite (solid line) and polyethylene terephthalate (dashed line). Plot is of number of electrons per energy in arbitrary units versus binding energy in electron volts. The lignite spectrum has been corrected for sample charging (11).

FIGURE 6. Electron micrograph of Beulah lignite showing organic region enriched in sodium (circular structure in lower center of view).

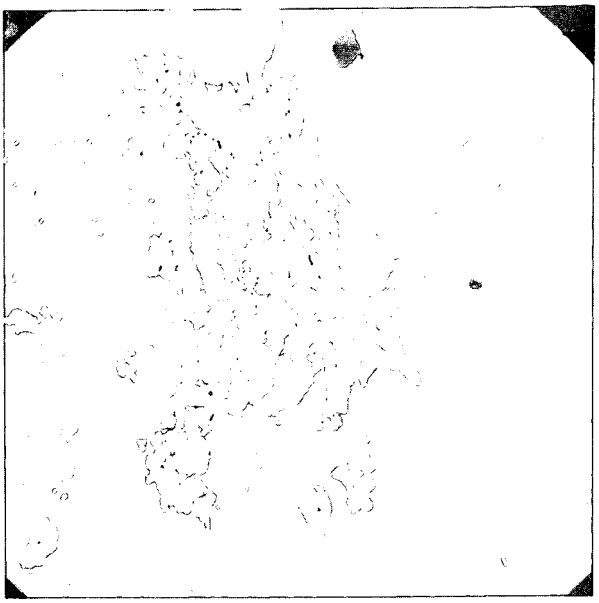

FIGURE 7. Electron micrograph of pyrite particles intergrown in carbonaceous structure of Beulah lignite, suggesting difficulty of removal by float/sink. 200x.

STRUCTURE AND REACTIVITY OF TEXAS LIGNITE

C. V. Philip, R. G. Anthony and Zhi-Dong Cui
Kinetic, Catalysis and Reaction Engineering Laboratory
Texas A&M University
College Station, Texas 77843

INTRODUCTION

The conversion of low rank coals such as lignites into gaseous and liquid fuels and chemical feed stocks received considerable attention in the last decade.[1-3] Data for liquefaction and gasification of various lignites have been reported.[1,3-16] Although extensive analytical data are available on lignite conversion product, their use to monitor chemical reactions involved in any liquefacation or gasification process is limited due to the enormous amount of time and effort required for the complete characterization of Lignite conversion products.[17-21] In the case of most of the reports on liquefaction experiments, the data are usually limited to total conversion, amount of certain fractions as oils, asphaltenes, preasphaltenes, tetrahydrofuran solubles, and certain physical characteristics.[17] This study involves one lignite sample from a Texas mine and its conversion products from mini reactor experiments using varying liquefaction conditions. The gaseous products are analyzed by gas chromatography (GC)[14] and the THF solubles are characterized by gel permeation chromatography (GPC)[8-15] and high resolution gas chromatography (HRGC).

EXPERIMENTAL

Lignite samples were collected fresh from the mine near Carlos, Texas and stored under distilled water prior to use. The Lignite was ground to less than 20 mesh size and stored in a closed jar which was kept in the refrigerator. The lignite liquefaction experiments were conducted in four 6.3 ml mini reactors which were heated in a fluidized sand bath. The reactors were fabricated using 'Autoclave' fittings. Each reactor was the same, but only one reactor was fitted with a pressure transducer. The absence of pressure gauges on the other three reactors allowed the minimization of the dead volume outside the sand bath. In most cases 1.5 gm lignite, 1ml solvent (decalin or tetralin) and a gas (nitrogen or hydrogen or 1:1 CO/H_2 mixture at 1000 psi) were charges to the reactor. The reactions were quenched by dipping the reactors in cold water. The gases from the reactors were analyzed using an automated multicolumn gas chromatograph equipped with sample injection and column switching valves.[4] The contents of the reactors were extracted with tetrahydrofuran (THF) by using an ultrasonic bath. The THF extract (about 15 ml) was filtered through a 1 micron micro-pore filter (Millipore) and separated into fractions by using a gel permeation chromatograph (GPC).[15]

The GPC fractions were obtained with a Waters Associate Model ALC/GPC 202 liquid chromatograph equipped with a refractometer (Model R401). A Valvco value injector was used to load about 100μ l samples into the column. A 5 micron size 100 Å PL gel column (7.5 mm ID, 600 mm long) was used. Reagent grade THF, which was refluxed and distilled with sodium wire in a nitrogen atmosphere, was used as the GPC carrier solvent. A flow rate of 1 ml per

minute was used. THF was stored under dry nitrogen, and all separations were conducted in a nitrogen atmosphere to prevent the formation of peroxides.

Straight chain alkanes from Applied Science, aromatics from Fisher Scientific Company and polystyrene standards from Waters Associate were used without purification for the linear molecular size calibration of the GPC. Since the solubility of the larger alkanes in THF is very low, approximately 0.2-1 mg of each standard was dissolved in 100 μl of THF for the molecular size calibrations. The fractions of the lignite derived liquid separated by GPC were analyzed by a gas chromatographic system (VISTA 44, Varian Associates) equipped with a 15 M long and 32 mm ID bonded phase fused silica capillary column and flame ionization detector.

RESULTS AND DISCUSSIONS

The lignite samples from Carlos, Texas have heating valves of 4000 to 6000 BTU/lb on an as received basis or about 12000 BTU/lb on dry mineral matter free (dmmf) basis. The samples may contain as much as 40% moisture which escapes from lignite even while stored in the refrigerator (water condenses on the walls of the container). The oxygen content varied from 20 to 30 % and has about 1 to 1.5 % sulfur on a dmmf basis. As much as 50% of the oxygen may exist as carboxylic groups which may produce carbon dioxide at the liquefaction conditions.[5] The substantial amount of hydrogen sulfide that was usually liberated, decreased rapidly as a function of sample ageing and storage conditions. The lignite seams are soaked with water under hydrostatic pressure in a virtualy anaerobic condition. Immediately after mining, the lignite samples continuously loose moisture and are oxidized by air. There is no ideal way the lignite samples can be stored to preserve its on seam characteristics.

The lignite liquefaction conditions are listed in Table 1. The composition of gaseous products are listed in Table 2. The data in Table 2 illustrate that the composition of gaseous products are unaffected by reaction conditions such as reactor pressure, feed gas or the solvent system (whether hydrogen donating or not). Higher temperatures favor the production of hydrocarbons. Apparently the fragile species produced by the pyrolytic cleavages of bonds in the coal structure are converted to stabler species which form the components of lignite derives gases without consuming hydrogen from the gaseous phase or from the hydrogen donor solvents. The species which require hydrogen for stabilization are abstracting hydrogen from carbon atoms in the vicinity. It is quite possible that the bond breaking and hydrogen abstraction are simultaneous and hydrogen from the donor solvent or the gaseous phase may not reach the reaction site in time to hydrogenate the fragile species.

To illustrate the gaseous hydrocarbon production from lignite, experiments were conducted using butylatedhydroxytoluene (BHT), a widely used antioxident and food preservative, aa a model compound (see Table 1 & 2). BHT decomposed to products including isobutylene and isobutane in an approximate 1:1 molar ratio in the absence of hydrogen from hydrogen donor solvent or gaseous phase. Addition of tetralin favored the production of isobutane over isobutylene. It appears that coal lignite can give some hydrogen to the isobutane formation but tetralin can readily reach the reaction vicinity in time for the hydrogen transfer reaction.

The elution pattern of the GPC using 5 micron 100 Å PL gel column is illustrated in Figure 1 where the GPC separation of a standard mixture containing straight chain alkanes and aromatics is shown. The polystyrene standard (mol. wt. 2350 and chain length 57 Å) gave a broad peak at 11 ml retention volume. The peak position is marked in the figure rather than using polystyrene standard in the mixture in order to save the $nC_{44}H_{80}$ peak from the enveloping effect of the broad polystyrene peak. The retention volume of several aliphatic phenolic, hetrocyclic, amine and aromatic compounds in THF and toluene have been reported elsewhere.[9] It is clear that aromatic compounds, as expected from their valence bond structures, have smaller linear molecular sizes compared to n-alkanes of similar molecular weight.[15] It is expected that most of the condensed ring aromatics such as naphthlene, anthracene and even big ones like coronene (seven fuzed rings with molecular weight of 300.4) are smaller than n-hexane and hence have retention volumes larger than that of n-hexane. The polystyrene standard with a 57 Å appears to be larger than expected from the alkane standard. The large number of phenyl groups on the main polyethelyene chain (57 Å) make the molecule into a large cylindrical structure with large steric hinderance for penetrating the pores of the gel. The two terminal phenyl groups also contribute to an increased chain length. The polystryrene peak (57 Å) is very close to the total exclusion limit of the 100 Å PL gel column.

The THF solubles of lignite liquefaction products were separated by GPC on the basis of effective linear molecule sizes in solution.[15] Although GPC can be used for molecular weight or molecular volume separation of homologous series such as polymers, such separations of complex mixtures like coal liquid is not feasible. The only molecular parameter which has the least variation from a calculated value is effective linear molecular size in solution. Lignite derived liquids are separated on the basis of effective molecular length which is expressed in carbon numbers of straight chain alkanes. The GPC fraction with species larger than $nC_{44}H_{80}$ is in fraction 1 which is composed of nonvolatile species. Fraction 2 has molecular sizes in the range of nC_{14} to nC_{44} and composed of volatile species mostly alkanes and nonvolatile species generally known as asphaltenes. Fraction 3 is composed of alkylated phenols such as cresols, alkyl indanols and alkyl naphthols as well as, some small amount of nonvolatiles namely low molecular weight asphaltenes. Fraction 4 is composed of species with molecular size less than that of $n\text{-}C_7H_{16}$. This fraction may not contain any straight chain alkanes as they are very volatile. It is composed of aromatic species such as alkylated benzenes, alkylated indans and naphthalene and even large species such as pyrenes and coronenes. The solvent system used for liquefaction (tetralin and decalin) separate from the bulk of the lignite derived products as the last peak (peak at 20.5 ml). Although the column is overloaded with respect to the solvent system, the efficiency of separation of the lignite derived products are unaffected. The volatile species of all fractions can be identified by GC-MS[15] and nonvolatiles by the IR and NMR spectroscopy.[12,13,17]

The effect of hydrogen donor solvent and feed gasea such as hydrogen and CO/H_2 mixture on lignite dissolution at 700°F is shown in Figure 2. Decalin dissolves less coal compared to tetralin. CO/H_2 as feed gas gave less liquid products which contained more larger molecular size species. When decalin with nitrogen (not shown in Figure 2) was used for liquefaction of lignite the

species appearing at total size exclussion limit of 100 Å gel column were totally absent. Figure 3 shows GCs of fraction 2s of two lignite derived liquids to illustrate the role of the hydrogen donor solvent on alkane production. If the alkanes are formed by breaking of alkyl chains from other groups, they are expected to contain more olefinic species in the absence of hydrogen donor solvents such as tetralin. Since the species in figure 4 a and b are very similar, the role hydrogen or hydrogen donor solvent plays in the production of alkanes are limited. Simple pyrolysis can liberate them from the coal matrix. The alkane may be existing as free while trapped inside the pores or their precursers are either carboxylic acids or species which decompose during heating to produce alkanes easily.

Figure 4 illustrates the effect of reaction time on liquefaction. Figures 5 and 6 show the liquefaction of lignite at 750°F and 800°F using different feed gases. Hydrogen tends to give more phenols and aromatics compared to nitrogen. CO/H_2 tends to produce higher molecular size species at the expense of phenols and aromatics. A qualitative estimation of the solvent systems can be obtained estimating the width of the solvent peak, and the area of the rest of the GPC may give the dissolved product from lignite. The use of CO/H_2 did not increase the total liquefaction yield while it has decreased the total yield of liquid products. The experiments using CO/H_2 gave liquid product which are difficult to filter through micro pore filters compare to the products obtained from experiments using either nitrogen or hydrogen as the feed gas. It could be assumed that CO/H_2 will give a product which contained more large size asphaltenes.

Based on our data on lignite liquefaction products and various coal liquids and their distillates, we proposed a structure for coal[7] as shown in figure 7. The major structural constituents of coal are derived from three sources namely cellulose, lignin and other plant components dispersed in the plant tissues. The first two are polymers. The coalification process which is mostly a deoxygenation process, might not create a sufficiently large number of tertiary bonds needed for binding various constituents of coal together to a strong three dimentional structure. The coals including lignite may have loose structures. The cellulose derived structures may have large pores in which species such as large alkanes could be trapped. Although low temperature (less than 300°F) extractions can extract some soluble components of coal, the alkanes are not liberated[5] except as smsll amount of carboxylic acids. The low temperature oxidation studies do not detect large alkanes. The higher temperatures (above 650°F) can either break the pore structures or the alkanes can distill out of the pores.

ACKNOWLEDGEMENTS

The financial support of The Texas Engineering Experiment Station, The Texas A&M University Center for Energy and Mineral Resources, is very much appreciated. The lignite was supplied by TMPA, Carlos, Texas.

REFERENCES

1. Sondreal, E. A., Wilson, W. G. and Sternberg, V. I. Fuel 1982 61, 925.

2. Proceedings of Low-Rank Coal Technology Development Workshop, San Antonio, Texas June 17-18, 1981.

3. Proceedings of the Basic Coal Science Workshop Houston, Texas, Dec. 8-9, 1981.

4. Philip, C. V., Bullin, J. A. and Anthony, R. G., J. Chromatogr. Sci., 1979, 17, 523.

5. Philip, C. V., and Anthony, R. G., Fuel Processing Technology, 1980.

6. Philip, C. V., and Anthony, R. G., Proceedings Coal Technology - 78, 2, 710.

7. Philip, C. V., and Anthony, R. G., Preprints ACS Org. Coat & Polym. Div., 20 August (1980).

8. Zingaro, R. A., Philip, C. V., Anthony, R. G., and Vindiola, A., Fuel Processing Technology (1981) 4, 169.

9. Philip, C. V. and Anthony, R. G., Am. Chem. Soc. Div. Fuel Chem. Preprints 1979, 24(3), 204.

10. Philip, C. V., Zingaro, R. A. and Anthony, R. G., Am. Chem. Soc. Fuel Chem. Preprints 1980, 25(1), 47.

11. Philip, C. V., Zingaro, R. A. and Anthony, R. G., "Upgrading of Coal Liquids" (Ed. R. F. Sullivan) Am. Chem. Soc. Symp. Ser., 1981, 156, 239.

12. Philip, C. V. and Anthony, R. G., Am. Chem. Soc. Div. Fuel Chem. Preprints 1977, 22(5) 31.

13. Philip, C. V. and Anthony, R. G., "Organic Chemistry of Coal," Am. Chem. Soc. 1978, p. 258.

14. Philip, C. V. and Anthony R. G., Fuel 1982, 61, 351.

15. Philip, C. V. and Anthony, R. G., Fuel 1982, 61 357.

16. Farnum, S. A., Olson, E. S., Farnum, B. W., Wilson, W. G., Am. Chem. Soc. Div. Fuel Chem. Preprints 1980 25 245.

17. Aczel, T., Williams, R. B., Pancirov, R. J. and Karchmer, J. H., "Chemical Properties of Synthoil Products and Feeds", Report prepared for US Enegry Research and Development Administration, FE8007, 1976.

18. Baltisberger, R. J., Klabunde, K. J., Sternberg, V. I., Woolsey, N. F., Saito, K. and Sukalski, W., Am. Chem. Soc. Div. Fuel Chem. Preprints 1977, 22(5), 84.

19. White, C. M., Sulz, J. L. and Sharkey, Jr. A. C., Nature 1970, 268, 620.

20. Pugmire, R. J., Grant, D. M., Zilm, K. W., Anderson, L. L., Oblad, A. G. and Wood, R. E. Fuel 1878, 57(4).

21. Seshadri, K. S., Albangh, E. W. and Bacha, J. D., Fuel 1982, 61, 336.

Table 1. Lignite Liquefaction Conditions

Run No.	Coal g.	Solvent 1 ml	Feed Gas	Initial Pressure (pai)	Temp °F	Time min.	Comments
1	1.5	tetralin	N_2	1000	700	30	+ BHT 0.2 g
2	1.5	tetralin	N_2	1000	700	120	+ BHT 0.2 g
3	1.5	tetralin	N_2	1000	700	120	
4	1.5	decalin	N_2	1000	700	120	+ BHT 0.2 g
11	1.5	tetralin	$CO+H_2$(1:1)	1000	700	120	
12	1.5	tetralin	N_2	1000	700	120	
13	1.5	decalin	N_2	1000	700	120	
14	1.5 (old)	tetralin	N_2	1000	700	120	
21	1.5	tetralin	N_2	1000	700	120	
22	1.5	tetralin	no	0	700	120	+ BHT 1 g
23	1.5	no	no	0	700	120	
24	1.5 (old)	tetralin	N_2	1000	700	120	
31	1.5	tetralin	H_2	1000	700	120	
32	1.5	tetralin	$CO+H_2$(1:1)	1000	700	120	
33	1.5	decalin	H_2	1000	700	120	
34	1.5	decalin	$CO+H_2$	1000	700	120	
41	1.5	tetralin	N_2	1000	700	15	
42	1.5	tetralin	N_2	1000	700	120	
43	1.5	tetralin	N_2	1000	700	360	
51	1.5	tetralin	N_2	1000	850	30	
52	1.5	tetralin	H_2	1000	850	30	
53	1.5	tetralin	$CO+H_2$(1:1)	1000	850	30	
61	1.5	tetralin	N_2	1000	800	30	
62	1.5	tetralin	H_2	1000	800	30	
63	1.5	tetralin	$CO+H_2$(1:1)	1000	800	30	
71	1.5	tetralin	N_2	1000	750	30	
72	1.5	tetralin	H_2	1000	750	30	
73	1.5	tetralin	$CO+H_2$	1000	750	30	

TABLE II Composition of Product Gas %

Run No.	H_2	CO_2	CO	H_2S	CH_4	C_2^o	$C_2^=$	C_3^o	$C_3^=$	n-C_4	i-C_4	i-$C_4^=$
1	13.0	11.2	26.1	-	8.4	1.3	1.9	0.8	0.15	0.07	12.6	24.1
2	2.1	61.5	3.6	-	9.2	2.8	2.8	1.8	0.28	0.19	11.9	5.9
3	0.9	80.0	0.9	-	11.8	3.7	7.3	1.2	0.13	0.17	0.1	0.03
4	0.3	61.9	2.1	-	8.6	2.0	1.5	1.0	0.10	0.07	8.7	13.2
11	3.2	60.4	2.5	22.4	6.8	2.6	0.2	1.0	0.12	0.14	0.1	0.01
12	3.7	70.5	2.8	10.5	7.9	2.6	0.3	1.0	0.14	0.15	0.1	0.1
13	0.5	75.9	3.8	7.8	8.4	2.2	0.6	0.6	0.10	0.06	0.04	0.02
14	2.3	78.2	2.9	1.1	9.7	3.4	1.2	1.1	0.10	0.13	0.1	0
21	1.1	80.7	1.5	-	9.5	2.6	0.3	1.5	0.15	0.16	1.8	0.8
22	5.2	51.2	3.4	-	28.1	3.6	0.04	3.2	0.01	0.06	3.9	0.9
23	-	76.5	3.6	-	11.4	3.9	0.2	2.0	0.31	0.41	0.2	0.1
24	0.8	83.7	1.6	-	8.3	3.1	0.3	1.2	0.18	0.17	0.1	0.03
31	0.7	71.3	2.7	13.1	7.3	2.6	0.7	0.9	0.12	0.18	0.2	0.2
32	0.7	70.1	1.9	12.7	5.3	1.8	0.4	0.6	0.10	0.09	0.1	0.1
33	0.7	75.5	2.1	11.3	7.3	1.9	0.1	0.7	0.12	0.07	0.1	0.03
34	0.8	63.0	2.4	-	19.1	4.2	1.1	2.2	1.64	0.90	1.3	1.1
41	-	80.8	2.1	11.5	3.9	0.8	0.3	0.2	0.09	0.03	0.03	0.03
42	1.0	74.3	1.5	10.2	7.5	3.2	0.8	1.1	0.13	0.15	0.1	0.02
43	5.6	41.2	1.3	37.1	9.2	3.7	0.1	1.4	0.11	-	0.1	0.01
51	8.8	44.7	4.7	8.8	21.0	5.5	0.4	2.2	0.26	0.44	0.2	-
52	8.1	46.6	5.3	7.6	23.2	6.6	0.4	1.7	0.23	0.17	0.1	0.02
53	9.9	47.5	5.4	9.9	19.0	5.5	0.1	1.8	0.24	0.29	0.2	-
61	1.7	65.8	6.0	9.4	11.1	4.3	1.2	0.1	0.23	0.21	0.1	0.03
62	1.6	65.8	6.0	8.8	11.8	3.9	0.6	1.0	0.16	0.11	0.1	0.02
63	1.6	66.1	5.9	10.4	11.5	3.2	0.1	0.9	0.14	0.09	0.1	0.02
71	0.7	78.4	3.7	4.9	8.3	2.4	0.4	0.7	0.14	0.11	0.1	0.03
72	0.7	76.9	2.4	6.6	9.2	2.9	0.1	0.8	0.14	0.10	0.1	0.02
73	0.7	75.2	2.9	8.7	8.0	2.8	0.5	0.8	0.16	0.10	0.1	0.02

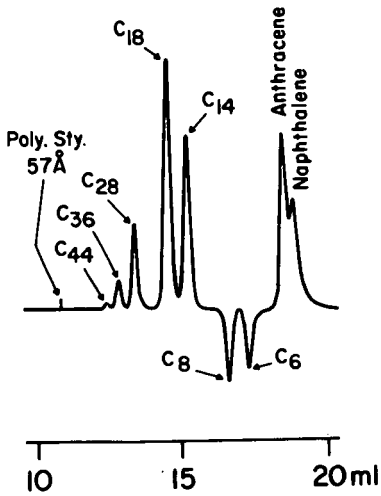

Figure 1. GPC of calibration mixture

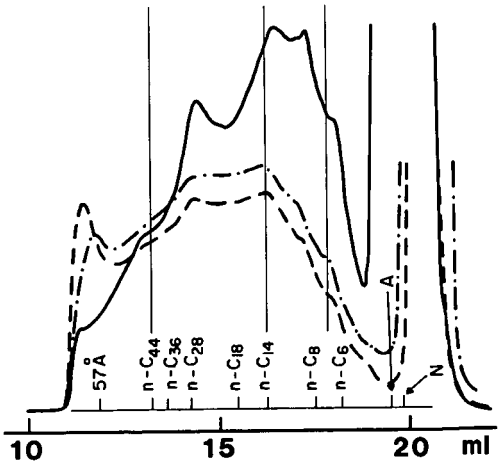

Figure 2. GPC of THF solubles of lignite from reactions at 700F in —— decalin and H_2 (33), --- tetralin and H_2 (31) -.- tetralin and CO/H_2 (32)

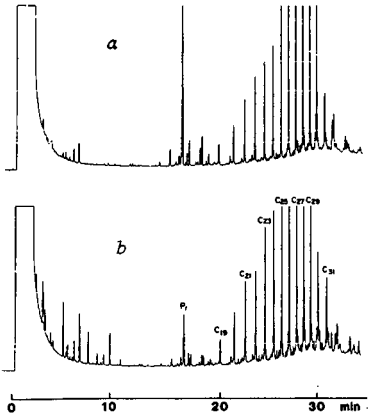

Figure 3. GC of alkane fractions from THF solubles of lignite a. tetralin and H_2 (21) b. Decalin and N_2 (13)

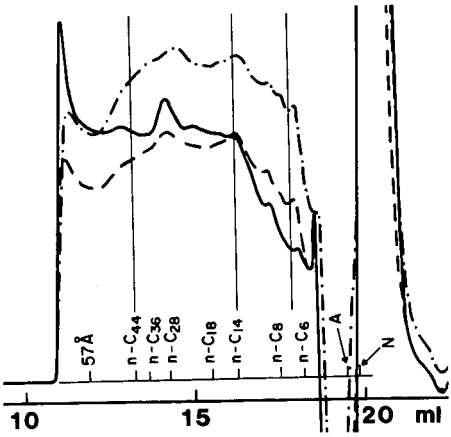

Figure 4. Effect of reaction time on THF solubles of lignite in tetralin and H_2 at 700F. —— 15 min. (41), --- 120 min. (42), -.- 360 min. (43)

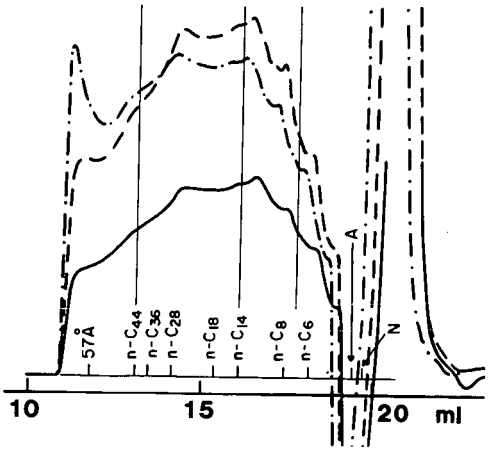

Figure 5. Effect of feed gas on lignite liquefaction in tetralin at 750 F —— N_2 (71), --- H_2 (72) -.- CO/H_2 (73)

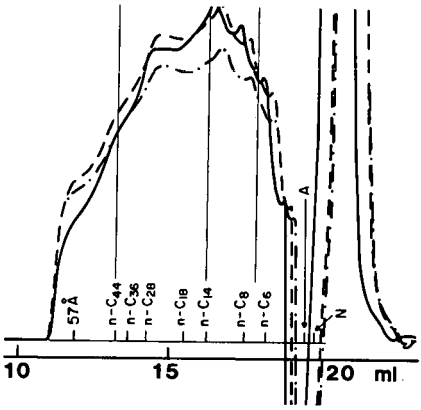

Figure 6. Effect of feed gas on lignite liquefaction in tetralin at 800 F. —— N_2 (61), --- H_2 (62), -.- CO/H_2 (63)

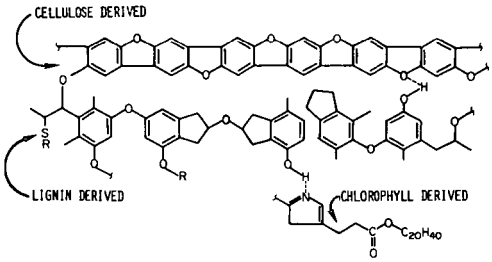

Figure 7. A structural model of coal

SOME SMALL-ANGLE X-RAY SCATTERING TECHNIQUES FOR STUDYING THE SUBMICROSCOPIC STRUCTURE OF COALS AND COAL-DERIVED LIQUIDS

Paul W. Schmidt, Chul Y. Kwak, and Mohanan Kalliat

Physics Department, University of Missouri, Columbia, MO 65211

Small-angle x-ray scattering is often useful for investigating submicroscopic structures--that is, structures with dimensions between about 20 and 2000 Å (1). This technique has been employed in several studies of the porosity and other submicroscopic structure of coals (2--7).

In this review, we will summarize the results we obtained in Reference (7), and we will discuss briefly some of our more recent scattering studies of coal porosity (8). We also will illustrate how scattering techniques can provide useful information about the properties of coal-derived liquids aged under oxygen for periods up to 8 weeks (9).

First, however, we will review some of the methods and techniques which we employed in our interpretation of the small-angle x-ray scattering data from coals. Figure 1 is a schematic drawing of a small-angle x-ray scattering system. X-rays from the tube T are formed into a beam by slits and fall on the sample S. A small fraction of the x-rays striking the sample are re-emitted, without change of wavelength, in directions different from that of the incoming beam. The intensity of these re-emitted x-rays, which are called the scattered rays, and their dependence on the direction in which they are emitted depend on the structure of the sample. In a scattering experiment, the intensity of the x-rays scattered in different directions is measured, and from an analysis of these data, an attempt is made to obtain information about the structure of the sample producing the scattering. Figure 1 shows a ray scattered at an angle θ with respect to the incoming beam. The scattered radiation is recorded by the detector C.

While no universal prescription can be given for analyzing the scattering pattern from an arbitrary sample, we will review some general principles useful for interpretation of scattering measurements. For a sample which has a structure characterized by a dimension a, most information obtainable from scattering measurements will be found at scattering angles θ in an interval for which

$$0.1 \leq ha \leq 10, \qquad (1)$$

where $h = (4\pi/\lambda)\sin(\theta/2)$; and λ is the x-ray wavelength. For angles no greater than about 7 degrees, $\sin\theta/2$ can be approximated by $\theta/2$, and so for small scattering angles, h can be considered proportional to θ. According to (1), for a structure with dimension a, the scattering is determined by the product ha, so that there is an inverse relationship between the size of the structure and the h values at which the scattered intensity from this structure is appreciable. Since the x-ray wavelengths are normally of the order of 1 or 2 Å and thus are of the same magnitude as the interatomic spacing in solids and liquids, Inequality (1) states that the x-ray scattering from structures with dimensions between about 20 and 2000 Å will be observed at scattering angles no greater than a few degrees. Small-angle x-ray scattering thus can be used to study these submicroscopic structures.

X-rays are scattered by electrons, and the small-angle scattering will be appreciable when the sample contains regions in which fluctuations or variations in electron density extend over distances of 20 to 2000 Å. At small angles, the scattering process is unable to resolve structures smaller than about 10 Å, and so in the analysis of the scattering data, the atomic-scale structure can be

neglected. For many scattering studies, it is therefore convenient to consider the sample to be composed of two phases, with constant but different electron densities.

If this two-phase approximation holds and the two phases always are separated by a sharp, discontinuous boundary, when the minimum characteristic dimension a_m of the structure satisifies the condition $ha_m > 3.5$, the scattered intensity I(h) can be approximated by (7)

$$I(h) = \frac{2\pi\rho^2(S/M)}{h^4} \frac{M}{A} I_e A, \qquad (2)$$

where ρ is the difference of the electron densities of the two phases, I_e is the intensity scattered by a single electron; S is the total surface area separating the two phases in the sample; M is the mass of the sample; and A is the cross-sectional area of the sample perpendicular to the incident beam. In the outer part of the small-angle scattering curve--that is, when $ha_m > 3.5$, the scattered intensity is proportional to h^{-4} and thus to the inverse fourth power of the scattering angle. Moreover, when I(h) has this angular dependence, the magnitude of the scattered intensity is proportional to the specific surface S/M, which is the surface area per unit sample mass separating the two phases.

As we explain in Reference (7), the quantities I_eA and M/A can be evaluated from the x-ray data, and so Equation (2) can be employed to calculate the specific surface S/M from the scattering data for samples with submicroscopic porosity.

We have made use of this technique to determine the specific surfaces of a number of PSOC coals. As our x-ray studies showed (7) that the almost all of the small-angle x-ray scattering was due to pores and that the scattering from the mineral matter in the coal was almost negligible, we have interpreted the small-angle x-ray scattering from coals as being due to submicroscopic pores, which are filled with air and for scattering purposes thus are essentially empty.

Our scattering studies show (7) that the rank of the coal is the main factor which determines the form of the angular dependence of the scattered intensity. The scattering curves for the coals which we studied can be grouped in four classes, as Figure 2 illustrates. Since both axes of Figure 2 are logarithmic, the curves in Figure 2 are straight lines with slopes -4 when Equation (2) describes the scattering. An angular dependence of this form is obtained for all types of coals at the smallest angles at which data could be recorded--that is, for scattering angles smaller than about 0.005 radian. For Pennsylvania Buck Mountain anthracite coal (PSOC 81, triangles), this inverse-fourth power continues to scattering angles as large as about 0.015 radian, and then the intensity decreases less rapidly with increasing scattering angle. Of all coals shown in Fig. 2, the scattering in the outer part of the plot is most intense for the anthracites. We interpret (8) this result as being due to the presence of a relatively large number of micropores, with average dimensions smaller than about 30 Å. As we have obtained similar curves for other anthracites, we have concluded that in these high-rank coals, there is a large fraction of micropores and an appreciable number of macropores, which have dimensions of 1000 Å or more. In a low-rank coal like Washington Queen #4 (PSOC 95, circles), there also are macropores, but since in the outer part of Fig 1 the intensity is lower than for the anthracite, we conclude that the anthracites have a larger fraction of micropores. Lignites gave scattering curves similar to the curve for PSOC 95. In the scattering curves for low volatile bituminous coals like Pennsylvania E. Kittaning coal (PSOC 127, plus signs), there is a maximum near 0.080 radians. This maximum has been ascribed (10) to interactions between the fundamental scattering units in these coals, which are planar aggregates of aromatic rings. In the fourth type of curve in Fig. 2, which we obtained for Illinois No. 6 coal (PSOC 22, squares) and for many other but not all low and medium-rank bituminous

coals, there is a shoulder on the scattering curve at intermediate scattering angles. On both sides of the shoulder or inflection, the intensity is proportional to the inverse fourth power of θ. (The shoulder on the curve in Fig. 3 occurs at such small angles that in this curve the inner region where the intensity is proportional to the inverse fourth power of θ is barely visible.) As we explain in Reference 7, we consider this shoulder to be the result of the fact that in these coals, there is a relatively high fraction of transitional pores, with average dimensions of the order of 50 to 200 Å. We calculated a specific surface from each part of the scattering curve which was proportional to the inverse fourth power of θ. These two surfaces are the specific surfaces of the macropores and the transitional pores. We have found that the presence of an inflection in the scattering curve is an indication that the coal has a relatively large number of transitional pores.

At the time we wrote the manuscript for Reference (7), we were unable to relate this high fraction of transitional pores to any other property of the coals. We have now found (8) that there are inflections only in coals with fixed carbon contents in the interval from about 72% through 83% per cent (dry, mineral-matter free). These results are summarized in Figure 3, which is a preliminary plot of the sum of the specific surfaces of the macropores and transitional pores as a function of carbon content.

The ability to distinguish between the specific surfaces associated with the macropores and the transitional pores is, we feel, a unique property of small-angle x-ray scattering.

By making some reasonable assumptions, we have also been able to estimate the specific surfaces and dimensions of the micropores in many coals (8).

The value of the specific surface obtained in studies of porous materials often depends on the techniques used for the measurement. For example, Gan, Nandi, and Walker (11), in their adsorption studies of a number of PSOC coals, obtained much larger specific surfaces by carbon dioxide adsoprtion at room temperature than by low-temperature adsorption of nitrogen. As we mentioned in Reference (7), the difference may be the result of the fact that carbon dioxide at room temperature can penetrate smaller pores than can be entered by nitrogen molecules at low temperature (12). As can be seen by comparison of the magnitudes of the specific surfaces in Figure 3 with the nitrogen specific surfaces in Figure 1 of Reference (11), the x-ray specific surfaces are much nearer to those measured by low temperature nitrogen adsorption than by room temperature carbon dioxide adsorption. As the micropores are too small to satisfy the conditions necessary to give a scattered intensity proportional to the inverse fourth power of the scattering angle, the "x-ray specific surface" includes only contributions from the macropores and transitional pores and does not take account of the specific surface of the micropores.

With reasonable assumtions, the dimensions and the specific surface of the micropores in anthracites and, at times, other coals can be estimated from the small-angle scattering data.

We have recently completed a small-angle x-ray scattering study of some coal-derived liquids prepared from West Virginia Ireland Mine coal in the U. S. Department of Energy Pittsburgh Energy Technology Center 400 lb/day Bruceton Liquefaction Unit and aged under oxygen for different lengths of time (9). To analyze the scattering data, we used the radius of gyration approximation, according to which, for independently-scattering, randomly-oriented particles (Ref. 1, pp. 24-28),

$$I(h) = I(0)\, e^{-(h^2R^2/3)}, \qquad (3)$$

where I(0) is the zero-angle scattered intensity, and R, the radius of gyration, is a characteristic dimension of the particle. According to Equation (3), which approximates the scattering when hR is not large with respect to 1, a plot of the logarithm of the scattered intensity as a function of the square of the scattering angle should be a straight line, from the slope of which the radius of gyration can be calculated. In Fig. 4, the radius of gyration plots, which are at least approximately linear, show that the radii of gyration of the coal-derived liquids, and thus the average size of the particles, at first grows slowly, but after the sample is aged for more the 4 weeks, there is a sharp rise in the radius of gyration. This increase in the radius of gyration is accompanied by a large increase in the viscosity. The scattering data thus relate the rise of the viscosity to the presence of relatively large, agglomerated colloidal particles in the coal-derived liquids.

By use of helium density and chemical composition measurements of the coal-derived liquids, we were able to show that in the early stages of aging--that is, before appreciable agglomeration took place, the number of colloidal particles remained essentially constant, and that the main effect of aging was to cause the colloidal particles already present to grow larger, rather than to produce new particles. We also have been able to make a rough estimate of the fractions of the volume occupied by the small and large colloidal particles.

Acknowledgements

We wish to express our sincere gratitudue to S. R. Koirtyohann for assistance with the preparation of the ash samples used in our tests of the contribution of the mineral matter to the scattering from the PSOC coals, to Robert G. Jenkins for measuring the specific surface of PSOC Coal 105, to Dennis H. Finseth for preparing the samples of the coal-derived liquids, to L. B. Thomas, C. Leon Krueger, and Clifford R. Holmes for their help in the design and construction of the sample cell, to Charles D. Crowder and Chul Y. Kwak for assistance during the measurements of the scattering from the coal-derived liquids, to Richard G. Lett for obtaining the helium density and chemical composition of the coal-derived liquids, and to S. S. Pollack, D. W. Houseknecht, B. E. Cutter, R. G. Jenkins, D. E. Briggs, and P. L. Walker, Jr. for advice and assistance. This work was supported by contracts from the U. S. Department of Energy.

References

1. Guinier, A.; Fournet, G.; Walker, C. B.; Yudowitch, K. L.; "Small-Angle Scattering X-Rays"; Wiley: New York, 1955.
2. Durif, S. J. Chim. Physique 1963, 60, 816-24.
3. Krőger, C.; Mues, G. Brennstoff-Chemie 1961, 42, 77-84.
4. Spitzer, Z.; Ulický, L. Fuel 1978, 11, 621-625.
5. Lin, J. S.; Hendricks, R. W.; Harris, L. A., Yust, C. S. J. Appl. Cryst. 1978, 11, 621-625.
6. Gonzales, J.; Torriani, I. L.; Luengo, C. A. J. Appl. Cryst. 1982, 15, 251-254.
7. Kalliat, M.; Kwak, C. Y.; Schmidt, P. W., in "New Approaches To Coal Chemistry"; B. D. Blaustein, B. C. Bockrath, and S. Friedman, eds., ACS Symposium Series No. 169, pub. 1981, Amer. Chem. Soc., Washington, 1981; pp. 3-22.
8. Kwak, C. Y.; Kalliat, M.; Schmidt, P. W. Research to be published. 1984.
9. M. Kalliat, Schmidt, P. W.; Finseth, D. H. Research to be published. 1984.
10. Hirsch, P. B. Proc. Roy. Soc. (London) 1954, 226A, 143-169.
11. Gan H.; Nandi, S. P.; Walker, P. L., Jr. Fuel 1972, 51, 272-277.
12. Gregg, S. J.; Sing, K. S. W. "Adsorption, Surface Area, and Porosity"; Academic Press: London and New York, 1967, pp. 211-217.

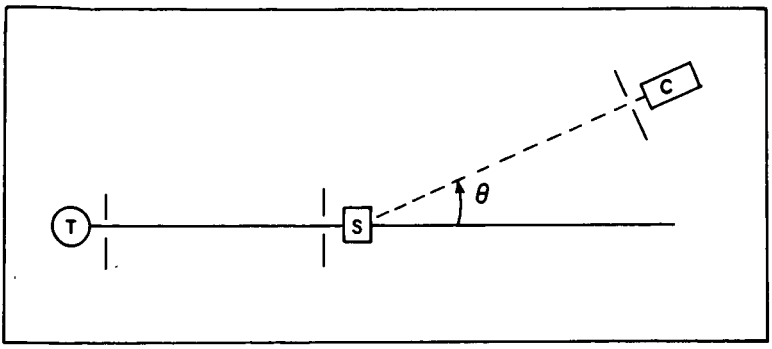

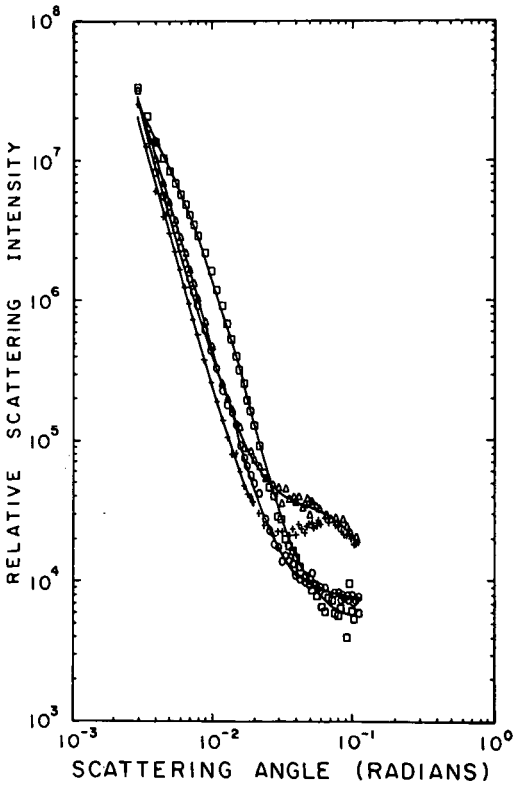

Fig. 1. (above) Schematic diagram of a small-angle x-ray scattering system. (Reproduced from Reference 7 by permission of the American Chemical Society.)

Figure 2. (left) Typical scattering curves for the coal samples. Curves 1--4 show the data for PSOC coals 95 (circles), 127 (plus signs), 81 (triangles) and 22 (squares). (This plot is reproduced from Reference 7 by permission of the American Chemical Society.)

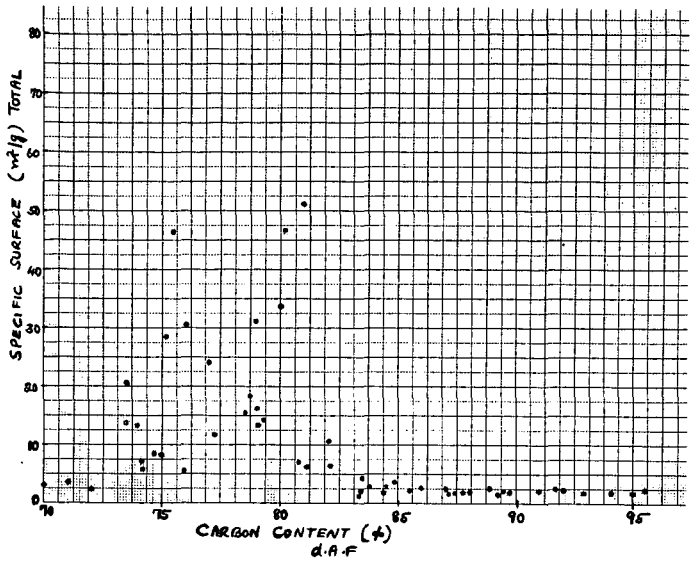

Figure 3. The combined x-ray specfic surfaces of the macropores and transitonal pores for coals of different carbon content (dry, ash-free).

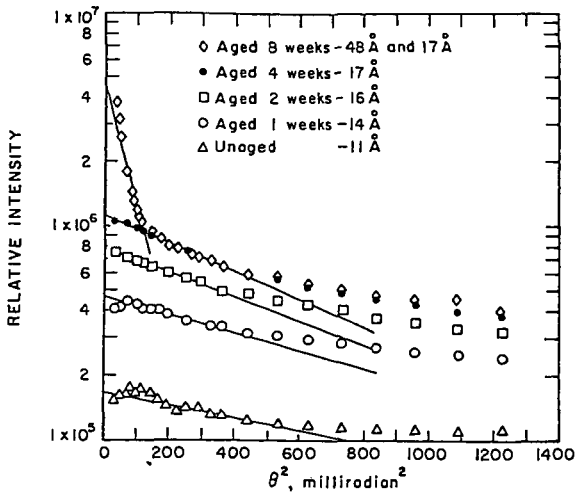

Figure 4. Radius of gyration plots for the coal-derived liquids.

DETERMINATION OF THE MICROSTRUCTURE OF WET AND DRY BROWN COAL BY MEANS OF X-RAY SMALL ANGLE SCATTERING

M. SETEK, I.K. SNOOK AND H.K. WAGENFELD

DEPARTMENT OF APPLIED PHYSICS
ROYAL MELBOURNE INSTITUTE OF TECHNOLOGY
124 LATROBE STREET, MELBOURNE, VICTORIA
AUSTRALIA 3000.

That brown coal is a highly porous substance and that a knowledge of this pore structure is vital to the efficient and diverse use of brown coal is obvious.

However, what is not so obvious is how to characterize and measure the pore structure of such a heterogeneous material as Victorian brown coal. Even defining what we mean by structure is difficult for such a complex material as coal which contains such diverse constituents as water, carbon, minerals, plant matter, pollen, etc. and whose composition may even vary within a seam. In practice, then, it seems that a Physicist must abandon his usual, precise but simplistic ideas of structure obtained from the study of objects with very regular structures such as crystals and give a description only in terms of such gross parameters as total pore volume, V, total surface area, S, and the distribution of some characteristic dimension, D, of the pores.

There appear to be currently two methods for the determination of the above mentioned parameter.

1) Gas Adsorption (GA) - where the total volume of a gas taken up by the coal is measured and V and S are obtained from this by the use of a model of the adsorption process.

2) Small Angle X-ray Scattering (SAXS) - where the intensity of radiation scattered by the coal is interpreted in terms of the pore structure which causes this scattering.

Both methods are to some extent dependent on models which are used in order to interprete the observed data. No known method can give a very detailed description of the microstructure at this stage. Indeed by the very nature of brown coal such a detailed description is not even, in principle, possible.

However, we will attempt to show that the SAXS method has very many advantages over other methods and we will also show what we have done to date using SAXS.

OUTLINE OF THE TECHNIQUE

Basically x-rays are scattered (just as is light) when a system contains regions which are inhomogeneous over some distance scale, d. These inhomogeneities cause scattering of intensity, I, through various angles, θ. The scattering curve, i.e. intensity as a function of θ or more precisely as a function of

$$h = \frac{2\pi}{\lambda} \sin \frac{\theta}{2}$$

(λ, the X-ray wavelength), contains information about the characteristic dimensions of the inhomogeneities (simplistically h is the reciprocal of d). However, when a wide range of characteristic distances are present the scattering

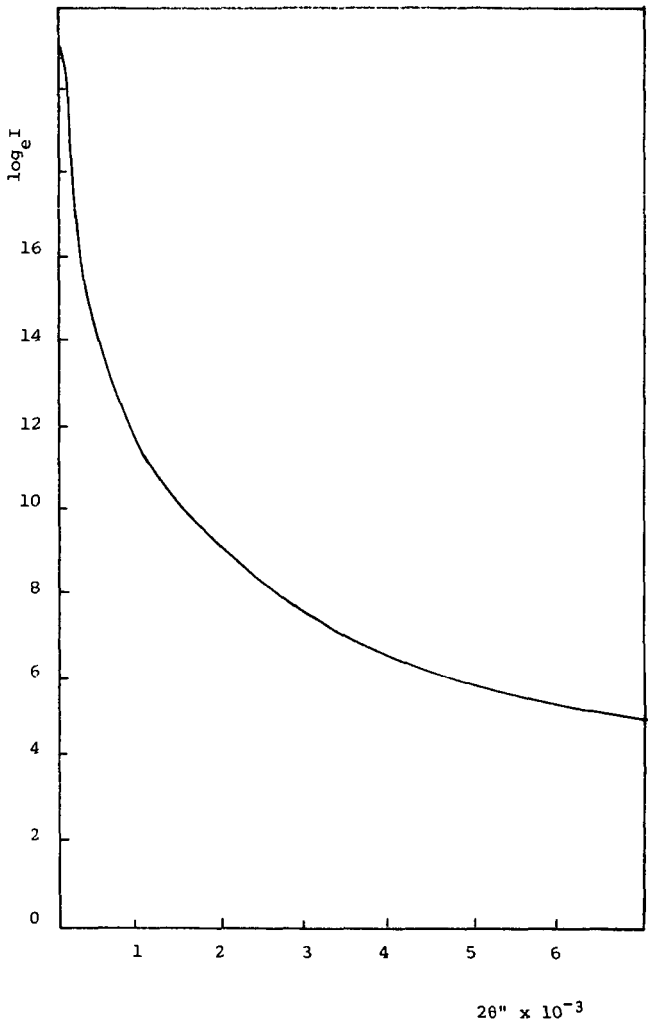

Fig. 1 Scattering curve of air dried coal (light lithotype).

curve is a superposition (convolution) of the effects of all these characteristic distances.

Thus, the scattering curve must be deconvoluted to obtain the information about the spacial distribution of inhomogeneities in the material, e.g. the pore structure in coal.

No known method can do this unambiguously, however, we believe realistic information may be readily and conveniently obtained by this method, e.g. total pore volume.

Furthermore, this method has several advantages over other available methods:

1) the sample can be wet or dry;

2) one can follow various stages of processes involving known coal or even, potentially, follow the material as it goes through these processes e.g. drying;

3) slurries may be studied.

DATA ANALYSIS AND RESULTS

Once the scattering curve has been obtained and stored in some convenient form it must be analysed (deconvoluted) to give details of the pore structure.

Technique to extract the micropore volume and the surface area from the scattering curves has been developed some years ago [1].

All scattering diagrams from brown coals (wet or dry) showed continuous strongly concave curves (Figure 1). This characteristic is assumed to be due to the presence of dilute system of micropores polydisperse in size but approximately identical in shape. From these curves several average pore length parameters can be obtained such as the mean radius of gyration, Rg, calculated by assuming a Maxwellian pore size distribution. Such parameters, although precise do not exactly define the form of the pores, however, can be used to calculate further physical quantities such as the micropore surface area. This quantity was obtained from the combined knowledge of the number of pores in the sample, the micropore volume (both quantities obtained by absolute intensity measurements), the mean radius of gyration, pore shape, and the pore size distribution. The micropore volume is computed directly from the scattering diagram in absolute units. Results are given in Table 1 together with data obtained by means of gas adsorption [2].

For the determination of the surface area we assumed two different shapes for the pores. In (1) we assumed a cylindrical shape and in (2) a disc shape.

Our method of interpretation of the scattering data shows only a partial success as can be seen when the results from the SAXS technique are compared to the results of the GA technique. Theoretically, this method seems to have several major faults:

1a) Assumption, that the pore size distribution is a single mode distribution. Pore size distribution may be more complicated, that is, it may follow a bimodal or even many modal type of distribution function. Indeed this can vary from sample to sample.

1b) Estimation of intensity scattered at zero angle. This point is not reachable experimentally and hence must be estimated, usually by some form of extrapolation. This is a very important quantity since it is directly proportional to the number of micropores within the irradiated volume.

1c) Assumption, that the shape of the micropores is identical. This is only an approximation that significantly simplifies the theoretical equations. It is quite possible that the micropores are not only polydispersed in size but also in shape.

TABLE 1 Comparison of microstructure parameters determined by gas adsorption (GA) and small angle X-ray scattering methods.

LITHOTYPE		MICROPORE VOLUME ml/g		SURFACE AREA m^2/g			RAD. OF GYR. nm
		GA	SAXS	GA	SAXS (1)	SAXS (2)	
DARK	WET	-	0.100	-	30	210	158
	DRY	0.079	0.095	298	90	1100	83
LIGHT	WET		0.110	-	40	390	136
	DRY	0.058	0.060	216	70	830	72

REFERENCES

[1] Kratky, O., 1940, Zs. El. Chem., 46, 550.

Porod, G., 1951, Koll. Zs., 124, 83.

Guinier, A., and Fournet, G., John Wiley & Sons, 1955, Chapter 2, New York.

[2] Wagenfeld, H.K., Setek, M., Kiss, L. and Stacy, W.O. (1981), Determination of porosity and pore size distribution of brown coal. Proceedings of International Conference on Coal Science, Dusseldorf.

Chemical Variation as a Function of Lithotype and Depth in Victorian Brown Coal

R. B. Johns, A. L. Chaffee and T. V. Verheyen

Department of Organic Chemistry, University of Melbourne, Parkville, Victoria, Australia, 3052.

Introduction

Victorian brown coal occurs in randomly sequenced stratified layers, known as lithotypes, which are distinguishable by their air-dried colour, maceral composition and many physical and chemical properties. The five major lithotypes can be related to generalized paleoenvironments of deposition and are known to influence many coal utilization parameters (1-3). Across the thick coal intervals which occur (up to 300 m) there is a small increase in coal rank observable via parameters such as % carbon and % volatiles (1). The purpose of this paper is to contrast the variation in the organic chemical nature of the coal occurring as a function of depth for a series of (nearly) identical lithotypes with that occurring as a function of lithotype. We have employed techniques giving both precise molecular level information (e.g., the distribution of extractable lipid classes) and average structural characterization of the whole coal (e.g., parameters derived from IR, solid state ^{13}C-NMR, etc.). All of these techniques have been able to provide much deeper insights into the varying nature of the coal than the conventional elemental and functional group type analyses which have been carried out extensively in the past.

Materials and Methods

Coal samples were taken from a single bore core (LY 1276) from the Flynn field in the Loy Yang region of the Latrobe Valley, Victoria, Australia. The core consists of > 100 m of continuous coal, but penetrates two coal seams, viz. Morwell 1A and Morwell 1B. These seams range from late Oligocene to Miocene in age. It is estimated that deposition of the 100 m of coal would have taken approximately 1 million years. Samples were chosen by visual examination of the air-dried colour of the coal. Lithotype classifications on this basis are usually, but not always correct; it was therefore found necessary to modify some of the initial classifications after a consideration of all the available petrographic and chemical data. This correction has not been incorporated in previous publications from our group (4). Further details relating to these samples, methods of fractionation and experimental techniques can be found elsewhere (5-6).

Characterization of Whole Coals

Before considering the results of other more sophisticated analyses it is useful to demonstrate the divergent chemical nature of the coal lithotypes by a more classical approach. When elemental analytical data are expressed in bond equivalence form it can be seen (Figure 1) that there is some inherent spread in the plotted points for the suite of light lithotype samples. The different lithotypes are, however, readily distinguishable due to the much greater variance in their analytical figures. The distinguishing features are especially exhibited at the extremes of the lithotype classification as an increase in the number of bonds associated with carbon at the expense of hydrogen for the dark lithotype and visa versa for the pale lithotype. For the light samples the bond equivalent data are most consistent for carbon, with the mean values for hydrogen and oxygen exhibiting higher proportional standard deviations. The bond equivalence data implies that the difference between the lithotypes resides in the type of chemical structure(s) that the elements form.

There are only a few solid-state techniques capable of providing structural information on "whole" coals. The CP-MAS ^{13}C-NMR spectra of Victorian brown coals exhibit significant fine structure including phenolic and carboxylic resonance envelopes which are consistent with their low aromaticity and rank. The proportion of aromatic carbon atoms, f(a), in the coal can be determined from the spectra and the variation in this parameter across the sample suite is illustrated in Figure 2. While there is some spread in the f(a) values amongst the light samples ($\bar{x}$ = 0.52, σ = 0.03) there is no obvious trend with depth. The variation as a function of lithotype transcends the inherent spread in the light samples and there is an obvious increase in aromaticity for the progression from paler to darker lithotypes. Only the medium-light sample cannot be adequately distinguished within the sample suite by this technique. In addition to their higher aromaticities the spectra of the medium-dark and dark lithotypes exhibit prominent phenolic and methoxyl carbon absorptions similar to the spectra of degraded lignins. Hence the variation in f(a) as a function of lithotype is considered to be predominantly the result of variation in the original organic input and in the relative preservation of various biopolymeric materials within the corresponding depositional paleoenvironments. Although aromaticity is known to correlate with coal rank over a wider regime, there is no suggestion of a regular increase in f(a) over the depth interval examined. The small variation in f(a) for the several light samples is probably a reflection of minor changes in the depositional paleoenvironments.

Absorption mode IR spectroscopy provides greater sensitivity for the observation of specific functional groups. The variation in the absorption coefficients K_{2920} (aliphatic C-H stretch) and K_{1710} (carbonyl, carboxyl stretch) across the suite of samples is illustrated in Figure 3. It is again obvious that the variation as a function of lithotype exceeds the spread inherent in the set of light samples. The proportional spread for the light samples is significantly more intense for K_{2920} ($\bar{x}$ = 14.1 cm mg^{-1}, σ = 2.9) than for K_{1710} ($\bar{x}$ = 36.2, σ = 2.2), but in neither case is there any definative trend with depth. A strong negative correlation (r = -0.95) exists between K_{1710} and f(a) for all samples examined. The correlation between f(a) and K_{2920} is significantly lower (r = -0.84) as would be expected from the higher proportional spread in the K_{2920} values. The structural implications of these relationships are not entirely clear, but the IR data provide a further clear indication of the effect of the depositional paleoenvironment upon the coal structure(s) which are ultimately preserved.

Rock-Eval analysis is a form of temperature programmed pyrolysis often applied to petroleum source rocks in which the level of evolved carbon dioxide and hydrocarbon-like material are quantitatively measured via oxygen (OI) and hydrogen (HI) indices. The temperature at which the maximum amount of volatile material is evolved (T_{max}) is also recorded, and this can be related to the rank of the organic substrate. The average T_{max} values for the samples under consideration was observed to be 397°C (σ = 2.6), a value which corresponds to a vitrinite reflectance of ~ 0.30. No significant regular variation in T_{max} was observed with either depth or lithotype and this method, also, does not provide any indication of the slight increase in rank over the 100 m coal interval. A plot of HI versus OI (Figure 4), however, provides a further method for distinguishing the lithotypes. Although there is a significant spread in the HI values for the light samples, the OI data enable better discrimination between the different lithotypes. This observation supports the NMR and IR data in suggesting that lithotype is a coal property especially influenced by the nature and concentration of oxygen containing species. HI is a measure of the hydrocarbon production potential and correlates strongly (r = +0.94) with the percentage of extractable material (see later); it is a parameter which has substantial significance for coal-to-oil conversion. It can be seen that the lighter lithotypes and especially the pale sample provide greater potential in this respect.

Characterization of Coal Fractions

The variation in the weight percentage of total solvent extractable (TSE) material (extraction with chloroform/methanol/toluene) and solvent extractable humic acid (SEHA) for the coal samples is illustrated in Figure 5. There is a substantial reduction in the weight % of these fractions in the progression from paler to darker lithotypes. It can also be seen that the variation with lithotype is significantly more extreme than the variation within the suite of light lithotypes. Within the latter suite there is a notably large difference in the weight percentages between the two adjacent samples from 59 m and 78 m depth in the core. The jump across this interval can be related to the Morwell 1A/Morwell 1B seam boundary which occurs at the 73 m depth. Taking into account this abberation the data are consistent with an increase in extractable material as a function of depth (for samples within a particular lithotype classification and seam). The increase across the interval from 78 to 119 m depth is quite marked by comparison with the increase in extractable material which accompanies increasing rank within the subbituminous rank regime (7). There have been, however, no previous systematic studies giving any indication of what to expect within this lower rank interval. A more intense study of rank dependent phenomena within this interval could significantly enhance our understanding of coal forming processes.

The distributions of extractable n-alkanes from the different lithotypes are illustrated in Figure 6. All the distributions exhibit a marked predominance of odd carbon chain length homologues and in this respect all are similar to the distribution of n-alkanes which occur in living higher plant waxes. In other respects, however, the distributions differ markedly. For example, the dark lithotype exhibits a primary maximum at C_{29} and a secondary one at C_{25}. The medium dark and pale lithotypes exhibit only primary maxima at C_{31} and C_{29}, respectively. By contrast, all the light samples exhibit primary maxima at C_{29} and secondary maxima at C_{37}. These C_{37} maxima appear to be a distinctive feature of the light samples and have almost certainly resulted from the input of some fairly specific taxon which was viable only in association with the paleoenvironment of deposition for this lithotype. The distribution can be further characterized by Carbon Preference Indices (CPIs), a parameter which is effectively the ratio of the abundance of odd relative to even carbon chain lengths. It can be seen (Figure 7) that there is considerable spread in the CPI values for the light samples and that only the CPI value for the dark lithotype lies significantly outside this margin. There is no apparent changes in the distribution of n-alkanes as a function of depth and it would appear that the distributions remain substantially representative of those contributed by the higher plant progenitors of the coal.

A consideration of the extractable n-fatty acid distributions gives a complimentary characterization of the sample suite. The distributions are again a reflection of those observed in the higher plant precursors to the coal. The distributional differences between lithotypes and the similarities within a single lithotype classification are less obvious than in the case of the n-alkanes, but a statistical approach involving the determination of covariance between sample pairs was able to effectively differentiate the divergent nature of the distributional variations as a function of depth and lithotype (5). CPI values for the n-fatty acid distributions are plotted in Figure 8 (CPI, in this case, is effectively the ratio of even relative to odd chain lengths). Again there is a considerable difference in the values for the various lithotypes, but the spread of values within the light sample suite is relatively small. Within this spread, however, it is possible to discern a general reduction in the CPI values with depth. There is again a discontinuity across the seam boundary. There is a corresponding general reduction in the level of extractable n-fatty acids over this depth interval and the consistent variation in these two parameters is believed to indicate that progressive diagenetic removal and alteration of the fatty acids is occurring with depth within this coal sequence. The discontinuity across the seam

boundary is an indication of the complex combination of paleobotanical, geochemical and microbiological factors which control the diagenetic progression.

Many coals contain extended chain (> 31 carbon atoms) hopanes and related compounds which appear to be diagenetically derived from the lipids of certain procaryotic organisms. Biologically produced hopanoids exclusively possess 17βH,

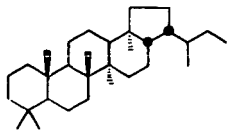

17βH,21βH-homohopane

21βH stereochemistry. The thermodynamically more stable 17αH,21βH stereochemistry has usually been explained to form in the geosphere via diagenetic acid catalyzed and temperature dependant isomerization from the biological diastereomers. Hence the diastereomeric ratio, 17αH,21βH/17βH,21βH has been observed to rise in simulated maturation studies and with increasing depth of burial in sedimentary sequences. The present data exhibit a reversal of this trend; that is, there is a reduction in this ratio with depth for the series of light samples (Figure 9). Although there must be some mechanism to account for the formation of the abiological 17αH,21βH-diastereomers in the first place, the data suggest that 17βH,21βH-diastereomers are being progressively produced with depth in the coal seam. On the basis of present understanding this could only occur by microbiologically mediated processes. The temperatures reached within the coal seam are obviously insufficient to force the isomerization towards its thermodynamic equilibrium. There is also a significant difference in the diastereomeric ratios determined by lithotype. This marked difference is probably substantially determined during the early stages of coal deposition where it may be significantly influenced by the pH of the surrounding swamp water or the coal surface acidity. The significant difference in the diastereomeric ratios (Figure 10) as a function of lithotype is consistent with the preceeding explanation; that is, the dark lithotypes can be generally associated with higher acidities (and hence pH) which would favour the formation of the abiological isomer, as observed.

The polycyclic aromatic hydrocarbons (PAHs) in brown coal consist predominantly of pentacyclic angularly condensed hydroaromatic moieties. These compounds appear to be derived from C_{30} triterpenoid precursors which occur as natural products in angiosperm waxes. It can be seen (Figure 10) that there is a marked variation in the concentration of PAHs as a function of both lithotype and depth. The variation as a function of lithotype is consistent with our views on the generalized paleoenvironments of deposition, i.e., the lighter lithotypes are deposited in relatively anaerobic environments more conducive to the preservation of the originally deposited organic material, while the darker lithotypes are deposited in relatively aerobic environments in which much of the less resistant organic material is removed by oxidation or substantially altered microbiologically. The increasing concentration in PAH concentration with depth for the series of light samples suggests that the formation of PAHs is also occurring within the coal seam. It seems most likely that this transformation, too, is microbiologically mediated.

Conclusions

The organic chemical nature of Victorian brown coal has been shown to vary as a function of both depth and lithotype. In the latter case the structural differences occur predominantly as a result of the differing nature of the depositional paleoenvironments and are readily distinguishable by both gross and molecular level parameters. The differences with depth are considerably more subtle and were observed only by specific molecular techniques; e.g., the level of PAHs, the diastereomeric ratio of hopanoids and the CPIs of the n-fatty acid distributions. Since the observed structural differences at the molecular level involve only a small proportion of the total coal substrate (parts per thousand level) it is hardly surprising that they are not manifested at the gross structural level. Although mild increases in temperature certainly occur across the sampled coal interval, the specific nature of the chemical changes observed with depth suggests that microbiological processes rather than geochemical (temperature dependent) processes are chiefly responsible. It may be that the warmer conditions deeper in the seam favour the viability of anaerobic microorganisms which can modify the coal substrate in the required manner, or more probably that the closer proximity of the deeper samples to underground aguifers (and potentail sources of oxygen and inorganic nutrients) favour the viability of aerobic microorganisms.

Acknowledgements

The authors acknowledge the Victorian Brown Coal Council and the State Electricity Commission of Victoria for the provision of coal samples. Mr S. Bombaci is thanked for technical assistance.

References

(1) Allardice D. J., George A. M., Häusser D., Neubert K. H. and Smith G. C., State Electricity Commission of Victoria, Research and Development Department, Report No. 342 (1977).

(2) Blackburn D. T., presented at "Cainozoic Evolution of Continental South-Eastern Australia" conference, Canberra, Nov. 1980.

(3) George A. M., State Electricity Commission of Victoria, Petrographic Report No. 17 (1975).

(4) Johns R. B., Verheyen T. V. and Chaffee A. L., "Proceedings of the International Conference on Coal Science, Düsseldorf, 1981", Verlag Glückauf, Essen, pp. 863-868 (1981).

(5) Chaffee A. L., "The Organic Geochemistry of Australian Coals", Ph.D. dissertation, University of Melbourne (1981).

(6) Verheyen T. V., "Structural Characterization of Selected Australian Coals", Ph.D. dissertation, University of Melbourne (1982).

(7) Radke M., Schaefer R. G., Leythauser D. and Teichmüller M., Geochim. Cosmochim. Acta, 44, 1787-1800 (1980).

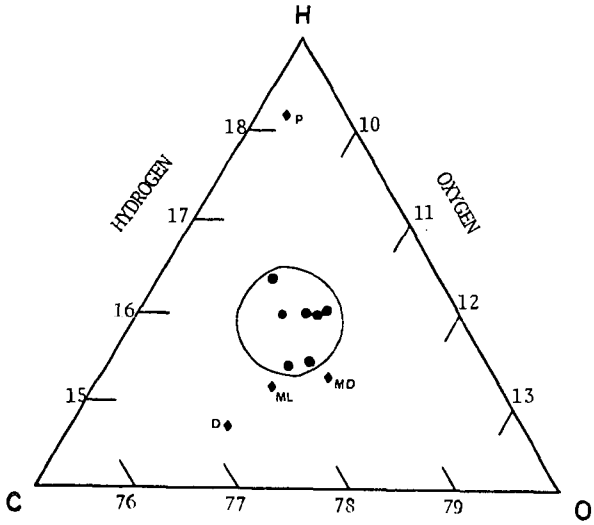

Figure 1 Ternary % bond equivalence diagram for whole coal samples. ● - Light lithotype samples; ♦ - other lithotypes as labelled: P - pale, ML - medium light, MD - medium dark, D - dark.

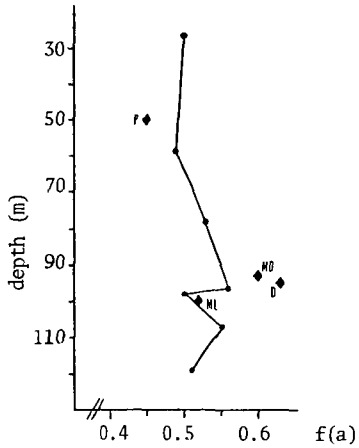

Figure 2 Aromaticity versus depth. Data for the light lithotype samples are joined to illustrate the spread of values.

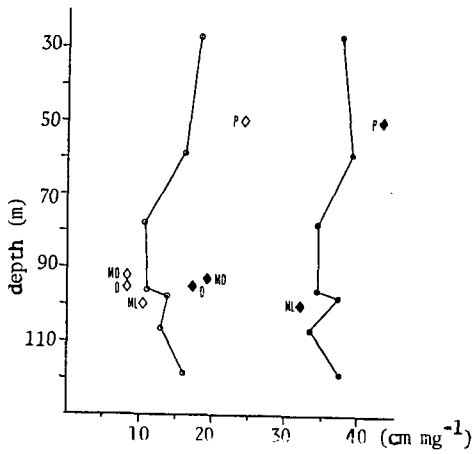

Figure 3 Infrared absorption coefficients versus depth. Closed symbols refer to K_{1710}; open symbols refer to K_{2920}.

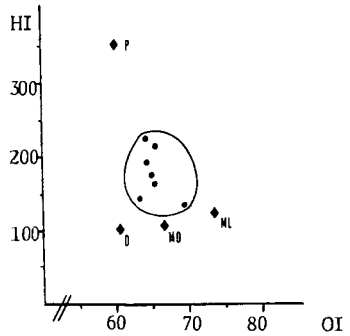

Figure 4 Hydrogen index (HI, mg HC/g TOC) versus oxygen index (OI, mg CO_2/g TOC) from Rock-Eval analysis.

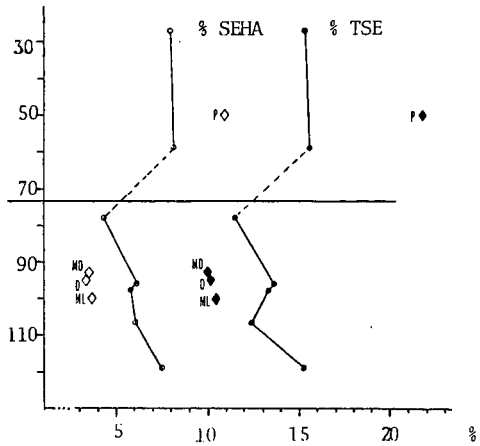

Figure 5 Weight % TSE (closed symbols) and SEHA (open symbols) versus depth. The horizontal line at 73 m represents the Morwell 1A/Morwell 1B seam boundary.

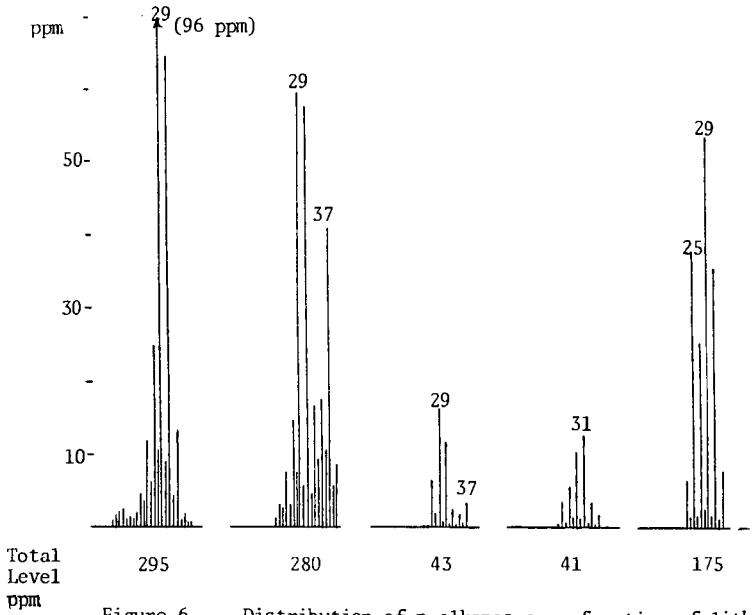

Figure 6 Distribution of n-alkanes as a function of lithotype.

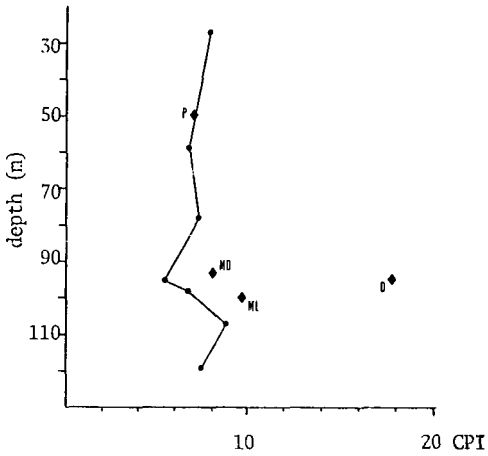

Figure 7 Carbon Preference Indices of n-alkanes versus depth.

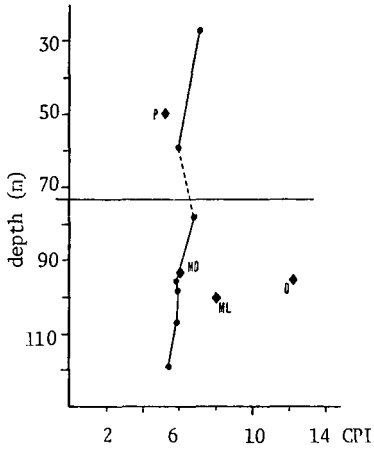

Figure 8 Carbon Preference Indices of n-fatty acids versus depth.

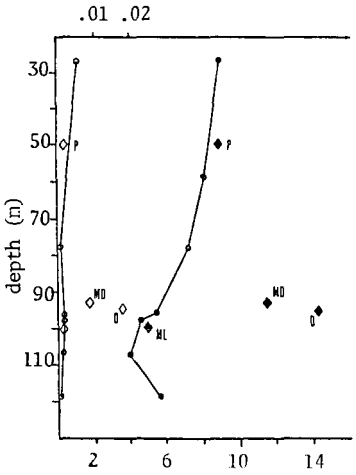

Figure 9 Ratio of diasteriomers, 17 H,21 H/17 H,21 H, for homohopane (closed symbols, bottom axis) and biohomohopanoic acid (open symbols, top axis).

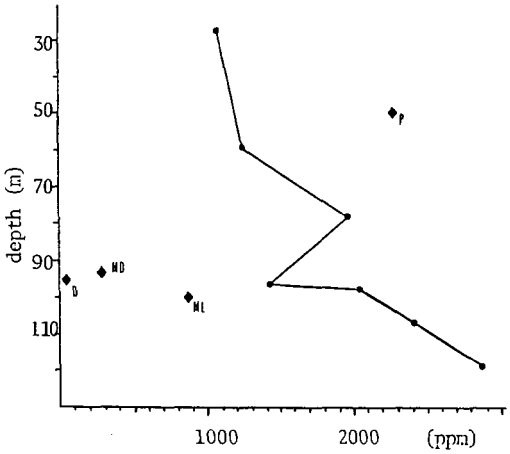

Figure 10 Level of extractable polycyclic aromatic hydrocarbons versus depth.

COMPARISON OF HYDROCARBON EXTRACTS FROM SEVEN COALS BY CAPILLARY GC AND GC/MS

Sylvia A. Farnum, Ronald C. Timpe*, David J. Miller, and Bruce Farnum

U.S. Department of Energy
Grand Forks Energy Technology Center
Box 8213, University Station
Grand Forks, North Dakota 58202

Coals have been shown to contain paraffinic hydrocarbons whose structures arise directly from biological precursors. The types of hydrocarbons usually considered in this group of biological markers include n-alkanes, acyclic isoprenoids, steranes and terpanes. The amounts of these materials that can be extracted from coal are small but even the characterization of these small amounts of alkanes can be very important in determining the origin and maturity of coals. A detailed understanding of the origin of coals and of the diagenesis and maturation of coals may someday be deduced by drawing upon the large body of available information on the relationships of biological markers to the geologic history of rocks, sediments, oil shales and petroleum. The subject has been reviewed (1,2). Some biological markers have also been detected in coal liquefaction products (3,4).

Seven coals were selected for analysis in this study. These seven coals have also been utilized for various liquefaction studies at the Grand Forks Energy Technology Center (GFETC). Their proximate and ultimate analyses are shown in Table 1.

The finely pulverized (-100 mesh) coals were sequentially extracted with chloroform (Soxhlet, 6 hr) and the ternary azeotrope chloroform: acetone: methanol, 47:30:23 (Soxhlet, 14 hr). Each extract was separated into a hexane-soluble and a hexane-insoluble portion. This report deals with the analysis of the hydrocarbons in the hexane-soluble portion (CHX) of the chloroform extract. This fraction contained the hydrocarbons of interest as biological markers. Extraction under these mild conditions gave the extraction yields shown in Table 2.

Capillary GC comparison of retention times with authentic standards and GC/MS were used to characterize the acyclic alkanes present in the CHX extracts. The extracts of Beulah 3 North Dakota lignite (B3), Wyodak Wyoming subbituminous coal (WY01), Highvale Alberta subbituminous coal (ALB1) and Powhatan Ohio bituminous coal (POW1) all contained homologous series of n-alkanes, Table 3. The low-rank coal CHX extracts for the limited members of the series present all gave Carbon Preference Indices, CPI's, (1), greater than one. The alkane distributions and the CPI values are shown in Figure 1. The observed n-alkane distributions were in agreement with the observation by Rigby et al. that increasing maturity of the coal was attended by a shift in maximum concentration to shorter chain length alkanes in extracts (5).

As has been previously reported, high temperature high pressure coal liquefaction as well as coal maturation lowers the odd/even carbon preference values to near 1.0 (3). This effect was also noted when the analyses of processed liquid products from the GFETC continuous processing liquefaction unit were compared with the CHX coal fractions extracted under mild conditions. CPI values of 1.0 were obtained for the processed liquids from B3 and WY01 low-rank coals compared with values of 1.8 for the fractions extracted under mild conditions. These coal extracts should contain alkanes that were present in the coal, whereas, the heat-altered, processed products also contain alkanes formed from cracking of waxes, other alkanes, and other aliphatic portions of the coal. In the case of the higher rank bituminous coal, POW1,

*Associated Western Universities, Inc., Summer Faculty Research Participant
present address -- Mayville State College, Department of Chemistry, Mayville, North Dakota 58275

TABLE 1

ANALYSIS OF COALS

	Beulah 3 (ND) B3	Morwell (Australia) MOC	Big Brown 1 BB1 (TX)	Big Brown 2 BB2 (TX)	Wyodak (Wyoming) WY01	Highvale (Alberta) ALB1	Powhatan (Ohio) POW1
Proximate Analysis As received:							
Moisture	28.84	10.19	27.55	28.87	30.99	17.79	4.00
Volatile Matter	28.99	43.00	32.10	38.27	30.43	39.83	39.47
Fixed Carbon	30.76	43.63	30.72	19.53	32.96	32.01	46.71
Ash	11.70	3.19	9.63	13.33	5.62	10.37	9.81
Ultimate Analysis Moisture-free:							
Ash	16.44	3.55	13.29	18.74	8.15	12.61	10.22
Moisture and ash-free (maf):							
Carbon	69.49	70.64	73.15	74.00	73.74	74.41	79.01
Hydrogen	4.43	5.01	5.22	6.09	5.38	4.92	5.43
Nitrogen	0.99	0.46	1.40	1.22	1.22	0.95	1.29
Sulfur	2.81	0.33	1.30	1.21	0.53	0.20	3.92
Oxygen (by difference)	22.26	23.56	18.93	17.48	19.12	19.52	10.35

the CPI was the same, 0.9 both before and after processing indicating maturation of the coal.

TABLE 2

SEQUENTIAL EXTRACTION OF COALS WITH $CHCL_3$ (SOXHLET), $CHCl_3$: ACETONE: METHANOL, 47:30:23, AZEOTROPE (SOXHLET) AND SEPARATION OF HEXANE SOLUBLES (% MAF COAL, DUPLICATES WERE AVERAGED)

	Total $CHCl_3$ Soluble (Soxhlet)	Hexane Soluble Portion of $CHCl_3$ Extract	Total Azeotrope Soluble (Soxhlet)	Hexane Soluble Portion of Azeotrope Extract
B3	2.8	1.0	1.6	0.13
MOC+	0.82	0.58	1.7	0.59
BB1+	4.2	1.7	2.2	0.16
BB2	3.7	1.7	2.4	0.19
WYO1	3.2	2.9	5.0	0.21
ALB1	0.58	0.35	1.8	0.28
POW1	0.70	0.51	5.8	1.1

+Values given from single extraction only.

The CHX extracts from B3 and POW1 were the only extracts of the seven that contained pristane. The bituminous coal, POW1, extract had more pristane than the B3 extract, Table 3. Phytane was not detected in any of the extracts, although both pristane and phytane were found in all of the coal liquefaction products from B3, BB1, WYO1, and POW1. The ratio of pristane to phytane was about 5:1. It has been reported that the pristane content of the saturated hydrocarbon fraction from subbituminous coals of more than 76% C begins to increase (1). The increase in phytane concentration corresponds roughly to 83-85% C.

Some of the cyclic hydrocarbons found in the CHX coal extracts are shown in Table 4. They were tentatively identified by capillary GC/MS except for the naphthalenes, for which authentic standards were available. Selected ion scans were used to detect sesquiterpenes (m/e 206, 191), sesquiterpanes (m/e 208), alkanes (m/e 141), alkyl benzenes (m/e 191, 163), steranes (m/e 217), and tricyclic terpenoids (m/e 191, 163) as well as the m/e values for the parent ion of specific compounds. Figure 2 shows the results of one of these selected ion scans, m/e 206, from the CHX extract of WYO1 along with a portion of the total ion chromatogram. The peaks shown in the m/e 206 trace between scan numbers 240 and 300 correspond to the sesquiterpenes listed in Table 4. All of these compounds showed M-15 peaks of various intensities (m/e 191), relatively intense M-29 peaks (m/e 177) and m/e 121 peaks. One compound, c, had a prominent even mass peak at 178. Six had more prominent M-43 (m/e 163) peaks than the others. The fragmentation patterns shown by these $C_{15}H_{26}$ sesquiterpenes resemble those reported by Richardson (6) for a series of $C_{15}H_{28}$ bicyclics identified in a crude oil. The sesquiterpene distribution for the CHX extracts of B3 and WYO1 were distinctive and similar. The distribution for ALB1 gave smaller concentrations of sesquiterpenes, Table 4, but the mass spectra were identical for comparable ALB1, WYO1, and B3 sesquiterpenes with the same GC retention times. POW1, MOC, BB1, and BB2 CHX extracts did not contain these compounds. No sesquiterpanes with (m/e 208) were detected in any of the CHX extracts. Gallegos (7) found a number of sesquiterpenes (m/e 206, 191) in pyrolysis products of six coals including Wyodak subbituminous coal and Noonan North Dakota lignite. Gallegos also detected cadalene (m/e 198, 183). Cadalene was present in the ALB1 extract and was probably a small component in the B3 extract. It was not found in the extracts of the other coals.

TABLE 3

ACYCLIC HYDROCARBONS FOUND IN EXTRACTS OF COALS AND THEIR DISTILLABLE LIQUEFACTION PRODUCTS
(Capillary GC, Area Percent, FID)

	Retention Time, min.	B3 Coal Extract	WY01 Coal Extract	ALB1 Coal Extract	POW1 Coal Extract
Isoprenoids:					
pristane (2,6,10,14,tetramethyl-pentadecane)	168.9	0.15			1.35
n-alkanes:					
C-14					
C-15	125.8	0.82			
C-16					
C-17					
C-18					
C-19	194.1	0.74			0.49
C-20	205.0	0.99			0.41
C-21	215.6	1.38			0.26
C-22	223.9	1.22	1.04		0.46
C-23	232.7	0.69	0.73	1.38	0.31
C-24	241.2	0.67	0.33	0.43	0.46
C-25	249.2	1.89	0.82	1.85	0.34
C-26	256.9	1.55	0.57	0.37	0.29
C-27	264.5	2.92	0.99	0.92	0.33
C-28	271.6	0.42	0.31	0.31	0.25
C-29	278.5	0.76	0.98	0.77	0.25
C-30	285.1	0.57	0.52	0.2	0.25
C-31	290.2	0.29	0.56	0.59	0.10
C-32	296.1				0.02
C-33	300.1				0.03
C-34	304.3				0.001
C-35	308.7			0.19	0.03
C-36	312.0			0.09	0.004
C-37	316.6				0.01
C-38	320.4				0.006
C-39	324.0				0.008

Another compound which gave identical mass spectra in two of the extracts, WYO1 and ALB1, appears to be one of the tricyclic alkanes, m/e = 276. An intense peak at m/e 247 corresponds to M-29. The mass spectrum was an excellent match with that presented by Philip, et al. (8) for which structure I was proposed. An intense peak at m/e 123 was noted and is probably due to the fragmentation shown.

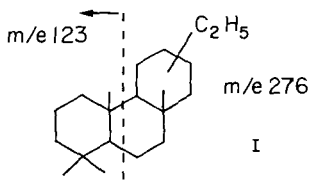

I

At a slightly longer retention time the component m/e 234 appears to be another tricyclic alkane, $C_{17}H_{30}$. Several similar tricyclic alkanes were reported by Jones et al. (4).

The spectrum of m/e 252, identical in WYO1 and ALB1 extracts, corresponds to $C_{18}H_{36}$ but is not dodecylcyclohexane (9). There is a prominent M-15 peak at m/e 237 and relatively intense peaks at m/e 111 and 195. The peak at 111 could be assigned as a dimethyl-cyclohexyl fragment.

The compounds detected in the mass range 398-454 in B3, BB1, BB2, and POW extracts appear to be pentacyclic triterpanes since all have prominent m/e 149, 177, 191, and 205 peaks (10). When selected ion chromatograms are compared, WYO1 extract shows no m/e 191 peaks for GC retention times in the pentacyclic triterpane region. The BB coal extracts, B3, ALB1 and POW1 all have numerous small peaks that are probably triterpenoids. Some of these gave appreciable GC FID responses and good mass spectra.

The spectrum of m/e 398 is identical for ALB1 and POW1 extracts. The compound is not adiantane since the m/e 191 is greater than 177, not of similar intensities (11). C_{27} - C_{31} triterpanes, especially adiantane, C_{29}, have been found in bituminous coal extracts (12).

The pentacyclic component at m/e 412 resembles the spectrum of oleanane (II) or gammacerane. It is also similar to that of lupane (11,13) but lacks the M-43 (369) fragment indicative of any isopropyl sidechain. Therefore, ring E is probably 6-membered, not 5-membered as in lupane or the hopanes. Although the mass spectrum is a slightly better match to gammacerane, the short retention time probably rules out gammacerane but not oleanane.

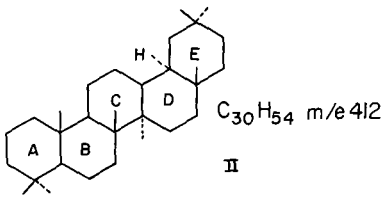

II

The two different $C_{31}H_{54}$ pentacycles (m/e 426), one observed in BB2 extract and one in POW1 extract had no M-29, M-43 or M-57 fragments. The m/e 205 was small ruling out structures like lupan-3-one (14). Other differences also eliminate friedelan-3-one and oleanan-3-one type of structure (14).

The m/e 440 pentacyclic representative found in BB1 and BB2 had an M-29 peak (411) and a prominent peak at 369. It could therefore be a homohopane. None of pentacyclic structures found in any of the extracts could correspond to the unaltered less stable 17βH, 21βH hopane series because m/e 191 is much larger than the secondary fragment in all cases. The structure could be a 17αH, 21βH hopane which is common in geologically altered sediments of all kinds (III).

TABLE 4

OTHER HYDROCARBONS FOUND IN EXTRACTS OF COAL CAPILLARY GC AND GC/MS, AREA %, FID

		Retention Time, Min.	m/e, Parent Ion	Capillary GC, Area %						
				B3	MOC	BB1	BB2	WY01	ALB1	POW1
Miscellaneous:										
naphthalene		47.9			0.32			0.18	0.12	1.2
2-methylnaphthalene		72.0			0.29			0.19	0.38	2.7
1-methylnaphthalene		75.6			0.04			0.09	0.13	2.0
C_2-naphthalene		95.3								0.68
cadalene		160.4	198	0.31						1.3
Alicyclic terpenoids:										
$C_{15}H_{26}$ sesquiterpene	a	100.7	206					2.8		
"	b	104.8	206					1.0		
"	c	106.8	206	1.9				13.2	0.70	
"	d	108.9	206	1.12				3.3		
"	e	111.2	206	0.24				8.3	0.17	
"	f	113.0	206					4.6	0.27	
"	g	114.9	206	2.3				1.5	1.9	
"	h	116.2	206	0.10				0.96	0.17	
$C_{20}H_{36}$ tricyclic alkane		230.3	276					0.96	0.46	
?		233.4	252						0.50	
$C_{17}H_{30}$ tricyclic alkene		236.4	234	1.2				1.0	0.50	0.10
?		272.5	Not Shown				0.66			
$C_{29}H_{50}$		284.6	398						0.27	0.13
$C_{30}H_{52}$		285.2	412							0.13
$C_{31}H_{54}$		287.0	426				3.3			
$C_{31}H_{54}$		295.8	426							0.03
$C_{32}H_{56}$		312.0	440			3.0	1.1			
$C_{33}H_{58}$		321.7	454	0.07		1.7	3.5			

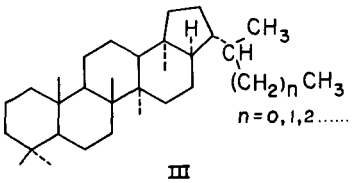

III

The m/e 454 pentacyclic triterpene (BB1, BB2 extracts) is also unidentified.

A number of hydrocarbon fractions from liquefaction products produced at GFETC from the coals studied here were investigated using selected ion scans of the capillary GC/MS analyses. None of the hydrocarbon biological markers other than the acyclic alkanes already discussed were detected. There were no sesquiterpenes, sesquiterpanes, steranes, triterpanes or other cyclic terpenoids found.

CHX extracts of the seven coals were profiled using capillary GC. The best results were obtained using a J.& W. DB5 60 N fused silica capillary column with H_2 carrier and flame ionization detector. Temperature programming from 50° to 125°C at 0.5°C/min, from 125° to 250°C at 1.0°C/min and from 250° to 350°C at 1.5°C/min, then an isothermal plateau at 350°C was used.

There were some striking similarities and differences between profiles for the coal CHX extracts. The profiles for CHX extracts of MOC, BB1 and BB2 were very similar. They show no detectable alkanes and very few peaks until 230 min when the maximum temperature was reached. Between 230 min. and 320 min. a large group of peaks form a dense envelope.

The capillary GC profiles for B3 and WY01 extracts are also strikingly similar, with nearly every major GC peak having a counterpart in each chromatogram. ALB1 extract shows some similarity to the WY01 trace but differs, the POW1 extract profile is also different. All of the GC profiles for B3, WY01, ALB1 and POW1 CHX extracts have continuous baseline resolved peak distributions from about 50 to 350 minutes with various recognizable patterns. From duplicate extractions of the same coal and by comparing BB1 and BB2 extracts, it may be seen that the profiling of the hydrocarbon extracts is reproducible and may be used to identify and group coals.

Each of the CHX extracts also contained some oxygen compounds. The elemental analyses showed 5-6% oxygen present. Although the characterization of these compounds is not complete, it may be noted that all of the extracts contained some 60-70 carbon nonvolatile waxes (long chain fatty acid esters). The presence of these esters was demonstrated by methanol/BF_3 transesterification followed by capillary GC and 200 MHz ^1H NMR analyses.

SUMMARY

The chloroform extraction of seven coals yielded extracts that gave unique capillary GC profiles. Several groups of hydrocarbon biological markers were detected in the coal extracts by mass spectrometry using selected ion scans. n-Alkanes, pristane, sesquiterpenes, several tricycle alkanes and pentacyclic triterpanes with molecular weights from 398 to 454 were detected. The coal extract profiles fell into four groups: 1) BB1, BB2 (Texas lignites) and MOC (Australian lignite); 2) B3 (North Dakota lignite) and WY01 (Wyoming, subbituminous); 3) ALB1 (Alberta, Canandian subbituminous), and 4) POW1 (Ohio, bituminous). Profiles were characteristic and reproducible for each coal.

ACKNOWLEDGEMENTS

The authors would like to thank Art Ruud for the extensive coal analyses he and his group carried out. Thanks also to John Diehl for running the capillary GC profiles of the seven coal extracts.

REFERENCES

1. Bartle, K.D., Jones, D.W., Pakdel, H. "Analytical Methods for Coal and Coal Products," Academic Press, New York, San Francisco, London, 1978; Part II, 209-262.

2. Bartle, K.D., Jones, D.W., Pakdel, H. "Coal and Coal Products: Analytical Characterization Techniques," American Chem. Society Symp. Ser., American Chemical Society, Washington, D.C., Volume 205, 1982, 27-45.

3. White, C.M., Shultz, J.L., Sharkey, A.G., Jr. Nature, 1977, 268, 620-622.

4. Jones, D.W., Pakdel, H., and Bartle, K.D. Fuel, 1982, 61, 44-52.

5. Rigby, D., Batts, B.D., and Smith, J.W. Org. Geochem., 1981, 3, 29-36.

6. Richardson, J.S. and Miller, D.E. Anal. Chem., 1982, 54, 765-768.

7. Gallegos, E.J. J. Chromatog. Sci., 1981, 19, 156-160.

8. Philip, R.P, Gilbert, T.D., and Friedrich, J. Geochim Cosmochim Acta, 1981, 45, 1173-1180.

9. Rubinstein, I. and Strausz, O.P. Geochim. Cosmochim Acta, 1979, 1387-1392.

10. Kimble, B.J., Maxwell, J.R., Philip, R.P, Eglinton, G., Albrecht, P., Ensminger, A., Arpino, P., and Ourisson, G. Geochim. Cosmichim. Acta, 1974, 38, 1165-1181.

11. Henderson, W., Wollrab, V., Eglinton, G. Advan. Org. Geochem. , Proc. Int. Meet., 4th, 1968, (1969), 181-207.

12. Allan, J., Bjorory, M., Douglas, A.G. Advan. Org. Geochem., Proc. Inst. Meet., 7th, 1975, (1977), 633-654.

13. Ekweozor, C.M., Okogun, J.I., Ekong, D.E.U., and Maxwell, J.R. Chem. Geol. 1979, 27, 11-28.

14. Budzikiewicz, H., Wilson, J.M., Djerassi, C.D. J. Am. Chem. Soc., 1963, 85, 3688-3699.

15. Ensminger, A., Van Dorsselaer, A., Spyckerelle, Ch., Albrecht, P., Ourrison, G. Adv. Org. Geochem., Proc. Int. Meet., 6th, 1974, (1976), 245-260.

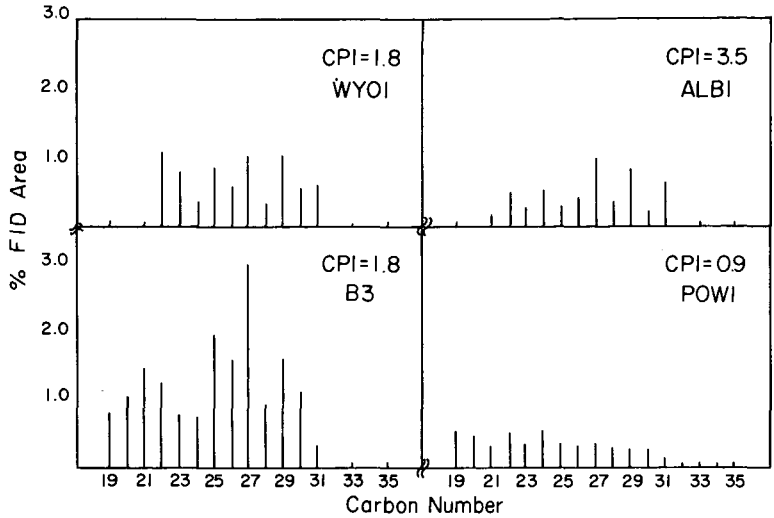

FIGURE 1. Alkane distribution in coal extracts.

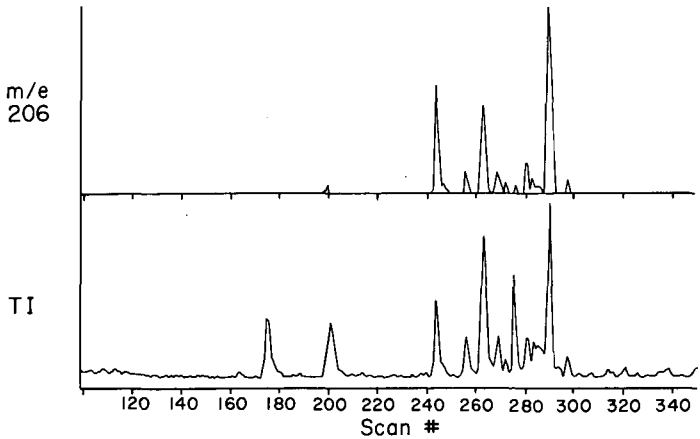

FIGURE 2. m/e 206 selected ion scan for sesquiterpenes and total ion current chromatogram, WY01 CHX extract.

THE ORGANIC CONSTITUTION OF WILCOX LIGNITE

N. Mallya, R.A. Zingaro, R.D. Macfarlane and J.H. Zoeller, Jr.

Department of Chemistry, Texas A&M University,
College Station, Texas 77843

The distribution of functional groups in low rank coals has been the subject of a body of investigations [summarized by Meyers (1982) and Spiro and Kosky (1982)] oriented towards a description of the kinetics and mechanism of thermal conversion processes. Use of the new technique of Californium-252 Plasma Desorption Mass Spectrometry (CFPDMS) as a probe to the structural features of coal have been described by Lytle, Tingey and Macfarlane (1982). The interpretation of CFPDMS spectra has necessitated a functional group characterization of the coal substrate by conventional spectroscopic and chemical techniques. CFPDMS requires the use of organic soluble fractions, and we have utilized DMSO extracts as they seem quite representative of the organic functionalities present. Dry Wilcox Lignite (WL) and some of its solubility fractions have been so characterized, including its DMSO solubles (SD), DMSO insolubles (ID), humic acids (HA), a sample demineralized (DM) by the method of Bishop and Ward (1958), the DMSO extract of this (SDM), and the insoluble residue (IDM). The coal sample used was obtained from a drill core near Rockdale, Texas.

Extraction of WL with DMSO for 24 hours at room temperature gives a 20% yield of extract. Humic acids were obtained by aqueous NaOH extraction and precipitation with HCl. Removal of residual DMSO in the solubles and insolubles can be accomplished by HI treatment with subsequent removal of dimethyl sulfide and HI, but at the cost of some iodine incorporation, ether cleavage, and mineral matter loss.

Acidic Group Titration

Titration for carboxylic acid content, (COOH), were carried out on WL, SD, DM, and SDM according to the methods of Schafer (1970a, 1970b); total acidity was determined on SDM and IDM. The results are reported on a daf basis in Table 1. An enrichment in (COOH) in the DMSO extracts of Wilcox lignite and the demineralized lignite amounts to 0.16 and 0.4 meg(COOM)/g respectively. Carboxylate bound cation content (COOM) is estimated from

$$\text{meq(COOM)/g} = (\text{COOH})_{\text{Demineralized}} - (\text{COOH})_{\text{Dry}}$$

Thus the bound cation content of WL and SD is some 1.5 and 1.8 meq(COOM)/g respectively. From the total acidity data, the concentration of hydroxyl and pyrrole hydrogen (OH,> NH) is estimated from

$$(\text{OH},> \text{NH}) = \text{total acidity} - (\text{COOH})$$

For the demineralized samples, DM and SDM, this amounts to 4.9 and 5.0 meq(OH, > NH)/g.

Nuclear Magnetic Resonance

Solid state C 13 NMRCPMS spectra for selected solubility fractions were obtained by the NMR Center at Colorado State University. Aromaticities derived from the spectra shown in Figure 1 for WL, ID, SD, and HA are 0.53 0.55, 0.52, and 0.72. The higher aromaticity of HA is due to both the enhanced height of the 123 ppm absorption due to the truly aromatic carbons, and to the profusion of carboxylates and aromatic oxygen functions in the skirt downfield of 150 ppm.

Proton NMR of SD in d_6-DMSO exhibits the proton populations shown in Table 2. The chemical shift of hydrogen attached to, or alpha to, oxygen atoms is not at all clear. What is apparent is that the high oxygen content

of this fraction gives rise to peaks in the 3.0-4.0 ppm region of the proton NMR spectrum.

Oxygen bound carbon also accounts for absorption in the downfield flanks of both aromatic and aliphatic peaks in the carbon 13 NMR spectra. Use of shift reagents (Shue and Yen (1983)) is under study in identifying the functionalities involved.

FOURIER TRANSFORM INFRARED SPECTROSCOPY (FTIR)

FTIR spectra of WL, ID, SD and HA were obtained on a Digilab 20C spectrometer in KBr discs. Although grossly similar in appearance, the spectra reveal some notable differences. Aliphatic absorptions at 2825 and 2920 cm^{-1} appear in all the spectra, but the 2825 cm^{-1} peak is much more intense in WL and ID. SD exhibits a prominent band at 2970 cm^{-1}, absent in the others. The carbonyl absorption at 1700 cm^{-1} appears as a shoulder in WL and ID, but is nearly as intense as the coal band (1600 cm^{-1}) in SD and HA. SD shows a pair of intense bands at 1260 and 1010 cm^{-1}, tentatively assigned to the asymmetric and symmetric aryl alkyl ether C-O-C stretch. Both bands are small in HA. In WL and ID, the 1260 cm^{-1} absorption is small, and the 1010 cm^{-1} absorption is masked by the kaolinite doublet at 1010 and 1035 cm^{-1}. Of the aromatic out of plane bending modes, only the 860 cm^{-1} band (isolated hydrogen) is present in all the fractions. The diminuitive aromatic C-H stretching band (3000-3100 cm^{-1}) in all the fractions, and the low population of aromatic protons (15.3%) seen in the ^{1}H-NMR spectrum of SD, suggests that the aromatic moieties are sparse and highly substituted. An unidentified absorption at 800 cm^{-1} appears in all the spectra, but is quite intense in SD.

Pertrifluoroacetic Acid Oxidation (PTFA)

The PTFA reaction described by Deno (1979) has been reinvestigated by Hessley et al (1982) in the analysis of Wyodak coal. In our laboratory, that procedure has led to low and variable product yields when applied to Wilcox lignite. Using a chloroform cosolvent during the oxidation moderates the degradation of aliphatic reaction products. This modification was developed by Lawrence Shadle at Pennsylvania State University. Wilcox lignite yields one hundred methyl esters, as detected by GC/MS, of which fifty comprise over 90% of the product. Fragmentation patterns indicate that the majority of the products are methyl esters of branched and napthenic hydrocarbons in the molecular weight range of 200 to 400. Methyl laurate is prominent among the straight chain esters present. Aromatic esters and oxirane carboxylates have not been detected among the products. Proton NMR of the crude acids of WL, SD, ID and HA discloses the presence of variable amounts of C_2 to C_5 mono- and dicarboxylic acids. No aromatic absorptions are seen in these spectra, with the notable exception of a 7.3 ppm absorption from SD.

Californium Plasma Desorption Mass Spectrometry (CFPDMS)

In the CFPDMS experiment described by Macfarlane and Torgerson (1976), a fission fragment of Cf-252 impinges on a thin film of substrate, forming high molecular weight ions whose mass is measured by a TOF mass spectrometer. Collision results in a localized hot spot for one picosecond, reaching temperatures of some 10^4 $\underline{o}$ K. Extracts of Wilcox lignite typically show positive and negative ions in clusters in the mass range of m/z 400 to 800. Isolated clusters of peaks are seen at low signal intensity up to m/z 2000. Although identification of these peaks is only tentative at this time, one of the

fragments does behave as a carboxylate functionality. In the positive ion spectrum of SD, peaks at m/z 646, 668 and 684 occur in a ratio of 8:5:1. The negative ion spectrum exhibits a peak at m/z 644. By analogy with the behavior of known carboxylic acids and their salts, these peaks correspond to structures $RCOOHH^+$, $RCOOHNa^+$, $RCOOHK^+$ and $RCOO^-$ respectively. The positive ion peaks at m/z 645 and 668 are also seen in the spectrum of HA.

Functional Description of Wilcox Lignite

On the basis of the ultimate analysis of Wilcox lignite, the organic constitution can be formulated as $C_{100}H_{76}O_{21}NS$. The titration data indicates 0.6 (COOH)/g., 1.6 meq(COOM)/g., and 4.9 meg.(OH, > NH)/g. In the C_{100} formulation, this corresponds to one carboxylic acid, three carboxylate salts, six hydroxyls and one pyrrole. The remaining seven oxygen atoms are semiarbitrarily distributed among two aryl alkyl ethers, three quinone carbonyls and one ester. By this accounting, eight of the carbons in the C_{100} formulation appear in the downfield skirt of the aromatic C-13 NMR absorption. From this we project forty eight aromatic carbons (not bound to oxygen) and forty three aliphatic carbons. Hydrogen atoms not bound to heteroatoms are assigned according to their integrated populations in the NMR spectrum of SD. Table 3 compiles this distribution within the C_{100} formulation.

Acknowledgements

Support for this project was provided by the Gas Research Institute and the Center for Energy and Mineral Resources. Carbon 13 NMR spectra were obtained by Dr. Bruce Hawkins at the NMR Center at Colorado State University. We thank Lawrence Shadle of the Pennsylvania State University for suggesting his modified procedure for the pertrifluoracetic acid oxidation.

References

Bishop, M. and Ward, D.L. (1958) "The Direct Determination of Mineral Matter in Coal": Fuel 37, 191.

Deno, N.C., Griegger, B.A., Jones, A.D., Rakitsky, W.G. and Stroud, S.G. (1979) "Coal Structure and Coal Liquefaction"; Final Report to Electric Power Research Institute from Pennsylvania State University, AF-960, RP-779-16.

Hesslly, R.K., Benjamin, B.M. and Larsen, J.W. (1982) "Deno Oxidation. Isolation of High Molecular Weight Aliphatic Material from Coals and Further Model Compound Studies"; Fuel 61, 1085.

Lytle, J.M. Tingey, G.L. and Macfarlane, R.D. (1982) "Californium-252 Plasma Desorption Mass Spectrometry of Solid Coal": Anal. Chem. 54, 1881.

Macfarlane, R.D. and Torgerson, D.F. (1976) "^{252}Californium Plasma Desorption Time of Flight Mass Spectrometry": Int. J. of Mass Spec. and Ion Physics.

Meyers, R.A. (1982) "Coal Structure": Academic Press, New York.

Schafer, H.N.S. (1970a) "Carboxyl Groups and Ion Exchange in Low Rank Coals": Fuel 49, 197.

Schafer, H.N.S. (1970b) " Determination of Total Acidity of Low Rank Coals": Fuel 49, 271.

Spiro, C.L. and Kosky, P.G. (1982) "Space Filling Models for Coal. 2. Extension to Coals of Various Ranks": Fuel 61, 1080.

Shue, F.F. and Yen, T.F. (1983) "Application of Lanthanide NMR Shift Reagents for Functional Group Studies of Shale Bitumen Asphaltenes" Fuel 62, 127.

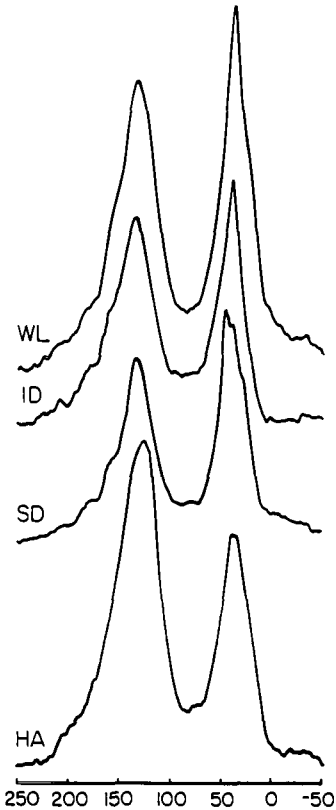

Figure 1. ^{13}NMR CP/MAS Spectra of Wilcox Lignite (WL), its DMSO Insolubles (ID), DMSO Solubles (SD) and Humic Acids (HA). Scale is in ppm.

Table 1. Acidic Group Concentration of Wilcox Lignite Fractions (meq/g., daf)

Sample	(COOH)	Total Acidity
Wilcox Lignite, (WL)	.55	---
DMSO Solubles of WL, (SD)	.71	---
Demineralized WL, (DM)	2.1	7.0
DMSO Solubles of DM, (SDM)	2.5	7.5

Table 2. Proton Population (Area %) in Wilcox Lignite DMSO Solubles, by H-NMR

Proton Type	δ(ppm)	%
H(AR)	4.5-9.0	15.3
H(α2)	3.3-4.5	14.2
H(α1)	2.0-3.3	24.0
H(N)	1.5-2.0	12.0
H(β)	1.0-1.5	20.8
H(γ)	0.5-1.0	13.7

Table 3. Accounting of Functional Groups and Atoms in the $C_{100}H_{76}O_{21}NSM_3$ Formulation of Wilcox Lignite Organic Matter. M = Na, Ca, etc.

Group	Population in the C_{100} Formulation	Atoms Present in Specified Groups					
		C	H	O	N	S	M
-COOH	1	1	1	2			
-COOX	3	3		6			3
-OH	6		6	6			
>N-H	1		1		1		
R-O-Ar	2			2			
>C=O	3	3		3			
RCOOR	1	1		2			
Aromatic C	49	49					
Aliphatic C	43	43					
H(AR)	10.4		10				
H(α2)	9.9		10				
H(α1)	16.3		16				
H(N)	8.2		8				
H(β)	14.1		14				
H(γ)	9.3		10				
Thiophene(?)							

Table 4. Analyses* of Wilcox Lignite and its Solubility Fractions (% Dry Basis).

Sample	C	H	O	N	S	Halogen	Ash
WL	62.75	4.45	19.38	1.28	1.32	0.83	14.16
SD	68.38	5.17	18.22	1.41	1.80	1.04	2.98
ID	64.89	4.67	17.92	1.28	1.50	1.06	8.09
HA	66.83	4.02	23.17	1.41	2.54	0.88	1.26
DM	70.49	5.01	19.57	1.48	1.97	0.78	0.23

*Huffman Laboratories, Inc.

ANALYSIS OF THE INORGANIC CONSTITUENTS IN LOW-RANK COALS

G. P. Huffman and F. E. Huggins

U.S. Steel Corporation, Research Laboratory
125 Jamison Lane, Monroeville, PA 15146

Introduction

In recent years, numerous modern analytical techniques have been applied to the analysis of the inorganic constituents in coal. At the U.S. Steel Research Laboratory, Mossbauer spectroscopy and computer-controlled scanning electron microscopy have been emphasized(1-5). With the advent of very intense synchrotron radiation sources, the technique of extended X-ray absorption fine structure (EXAFS) spectroscopy has been applied in many areas of materials science, and several very recent articles on EXAFS studies of the inorganic constituents of coal have appeared(6-8). For the most part, previously published work has reported investigations of bituminous coals by these three techniques. In the current article, we present some examples of the analysis of the inorganic constituents of lower-rank coals, principally lignites, by these methods. Although the suite of low-rank coals investigated is rather limited, some distinct differences between the inorganic phase distributions in these coals and those in bituminous coals are apparent.

Experimental

Mossbauer spectroscopy is a spectroscopy based on the resonant emission and absorption of low-energy nuclear gamma rays. The ^{57}Fe nucleus exhibits the best Mossbauer properties of all isotopes for which the Mossbauer effect has been observed, and ^{57}Fe Mossbauer spectroscopy is perhaps the best method available for quantitative analysis of the iron-bearing phases in complex, multiphase samples. As discussed in recent review articles(2,9,10) every iron-bearing compound exhibits a characteristic Mossbauer absorption spectrum, and the percentage of the total iron contained in each phase can be determined from absorption peak areas. Detailed descriptions of the Mossbauer spectrometer and data analysis programs used in this laboratory, and discussion of the physical basis of the Mossbauer technique are given elsewhere(10).

The computer-controlled scanning electron microscope (CCSEM) developed in this laboratory consists of an SEM interfaced by minicomputer to a beam-control unit and an energy dispersive X-ray analysis system. Detailed descriptions of this instrument and its use in the determination of coal mineralogy and other applications are given elsewhere(3,11). Briefly, the beam is stepped across the sample in a coarse grid pattern, with typically 300 x 300 grid points covering the field of view. At each point, the backscattered electron intensity is sampled, and the minicomputer decides whether or not the beam is on a particle. Once a particle is identified, the grid density is increased to 2048 x 2048 and the area of the particle is measured. The beam-control unit then places the electron beam back

at the center of the particle and an energy dispersive X-ray spectrum is collected. Each particle is then placed into one of up to 30 categories (minerals, compounds, etc.) on the basis of the chemistry indicated by its X-ray emission spectrum, and approximate weight percentages of all categories are calculated. CCSEM is capable of measuring the size and chemical composition of up to 1000 particles per hour for many kinds of particulate samples.

EXAFS spectroscopy examines the oscillatory fine structure above the absorption edge in the X-ray absorption spectrum of a particular element. These oscillations arise from interference between the outgoing photoelectron wave and scattered waves produced by interaction of the photoelectrons with neighboring atoms. As discussed elsewhere (12,13), Fourier transform techniques can be used to extract from these oscillations information about the bond distances, coordination numbers, and types of ligands surrounding the absorbing element. Additional information about the valence or electronic state of the absorbing ion and the ligand symmetry can be obtained from examining the X-ray absorption near-edge spectra, or XANES, in the energy region very close to the absorption edge (within approximately $\pm$20-30 eV). Such XANES spectra frequently provide characteristic fingerprints for different types of ligand bonding to an absorbing ion(6,7,14,15).

The X-ray absorption spectra of calcium-containing coals and reference compounds discussed in this paper were recorded at the Stanford Synchrotron Radiation Laboratory (SSRL) during a dedicated run of the Stanford Positron-Electron Acceleration Ring at an electron energy of 3.0 GeV. The calcium K-edge occurs at 4038 eV and data were collected from 3800 to 5000 eV, using a double Si (111) monochromator and a fluorescence detector similar to that of Stearn and Heald(16). A more detailed discussion of this work will appear elsewhere(17).

The samples examined were predominantly lignites from the Pust seam in Montana. However, data for two North Dakota lignites, for slagging and fouling deposits produced by those lignites, and for several subbituminous coals are also included.

Results and Discussion

Mossbauer spectroscopy results for all samples investigated are summarized in Table I. The percentages of the total sample iron contained in each of the iron-bearing minerals identified are given in columns 1 to 4, and the weight percentage of pyritic sulfur, determined from the pyrite absorption peak areas as discussed elsewhere(1), are given in column 5. It is seen that pyrite and minerals (iron sulfates and iron oxyhydroxide) that are probably derived from pyrite by weathering are the only iron-bearing species in these low-rank coals. Notably absent are contributions from iron-bearing clays and siderite which are common constituents of bituminous coals(1,2). Pyrite and iron oxyhydroxide are difficult to separate with room temperature Mossbauer spectroscopy(18). For example, in Figure 1 are shown the room temperature and 77 K spectra obtained from the Pust seam, C, lignite, which had been stored for several years prior to measurement. Although it is quite difficult to determine the relative amounts of pyrite and oxyhydroxide from the room temperature Mossbauer spectrum, the spectral contributions of the two phases are

readily resolved at 77 K.

CCSEM results for the approximate weight percentages of all inorganic phases are given in Table II. Perhaps the most interesting aspect of the CCSEM results for these low-rank coals as compared with similar data for bituminous coals is the abundance of Ca-rich phases. In most cases, these phases are not calcite, but are Ca-enriched macerals in which the Ca is uniformly dispersed throughout the coal, as illustrated by the SEM micrograph in Figure 2. The Ca-enriched macerals appear gray in this inverted backscattered electron image. An energy dispersive X-ray spectrum obtained from an individual maceral is shown on the right. As discussed below, EXAFS data indicate that this calcium is dispersed as salts of carboxylic acids.

The backscattered electron intensity of the Ca-enriched macerals is significantly smaller than that of calcite, and CCSEM can make a distinction, albeit somewhat imprecisely, between Ca-enriched macerals and calcite or other Ca-rich minerals on this basis. However, the CCSEM programs have not been properly calibrated to deal with the case of macerals enriched in an inorganic component such as Ca at this point. Consequently, the percentages indicated in Table II for the Ca-rich category are only a qualitative indication of the relative amounts of this species in the various low-rank coals examined. On the basis of the backscattered electron intensity, it appears that calcium is dispersed throughout the macerals of the lignites that have been examined, and is present partially in dispersed form and partially as calcite in the subbituminous coals. In fresh bituminous coals, calcium is present almost exclusively as calcite(3-5).

For comparison with Tables I and II, Table III gives the range and typical values of the mineral distributions observed in bituminous coals by the CCSEM and Mossbauer techniques, derived from studies of perhaps a hundred different bituminous coal samples in this laboratory. Some obvious differences in mineralogy are apparent. In addition to the difference in calcium dispersion and abundance already noted, it is seen that certain minerals common in bituminous coals, such as Fe-bearing clays (illite and chlorite) and siderite, are virtually absent in the low-rank samples of Tables I and II. Conversely, minerals such as barite ($BaSO_4$), apatite ($Ca_5(PO_4)_3OH$), and other Ca, Sr phosphates, are rather uncommon in bituminous coals.

EXAFS and XANES data for a Ca-rich sample of the Pust seam, A, lignite can be briefly summarized by reference to Figures 3 and 4. Figure 3 shows the XANES of the lignite, Ca acetate, and a fresh bituminious coal from the Pittsburgh seam rich in calcite. The strong similarity between the lignite and calcium acetate spectra is apparent. Similarly, a close similarity is also observed for the XANES of the fresh bituminous coal and that of a calcite standard. Examination of the XANES of several other standard compounds (CaO, $Ca(OH)_2$, and $CaSO_4 \cdot 2H_2O$) showed that none of these phases were present in detectable amounts in either coal. The strong similarity of the XANES of calcium acetate and that of the lignite is direct evidence that the calcium in this coal is associated with carboxyl groups in the macerals and is not contained in very fine (<0.1 μm) mineral matter.

Mathematical analysis of the EXAFS associated with the nearest-neighbor oxygen shell surrounding the Ca ions in the lignite was

accomplished using programs developed by Sandstrom(13). Briefly, the results indicate that the Ca is coordinated by six oxygens, possibly contributed in part by water molecules, at an average nearest neighbor distance of 2.39 Å. Additionally, the EXAFS data indicate that structural order at distances further from the Ca ions than the first coordination shell is essentially absent in the lignite, implying that the Ca sites are more or less randomly distributed throughout the macerals. This point is well illustrated by phase-shift subtracted Fourier transforms of the EXAFS data, which, as discussed elsewhere (12,13), should bear a reasonably close relationship to the radial distribution functions appropriate for the local environment of the Ca ions. In Figure 4, the magnitude of the phase-shift subtracted Fourier transform, $|F(r)|$, is shown for the lignite sample, calcium acetate, and a calcite-rich bituminous coal from the Pittsburgh seam. It is seen that the $|F(r)|$ curves for calcium acetate and the calcite-rich bituminous coal exhibit maxima corresponding not only to the nearest-neighbor oxygen shell, but also at the approximate locations of more distant calcium neighbor shells. The $|F(r)|$ curve of the lignite exhibits a clear maximum only at the oxygen nearest-neighbor shell distance. It is possible, however, that the small shoulder that appears on the high side of the oxygen shell peak in the lignite $|F(r)|$ curve (at approximately 3.5 Å) could correspond to the initial stages of Ca ion clustering.

Finally, it is noted that XANES and EXAFS spectra obtained from a severely weathered bituminous coal were nearly identical to those obtained from the lignite sample. This indicates that in the weathered coal calcium is also present in a dispersed form in which it is bonded to carboxyl groups in the macerals. A more detailed report of the Ca EXAFS investigation of lignite, fresh and weathered bituminous coal, and Ca reference compounds will appear elsewhere(17).

Analysis of Fouling and Slagging Deposits. It was observed that one of the two North Dakota lignites listed in Tables I and II produced heavy fouling deposits during combustion in a large utility furnace, while little or no difficulty was experienced in firing the other. As seen in Tables I and II, the inorganic phase distributions of these two coals are rather similar. Additionally, CCSEM and Mossbauer analysis of boiler-wall slag deposits produced by both coals gave rather similar results. A typical Mossbauer spectrum obtained from a boiler wall deposit (wall temperature ~1250°C) is shown in Figure 5, and a summary of the approximate phase distributions of the wall slag deposits produced by both coals is given in the inset. From the observed phases, it appears that the CaO-SiO_2-Fe_2O_3 phase diagram plays a key role in determining the slagging behavior of these coals. CCSEM analyses of fouling deposits produced by the two lignites are given in Table IV. It is seen that the only significant difference between the light and heavy deposits is the presence of an alkali sulfate mixture, containing Na, K, and Ca sulfates, in the latter. It is well known that alkali sulfates can react strongly with metal surfaces to produce alkali-iron sulfate mixtures that are partially molten over the temperature range from approximately 700 to 1100°C, causing severe fouling and corrosion problems(19).

Conclusions

In this paper, we have presented some examples of the usefulness of three techniques, Mossbauer spectroscopy, CCSEM, and EXAFS in the analysis of low-rank coals and combustion products of low-rank coals. Points of interest regarding the inorganic constituents of these coals include the high abundance of calcium bonded to carboxyl groups and dispersed throughout the macerals, the low abundance of illite, siderite, and calcite, and the presence of significant amounts of accessory minerals such as barite, apatite, and other phosphates. Areas that merit further investigation by these techniques include the analysis of fouling and slagging deposits, and structural studies of inorganic elements such as calcium that are dispersed through and bonded to the coal macerals.

Acknowledgments

The EXAFS experiments discussed in this paper were conducted in collaboration with F.W. Lytle and R.B. Greegor of the Boeing Company at the Stanford Synchrotron Radiation Laboratory, which is supported by the National Science Foundation and the Department of Energy.

References

1. Huffman, G.P., Huggins, F.E., Fuel, 1978, 57, 592-604.
2. Huggins, F.E., Huffman, G.P., Anal. Methods for Coal and Coal Products, Clarence Karr, Jr., Ed.; Academic: New York, 1979, Vol. 3, 371-423.
3. Huggins, F.E., Kosmack, D.A., Huffman, G.P., Lee, R.J., SEM/1980/I, 531-540, SEM Inc., AMF O'Hare (Chicago), IL (1980).
4. Huffman, G.P., Huggins, F.E., Lee, R.J., Proc. Int. Conference on Coal Science, Dusseldorf, 1981, 835-840, Verlag Glückauf GmbH, Essen, Germany (1981).
5. Huggins, F.E., Huffman, G.P., Lee, R.J., Coal and Coal Products: Analytical Characterization Techniques, E.L. Fuller, Jr., Ed.; ACS Symposium Series No. 205, 1982, 239-258, Amer. Chem. Soc., Washington, D.C.
6. Maylotte, D.H., Wong, J., St. Peters, R.L., Lytle, F.W., Greegor, R.B., Science, 1981, 214, 554.
7. Sandstrom, D.R., Filby, R.H., Lytle, F.W., Greegor, R.B., Fuel, 1982, 61, 195.
8. Hussain, Z., Barton, J.J., Umbach, E., Shirley, D.A., SSRL Activity Report, May 1981, A. Bienenstock and H. Winick, Eds.; p. VII-102.
9. Huffman, G.P., Huggins, F.E., Mossbauer Spectroscopy and Its Chemical Applications, J.G. Stevens and G.K. Shenoy, Eds.; Advances in Chemistry Series No. 194, 1981, 265-301, Amer. Chem. Soc., Washington, D.C.
10. Huffman, G.P., Huggins, F.E., Physics in the Steel Industry, F.C. Schwerer, Ed.; AIP Conf. Proc. No. 84, Amer. Inst. Physics, 1982, 149-201.

11. Lee, R.J., Kelly, J.F., SEM/1980/I, 303-310, SEM Inc., AMF O'Hare (Chicago), IL, (1980).
12. Lee, P.A., Citrin, P.H., Eisenberger, P., Kincaid, B.M., Rev. Mod. Phys., 1981, 53, 769.
13. Sandstrom, D.R., Proc. Workshop on EXAFS Analysis of Disordered Systems, Parma, Italy, 1981, to be published in Nuovo Cimento B.
14. Kutzler, F.W., Natoli, C.R., Misemer, D.K., Doniack, S., Hodgson, K.O., J. Chem. Phys., 1980, 73, 3274-88.
15. Bair, R.A., Goddard, W.A., Phys. Rev. B, 1980, 22, 2767-76.
16. Stearn, E.A., Heald, S., Rev. Sci. Instrum., 1979, 50, 1579.
17. Huggins, F.E., Huffman, G.P., Lytle, F.W., Greegor, R.B., "An EXAFS Investigation of Calcium in Coal," to be published in Proc. Int. Conference on Coal Science, Pittsburgh, 1983.
18. Huggins, F.E., Huffman, G.P., Kosmack, D.A., Lowenhaupt, D.E., Int. J. Coal Geology, 1980, 1, 75-81.
19. Reid, W.T., Chemistry of Coal Utilization, 1983, M.A. Elliot, Ed.; Suppl. Vol., Chapt. 21, 1389-1445, John Wiley & Sons, Inc.

TABLE I

Mossbauer Results For Low-Rank Coals

Sample	Percent of Total Iron Contained in: Pyrite	Jarosite	Ferrous Sulfate	Iron Oxy-hydroxide	Wt.% of Pyritic Sulfur
Pust seam, A-3	100	-	-	-	0.30
Pust seam, A-4	92	7	1	-	2.26
Pust seam, A-6	91	9	-	-	0.15
Pust seam, A-7	∿100+	-	-	-	≲0.03+
Pust seam, B-3	100	-	-	-	0.06
Pust seam, B-5	100	-	-	-	0.05
Pust seam, B-7	100	-	-	-	0.09
Pust seam, C	43	26	-	31	0.29
N.Dakota lignite, heavy fouling	91	6	2	-	0.50
N.Dakota lignite, light fouling	95	5	-	-	0.38
Rosebud subbituminous	65	16	19	-	0.15
Colstrip subbituminous	81	19	-	-	0.27

+Very weak spectrum; sample contained only 0.07% iron.

TABLE II

CCSEM Results for Low-Rank Coals (approximate weight percentages)

Sample	Quartz	Kaolinite	Mixed Silicates	Illite	Pyrite	Fe Sulfates	Fe-rich	Ca-rich+	Barite	Apatite	Other Phases Phase	Other Phases Percent
Pust seam, A-3	7	45	8	-	1	-	6	26	1	-	Montmorillonite	1
											Rutile	1
Pust seam, A-4	12	20	3	-	26	4	7	15	7	2	Fe-Ca-S	3
Pust seam, A-6	7	27	-	-	1	-	-	51	5	3	-	-
Pust seam, A-7	7	35	3	-	1	-	-	49	3	-	-	-
Pust seam, B-3	10	43	13	1	1	-	-	22	3	3	Montmorillonite	4
Pust Seam, B-5	14	38	3	-	1	-	-	38	5	-	Rutile	1
Pust seam, B-7	16	38	2	-	5	-	-	27	5	-	Ca-Fe-S	1
Pust seam, C	9	29	5	1	4	5	14	13	4	-	Ca-Fe	6
											Ca-Sr-Al-P*	4
											Jarosite	2
N.Dakota lighite, heavy fouling	24	13	20	3	19	1	1	14++	-	-	Montmorillonite	1
N.Dakota lignite, light fouling	28	16	13	2	10	-	2	23++	-	-	Montmorillonite	1
Rosebud, subbituminous	23	36	6	2	6	2	3	8	1	1	Ca-Sr-Al-P*	6
											Montmorillonite	1
											Rutile	1
Eveleth, subbituminous	18	23	22	12	4	-	3	7	-	1	Ca-Sr-Al-P*	8
Colstrip, subbituminous	22	25	6	3	8	-	3	29	-	-	Gypsum	4
Absaloka subbituminous	56	22	8	-	3	-	-	5	-	-	Rutile	3

+As discussed in the text, percentages given for the Ca-rich category are not quantitative.
*Minerals denoted by Ca-Sr-Al-P are probably crandallite $(Ca,Sr)Al_3(PO_4)_2(OH)_5H_2O$.
++Macerals enriched in Ca and S, with Ca/S ratios ∿1/1 to 6/1; some gypsum is probable.

TABLE III

Mineralogy of Bituminous Coals

CCSEM Analysis, Wt.% of Mineral Matter			Mossbauer Analysis, % of Total Sample Iron		
Mineral	Range	Typical	Mineral	Range	Typical
Quartz	5-44	18	Pyrite	25-100	62
Kaolinite	9-60	32	Ferrous Clay	0-56	18
Illite	2-29	14	Siderite/Ankerite	0-58	9
Chlorite	0-15	2	Ferrous Sulfate	0-18	3
Mixed Silicates	0-31	17	Jarosite	0-21	4
Pyrite	1-27	8	Wt.% Pyritic Sulfur*	0.08-1.51	0.35
Calcite/Dolomite	0-14	3			
Siderite/Ankerite	0-11	2			
Other	0-12	4			

*Determined by method of Ref. 1.

TABLE IV

CCSEM Results For Fouling Deposits, 800-1000°C

Species	Heavy (wt%)	Light (wt%)
Al, Si-rich	5	5
Quartz	3	8
Hematite	2	3
Ca-rich	10	7
Mg-Ca	3	5
Ca Ferrite	2	<1
Ca-Si-Fe Glass	21	22
Ca-Si + Glass	40	40
Alkali Sulfate	2	0
$CaSO_4$ + Alkali Sulfate	4	6 $CaSO_4$ only
Other	8	4

Alkali Sulfate - Na/Ca/K = 1.0/0.5/0.1

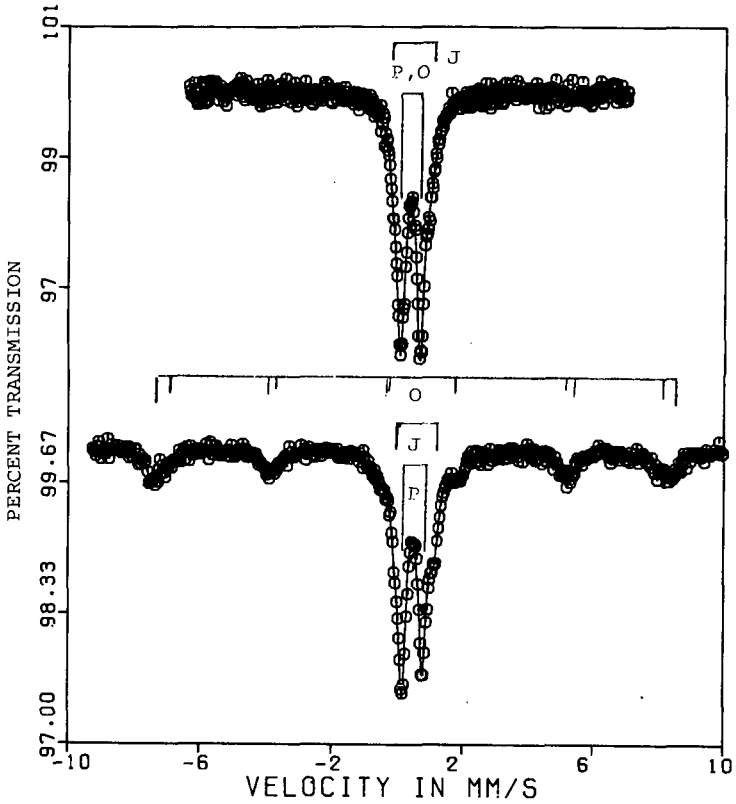

Fig. 1 Mossbauer spectra of the Pust seam, C, lignite. Pyrite (P), jarosite (J), and iron oxyhydroxide (O) are indicated.

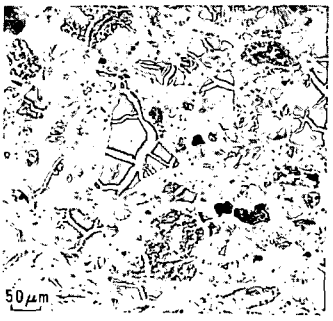

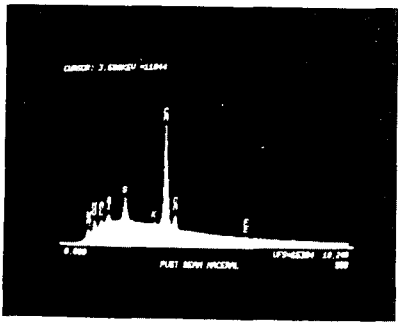

Fig. 2 **BACK-SCATTERED ELECTRON IMAGE** **ENERGY-DISPERSIVE X-RAY SPECTRUM**

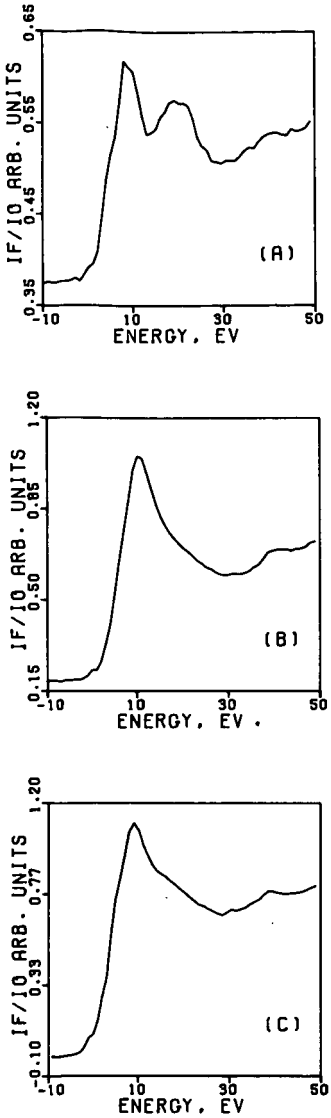

Fig. 3 XANES of: (A) calcite-rich bituminous coal; (B) the Pust seam lignite; (C) calcium acetate.

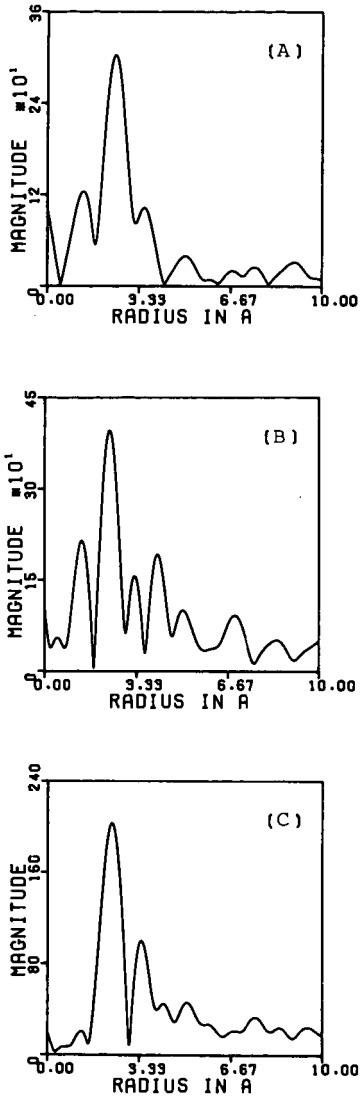

Fig. 4 Magnitudes of the phase-shift subtracted Fourier transform of: (A) the Pust seam lignite; (B) calcite-rich bituminous coal; (C) calcium acetate.

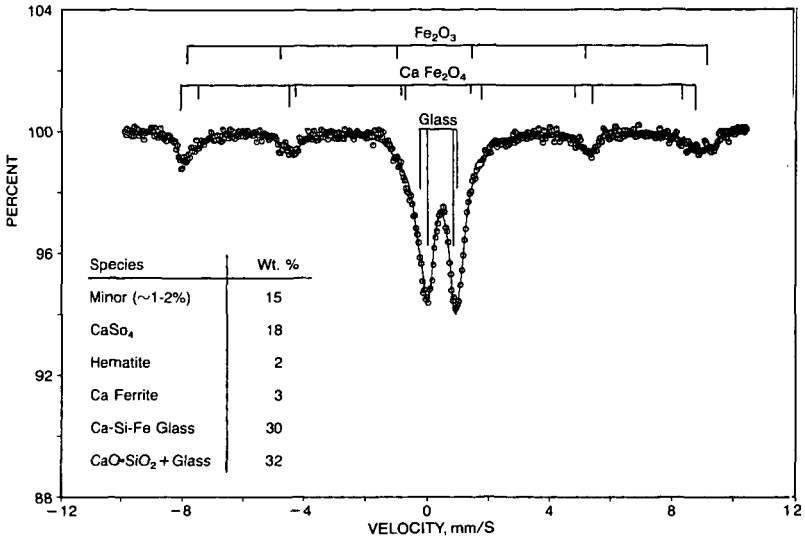

Fig. 5 Mossbauer spectrum of boiler-wall slag deposit. The approximate phase distribution determined from CCSEM and Mossbauer results is shown in the inset.

GEOCHEMICAL VARIATION OF INORGANIC CONSTITUENTS IN A NORTH DAKOTA LIGNITE

Frank R. Karner, Steven A. Benson, Harold H. Schobert, and Robin G. Roaldson

U.S. Department of Energy
Grand Forks Energy Technology Center
Box 8213, University Station
Grand Forks, North Dakota 58202

INTRODUCTION

This paper summarizes information on the distribution of major and trace elements in a stratigraphic sequence of sedimentary materials in a major lignite producing portion of the Fort Union region of the Northern Great Plains. Previous study of the geochemical variation in these sediments is summarized in the literature (1,2). Major patterns of elemental variations in lignite are related to factors affecting accumulation of both organic and inorganic components during deposition and aqueous precipitation, dissolution, and ion-exchange processes after deposition. Variations in overburden and underclay are dependent upon specific clay mineral variation and relative abundances of quartz- and feldspar-rich silt fractions versus clay mineral-rich fractions of the sediment, as well as upon local variation in carbonates and other elements.

GEOLOGIC RELATIONSHIPS

The Center mine, Oliver County, North Dakota is in the Fort Union Coal Region, which is one of the largest reserves of lignite in the world. The Fort Union Coal Region lies within the North Great Plains Coal Province and encompasses portions of north-central United States and south-central Canada, including both the subbituminous coals of the northern Powder River Basin and the lignites of the Williston Basin (2), a broad structural and sedimentary intracratonic basin that extends over an area of about 40,000 km^2. Over 4600 m of sedimentary rocks overlie the Williston Basin in its deepest portions of McKenzie County, North Dakota.

Important lignite beds of the Fort Union Region occur within Ludlow, Slope, Bullion Creek, and Sentinel Butte Formations of the Paleocene Fort Union Group.

The Sentinel Butte Formation has been described as a "lignite-bearing, nonmarine, Paleocene unit whose outcrops are somber gray and brown" (3). Rock types include sandstone, siltstone, claystone, lignite, and limestone. The lignite beds typically vary from less than 1 meter to 3-5 meters in thickness (4). The Oliver-Mercer County district is located in eastern Mercer and northeastern Oliver Counties with the principal bed, the Hagel bed, ranging in thickness from 3 to 4 meters at the Center Mine (4).

The sampling program (5) was designed to obtain stratigraphically controlled specimens for a study of the character, distribution, and origin of the inorganic constituents in lignite. The objectives of the field sampling were to obtain:

1. Incremental samples of underclay, lignite, and overburden at each mine.

2. Duplicate vertical sections and lateral samples to test variation.

3. Samples of specific beds, lenses, fault zones, mineral concentrations, or other areas of unusual aspect.

Lignite, lignite overburden, and underclay were collected from a vertical section on the high walls at the Center mine. Figure 1 illustrates the stratigraphic sections and sample locations. Choice of sections to be sampled was based on accessibility to areas in the mines due to mining activity.

To minimize contamination, material from slope wash and mining activity was first removed from each section. In order to obtain samples of underclay it was necessary to dig down at the base of the lowest lignite, since in surface mining the underclay is normally left undisturbed. Once the section to be sampled was exposed it was measured and marked at 30 cm intervals (through the lignite, starting at the base) and then at additive increments of 1 m through the extent of the overburden in the mine cut.

Samples were collected (Table 1) over a 10 cm by 50 cm area at the bottom of each marked interval of the measured section. Samples were collected at all contacts between lithologic units when the contact was found and at points of interest (for example: iron sulfide-coated joints, clay partings, sand lenses, concretions). All samples were stored in plastic bags inside cardboard cartons.

TABLE 1

SAMPLE DESCRIPTIONS AND LOCATION, CENTER MINE

Sample #	Height, meters*	Description
1-1-D	-0.05	Underclay, gray
1-2-D	0.05	Black lignite, very hard
1-3-D	0.40	Black lignite, very hard
1-4-D	0.70	Black lignite, very hard
1-5-D	1.00	Black lignite, very hard
1-6-D	1.25	Black lignite, very hard
1-7-D	1.50	Black lignite, very hard
1-8-D	1.70	Black lignite, very hard
1-9-D	1.90	Black lignite, very hard
1-10-D	2.10	Black lignite, very hard
1-11-D	2.45	Black-brown lignite, soft and fractured, top of seam
1-12-D	2.55	Dark gray organic rich silt
1-13-D	3.65	Gray sand, fine-grained, fossilized
1-14-D	4.15	Gray sand with a clay matrix
1-15-D	4.50	Concretion zone
1-16-D	4.75	Brown lignite, very soft, silty
1-17-D	4.85	Gray-green clay
1-18-D	5.15	Brown lignite, very soft, silty
1-19-D	5.45	Brown lignite, top of seam
1-20-D	5.60	Gray silty clay
1-21-D	5.75	Brown lignite with silty interbedded layers
1-22-D	5.85	Gray siltstone
1-23-D	6.45	Gray siltstone, 1-2 mm laminae

*Height from base of major lignite seam.

GEOLOGICAL CHARACTERISTICS

The Center mine lignite is a black to brownish black coal that slacks rapidly on exposure to the atmosphere and typically contains dark carbonaceous clay or grey clay partings (4). The underclay is a grey-green clay with lignite fragments. The overburden is grey fine-grained sediment primarily consisting of clayey silts and silty clays with minor concretionary zones and sands. Logan (6) has described the overburden sequence as the Kinneman Creek interval and has interpreted it to be of lacustrine origin. Generally the early Cenozoic sediments in this region are believed to have been deposited in a coastal complex of stream channel and flood plain, swamp, lake, and delta environment.

INORGANIC CONSTITUENTS

Inorganic constituents in the Sentinel Butte sediments are present as 1) detrital mineral grains and volcanic glass fragments, 2) components of organic debris, 3) authigenic mineral grains and cement, and 4) ions adsorbed by clay and other minerals and organic material (7,8,9,10).

A summary of minerals observed in the Sentinel Butte Formation is given in Table 2 (9). Major original detrital constituents include montmorillonite, quartz, plagioclose, alkali feldspar, biotite, chlorite, volcanic glass and rock fragments. Major minerals formed during deposition and diagenesis by conversion of original detrital constituents consist of montmorillonite, chlorite, and kaolinite. Pyrite, gypsum, hematite, siderite, and calcite (?) formed in post-depositional reducing and oxidizing reactions related to changing conditions of deposition, burial, and groundwater movements.

TABLE 2

INORGANIC CONSTITUENTS IN THE SENTINEL BUTTE FORMATION

Constituent	Overburden	Lignite	Underclay
Alkali feldspars	XX	X	X
Augite		X	
Barite		X	
Biotite	X		
Calcite/Dolomite	XX	X	
Siderite	XX		
Chlorite	XX	X	X
Gypsum		XXX	
Hematite		XX	
Hornblende	X		
Illite	XX	X	X
Kaolinite	XX	XXX	XXX
Magnetite	X		
Montmorillonite	XXX	X	XXX
Muscovite	X		
Plagioclase	XXX	X	X
Pyrite		XX	
Quartz	XXX	XXX	XXX
Volcanic Glass	X		
Rock fragments	XX		

XXX = Abundant
XX = Common
X = Minor

GEOCHEMICAL VARIATION IN OVERBURDEN AND UNDERCLAY

Previous work (7,8) and our current work seeks to relate chemical variations to variations in the original mineral content of the sediments and to variations due to post-depositional mineral reactions.

Overburden sediments are typically silty clays with about 80 pct clay and 20 pct silt. Other sediments include clayey silts and fine sands with varying organic content and calcareous cement. Sideritic concretion zones are present. Clay-rich sediments are enriched in some elements particularly Al, Mg, and Ti. Carbonate-rich sediments are enriched in Ca and Fe (concretionary zones). Sodium shows a tendency to increase downward to a high in organic-rich silty clay, above the lignite. Specific beds, including the underclay, are markedly enriched in potassium, possibly related to high mica content.

EXPERIMENTAL

Samples of coal, overburden, and underclay were dried and analyzed by neutron activation (NAA) and x-ray fluorescence analysis (XRF). NAA analysis was performed by the Nuclear Engineering Department, North Carolina State University. The system description and detection limits for coal and coal fly ash are summarized by Weaver (11). XRF was done at GFETC with an energy dispersive x-ray system. Mineralogy of the overburden and underclay was determined by x-ray diffraction (XRD). The crystalline phases present in the coal were determined by XRD of the low-temperature ash of the coal.

RESULTS AND DISCUSSION

Mineralogy of the Statigraphic Sequence - X-ray diffraction was used to determine the major minerals present in the overburden, underclay, and of the low-temperature ash of the coal. The results are summarized in Figure 2, which illustrates the distribution of minerals throughout the sequence. The most distinct variation in the overburden is the concretion zone, which is a very compact, cemented zone rich in siderite and dolomite. The remaining fractions of the overburden are consistent with varying amounts of quartz, kaolinite, muscovite, and plagioclase.

The bulk mineralogy of the coal also represented in Figure 6 reveals the presence of quartz, calcite, bassonite, kaolinite, and pyrite in varying amounts. Bassonite is possibly a product of organic sulfur fixation with organically bound calcium (12). Pyrite appears to increase with depth in the seam.

Variations of Elements in the Stratigraphic Sequence - The results of the neutron activation and x-ray fluorescence analysis for the stratigraphic sequence are listed in Table 3. Descriptions of the samples are listed in Table 1.

Variation Within Major Coal Seam - The distribution of elements throughout the section sampled in the coal seam can be summarized by four general trends: 1) concentration of elements in the margins; 2) concentration in the lower part of the seam; 3) even distribution; 4) without a clear pattern. These trends can be best examined by plotting or charting them with location in the seam.

The elements which were concentrated at or near the margins of the coal seam included Al, Ti, Fe, Cl, Sc, Cr, Co, Ni, Zn, As, Ru, Ag, Cs, Ba, La, Ce, Sm, and U. An example of a typical distribution is a graph of Zn shown in Figure 3, which illustrates the distribution of zinc throughout the entire stratigraphic sequence.

The elements which are concentrated at the margins of the lignite seam are most likely associated with the detrital constituents, such as finely divided clay min-

TABLE 3

ELEMENTAL ANALYSIS FOR SELECTED MAJOR AND MINOR ELEMENTS, PARTS PER MILLION
(Dry Basis)

ID		Height* M.	Na	Mg	Al	K	Ca	Ti	Fe	Cl	Sc	V	Cr	Mn	Co	Ni	Zn	As
1-1-D	Underclay	-0.05	5332	9534	95268	26788	9605	4052	26761	411	15	137	99	144	5	59	42	4
1-2-D	Lignite	0.05	1518	1736	10200	2153	6247	724	9377	132	6	219	49	39	2	34	25	16
1-3-D	Lignite	0.40	1307	1607	5586	806	5984	246	6685	55	2	25	6	49	2	21	14	20
1-4-D	Lignite	0.70	1398	1677	2595	1000	7658	119	2909	44	1	4	2	69	1	16	10	6
1-5-D	Lignite	1.00	1398	1375	3313	615	6888	323	2326	59	1	22	5	47	1	12	6	6
1-6-D	Lignite	1.25	967	1861	2949	1000	6820	124	1745	55	1	4	1	68	0	13	8	5
1-7-D	Lignite	1.50	1115	2209	6051	1000	6994	298	2182	67	1	16	5	76	1	16	12	8
1-8-D	Lignite	1.70	804	827	1970	1000	4689	78	6128	36	0	1	1	24	1	13	6	31
1-9-D	Lignite	1.90	1006	1979	10813	1104	6330	357	7323	74	3	47	10	61	4	28	19	15
1-10-D	Lignite	2.10	3685	9219	100370	1000	8691	2578	17133	407	11	101	68	100	3	33	34	7
1-11-D	Lignite	2.45	737	1848	6620	1000	7935	191	4070	51	7	12	5	56	1	33	25	21
1-12-D	Overburden	2.55	5814	10564	79761	25718	10564	3119	29506	336	13	138	80	257	11	47	44	8
1-13-D	Overburden	3.65	5331	10921	71239	1000	16988	3393	24822	407	11	116	72	287	11	36	36	3
1-14-D	Overburden	4.15	4461	11465	95029	1000	7838	3540	31466	508	15	170	94	175	15	55	54	3
1-15-D	Overburden	4.50	1422	3673	96920	5000	5824	4320	233070	116	29	138	21	128	1	190	108	2
1-16-D	Lignite	4.75	750	1762	5813	1000	6754	419	28510	113	15	185	34	66	10	46	40	28
1-17-D	Overburden	4.85	5767	10951	96097	30645	7483	4103	30072	428	14	165	93	187	16	49	45	8
1-18-D	Lignite	5.15	718	1652	2512	233	6391	125	3552	43	4	6	4	79	1	25	20	17
1-19-D	Lignite	5.45	609	2208	7230	1000	6560	145	3724	63	3	24	10	108	4	24	18	27
1-20-D	Overburden	5.60	4485	11779	82608	1000	12364	3869	30382	471	14	134	75	424	14	67	47	2
1-21-D	Lignite	5.75	3510	6974	50912	21576	7039	2133	28376	314	11	158	92	242	13	64	37	44
1-22-D	Overburden	5.85	4900	10756	87974	1000	8418	3429	30294	499	14	151	106	387	19	96	46	7
1-23-D	Overburden	6.45	7708	9368	64715	19274	18107	3081	30374	395	13	106	119	436	15	50	38	11

*Height from base of major coal seam.

TABLE 3

(Continued)

ID		Se	Br	Ru	Ag	Cd	Sb	Cs	Ba	La	Ce	Sm	Eu	Yb	Th	U
1-1-D	Underclay	2	1	160	2.48	3	2	5	1132	27	53	3	1	1	10	4
1-2-D	Lignite	2	1	16	1.42	5	19	4	370	9	18	2	1	1	4	5
1-3-D	Lignite	1	3	5	0.83	9	5	1	185	3	9	2	0	0	1	6
1-4-D	Lignite	1	2	3	0.60	5	1	0	64	3	5	1	0	0	0	0
1-5-D	Lignite	1	2	3	0.71	5	2	0	39	3	4	0	0	0	1	1
1-6-D	Lignite	0	2	3	0.49	5	0	0	45	2	3	0	0	0	0	0
1-7-D	Lignite	1	3	3	0.67	4	1	0	66	4	6	1	0	0	1	2
1-8-D	Lignite	0	1	3	0.46	1	1	0	496	1	4	0	0	0	1	0
1-9-D	Lignite	1	1	5	1.12	9	5	1	114	4	8	2	0	1	2	5
1-10-D	Lignite	2	1	119	2.05	5	1	6	745	26	50	2	1	1	11	4
1-11-D	Lignite	1	4	6	1.44	7	4	0	246	5	9	2	0	1	3	4
1-12-D	Overburden	2	1	147	2.57	5	2	4	661	35	58	4	1	2	10	4
1-13-D	Overburden	2	3	107	2.19	5	1	3	673	31	60	3	1	2	11	2
1-14-D	Overburden	2	1	144	3.11	5	2	5	781	32	63	4	1	2	11	3
1-15-D	Overburden	9	3	46	7.14	20	0	0	595	23	6	3	1	3	3	3
1-16-D	Lignite	2	2	9	2.33	18	15	6	179	5	1	3	0	1	2	9
1-17-D	Overburden	2	1	138	2.00	5	2	1	761	32	56	3	1	2	10	3
1-18-D	Lignite	1	3	4	1.09	0	5	1	161	3	6	1	0	1	1	1
1-19-D	Lignite	1	3	4	1.00	4	4	1	95	2	4	1	0	0	2	3
1-20-D	Overburden	2	1	122	2.74	5	1	4	640	29	57	3	1	2	10	2
1-21-D	Lignite	4	3	66	2.21	8	8	4	559	10	36	3	1	2	8	5
1-22-D	Overburden	2	2	131	2.75	2	2	4	911	26	49	3	1	1	9	2
1-23-D	Overburden	1	2	90	2.30	5	2	2	691	29	55	3	1	2	9	2

*Height from base of major coal seam.

erals. The possible associations of trace and minor elements with clays are summarized by Finkelman (13). The elements which have possible affinities to clay and other sedimentary environments in relation to coal seams include Al, Sc, Ti, Cl, Cr, La, Mg, and Fe. A second group of elements, including Fe, Co, Ni, Zn, As, and Ag, may associate in the margins with pyrite or other sulfides. Uranium can be associated with the organic part of the coal but can be associated with a diverse suite of uranium minerals (13). Other elements, such as Ru, Ce, Sm, have not been extensively studied but appear to have an association with detrital minerals.

The elements which have an even distribution include Cd, Mn, Mg, Na, and Ca. As an example, Figure 4 represents the distribution of Ca within the stratigraphic sequence. The majority of these elements are organically bound or associated with authigenic minerals. The elements which are considered to be organically bound include Ca, Na, Mg, and Mn (14). This association would be as the counter ion with the carboxylic acid functional groups of the carbonaceous structure. Calcium, Mg, and Mn may also exist as carbonates which form in the coal during coalification. Calcite ($CaCO_3$), for example, was identified in the low-temperature ash of the coal. Cadmium in other coals has been found associated with sulfides (13). Its inclusion in this group may rather indicate an organic association, at least in this lignite. The calcium and cadmium ions have similar ionic potentials (~ 2) and may therefore behave similarly toward carboxylic groups.

Elements which showed a tendency to concentrate toward the base of the lignite seam are V, K, and Sb. Figure 5 represents this trend by a graph of the distribution of Sb. The increased concentration of K toward the base of the seam is very subtle. Vanadium and Sb increase sharply at the base of the seam. Vanadium has strong organic tendencies (13). Sb has strong chalcophile tendencies (15) so it is possible that Sb is associated with the sulfides.

The elements which reveal no clear pattern of distribution include Se, Br, Cs, Eu, and Yb. Bromine is an example, as illustrated in Figure 6. The probable reason is that low concentrations of these elements are near the detection limits of the analysis and thus may have greater experimental error.

Although the concentrations of rare earth elements are quite low, there is nevertheless a reasonable agreement with the rare earth abundance pattern in sedimentary rocks. This pattern can be seen in Table 4, which compares average concentrations in the main seam of lignite (samples 1-2-D through 1-11-D), after rejection of outliers, with the sedimentary rock pattern. For convenience in comparing the data, both sets of data have been calculated as ratios. The sedimentary rock data is from reference 16. Note that this comparison is only of the patterns of abundance, and not of the magnitudes. In the case of europium, the comparison is certainly influenced by working near the detection limit in the lignite samples.

TABLE 4

PATTERNS OF ABUNDANCE OF RARE EARTHS
IN LIGNITE AND SEDIMENTARY ROCKS

Element	Lignite Ratio, La/x	Sedimentary Rock Ratio, La/X
La	1.0	1.0
Ce	0.91	0.63
Sm	3.1	3.1
Eu	10	19
Yb	9.1	9.4

Reasonable qualitative agreement exists among the elemental variations observed here, the ionic potential of the elements, and the chemical fractionation behavior. Chemical fractionation determines the amount of each element present as ion-exchangeable cations, as acid-soluble minerals or coordination complexes, and as insoluble minerals. Our application of this procedure to other lignites has been discussed previously (17). In general, those elements which would be predicted to form insoluble hydrolysates on the basis of their ionic potential (that is, $3 < Z/r < 12$) are found concentrated near the margins of the seam and, in chemical fractionation, mainly occur as acid-insoluble minerals. Examples of elements in this category are Al, Ti, Cr, and Ni. On the other hand, elements of $Z/r < 3$ would likely exist as hydrated cations; these elements generally show even distribution through the seam and are removed by ion-exchange with ammonium acetate in chemical fractionation. Examples are Ca, Mg, and Na.

Variation Within the Overburden - The distribution of elements in the overburden is consistent in the clay-silt-sand regions with the exception of the concretion zone. This zone is extremely high in iron due to the siderite. The other elements which are concentrated in the concretion zone include Ag, Ni, Fe, Sc, Yb, Cd, Se, and Zn. The elements which are depleted are Co, Ce, Cs, As, Cr, Ru, Cl, and Na. The small coal seam directly above the concretion zone has high concentrations of As, V, Sb, and U. Figure 7 represents uranium distribution throughout the stratigraphic section, note that the highest concentration of uranium anywhere in the section is in the lignite seam directly above the concretion zone.

Many of the minor metallic elements have concentrations lying within 20% of the average values for shales. This comparison is illustrated by the data in Table 5, which compares the average concentrations in the underclay and overburden samples, after statistical rejection of outliers, with tabulated values from the literature (18). The most notable exception is manganese.

TABLE 5

COMPARISON OF AVERAGE MINOR ELEMENT CONCENTRATIONS FOR OVERBURDEN/UNDERCLAY SAMPLES WITH AVERAGE CONCENTRATIONS FOR SHALES

CONCENTRATIONS IN PPM

Element	Overburden/Underclay	Shales	Element	Overburden/Underclay	Shales
Ba	760	600	Sc	15	15
Ce	56	70	Th	10	12
Co	13	20	Ti	3650	4600
Cr	92	100	U	2.8	3.5
Mn	269	850	V	139	130
Ni	72	80	Zn	51	90

The variation of potassium in the overburden and underclay is extreme, ranging from 1000 to 30,000 ppm. The reasons for this variability are not clearly understood, but may be due to the minerals in the overburden and underclay, some of which would be potassium-containing clays and others not. Figure 8 represents the distribution of potassium within the stratigraphic sequence.

INTERPRETATION OF PATTERNS OF ELEMENT DISTRIBUTION

The observed patterns of element distribution in the lignite seam may be explained by both changes in depositional conditions during accumulation and subsequent chemical changes during diagenesis and post-diagenetic processes. Depositional factors involving addition of greater fractions of detrital clay and silt at the beginning and end of peat deposition would increase Si, Al, Mg, Ca, Na, K, and possibly other elements in the margins of the lignite. Other possible depositional factors include changing of Eh or pH, influx of ash, or changing botanical factors at the beginning and end of peat deposition. Post-depositional factors related to the flow of meteoric water (i.e., water derived from the atmosphere) through the lignite laterally might selectively concentrate elements in the margins of the seam or at its center. Vertical flow might concentrate elements at either the upper or lower margin, depending on flow direction and on the nature of the adjoining sediments. Other post-depositional factors might be related to the changing geochemistry of the lignite-forming environment, such as Eh and pH changes, botanical changes due to breakdown of plant material, and geological factors such as depth of burial, temperature, compaction, or changes in groundwater chemistry. The existence of several types of patterns suggests that several processes have been operative during the geological history of this sequence.

Future work will include a very detailed sampling of several vertical sections of a mine to describe groundwater influences on the formation of authigenic minerals and on the distribution or organically associated elements.

ACKNOWLEDGEMENTS

The authors would like to thank Diane K. Rindt for the x-ray diffraction work and Arthur L. Severson for x-ray fluorescence analysis. Mr. Roaldson acknowledges support from Associated Western Universities, Inc. as a part of their summer undergraduate research participation program.

REFERENCES CITED

1. Sondreal, E.A., W.R. Kube, and J.L. Elder. Analysis of the Northern Great Plains Province Lignites and Their Ash: A Study of Variability. U.S. Bureau of Mines Report RI 7158 (1968).

2. Energy Resources Co. Inc., Walnut Creek, CA 94596. Low-rank Coal Study, National Need for Resource Development-Resource Characterization. DOE/FC/10066-TI (Vol. 2) Nov. 1980.

3. Jacob, A.F. Geology of the upper part of the Fort Union Group (Paleocene), Williston Basin, with reference to uranium: North Dakota Geol. Survey Report of Investigation No. 58, 1976, 49 p.

4. Groenewold, G.H., L.A. Hemish, J.A. Cherry, B.W. Rehm, G.N. Meyer, and L.M. Winczewski. Geology and geohydrology of the Knife River Basin and adjacent areas of west-central North Dakota: North Dakota Geol. Survey Report of Investigation No. 64, 1979, 402 p.

5. Karner, F.R., S.F. White, D.W. Brekke, and H.H. Schobert. Geologic Sampling of Lignite Mines in Mercer and Oliver Counties, North Dakota. DOE/FC/FE-1, 1983, (in preparation).

6. Logan, Katherine J. The Geology and Environment of Deposition of the Kinneman Creek Interval Sentinel Butte Formation (Paleocene), North Dakota. Unpublished Masters Thesis, University of North Dakota (1981).

7. Karner, F.R., W. Beckering, D.K. Rindt, and H.H. Schobert. Inorganic Constituents in Lignite: Overview and Some Effects on Coal Utilizations. Geological Society of America Abstracts with Programs 11 454 (1979).

8. Karner, F.R., G. Winbourn, S.F. White, and A.K. Gatheridge. Sodium and calcium in overburden, lignite and underclay at the Beulah and Baukol-Noonan Mines, Mercer and Oliver Counties, North Dakota [abs.]: North Dakota Academy of Science Proceedings, vol. 33, pt. 1, 1979, p. 70.

9. Schobert, H.H., S.A. Benson, M.L. Jones, and F.R. Karner. Studies in the Characterization of United States Low-rank Coals. Proceedings, International Conference on Coal Science, Dusseldorf, Sept. 1981, p. 10-15.

10. Karner, F.R., S.A. Benson, H.H. Schobert, R.G. Roaldson, and Cirtchlow. Organic and Inorganic Components of Lignite: A Scanning Electron Microscope and Microprobe Study. Geological Society of America Programs with Abstracts, (Abstract), v. 14, 1982.

11. Weaver, J.N. in Analytical Methods for Coal and Coal Products, Vol. I, p. 377-401, Karr, C., Jr. (Ed.), Academic Press, Inc., New York (1978).

12. Miller, R.N. and P.H. Given. A geochemical study of the inorganic constituents in some low-rank coal. U.S. DOE report FE-2494-TR-1 (1979).

13. Finkelman, R.B. Modes of Occurrence of Trace Elements in Coal. University of Maryland. Ph.D. dissertation (1980), 301 p.

14. Holm, P.L. Distribution of Inorganics in Selected Low-rank Coals. GFETC IR-5, 1982.

15. Goldschmidt, V.M. Geochemistry, Oxford Press, 1954, 730 p.

16. Henderson, P. Inorganic Geochemistry, Pergamon Press, New York, 1982, p. 27.

17. Benson, S.A. and P.L. Holm. Comparison of Inorganics in the Three Low-Rank Coals. ACS Division of Fuel Chemistry Preprints, 28 (2), 234 (1983).

18. Krauskopf, K.B. Introduction to Geochemistry, McGraw-Hill Book Co., New York, 1979, p. 482.

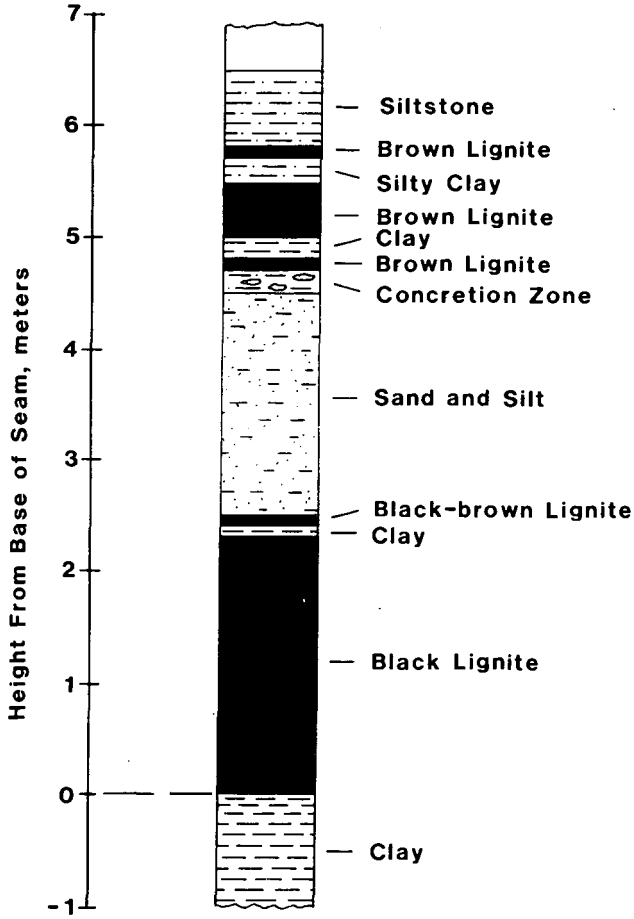

FIGURE 1. Description of stratigraphic sequence.

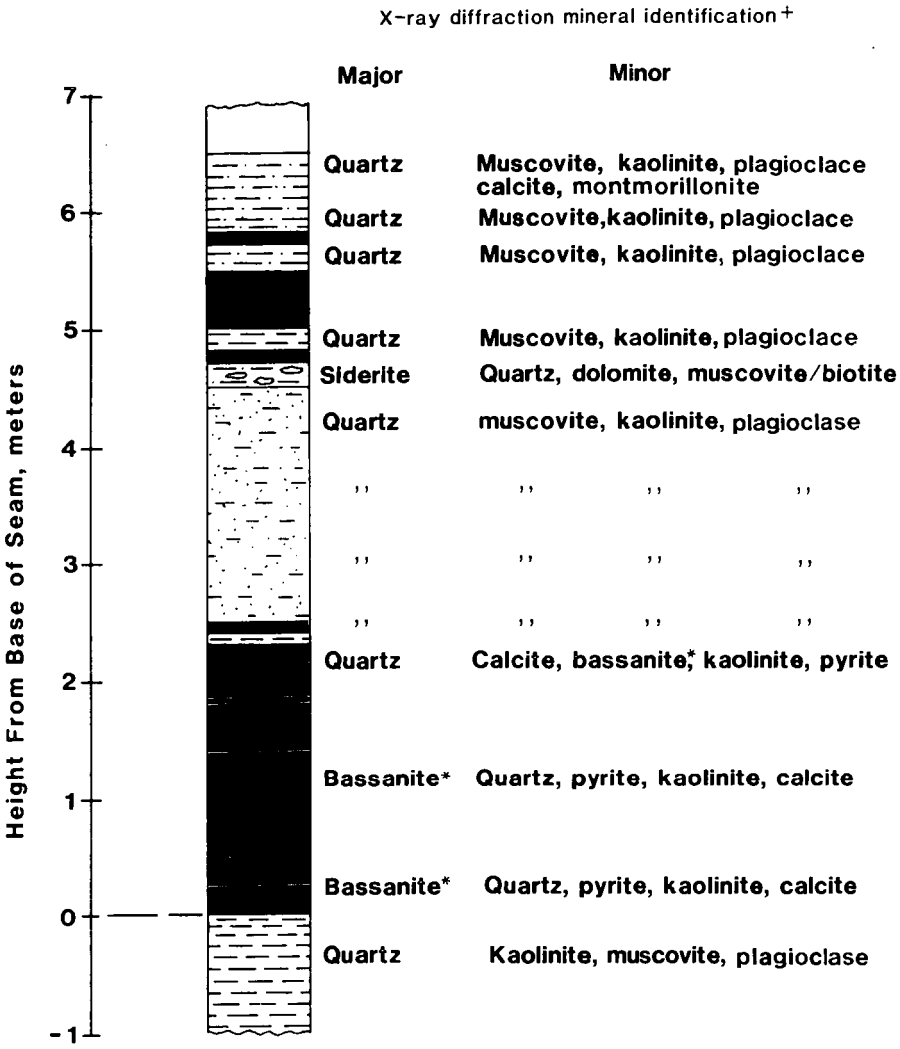

+Abundance listed in decreasing order

*Bassanite may be a product of the Low-temperature ashing procedure

FIGURE 2. Mineralogy of the stratigraphic sequence.

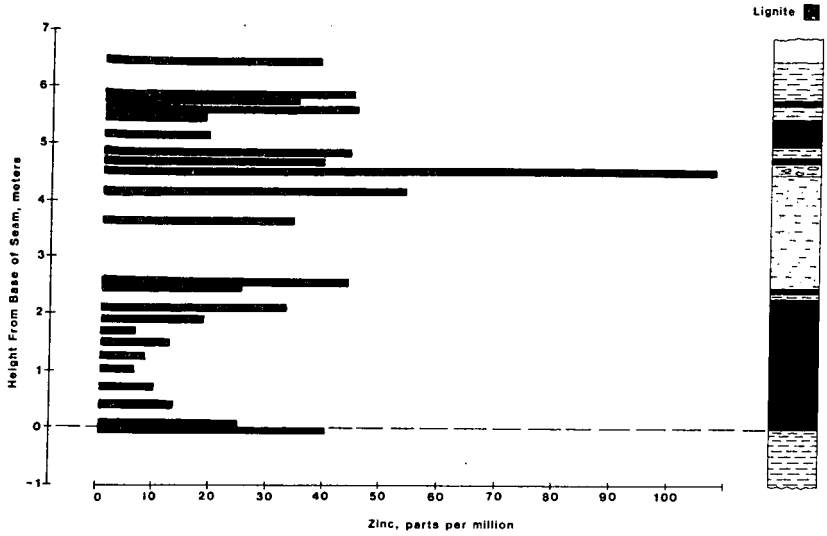

FIGURE 3. Zinc distribution in the stratigraphic sequence.

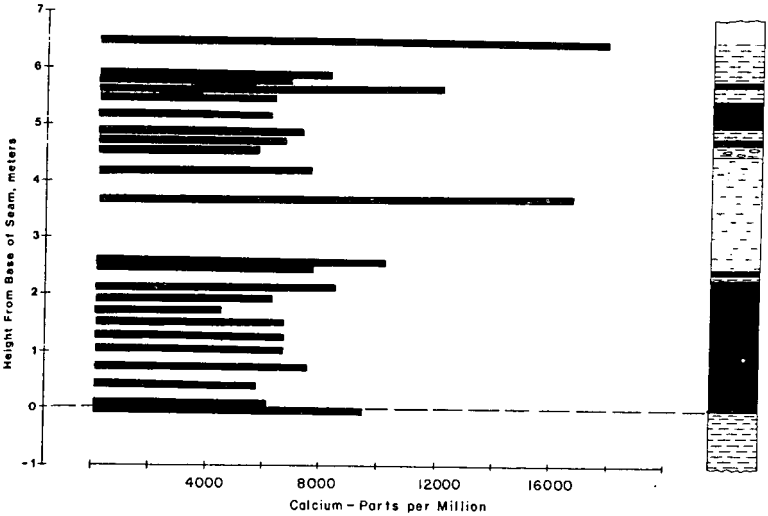

FIGURE 4. Calcium distribution in the stratigraphic sequence.

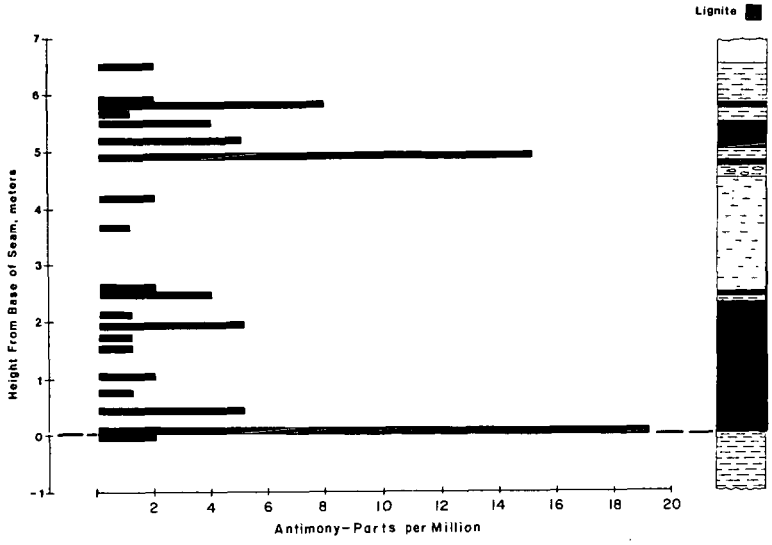

FIGURE 5. Antimony distribution in the stratigraphic sequence.

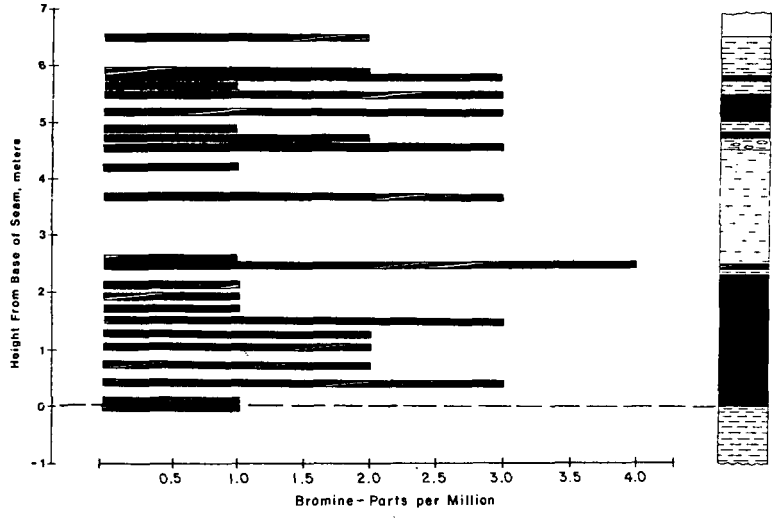

FIGURE 6. Bromine distribution in stratigraphic sequence.

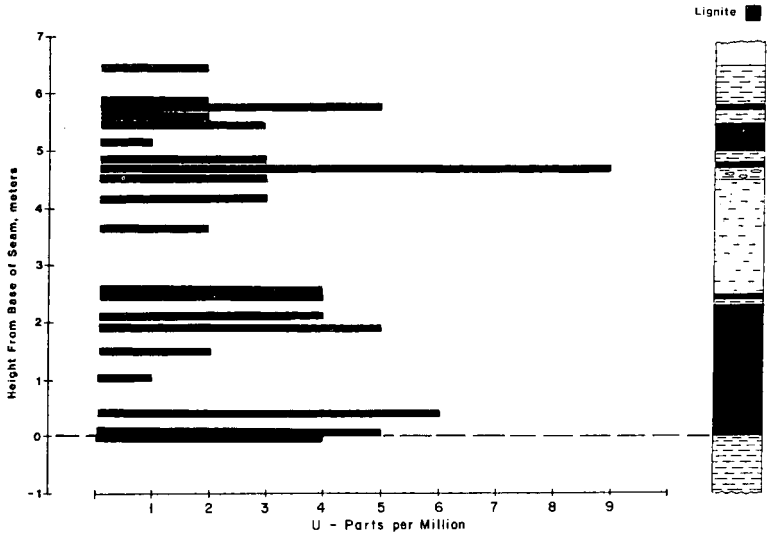

FIGURE 7. Uranium distribution in the stratigraphic sequence.

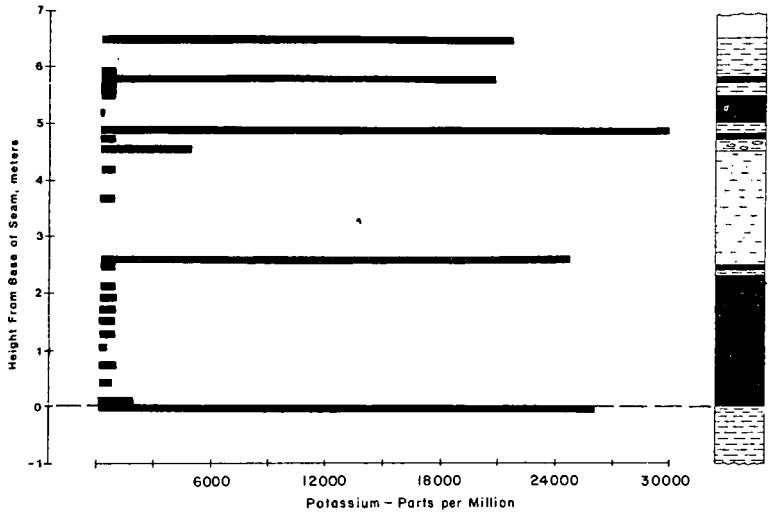

FIGURE 8. Potassium distribution in the stratigraphic sequence.

ROLE OF EXCHANGEABLE CATIONS ON THE RAPID PYROLYSIS OF LIGNITES

Mark E. Morgan* and Robert G. Jenkins

Department of Materials Science and Engineering
The Pennsylvania State University
University Park, PA 16802

INTRODUCTION

Recently, research concerned with utilization of the vast reserves of American lignites has expanded greatly. Studies have shown that lignites react quite differently than coals of higher rank when subjected to utilization and conversion schemes. The behavior of lignites is believed to be greatly influenced by the inorganic constituents present. The most significant feature of the inorganic constitutents of lignites is the large concentration of exchangeable metal-cations. These cations are mainly alkali and alkaline earth metals associated with the carboxyl groups present in lignites. This research is concerned with the effect of exchangeable cations on rapid pyrolysis of a lignite.

EXPERIMENTAL

Pyrolysis was carried out in a dilute-phase entrained-flow reactor. The system is a modified version (1) of that utilized by Scaroni et al. (2). The system allows pyrolysis to be studied under high heating and cooling rates (10^4 - 10^5 K/s). Under these conditions, examination of pyrolysis over residence times from 0.03 to 0.30 s and at temperatures up to ~1300 K is possible. Pyrolysis occurs in a dilute stream in order to reduce the role of secondary reactions resulting from contact between the pyrolysis products.

A Montana lignite (Fort Union Seam) was utilized in this study. Details of the organic and inorganic analyses of this coal can be found elsewhere (3). In this study, three types of samples were utilized: raw lignite, acid-washed lignite and cation-loaded lignite. In the acid-washed lignite the carboxylate cations are in the hydrogen (acid) form. In the acid washing procedure, 50 g of raw lignite were mixed with 900 ml of 0.1 N HCl for 16-24 h, filtered, mixed with a new batch of HCl for an additional 4 h, filtered, and washed repeatedly. It was then refluxed in 1000 ml of boiling distilled water for 1 h to remove excess HCl (3,4).

Cation loading was always performed on the acid-washed samples because it facilitates the determination of the extent of cation loading and eliminate complexities caused by the presence of more than one cation. The conditions utilized for ion exchange can be seen in Table 1. Further details can be found elsewhere (5). Also shown in Table 1 are the results of the cation loading. As can be seen, there are four different loadings of calcium. Calcium was chosen as the cation to be studied most, because it is the predominant cation in American lignites (3).

A number of gauges of the effects of pyrolysis were utilized, the most informative is weight loss. Because of experimental conditions, weight loss was determined by using ash as a tracer. This technique has been used previously by a number of workers (2,6,7).

In addition, the decomposition of the carboxyl groups was studied by measuring the carboxylate concentrations in the chars after pyrolysis. The technique to determine the carboxyl group content is outlined in detail elsewhere (3), and is based on the work of Schafer (8). There are three basic steps involved: acid washing, exchange with barium acetate and determination of the extent of exchange.

*Current address: Atlantic Research Corporation, Alexandria, VA, 22314.

TABLE 1

ION EXCHANGE CONDITIONS AND RESULTS

Sample	Exchange Media	Starting pH	g coal/l	Stir Period	m moles/g DICF Coal
Cal	1 M Ca Acetate	8.0	55	24 h	0.84
Ca2	.25 M Ca Acetate + .25 M CaCl	6.0	100	24 h	0.75
Ca3	.25 M Ca Acetate	5.5	160	24 h	0.49
Ca4	1 M Ca Acetate	8.0	55	24 h + 24 h + 24 h + 24 h	1.11
Na	1 M Na Acetate	8.0	55	24 h	0.94
Mg	1 M Mg Acetate	8.0	55	24 h	0.71
Raw	----------	---	---	------	0.94

RESULTS AND DISCUSSION

Total Weight Loss -- In Figure 1, the weight loss versus time behavior for the raw, acid-washed and Cal-form samples are displayed. As can be seen, the presence of metal-cations dramatically affects the weight loss behavior in the entrained flow reactor. All three samples undergo a period of rapid weight loss followed by a region of slow weight loss. In the case of the raw and Cal-form samples, weight loss lasts for about 0.15 s until a value of about 30 wt% (Dry Inorganic Content Free-DICF) is achieved. For the acid-washed sample, the rapid weight loss is completed in 0.05 s and the final weight loss value is 50 wt% (DICF). It is very interesting to note the similarity between the behavior of the raw and Cal samples. This similarity indicates the reversibility of the ion exchange treatments in terms of coal pyrolysis behavior. This strongly suggests that the difference in pyrolysis behavior between the metal cation and hydrogen-form samples is mainly due to the presence of cations, and not to the chemical treatments to which the coals were subjected.

While Cal contains about the same amount of exchangeable cations as the raw coal, it is possible to load various amounts of calcium onto the acid-washed lignite. Figure 2 displays the results of a study on the effects of varying the quantity of exchanged calcium. In this figure, the weight loss at maximum residence time in the entrained flow reactor at 1173 K is plotted for samples (270x400 mesh) with five levels of calcium ranging from 0 to 4.7 wt% (DICF). As can be seen, as the calcium content of the coal is increased there is a gradual and significant decrease in the maximum weight loss. This behavior is similar to that observed by Tyler and Schafer (9).

Other exchangeable cations are found in lignites, thus, a study was made into the effects of sodium and magnesium on pyrolysis. Results of this study are summarized in Table 2 which lists weight loss values at maximum residence time for a number of different cation loaded samples pyrolyzed at 1173 K. Firstly, it can be seen that the presence of metal cations always results in a decrease in weight loss. This result is important in itself in that it reemphasizes the importance of cations in lignite pyrolysis. Secondly, information can be gained about the relative activity of the various cations studied. If one compares the two divalent cations (calcium and magnesium), it can be seen that the elements have a similar effect on a per mole basis. The samples Ca2 and Mg have almost the same number of moles of cations, and both samples lose approximately the same weight. If one tries to assess the relative activity of sodium, it can be seen that, in general, the sodium-form coal undergoes a relatively large weight loss during pyrolysis.

TABLE 2

EFFECT OF CATIONS ON MAXIMUM WEIGHT LOSS IN ENTRAINED FLOW REACTOR
1173 K, DICF BASIS

Sample	Weight Loss
Raw	30.8
Ca1	28.7
Ca2	34.9
Mg	33.4
Na	38.7
Acid Washed	49.4

The monovalent nature of sodium makes a comparison of the concentrations difficult. It contains the highest molar concentration of cations, but they cover the least number of carboxyl groups.

Extended Residence Time Studies -- It was just pointed out that coals undergo rapid weight loss followed by what appears to be a region of little weight loss in the entrained flow reactor. However, although samples reach this region of constant weight loss, no samples undergo complete pyrolysis in the residence times available. Rather, this "plateau" region of weight loss is a regime of relatively slow decomposition. While it takes as little as 0.05 to 0.15 s to reach this leveling off point, it can take on the order of minutes to complete pyrolysis.

In order to determine the total pyrolysis yield, another technique was used. Basically, the approach involves capturing the pyrolyzing coal particles in a crucible at the maximum residence distance in the reactor. The captured samples are then held in the reactor for 10 min to complete pyrolysis. It is thought that this technique gives a reasonable estimation of the total pyrolysis yield possible in an entrained flow reactor.

The results of this study can be seen in Table 3 in which weight loss values for extended residence time runs are listed. If one compares the weight loss of

TABLE 3

EXTENDED RESIDENCE TIME RUNS IN THE ENTRAINED FLOW REACTOR
1173 K, DICF BASIS

Sample	Weight Loss	A.S.T.M. Volatile Matter Content
Raw	54.0	43.7
Acid Washed	63.3	43.2
Ca1	46.1	43.0

these samples, it can be seen, once again, that the presence of metal-cations greatly reduces the amount of volatile material evolved. It is interesting to compare these results with those gained by the ASTM volatile matter test. The ASTM volatile matter contents display no effect of cation-loading. It will be recalled that this test is performed in a fixed bed (crucible) which is felt to increase the amount of secondary char-forming reactions. Thus, when secondary char-forming reactions are increased, there is little difference in the weight loss values for pyrolysis. However, decreasing the likelihood of these reactions leads to large differences in total weight loss.

Kinetics of Total Weight Loss -- The method chosen is a simple first order Arrhenius treatment in which a single overall activation energy is utilized. The technique has been applied to the kinetics of the initial weight loss, and therefore, the weight loss values were compared to the maximum weight loss in the entrained flow reactor. Values of the apparent activation energy and preexponential factor found in this study are displayed in Table 4. It is clear that there is a similarity in the behavior of the raw and calcium-form coals. The acid-washed coal exhibits the largest activation energy, almost three times larger than that found for the raw lignite and 50% greater than that of the calcium form. Again, it is obvious that the absence of metal-cations can have a profound effect on pyrolysis kinetics and mechanisms.

TABLE 4

KINETIC PARAMETRS FOR TOTAL WEIGHT LOSS

Sample	Activation Energy (kJ/mole)	Preexponential Factor (s^{-1})
Raw	58	8×10^3
Acid Washed	147	2×10^3
Cal	99	5×10^5

Effect of Exchangeable Cations on Tar Release -- Table 5 lists the results of a study in which the quantity of tar, collected on a filter, in the outlet gas

TABLE 5

TARS RELEASED IN ENTRAINED FLOW REACTOR

Residence Time (s)	mg Tar/g Coal Fed	
	Raw Coal	Acid Washed Coal
0.042	3	10
0.078	9	30
0.112	3	48

stream, was measured for the raw and acid washed samples at 1173 K at three residence times. At each residence time the amount of tar released by the acid-washed coal was significantly greater than those released by the raw coals. This trend is in the same direction as the weight loss data. That is, increases in total weight loss when metal cations are removed are also accompanied by increases in tar yield.

Tar samples (1173 K, 0.078 s) were analyzed by Fourier Transform Infrared Spectroscopy, spectra were created by use of KBr pellets in the manner described by Painter et al. (10). Spectra from the raw and acid-washed coal tars were recorded as well as the "difference spectrum" from the two samples.

The spectra of these tars from the raw and acid-washed coals were similar in many ways. The same general major features were present, such as methyl, phenol and carboxyl groups. However, there is a significant difference between the two spectra in the intensities of the carbon-hydrogen aliphatic bond stretching absorbances at about 2800 - 3000 cm^{-1}. Integration of this band for the two samples leads to the conclusion that tars from the raw coal contain three times the quantity of aliphatic hydrogen as do the tars from the acid-washed coal.

Effect of Exchangeable Cations on Carboxyl Group Decomposition -- Decomposition of the carboxyl groups was followed by measuring the quantity of carboxyl

groups in the parent coal and in the resulting chars. It should be pointed out that data on the decomposition of carboxyl groups enables one to study the behavior of a single species during pyrolysis, thus yielding information that cannot be extracted from overall weight loss data. Also, it should be noted that since there are about 3.1 meq/g DICF of carboxyl groups on this lignite, the decomposition of this species can account for a weight loss of up to 14% of the lignite.

Results from this study can be seen in Figure 3 in which the quantities of carboxyl groups remaining on the raw lignite as a function of residence time at 1173 are shown. The loss of the carboxyl groups is very similar to the total weight-loss behavior presented in Figure 1. That is, there is a very rapid loss of carboxyl groups followed by a region of slow decomposition. It is interesting to note that both the raw and Cal-form samples appear to complete decarboxylation at about 2.6 meq/g DICF while the acid-washed sample releases all of the 3.1 meq/g DICF present.

Although previous researchers have studied the effects of cations on the pyrolysis of carboxyl groups, most of the work has been concerned with weight loss as a function of temperature and/or the evolution of oxides of carbon. Little work has been concerned with direct determination of the kinetics of decarboxylation. Table 6 lists the results of a first-order kinetic analysis of decarboxylation of the raw and acid washed forms of the lignite. The activation energies for decarboxylation are somewhat different for the two samples studied, that found for the raw lignite is about 20% greater than that calculated for the acid-washed coal. However, the values are quite similar when compared to the spread of activation energies found for the overall weight loss data (Table 4).

CONCLUSIONS

It must be concluded that the presence of metal cations in lignites dramatically affects pyrolysis behavior under rapid heating conditions. The presence/absence of metal cations are important in terms of the rate of evolution total weight loss and nature of the pyrolysis products. It is suggested that these data have significant importance in gasification and combustion of lignites.

ACKNOWLEDGEMENTS

This study was supported by USDOE under Contract No. DE-AC01-79ET14882.

REFERENCES

1. Maloney, D. J., Ph.D. Thesis, The Pennsylvania State University, 1983.

2. Scaroni, A. W., Walker, P. L., Jr. and Essenhigh, R. H., Fuel, 1981, (60), 71.

3. Morgan, M. E., M.S. Thesis, The Pennsylvania State University, 1980.

4. De, G. S., Tumuluri, S., Lahari, K. C., Fuel, 1971, (50), 272.

5. Morgan, M. E., Ph.D. Thesis, The Pennsylvania State University, 1983.

6. Anthony, D. B. and Howard, J. B., AIChE Journal, 1976, (22), 625.

7. Badzioch, S. and Hawksley, P. G. W., Ind. Eng. Chem. Process Des. Dev., 1970, (9), 521.

8. Schafer, H. N. S., Fuel, 1970, (49), 197.

9. Tyler, R. J. and Schafer, H. N. S., Fuel, 1980, (59), 487.

10. Painter, P. C., Kuehn, D. W., Snyder, R. W. and Davis, A., Fuel, 1982, (61), 691.

TABLE 6

KINETIC PARAMETERS FOR DECARBOXYLATION

Sample	Activation Energy (kJ/mole)	Preexponential Factor (s^{-1})
Raw	106	4×10^5
Acid Washed	80	8×10^4

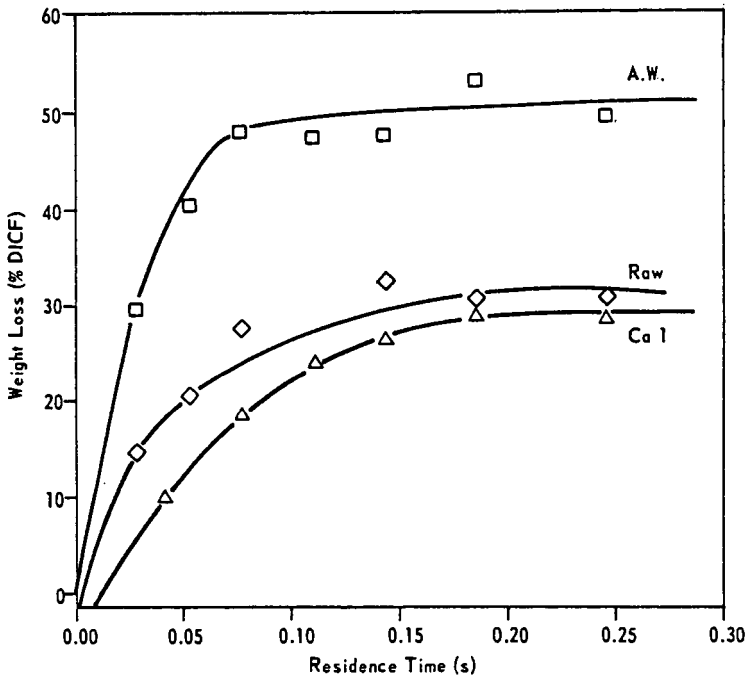

Figure 1. WEIGHT LOSS IN ENTRAINED FLOW REACTOR
270 x 400 mesh Lignite at 1173 K

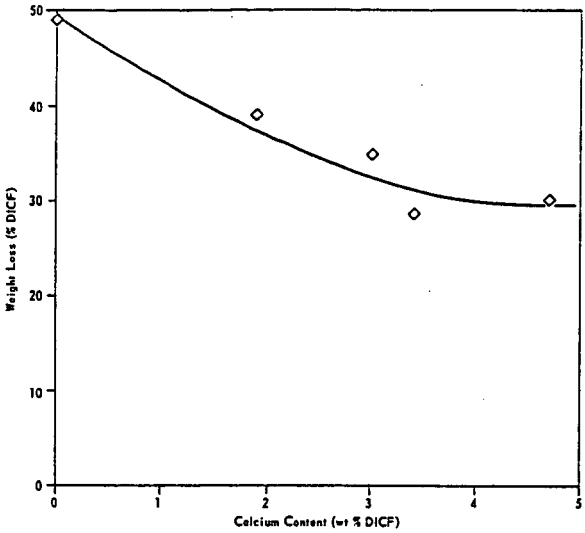

Figure 2. WEIGHT LOSS IN ENTRAINED FLOW REACTOR
Effect of Ca Loading at 1173K

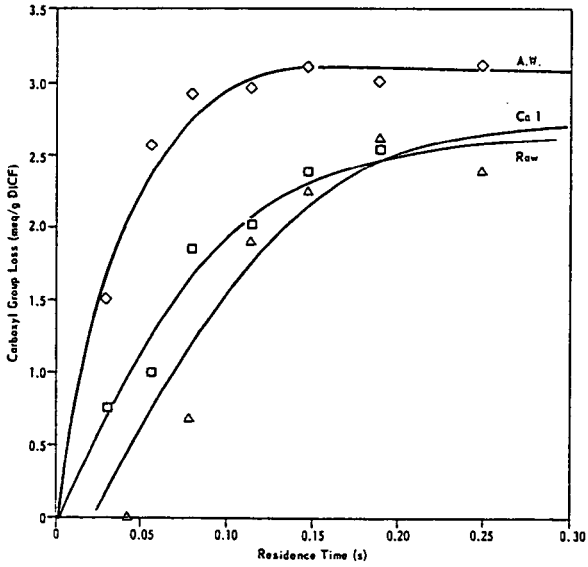

Figure 3. DECOMPOSITION OF CARBOXYL GROUPS (1173 K)

INVESTIGATION OF LOW-RANK COAL HYDROPYROLYSIS

C. S. Wen and T. P. Kobylinski

Gulf Research & Development Company, P. O. Drawer 2038, Pittsburgh, PA 15230

INTRODUCTION

Recently, increased attention is being directed toward the pyrolysis route of processing coal to produce liquid and gaseous fuels, in particular when coupled with the use of char by-product for power generation.(1) In view of the increased interest in coal pyrolysis, a better understanding of the thermal response of coals as they are heated under various conditions is needed.

Conventional liquefaction processes developed for Eastern bituminous coals might not be the best choice for Western low-rank coals because of the substantial property and structural differences between them. In general, low-rank coals are more susceptible to reaction with H_2, CO, or H_2S.

Coal hydropyrolysis is defined as pyrolysis under hydrogen pressure and involves the thermal decomposition of coal macerals followed by evolution and cracking of volatiles in the hydrogen. It is generally agreed that the presence of hydrogen during the pyrolysis increases overall coal conversion.(2,3)

In the present study we investigated pyrolysis of various ranks of coals under different gaseous environments. Low-rank coals such as Wyoming subbituminous coal and North Dakota lignite were pyrolyzed and their results were compared with Kentucky and Illinois bituminous coals.

EXPERIMENTAL

The coals used in this study included Wyoming subbituminous coal, North Dakota lignite, Kentucky bituminous coal, and Illinois No. 6 bituminous coal. Proximate and ultimate analyses of the coals studied are given in Table I.

All pyrolysis experiments were carried out in the thermogravimetric apparatus (TGA) having a pressure capacity of up to 1000 psi. A schematic of the experimental unit is shown in Figure 1. It consists of the DuPont 1090 Thermal Analyzer and the micro-balance reactor. The latter was enclosed inside a pressure vessel with a controlled temperature programmer and a computer data storage system. The pressure vessel was custom manufactured by Autoclave Engineers. A similar set-up was used previously by others.(4) A chromel-alumel thermocouple was set in close proximity to the sample inside a reactor. The reactor was made of a quartz tube which was surrounded by a tubular furnace. In a typical coal pyrolysis run, the coal sample (20-30 mg) was placed in a platinum boat which was suspended from the quartz beam of the TGA balance. The coal particle size used was 100-200 mesh. Samples were heated to desired temperatures at linear heating rates or heated isothermally under various gaseous environments.

FT-infrared was also used to monitor the degree of pyrolysis for various samples at different temperatures. The KBr (potassium bromide) pellet of sample was prepared for FTIR analysis.

RESULTS AND DISCUSSION

Typical thermograms of Wyoming coal under hydrogen pressure are given in Figure 2. The TGA and the weight loss rate thermograms show a major weight loss at temperatures ranging from 350-600°C. A secondary hydropyrolysis peak occurs above 600°C most likely due to the gas releases from the further decomposition of coal.

Figure 3 shows a comparison of derivative thermograms for four different rank coals. The differences of devolatilization rate are not large at temperatures up to 500°C, however, above 500°C, the secondary hydropyrolysis peak of low-rank coal becomes dominant.

The influence of heating rate on coal hydropyrolysis was studied over a range of 5-100°C/min. As shown in Figure 4, the two peaks were observed, the first of which we call the primary volatilization, and the second, characteristic of local hydropyrolysis. The first peak increased rapidly with the increase of the heating rate. The second characteristic peak becomes relatively dominant at lower heating rates. It seems that the hydropyrolysis peak is favored by slow heating rates, indicating a heat transfer limitation within the secondary hydropyrolysis region. In contrast, coal pyrolyzed under an inert nitrogen atmosphere results in an increase of weight loss rate with increasing heating rates, but the shape of the curves remains the same (Figure 5).

The effect of hydrogen on coal pyrolysis can further be illustrated by Figure 6, where we compared derivative thermograms of Wyoming coal pyrolyzed at 200 psig of N_2 and 200 psig of H_2 at the same heating rates (20°C/min). The secondary hydropyrolysis peak observed at 580°C in the H_2 run was absent in the N_2 atmosphere.

FTIR spectra of the original coal and char from pyrolyzing Wyoming coal under H_2 pressure at various temperatures are shown in Figure 7 (only wave numbers between 1700 and 400 cm^{-1} were shown here for comparison). The strongest absorption band located at 1600 cm^{-1} begins to decrease in intensity at 470°C. This band has been assigned to aromatic ring C-C vibration associated with phenolic/phenoxy groups.(5) Similarly, the aromatic-oxygen vibration band near 1260 cm^{-1} shows an equivalent decrease. The absorption bands between 720 to 870 cm^{-1} (which arise from the out-of-plane aromatic CH vibrations) increase markedly at 470°C, indicating a growth in size of aromatic clusters in the reacted coal. At 650°C, most organic absorption bands were diminished except for a broad band ranging from 1000-1090 cm^{-1} due to clay mineral absorption.(7) An increase in the structureless background absorption is observed, suggesting a growth of graphitization in the residue coal.

The kinetics of coal pyrolysis are complicated because of the numerous components or species which are simultaneously pyrolyzed and decomposed. For measuring kinetic parameters, we treated data following the procedure of Coats and Redfern (8) and Mickelson and Einhorn.(9) The kinetic parameters for four different coals heated under H_2 pressure are presented in Table II. A reaction order equal 2.3 to 2.9 was observed for the primary hydropyrolysis peaks. A high reaction order was obtained for the secondary reaction peak under hydrogen pressure. The kinetic parameters for four different coals heated under N_2 atmosphere compared with data presented in the literature are listed in Table III.

Kinetic parameters for n (reaction order) and E (activation energy) in the literature show significant variation for different techniques and coal (Table III). By considering the complexity of coal thermal degradation, many authors have contented that a simple, first-order reaction is inadequate. Wiser et al. (10) found that n=2 gave the best fit to their data, while Skylar et al. (11) observed that values of n above 2 were required to fit nonisothermal devolatilization data for different coals. The kinetic parameters obtained in this study also show a non-integer reaction order. The thermal decomposition of coals are complex because of the numerous components or species which are simultaneously decomposed and recondensed.

Figure 8 demonstrates the influence of CO on devolatilization for different ranks of coal. For the higher rank coals (i.e., Kentucky and Illinois bituminous coals), pyrolysis in the presence of CO plus H_2 or H_2 alone follows the

same path. However, lignite showed a marked increase of pyrolysis rate in the run where CO was added. A higher content of reactive oxygenated bonds (i.e., carboxyl or ether linkages) in low-rank coals could be the reason for the high reactivity in the presence of CO. The kinetic parameters determined for coal pyrolyzed in syngas (CO/H_2 mixture) are listed in Table IV. As shown in the table, a high reaction order was obtained for the H_2 and CO/H_2 runs, particularly for the low-rank coals which showed a secondary reaction occurring at temperatures above 500°C.

CONCLUSIONS

Laboratory microscale studies have demonstrated that the coal pyrolysis in a hydrogen atmosphere gave higher degree of devolatilization in low-rank coals than pyrolysis in an inert atmosphere. In hydrogen atmosphere two distinct steps in coal devolatilization were observed as shown by the double peak of the devolatilization rate. Only one step was observed under nitrogen atmosphere. In a comparison of kinetic parameters, a high reaction order and a low activation energy were also obtained in the coal hydropyrolysis. Application of data and observations from this study could lead to a better understanding of chemical and physical changes during the coal hydropyrolysis and seek alternative coal conversion routes.

REFERENCES

1. H. W. Parker, "Liquid Synfuels Via Pyrolysis of Coal in Association with Electric Power Generation," Energy Progress, 2(1), 4, 1982.

2. R. J. Belt and L. A. Bissett, "Assessment of Flash Pyrolysis and Hydropyrolysis," DOE Report METC/RI-79/2, 1978.

3. P. Arendt and K. H. Van Heek, Fuel, 6099), 779, 1981.

4. J. G. Speight, "Assessment of Structures in Coal by Spectroscopic Techniques," in Analytical Methods for Coal and Coal Products, (Ed. by C. Karr, Jr.), Vol II, Chapter 22, pp 75-101, Academic Press, New York, 1978.

5. V. T. Ciuryla, R. F. Weimer, D. A. Bivans, and S. A. Motika, Fuel, 58(10), 748, 1979.

6. P. C. Painter and M. M. Coleman, "The Application of Fourier Transform Infrared Spectroscopy to the Characterization of Coal and Its Derived Products," DIGILAB FTS/IR Notes No. 31, January 1980.

7. A. W. Coats and J. P. Redfern, "Kinetic Parameters from Thermogravimetric Data," Nature, 201, 68, 1964.

8. R. W. Mickelson and I. N. Einhorn, Thermochim. Acta, 1, 147, 1970.

9. W. H. Wiser, Fuel, 47, 475, 1968.

10. W. H. Wiser, G. R. Hill, and N. J. Kertamus, I&EC Process Design and Develop., 6(1), 133, 1967.

11. M. G. Skylar, V. I. Shustikov, and I. V. Virozub, Intern. Chem. Eng., 9, 595, 1969.

Table I

COAL ANALYSIS

	Wyoming Subbituminous Coal		North Dakota Lignite		Kentucky Bituminous Coal		Illinois Bituminous Coal	
	As Received	Dry Basis	As Received	Dry Basis	As Received	Dry Basis	As Received	Dry Basis
Proximate Analysis, wt%								
Moisture	6.1	--	21.2	--	3.0	--	3.9	--
Volatile	39.9	42.5	35.3	44.7	39.8	41.0	38.1	39.6
Fixed Carbon	45.6	48.6	35.9	45.6	48.6	50.1	46.8	48.7
Ash	8.4	8.9	7.6	9.7	8.6	8.9	11.2	11.7
Ultimate Analysis, wt%								
Moisture	6.1	--	21.2	--	3.0	--	3.9	--
Carbon	64.6	68.8	50.5	64.1	70.3	72.5	67.5	70.3
Hydrogen	4.3	4.6	3.5	4.4	4.8	5.0	4.5	4.7
Nitrogen	0.9	1.0	1.1	1.4	1.2	1.2	1.3	1.4
Sulfur	0.5	0.5	0.5	0.6	3.0	3.1	3.4	3.5
Ash	8.4	8.9	7.6	9.7	8.6	8.9	11.2	11.7
Oxygen (diff.)	15.1	16.1	15.6	19.7	9.1	9.4	8.2	8.4

Table II

KINETIC PARAMETERS OF COAL HYDROPYROLYSIS[a]

Coal	Reaction Order		Activation Energy (kcal/mole)		Frequency Factor (min^{-1})	
	1st Peak	2nd Peak	1st Peak	2nd Peak	1st Peak	2nd Peak
Wyoming	2.5	3.4	18.9	64.5	1.6×10^{5}	1.3×10^{15}
North Dakota Lignite	2.9	4.7	23.9	70.4	4.2×10^{7}	1.2×10^{18}
Kentucky	2.3	--	23.4	--	3.1×10^{6}	--
Illinois	2.4	--	29.2	--	1.9×10^{8}	--

[a] Samples were heated at 50°C/min under 500 psig H_2.
[b] Hydropyrolysis characteristic peak occurred in low-rank coals.

Table III

A COMPARISON OF KINETIC PARAMETERS IN COAL PYROLYSIS

Investigators	Coal	Reaction Order	Activation Energy (kcal/mole)	Frequency Factor (min^{-1})	Reference
Wiser et al.	Utah Bituminous	2	15.0	2.9×10^{3}	(9)
Stone et al.	Pittsburgh Seam Bituminous	1[a]	27.3	3.2×10^{8}	(11)
Ciuryla et al.	Pittsburgh Seam Bituminous	1[a]	39.5	1.7×10^{11}	(5)
	North Dakota Lignite	1[a]	53.6	1.7×10^{15}	(5)
	Illinois Bituminous	1[a]	52.3	1.7×10^{15}	(5)
Skylar et al.	Soviet Coal	2.3	10.0	1.3×10^{5}	(10)
	Soviet Gas Coal	2.1	14.6	5.1×10^{6}	(10)
This Work[b]	Wyoming Subbituminous	2.1	25.1	6.1×10^{5}	
	North Dakota Lignite	2.2	23.2	1.2×10^{6}	
	Kentucky Bituminous	1.9	26.9	4.2×10^{8}	
	Illinois Bituminous	1.8	30.9	4.8×10^{8}	

a Based on a series of first-order reactions.
b Samples were heated at 50°C/min under 50 cc/min ambient N_2 flow.

Table IV

KINETIC PARAMETERS OF COAL PYROLYSIS UNDER SYNGAS[a]

Coal	Reaction Order		Activation Energy (kcal/mole)		Frequency Factor (min^{-1})	
	1st Peak	2nd Peak	1st Peak	2nd Peak	1st Peak	2nd Peak
Wyoming Coal	2.8	3.6	23.1	57.5	1.1×10^{7}	7.1×10^{14}
North Dakota Lignite	2.6	2.8	20.8	32.6	2.6×10^{6}	1.8×10^{12}
Kentucky Coal	2.3	--	22.9	--	2.3×10^{6}	--
Illinois Coal	2.3	--	25.4	--	3.5×10^{7}	--

[a] Samples were heated at 50°C/min under 500 psig H_2 /CO (3/1 mole ratio).

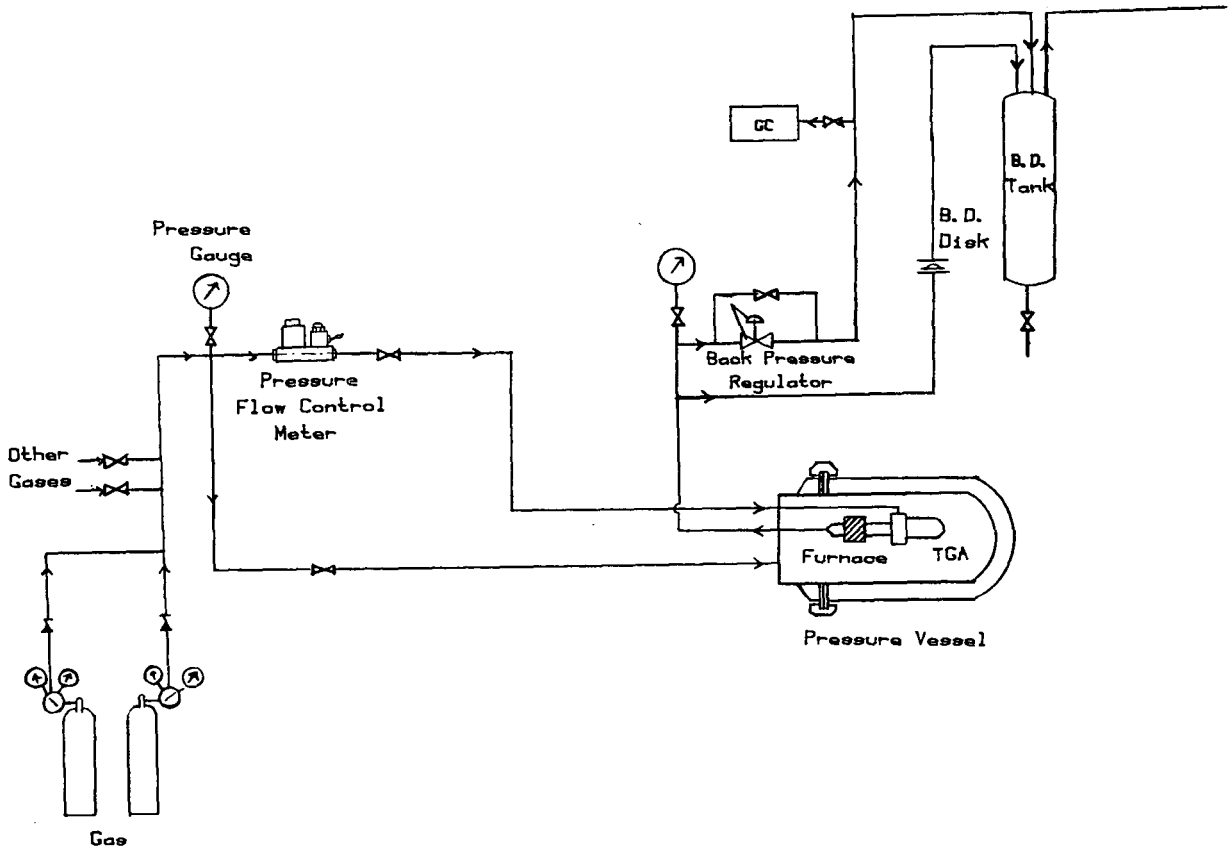

Fig. 1 Schmatic Set-up of the Pressure Pyrolysis Apparatus.

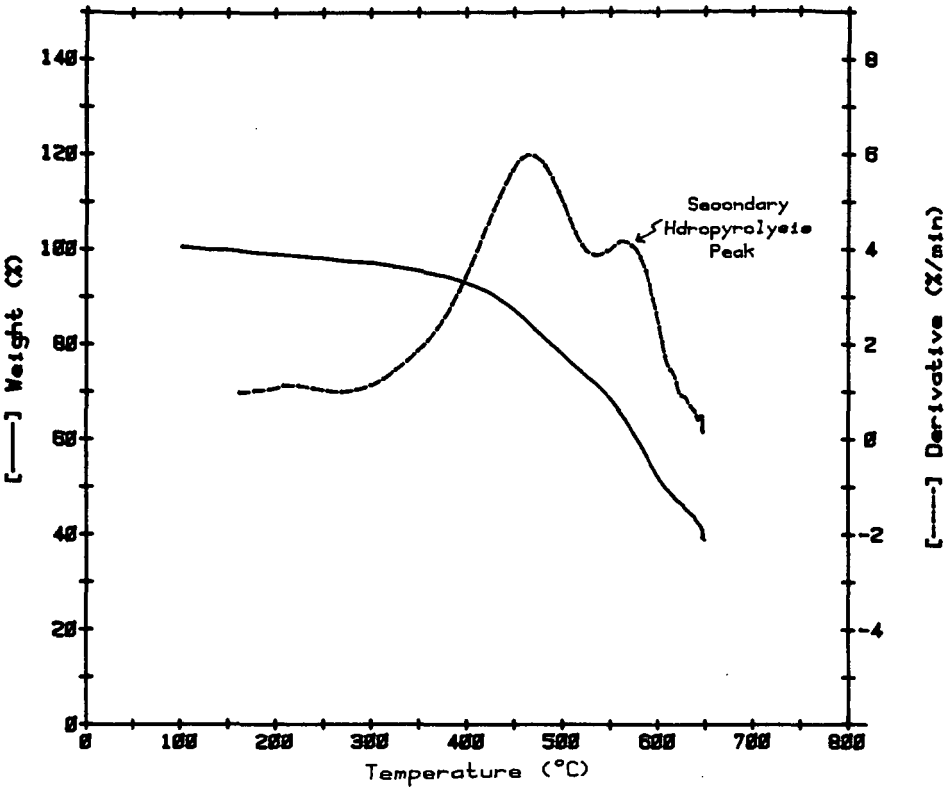

Fig. 2 Typical Pressure TGA Thermograms of Wyoming Coal Heated at 50°C/min and 500 psig H2.

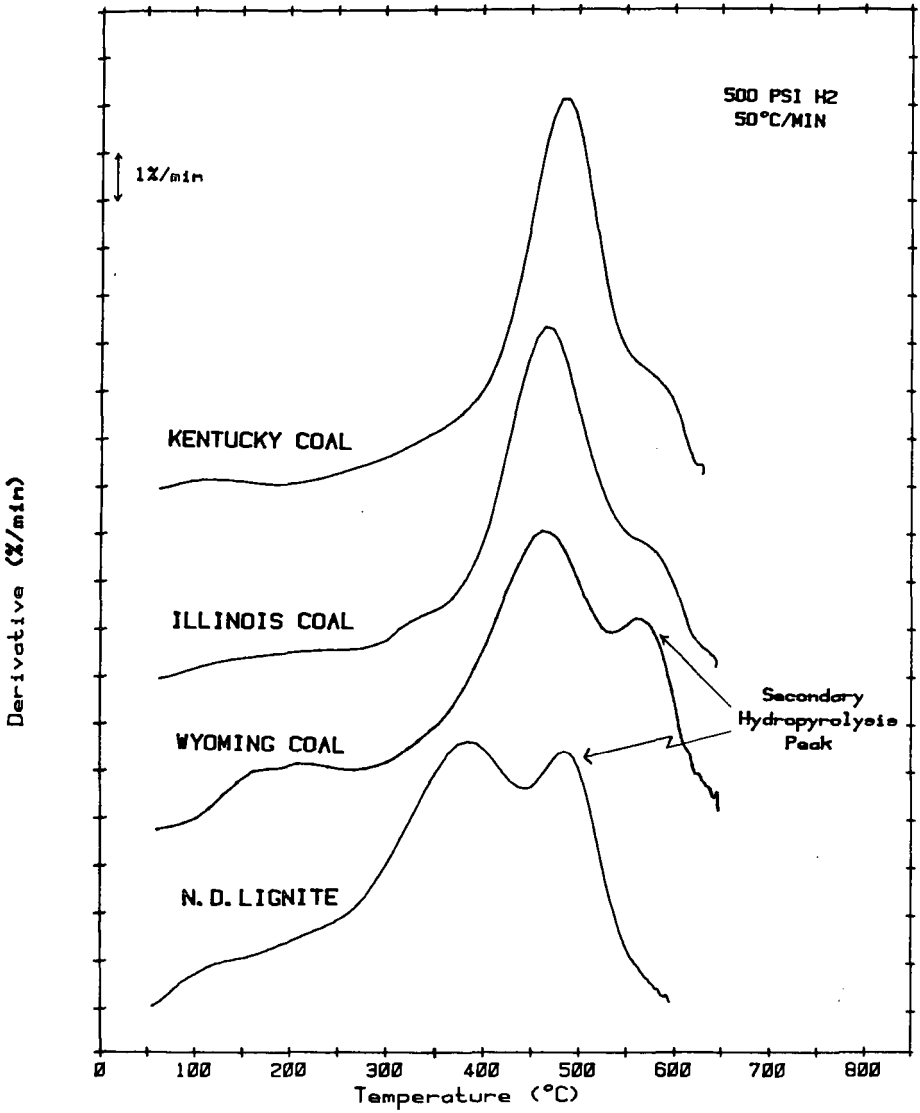

Fig. 3 A Comparison of Hydropyrolysis Derivative Thermograms for Various Coals at 50 °C/min and 500 psig H2.

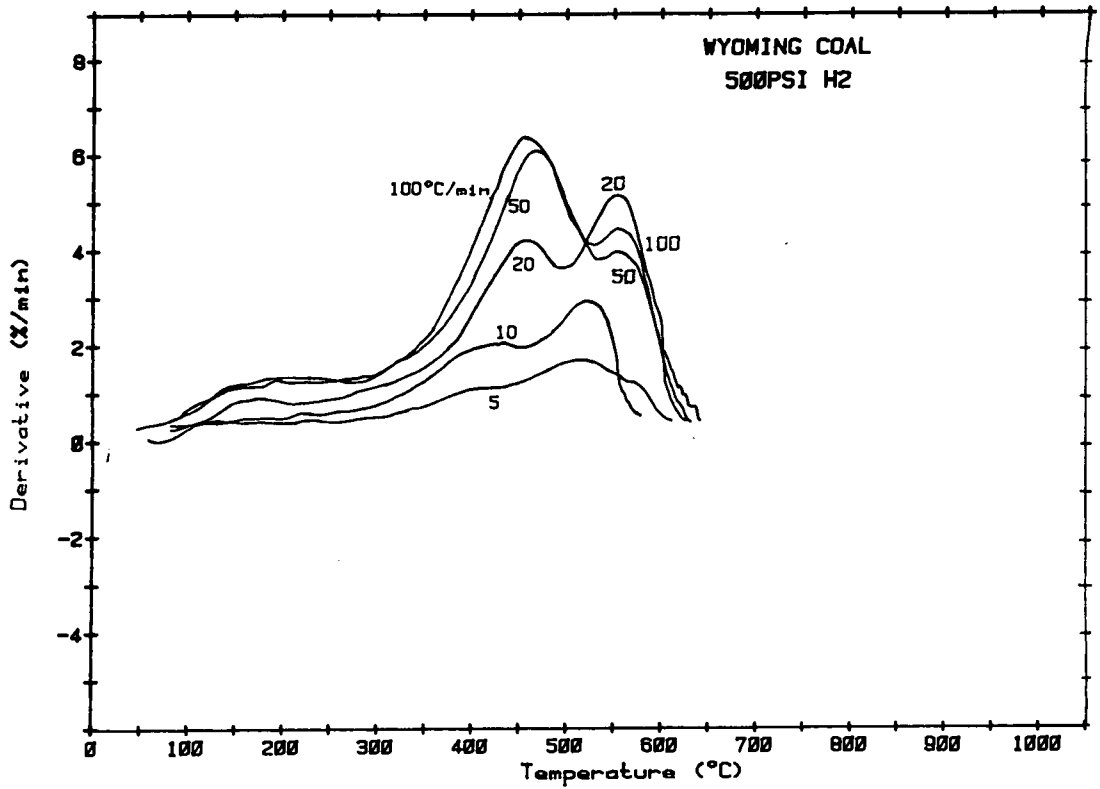

Fig. 4 The Effect of Heating Rate on Devolatilization Rate of Wyoming Coal Hydropyrolysis.

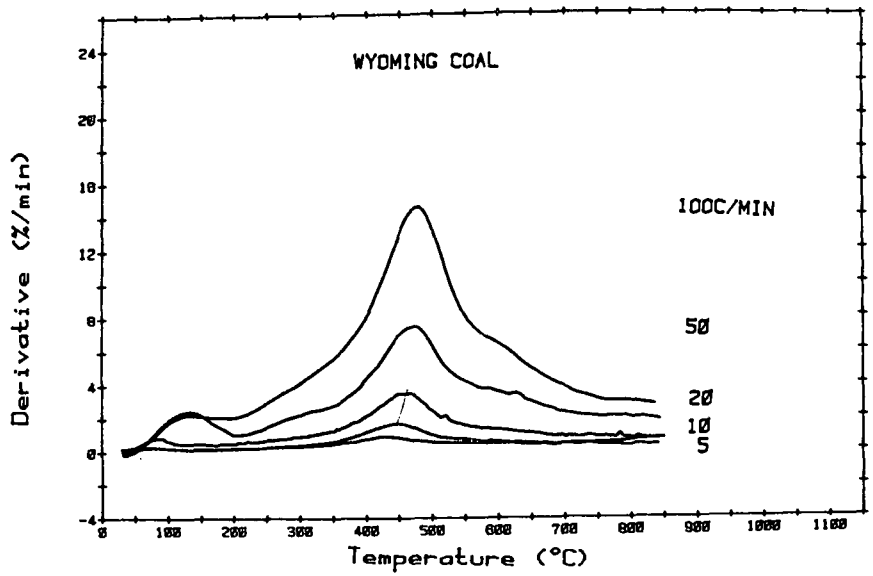

Fig. 5 Derivative Thermograms of Coal Pyrolysis at Different Heating Rates Under 1atm N2.

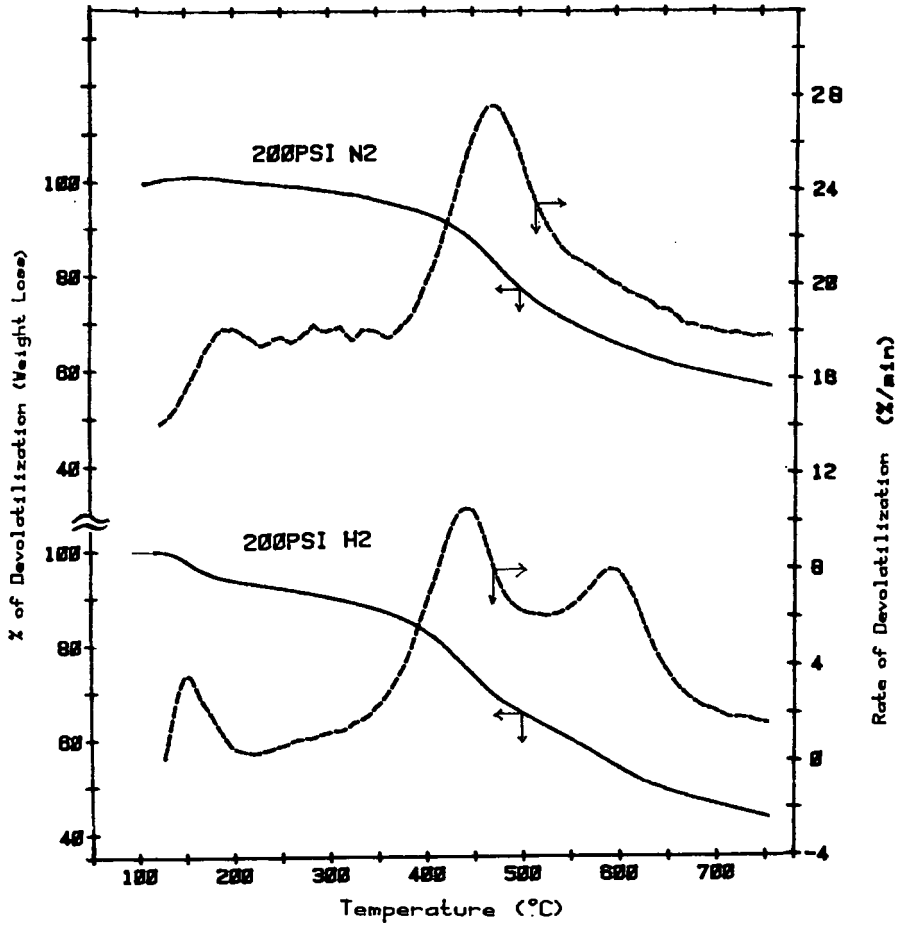

Fig. 6 A Comparison of Thermograms between Wyoming Coal Pyrolyzed in 200 psig N2 and 200 psig H2 at 20°C/min.

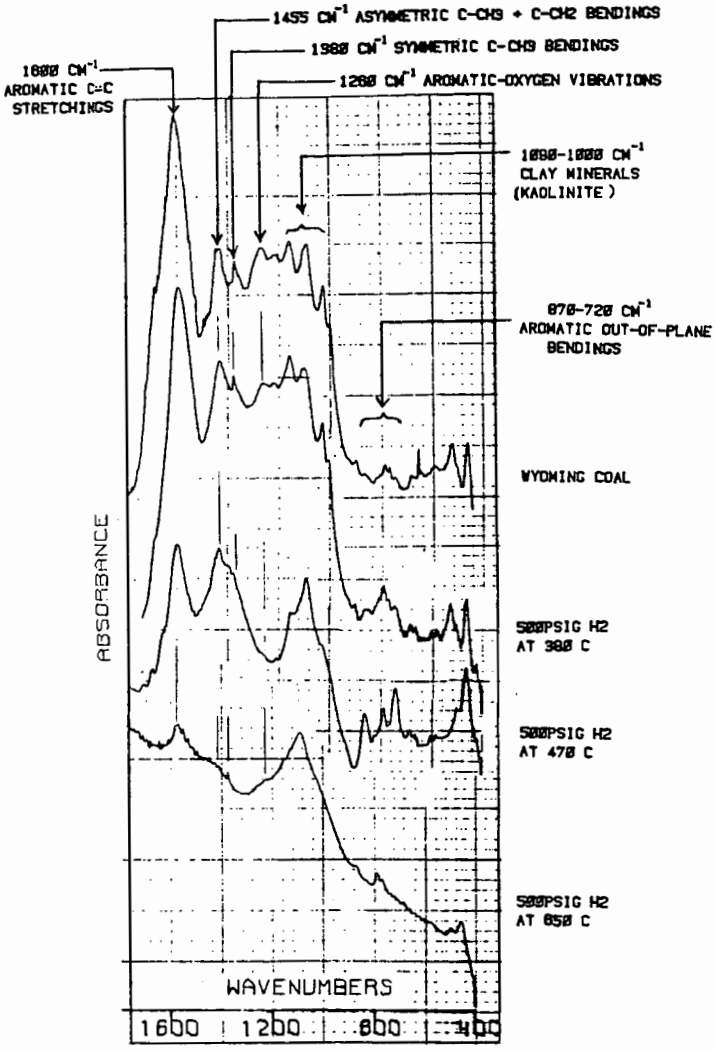

Fig. 7 FT-IR Monitor of Wyoming Coal Pyrolysis under 500 psig H2 at Various Temperatures.

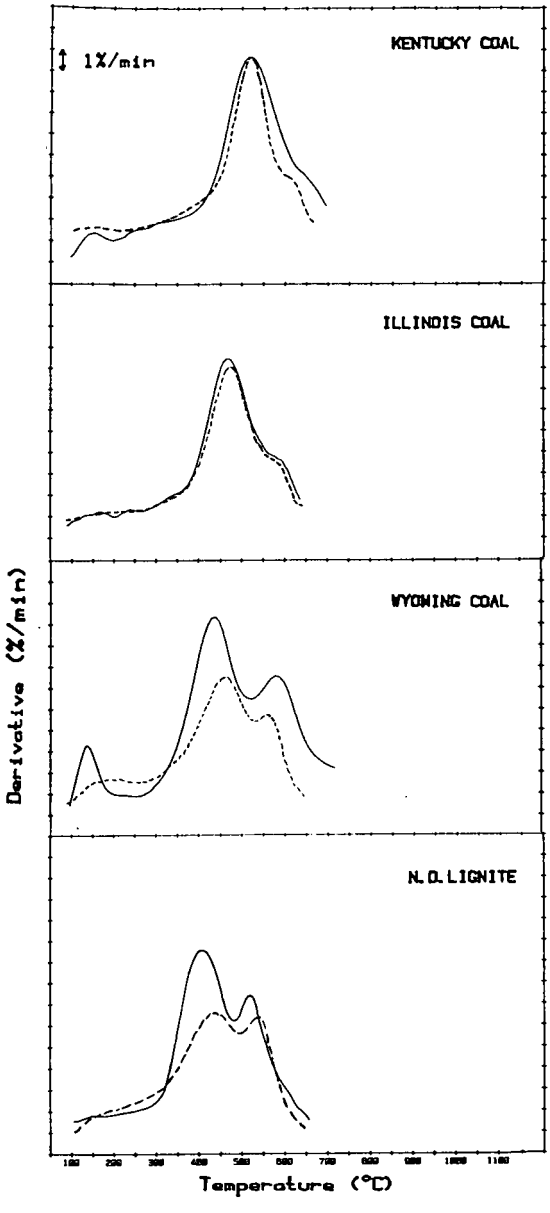

Fig. 8 The Influence of CO on Coal Devolatilization, where —; 500 psig CO/H2 and---; 500 psig H2.

COMBUSTION REACTIVITY OF LOW RANK COAL CHARS

B.C. YOUNG

CSIRO Division of Fossil Fuels, PO Box 136, North Ryde, NSW 2113, Australia

Introduction

For many years the CSIRO has been involved in studies on the combustion kinetics of coal chars and related materials. Early work included studies on a char produced from a Victorian brown coal (1). More recently, the combustion kinetics of chars produced during the flash pyrolysis of sub-bituminous coals have been determined (2,3).

In this paper data are given for the combustion reactivities of four flash pyrolysis chars. Their reactivities are compared with the results for chars produced from low and high rank coals, and petroleum coke. Reactivity is expressed as the rate of combustion of carbon per unit external surface area of the particle, with due correction being made for the effect of the mass transfer of oxygen to the particle.

Experiment and Theory

Details of the method of producing the flash pyrolysis chars are available elsewhere (4), as is information on the procedure for measuring their combustion rates (2,3,5). In brief, pulverized Millmerran and Wandoan coals (Queensland, Australia) were flash pyrolysed at various temperatures between 500 and 800°C. The resulting chars were screened to yield a size fraction having a median mass size around 80 μm. The properties of the chars are presented in Table 1.

TABLE 1 Properties of the Chars

	Millmerran					Wandoan
Pyrolysis temperature, °C	540	585	610	780	800	550
Median mass size, μm	85	76	90	70	88	76
Size below which 90% of material lies, μm	100	95	118	92	98	96
Size below which 10% of material lies, μm	66	52	61	47	74	49
Particle density, g/cm^3	0.88	0.80	0.78	0.99	0.78	1.05
Chemical analysis, % w/w (as received)						
Moisture	2.7	2.2	3.3	2.5	4.7	2.9
Ash	28.0	30.4	35.6	60.1	38.2	22.1
Elemental composition						
C	56.6	55.3	50.7	31.3	50.3	60.3
H	3.8	2.8	2.7	1.1	1.3	3.3
N + S + O	8.9	9.3	7.7	5.0	5.5	11.4

Rate measurements were carried out, using an entrainment reactor, on flowing suspensions of particles in preheated oxygen-nitrogen. From progressive changes in gas composition and gas and wall temperatures along the reactor, the rate of carbon burned per unit external area of particle (ρ) was calculated.

From ρ, the chemical rate coefficient, R_c, was evaluated (6):

$$\rho = R_c \, [p_g \, (1 - \chi)]^n \qquad g/cm^2s \qquad (1)$$

where p_g is the partial pressure of oxygen in the bulk gas, n is the order of reaction in relation to p_g and λ is the ratio of ρ to the maximum possible (i.e. mass transfer limited) burning rate calculated from known physical properties (6,7).

R_c, as will be shown, is strongly dependent on particle temperature, T_p. This temperature is calculated from a heat balance over the burning particle (6).

Results and Discussion

Combustion rate data for Millmerran and Wandoan chars are shown in Arrhenius form in Fig. 1. Data for Millmerran chars produced at 585 and 610°C were combined into a single set, as were the data for the chars produced at 780 and 800°C. Rate data for other chars (derived from low and high rank coals) and also for petroleum coke are also included in Fig. 1. To permit the comparison of results for different materials exhibiting different values of n, the rate data were calculated from the relation:

$$\rho_c = R_c \, p_g^{\,n} \qquad g/cm^2s \qquad (2)$$

where p_g is taken as 1 atm. Values of the Arrhenius parameters, A (pre-exponential factor) and E (activation energy), together with the magnitude of n for each material referred to in Fig. 1 are listed in Table 2.

TABLE 2 Kinetic Data for the Combustion of Chars and Coke

Material	A $g/\{cm^2s\ (atm\ O_2)^n\}$	E kcal/mol	n	Reference
Millmerran char (540°C)	15.6	17.5	0.5	2
Millmerran char (585 and 610°C)	22.3	18.8	0.5	3
Millmerran char (780 and 800°C)	73.3	21.7	0.5	3
Wandoan char (550°C)	39.1	18.3	0.5	3
Yallourn brown coal char	9.3	16.2	0.5	1
New Zealand bituminous coal char	8	16.0	1.0	7
Anthracites and semi-anthracites	20.4	19.0	1.0	8
Petroleum coke	7.0	19.7	0.5	5

The data exhibit several notable features:

(1) The combustion rates of all the materials show a strong dependence on temperature, the values of the activation energies ranging from 16.0 to 21.7 kcal/mol.

(2) The activation energy increases and the reactivity of Millmerran chars decreases with increasing pyrolysis temperature.

(3) The most reactive char is that produced from Wandoan coal at 550°C. This material is about twice as reactive as chars produced from other low rank coals (Millmerran and Yallourn) and high rank coals (New Zealand bituminous, anthracites and semi-anthracites), and about ten times as reactive as petroleum coke.

(4) The low rank coal chars and petroleum coke show an order of reaction of 0.5. Earlier determinations on chars from high rank coals indicate a value of unity. However, a reanalysis (5) of an earlier set of data (9) showed, in the case considered, little to choose between n equal to 0.5 or 1.0.

The values of the activation energy for the Millmerran and Wandoan chars (~ 20 kcal/mol), together with those of the other materials listed in Table 2, imply reactions under circumstances where pore diffusion as well as chemical reaction exercises strong rate control, i.e. regime II (10) conditions apply. Confirmatory evidence that these materials are indeed burning under regime II conditions is provided by the steady decrease in particle size and slight reduction in the particle density of the particles as they burn away (6). This behaviour is illustrated in Fig. 2 by the data on the lowest temperature chars produced from Millmerran and Wandoan coal. Also shown are some theoretical curves indicating the changes in particle size and density to be expected for combustion at constant particle density or at constant particle size (6).

Conclusions

It has been shown that the reactivities to oxygen of chars produced from Millmerran sub-bituminous coal decrease with increasing pyrolysis temperature but are similar in magnitude to the reactivities of chars derived from a brown and a bituminous coal and to the reactivities of anthracites and semi-anthracites. However, Wandoan char, also of sub-bituminous origin, exhibits about twice the reactivity of Millmerran char and about ten times the reactivity of petroleum coke. On the basis of observed activation energy values, particle size and particle density behaviour it is concluded that the combustion rates of Millmerran and Wandoan chars are controlled by the combined effects of pore diffusion and chemical reaction.

Acknowledgements

The author is grateful to R.J. Hamor for carrying out the experimental measurements and to I.W. Smith for valuable discussions.

References

1. Hamor, R.J., Smith, I.W. and Tyler, R.J. Combustion and Flame, 21, 153-162 (1973).
2. Young, B.C. Proceedings of the International Coal Science Conference, Düsseldorf: Verlag Glückauf, Essen, pp. 260-265, 1981.
3. Hamor, R.J. and Young, B.C. Proceedings of the International Science Conference, Pittsburgh, in press (1983).
4. Edwards, J.H., Smith, I.W. and Tyler, R.J. Fuel, 59, 681-686 (1980).
5. Young, B.C. and Smith, I.W. Eighteenth Symposium (International) on Combustion, The Combustion Institute, Pittsburgh, pp. 1249-1255 (1981).
6. Smith, I.W. Nineteenth Symposium (International) on Combustion, The Combustion Institute, Pittsburgh, in press (1983).
7. Smith, I.W. Combustion and Flame, 17, 303-314 (1971).
8. Smith, I.W. Combustion and Flame, 17, 421-428 (1971).
9. Field, M.A. Combustion and Flame, 13, 237-252 (1969).
10. Mulcahy, M.F.R. and Smith, I.W. Review of Pure and Applied Chemistry, 19, 81-108 (1969).

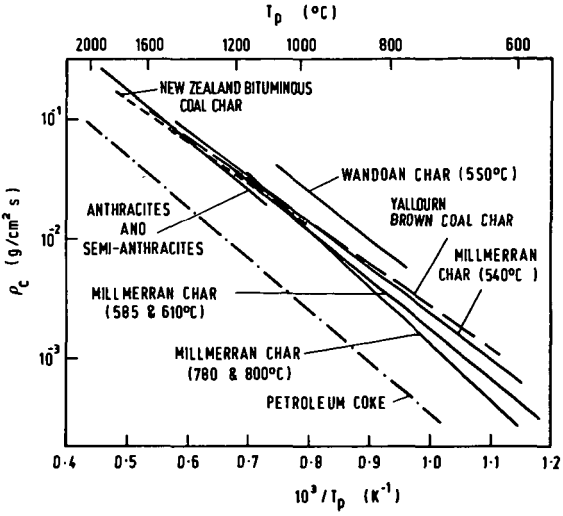

Figure 1 Combustion rate data for chars and coke

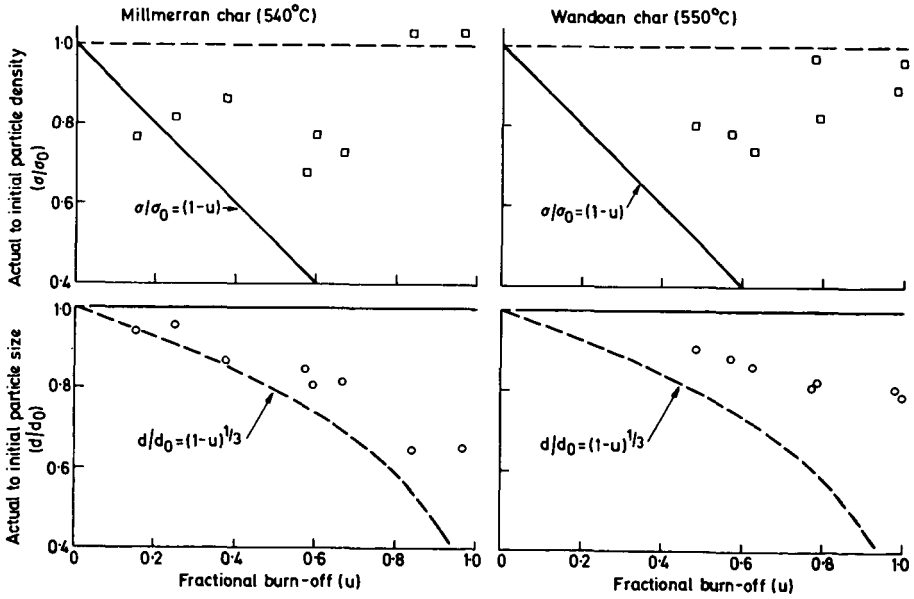

Figure 2 Burning behaviour of Millmerran and Wandoan chars (--- theoretical lines for particles burning with constant density, — theoretical lines for particles burning with constant size)

THE EFFECTS OF CATIONS ON PULVERIZED COAL COMBUSTION

Bruce A. Morgan and Alan W. Scaroni

Fuels and Combustion Laboratory
The Pennsylvania State University
University Park, PA 16802

INTRODUCTION

Although coal has been burned for centuries, many fundamental aspects of the process remain poorly understood. Conflicting theories appear in the voluminous combustion literature. There is, however, general agreement that coal combustion occurs in two stages: pyrolysis or devolatilization of the coal followed by heterogeneous combustion of the char (1-3). In most practical combustors, the latter acts as the rate determining step for the overall process. For more efficient coal combustion, therefore, it is essential to understand the parameters which most affect the rate of heterogeneous char combustion.

Char combustion rate depends primarily on the reactivity of the carbonaceous material to oxygen. This reactivity is controlled by several parameters such as gas diffusion rates to and from the reactive surface and catalysis of combustion by inorganic species present in the char. This research concentrates on the effect of various inorganic species on the rate of pulverized lignite combustion.

Jenkins et al. (4) have shown that the reactivity of coal chars is rank related. Chars from low rank coals such as lignites were found to be more reactive than chars produced from high rank bituminous coals. This has been attributed to the presence of inorganic constituents, in particular ion exchangeable cations, in low rank coals and their chars (5-7).

Walker (7) and McKee (8) have shown that alkali and alkaline-earth metals are catalysts for the carbon-oxygen reaction. Furthermore, the predominant ion exchangeable cations on American lignites are alkali (Na, K) and alkaline-earth (Ca, Mg, Ba) metals (9). Therefore, it is possible that highly dispersed cations on low rank coal chars catalyze the heterogeneous combustion step.

Reactivity data have been generated previously under isothermal conditions in the absence of particle ignition (5-7). The present work reports on lignite combustion under nonisothermal conditions. It was directed primarily towards understanding the effects of cations (K, Ca, Na) on the initial stages of pulverized coal combustion.

EXPERIMENTAL

Sample Preparation. The ion exchangeable cations located on the carboxyl groups of a Texas lignite (PSOC-623) were removed by acid washing with 0.04 M HCl. Alkali (Na, K) and alkaline-earth (Ca) metals were back exchanged on the acid-washed coal using 1 M metal acetate solutions. Details of the procedure are outlined elsewhere (10). The quantity of exchanged cations was determined by atomic absorption spectroscopy.

Combustion Experiments. Raw and modified lignite (mean weight particle size 62 μm) were combusted in an entrained-flow reactor at an initial furnace (gas and wall) temperature of 973 K. The reactor configuration and operating principle have been well documented (10-12). Weight loss rate data were obtained using an ash tracer technique.

RESULTS AND DISCUSSION

Sample Characteristics. Proximate analyses of the raw and modified Texas lignite are shown in Table 1. Acid washing with HCl reduced the total ash yield

TABLE 1

PROXIMATE ANALYSES OF TEXAS LIGNITE (PSOC 623)

	Ash, wt% (Dry)	VM, wt% (Dry)	Moisture, wt%
Raw	15.9	44.7	10.8
Ca Loaded	14.0	46.5	8.0
Na Loaded	13.0	43.4	12.3
K Loaded	15.0	43.9	12.4
Acid-Washed	10.7	46.1	7.7

of the coal by 33 wt%. Subsequent addition of the cations increased the ash yields by between 18% (Na) and 29% (K), based on the raw lignite. The quantity of each cations back exchanged, wt% dry basis, is shown in Table 2. The acid washing was

TABLE 2

CATION LOADINGS ON THE LIGNITE*

Cation	wt% (Dry)	milliequivalents/g of coal (Dry)
Ca	3.8	1.2
Na	2.6	1.0
K	5.0	1.1

*The acid-washed sample had less than 0.1 wt% (dry) cations on the coal.

an efficient procedure since less than 0.1 wt% (dry basis) of the cations remained on the acid washed coal.

Weight Loss Rate Data. Figure 1 illustrates weight loss rate data (wt%, daf) in air for raw and exchanged lignites. Residence times were determined using the model formulated by Morgan (10). Essentially, the model accounts for slip velocity between particles and flowing gas.

In the initial 0.1 s, the acid-washed lignite had the greatest rate of weight loss. The initial step in the combustion process accounting for weight loss is pyrolysis. Figure 2 illustrates the effect of cations on the rate of pyrolysis. These data were obtained in N_2 at a furnace temperature of 973 K. During pyrolysis, the acid-washed lignite had a greater rate of weight loss and a greater total weight loss in the residence time of the reactor. It is suggested that cations catalyze secondary char forming reactions of the primary volatiles, particularly the tars (10). These cracking and/or polymerization reactions on the surface of particles reduced the initial rate of weight loss (when tar evolution was predominant) and the total yield of volatiles due to surface carbon deposition.

As shown in Figure 1, when heterogeneous combustion predominated (residence times >0.1 s) the modified coals lost weight more rapidly than the acid-washed lignites. Alkali and alkaline-earth metals are known to be excellent catalysts for the carbon-oxygen reaction (7,8). Hence, it is suggested that cations exchanged on the coal catalyzed the heterogeneous combustion of the char.

The Na and K loaded lignites underwent greater total weight loss (by about 20 wt%) than the calcium loaded lignite in the total residence time of the furnace. Isothermal reactivity data have shown that K and Na are better catalysts than Ca for the carbon-oxygen reaction (5,7). However, the low weight loss by the Ca loaded coal may be the result of a combination of two factors: catalysis of secondary reactions and catalysis of the carbon-oxygen reaction.

SUMMARY

The effect of cations on the combustion behavior of pulverized lignite can be divided into three main areas: the rate of weight loss due to pyrolysis, the total weight loss due to pyrolysis and the rate of heterogeneous char combustion. The presence of cations (Na, K, Ca) reduced the rate of pyrolysis and the total weight loss due to pyrolysis but increased the char combustion rate.

REFERENCES

1. Field, M. A., Gill, D. W., Morgan, B. B., Hawksley, P. G. W., Combustion of Pulverized Coal, The British Coal Utilization Research Association, Leatherhead, 1967.

2. Smith, I. W., Combustion and Flame, 17, 303, 1971.

3. Field, M. A., Combustion and Flame, 14, 237, 1970.

4. Jenkins. R. G., Nandi, S. P., and Walker, P. L., Jr., Fuel, 52, 288, 1973.

5. Hippo, E. J. and Walker, P. L., Jr., Fuel, 54, 245, 1975.

6. Radovic, L., Ph.D. Thesis, The Pennsylvania State University, 1982.

7. Walker, P. L., Jr., Fuel, 62, 140, 1983.

8. McKee, D. W., Fuel, 62, 170, 1983.

9. Morgan M. E., Jenkins, R. G., and Walker, P. L., Jr., Fuel, 60, 189, 1981.

10. Morgan, M. E., Ph.D. Thesis, The Pennsylvania State University, 1983.

11. Scaroni, A. W., Walker, P. L., Jr., and Essenhigh, R. H., Fuel, 60, 71, 1981.

12. Maloney, D. J., Ph.D. Thesis, The Pennsylvania State University, 1983.

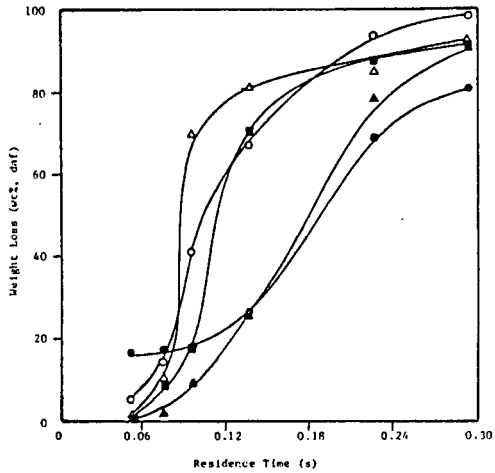

Figure 1. Effect of Cations on Combustion at a Furnace Temperature of 973 K. ■ Na; ○ K; ● Ca; △ Acid-washed; ▲ Raw.

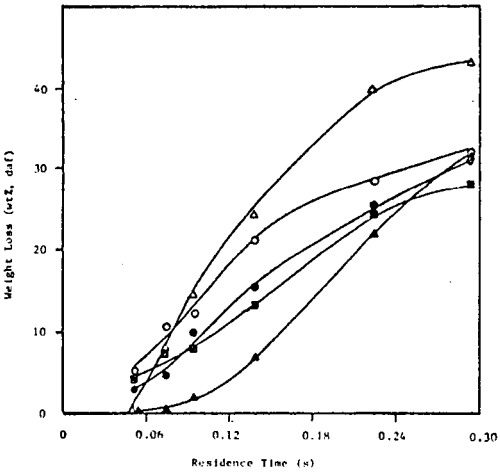

Figure 2. Effect of Cations on Pyrolysis in Nitrogen at 973 K. ■ Na; ○ K; ● Ca; △ Acid-washed; ▲ Raw.

CATALYSIS OF LIGNITE CHAR GASIFICATION BY EXCHANGEABLE CALCIUM AND MAGNESIUM

T. D. Hengel and P. L. Walker, Jr.

Department of Materials Science and Engineering
The Pennsylvania State University, University Park, PA 16802

INTRODUCTION

The high intrinsic reactivity of chars derived from lignite coals is primarily due to the presence of well dispersed metal oxide particles, which are formed when carboxyl groups on the lignite surface, having been exchanged with various cations from the local groundwater, decompose as the lignite is heated to gasification temperatures. Roughly half of the carboxyl groups on American lignites have undergone exchange, with Ca and Mg predominantly, and to lesser extents with other alkali and alkaline-earth cations (1). These cations have been shown to be good catalysts for lignite char gasification in air, CO_2 and steam (2).

It is noted, however, that lignite char reactivity decreases rapidly as final heat treatment temperature increases (3,4) or as soak time at temperature increases (4). Radovic and co-workers (5) have shown that the majority of this decrease can be correlated with a decrease in CaO dispersion in the case of Ca loaded demineralized (Dem) lignite chars.

Exchangeable cations play an important role in the behavior of lignite coals in coal conversion processes. It is, therefore, important that a fundamental understanding be attained, first of the possible interaction of exchangeable cations in lignites with each other, and, second, of the possible effects on the subsequent catalytic activity of the cations for lignite char gasification. The aim of this study was to develop such an understanding using the two most abundant cations in American lignites: Ca and Mg. The objective of this work was to study the effect which adding Mg, which is a poor gasification catalyst, to Ca, which is a good gasification catalyst, has on the catalytic behavior of Ca for lignite char gasification. That is, will the presence of Mg in some way affect the sintering of Ca and, hence, affect the catalytic activity of Ca?

EXPERIMENTAL

A Montana lignite (6) was subjected to essentially complete demineralization with HCl and HF in order to remove essentially all the inorganic constituents (exchangeable cations and mineral matter) present (1). The Dem lignite was then ion-exchanged with Ca or Mg using solutions of their acetate salts. Seven levels of Ca and three levels of Mg were obtained using loading solutions of varying concentrations. A sample of Dem lignite was also co-exchanged with Ca and Mg in order to study the effect of their interaction on subsequent char reactivity. Chars were prepared by slowly heating (10 K/min) the treated lignites in a box furnace equipped with an air tight retort under N_2 to final temperatures of 973 or 1273 K and held (soaked) for 1 h. Char reactivities were determined by isothermic thermogravimetric analysis (TGA) in 0.1 MPa air, 0.1 MPa CO_2 and 3.1 kPa steam (saturated N_2). The maximum slope (R_{max}) of the TGA recorder plot was used as a measure of gasification reactivity (normalized to initial weight of char, daf basis). From a series of preliminary runs (7) reaction conditions were selected in order to eliminate heat and mass transfer limitations. Therefore, reported reactivities are believed to be intrinsic, chemically controlled rates.

Selected chars were examined by x-ray diffraction (XRD) to identify Ca and Mg containing species present in the chars. Average crystallite diameters of selected species were determined using the line broadening concept and the Scherer equation (8).

RESULTS AND DISCUSSION

Figures 1 and 2 show the reactivity results in 0.1 MPa air for the 973 and 1273 K chars, respectively. As seen previously, Ca is a good catalyst for char gasification in air, while Mg is a poor char gasification catalyst (2). For Ca loaded chars at both heat treatment temperatures, it is seen that two distinct regions of reactivity behavior are present. For loadings up to ~4 wt% Ca, the reactivity increases linearly with increasing Ca content. For loadings greater than ~4 wt% Ca, however, reactivity remains essentially constant with increasing Ca content. This is contrary to the behavior seen by Hippo et al. (9)., who reported a linear increase in reactivity with increasing Ca content up to 12.9 wt% in 0.1 MPa steam for a Texas lignite. Since mass transport limitations are believed to be absent, the plateau is not due to diffusional effects. This suggests that the plateau is the result of a catalyst "saturation effect," that is, adding of catalyst beyond a certain amount does not further increase the observed rate. For the relatively small range of Mg contents a similar saturation effect appears to be operating. Examination of the cation exchanged 1273 K chars by XRD revealed that CaO and MgO were the major species present in the Dem+Ca and Dem+Mg chars, respectively.

Reactivity results for the 1273 K chars reached in 0.1 MPa CO_2 and 3.1 kPa steam at 1053 K are shown in Figures 3 and 4, respectively. The same trends evident for the 1273 K chars reacted in 0.1 MPa air are also seen in these reactant gases. Two regions of reactivity behavior are present in both cases. Calcium is seen to be a good char gasification catalyst, while Mg has very little catalytic effect.

The purpose of this work was to study the effect that adding Mg to Ca has on the subsequent catalytic behavior of Ca for lignite char gasification. To study this effect, the chars of the co-exchanged Dem lignite were used. It was reasoned that the co-exchanged chars should have a Ca content which was in the region where reactivity increased with metal content, as to avoid the saturation region. Also, the char should contain more Mg than Ca on a molar basis, since an effect is more likely to be observed under these conditions. Metal contents of the co-exchanged chars are presented in Table 1.

TABLE 1

METAL CONTENTS IN THE CO-EXCHANGED CHARS (DRY BASIS)

	Calcium		Magnesium	
Char	mmol/g	wt%	mmol/g	wt%
973 K	0.54	2.2	0.91	2.2
1273 K	0.56	2.2	0.94	2.3

To determine if there was any effect, reactivity data of the mono-exchanged chars were used to calculate an expected reactivity. Calculation of these expected reactivities was straight forward, which assumed that the catalytic activities of Ca and Mg were simply additive. From the metal contents in Table 1, the contributions of Ca and Mg to the calculated reactivities could be determined from Figures 1-4 by reading the reactivity value corresponding to that amount of Ca or Mg directly from the appropriate figure. The reactivity of the Dem-char is subtracted once because it is included in both the Ca and Mg contributions, while it is included only once in the co-exchanged char. This step is not necessary when the rate of the uncatalyzed (Dem) reaction is low; but is necessary when the uncatalyzed rate is high, as is the case in CO_2 (Figure 3). For consistency, the Dem reactivity

was always subtracted once. The calculated reactivity is the sum of the Ca and Mg contributions, with the rate of the Dem reactivity subtracted once. By comparing the calculated reactivity with that actually observed for the co-exchanged chars, one will be able to tell if indeed there is an effect. The calculated and observed reactivities are given in Table 2 for the various gases.

TABLE 2

CALCULATED AND OBSERVED REACTIVITIES OF THE CO-EXCHANGED CHARS

Char	Reactivity Contributions (mg/mg h)			Reactivities (mg/mg h)	
	Ca	Mg	Dem	Calculated	Observed
			Air		
973 K	0.31	0.09	0.01	0.39	0.42
1273 K	0.34	0.22	0.03	0.53	0.60
			CO_2		
1273 K	0.60	0.34	0.32	0.62	0.64
			Steam		
1273 K	0.30	0.10	0.05	0.35	0.31

It is quite clear from Table 2 that the addition of Mg to Ca does not have a significant effect on the subsequent activity of Ca. The observed reactivities are, within experimental error, the same as the calculated reactivities. This shows that the catalytic effects of Ca and Mg are additive and they do not interact in a significant way to either increase or decrease their combined catalytic effects. This is perhaps due to the fact that MgO is not significantly soluble in CaO below 1900 K (10). The presence of MgO does not reduce the sintering of CaO. This is supported by examination of the 1273 K co-exchanged char by XRD. The average crystallite diameter of the CaO was calculated to be 30 nm. This is the same value obtained for a 1273 K Dem+Ca char that has a similar Ca content (1.4 wt%).

CONCLUSIONS

The addition of Mg to Ca does not have a significant effect on the subsequent activity of Ca for lignite char gasification under the slow heating conditions used in this study. Their catalytic effects were found to be additive, indicating that they did not interact in any significant way. This was supported by XRD results which showed that the sintering of CaO was not reduced by the presence of MgO.

REFERENCES

1. Morgan, M. E., Jenkins, R. G. and Walker, P. L., Jr., Fuel 60, 189 (1981).

2. Walker, P. L., Jr., Matsumoto, S., Hanzawa, T., Miura, T. and Ismail, J. M. K., Fuel 62, 140 (1983).

3. Jenkins, R. G., Nandi, S. P. and Walker, P. L., Jr., Fuel 52, 288 (1973).

4. Radovic, L., "Importance of Catalysis and Carbon Active Sites in Lignite Char Gasification," Ph.D. Thesis, The Pennsylvania State University, 1982.

5. Radovic, L., Walker, P. L., Jr. and Jenkins. R. G., J. Catalysis, in press.

6. Penn State/DOE Coal Data Base, PSOC 833, Coal Research Section, The Pennsylvania State University.

7. Hengel, T., "Catalysis of Lignite Char Gasification by Exchangeable Cations: Calcium and Magnesium," M.S. Thesis, The Pennsylvania State University, 1983.

8. Klug, H. P. and Alexander, L. E., "X-ray Diffraction Procedures," 2nd Edition, Wiley, NY, 1974.

9. Hippo, E. J., Jenkins, R. G. and Walker, P. L., Jr., Fuel 58, 338 (1979).

10. Doman, R. C., Barr, J. B., McNally, R. N. and Alper, A. M., J. Amer. Cer. Soc. 46, 313 (1963).

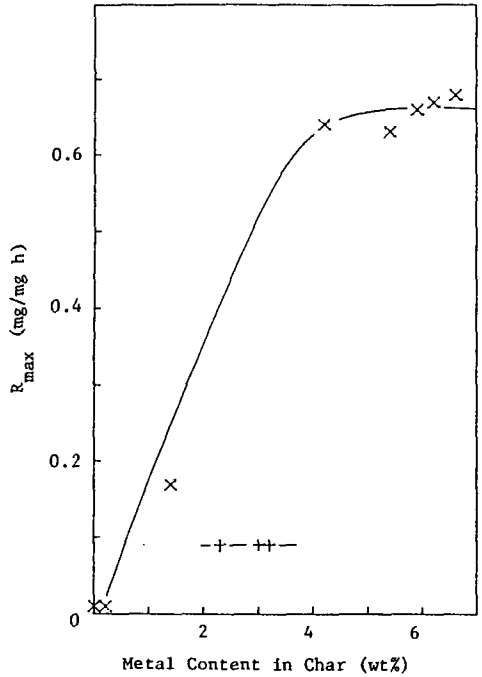

Figure 1

Reactivities of the 973 K Chars
in 0.1 MPa Air at 603 K.
x Dem+Ca, + Dem+Mg

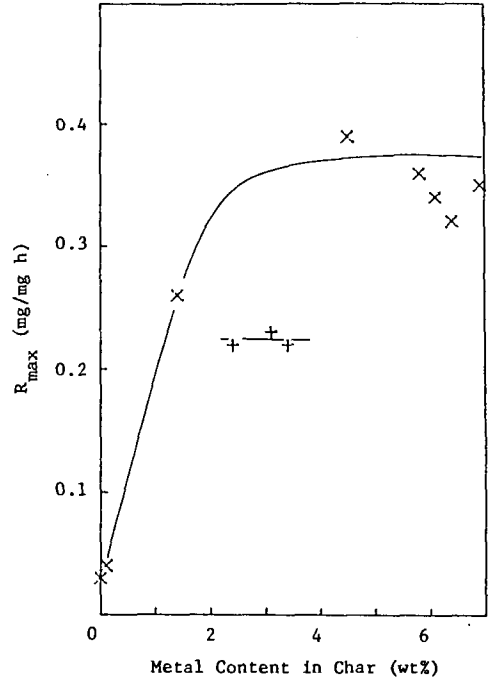

Figure 2

Reactivities of the 1273 K Chars
in 0.1 MPa Air at 603 K.
x Dem+Ca, + Dem+Mg

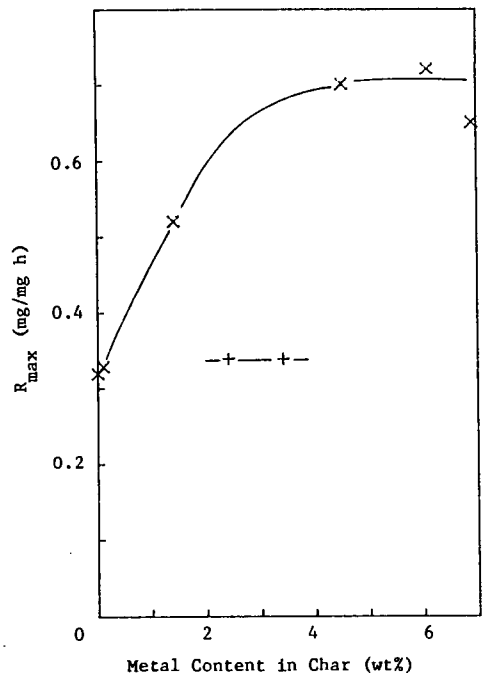

Figure 3

Reactivities of the 1273 K Chars
in 0.1 MPa CO_2 at 1053 K.
x Dem+Ca, + Dem+Mg

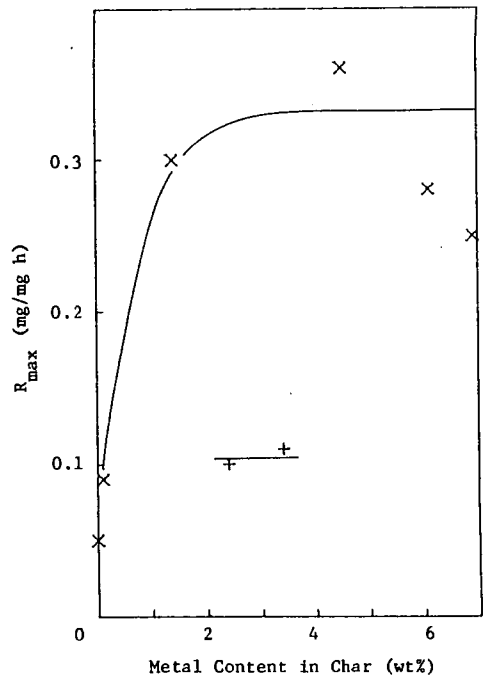

Figure 4

Reactivities of the 1273 K Chars
in 3.1 kPa Steam at 1053 K.
x Dem+Ca, + Dem+Mg

Measurement and Prediction of Low-Rank Coal Slag Viscosity

Robert C. Streeter,[1] Erle K. Diehl,[2] and Harold H. Schobert[3]

Bituminous Coal Research, Inc., Monroeville, PA 15146
and
Grand Forks Energy Technology Center, Grand Forks, ND 58202

INTRODUCTION

Since 1980, Bituminous Coal Research, Inc., (BCR) has been conducting measurements on the viscosity of western U. S. low-rank coal slags under a contract with the Grand Forks Energy Technology Center (GFETC), U. S. Department of Energy. This work has been motivated by the realization that 1) very few data exist in the literature on the viscosity of low-rank-coal slags; 2) published correlations relating slag viscosity to coal ash composition were derived from work with bituminous-coal slags, and attempts to apply them to data from low-rank coal slags generally have been unsuccessful; and, 3) from a practical standpoint, data on slag rheology are of considerable interest in support of the operation of a slagging fixed-bed lignite gasifier at GFETC. As a matter of related interest, BCR's slag viscometer was originally put into operation in 1976 to obtain data on the slagging properties of coals intended for use in the BI-GAS coal gasification pilot plant at Homer City, Pennsylvania; the BI-GAS process incorporates an entrained-bed, slagging gasifier.

Although the data obtained in these studies have been valuable in interpreting the slagging phenomena observed in the Grand Forks gasifier tests, a more fundamental objective of the current work is to develop correlations that can be used to predict *a priori* the viscosity behavior of low-rank-coal slags from a knowledge of the ash or slag composition.

EXPERIMENTAL

The slag-viscosity apparatus was assembled for BCR by Theta Industries, Inc. It includes a Lindberg furnace with globar heating elements of silicon carbide, rated for operation at temperatures up to 2732 F (1500 C). The rotating bob viscometer is a Haake RV-2 Rotovisco unit with a DMK 50/500 dual measuring head, which allows adjustment of torque by a factor of 10 (i.e., ranges of 0 to 50 and 0 to 500g-cm).* The torque on the viscometer bob twists a spiral spring inside the measuring head; the angular displacement of the spring is proportional to shear stress, and is converted to an electrical signal that is plotted on an X-Y recorder as a function of the rotational speed of the bob (shear rate). A microprocessor has been incorporated into the original system to provide automatic temperature programming at the rate of about 1°F/min, and stepwise bob rotation from 0 to 64 rpm in increments of 4 rpm.

To simulate conditions existing in the slagging coal gasifier, all tests are carried out in a reducing atmosphere consisting of 20 percent hydrogen and

---

[1] Supervising Scientist, Bituminous Coal Research, Inc.
[2] Manager, Applied Research, Bituminous Coal Research, Inc.
[3] Project Manager, Coal Science, Grand Forks Energy Technology Center

* Reference to a company or product name does not imply endorsement of the product to the exclusion of others that may be suitable.

80 percent nitrogen. The gas mixture is injected into the furnace at a flow rate of 500 cc/min through an alumina tube that extends to within 1 inch of the top of the sample crucible.

Although a platinum/rhodium bob was employed initially, some problems were encountered with attack on the bob by molten iron in the slag. In all of the tests discussed herein, the bob was fabricated from 1/2-inch molybdenum bar stock; the bob is approximately 1-inch long with a 30°-angle taper machined on both ends. The top of the bob terminates in a 5/8-inch long, 1/4-inch-diameter shaft which is drilled and tapped to accommodate a 1/8-inch- diameter x 16.5-inch long molybdenum stem. The bob stem is covered by a tubular alumina sleeve to minimize erosion during a test. As originally designed, the viscometer incorporated a universal joint in the measuring head shaft and a Jacobs-type chuck to hold the bob stem. However, this arrangement allowed too much lateral motion of the bob in the slag, and the bob is now attached to the measuring head by a rigid shaft containing three set screws to hold the stem. During a viscosity test, the bob is immersed until the slag just covers its top; the position of the bob can be determined accurately using a depth gauge attached to the measuring head.

In the earlier tests, the slag was melted in crucibles of vitreous carbon, 1-1/4-in. I.D. x 1-3/8-in. high (Atomergic Chemetals Co.). The carbon sample crucible was contained in a larger alumina guard crucible (1-7/8-in. I.D. x 6-in. high) and the annular space between the two crucibles was packed with 60-mesh alundum. The use of carbon crucibles was somewhat influenced by the observation that slag from the gasifier frequently contained particles of devolatilized coal (char), which might be involved in reactions with the molten slag. It soon became evident that iron oxides in the slag were being reduced by reaction with the carbon crucible, as small pools of molten iron invariably settled from the slag during the carbon-crucible tests. With certain coal ashes containing comparatively high amounts of Fe_2O_3, destruction of the carbon crucible was so severe that the portion in contact with the slag virtually disappeared during the viscosity test. Consequently, the carbon crucibles were eventually replaced with high-purity alumina crucibles (McDanel Refractory Co.) of the same dimensions.

Since the alumina crucibles were put into use, metallic iron has only rarely been observed in the slag; if formed at all, the iron usually tends to cling to the top of the bob at the gas/liquid interface. On the other hand, varying degrees of attack on the alumina crucible by the slag have been observed. Generally, dissolution of Al_2O_3 by the slag has been slight, but in a few cases noticeable thinning of the crucible walls has occurred. In addition, with the low-form alumina crucibles, there was a tendency for the slag to overflow the sample crucible and seep into the alundum packing. In a few cases, the slag managed to seep beneath the sample crucible, whereupon subsequent outgassing of the slag actually raised and tilted the sample crucible. To alleviate this problem, high-form (3-in. high) sample crucibles have been employed since September, 1982.

Since measured viscosities will vary depending on the dimensions of and the materials employed for the sample crucible and the rotating bob, measured values are related to absolute viscosities by means of an instrument factor. In these studies, the instrument factor was determined by tests with NBS glass viscosity standards whose viscosities are precisely defined and similar to those of the slags over the temperature range of interest. The instrument factor is related to viscosity by the equation:

$$\text{Viscosity} = \text{Instrument factor} \times \text{torque reading} \div \text{bob speed (rpm)}$$

In preparation for a slag-viscosity test, the coal is pulverized to minus-60 mesh and ashed in B&W K-3000 insulating firebrick dishes for 3 hours at 1850 F (1010 C) in a large muffle furnace. This higher-than-normal ashing temperature was chosen after preliminary work showed that sufficient volatiles remained in the ash prepared

at the standard "ASTM temperature" of 1382 F (750 C)* to cause severe frothing and foaming during the ash melting process. This difficulty is still experienced to some extent during melting of the high-temperature ash and is believed due to decomposition of residual sulfates and volatilization of alkali-metal oxides in the ash. The coal ash is sieved again at 60 mesh to remove any foreign particles of firebrick, then compressed into pellets 5/8-inch in diameter weighing about 5 grams each. The ash pellets are dropped, one or two at a time, into the previously heated sample crucible through a long quartz tube; a typical coal-ash charge in the high-form alumina crucibles is about 60 to 70 grams.

Viscosity measurements are normally commenced at the highest temperature at which an on-scale reading can be obtained with a bob speed of 64 rpm. The temperature is then decreased slowly (under microprocessor control) and viscosity measurements are taken at approximately half-hour intervals. This "cooling cycle" is continued until the upper limit of the measuring head is approached (typically about 3000 poises**), then the slag is gradually reheated to observe changes in viscosity during a "heating cycle."

Following each test, samples of the solidified slag and high-temperature ash are submitted to GFETC for compositional analyses by X-ray fluorescence and X-ray diffraction techniques. A Kevex Model 0700 energy dispersive X-ray spectrometer is employed for X-ray fluorescence analysis. Samples are ground to minus 60-mesh and pressed into a pellet using either cellulose or lithium tetraborate as a binder. The instrument is calibrated using mixtures of reagent-grade oxides, blended to approximate the relative amounts present in the slag. X-ray diffraction measurements are conducted on minus 325-mesh samples using a Philips 3600 automated X-ray diffractometer. Compound identification is accomplished with the aid of a computer-based index file.

The selection of low-rank coals for these studies was based to some extent on those which had actually been tested or were candidate feedstocks for the GFETC lignite gasifier; in addition, an effort was made to choose samples that would represent a wide range of ash compositions and diverse geographical locations. The coals selected for these viscosity studies are listed in Table 1.‡

RESULTS AND DISCUSSION

Viscosity can be defined as the resistance to flow offered by a fluid and is customarily expressed as the ratio of shear stress to shear rate. The most commonly encountered regime of viscous flow is termed "Newtonian" flow, in which shear stress is a linear function of shear rate (i.e., viscosity is constant at any given shear rate). For Newtonian substances, the dependence of viscosity (η) on

---

* ASTM Method D 3174-73, "Ash in the Analysis Sample of Coal and Coke."

**Throughout this paper, viscosities are given in the more familiar units of poises; the accepted SI unit for viscosity is the Pascal-second, and the conversion is poises x 0.1 = Pa·sec.

‡ In view of the considerable within-seam or within-mine variability of low rank coals, it should be understood that these coal samples are not necessarily representative of the total production of a particular mine.

temperature (T) is exponential, such that a plot of log η vs. T yields a straight line.* Three other regimes of non-Newtonian behavior are less commonly encountered:

1. Pseudoplastic - viscosity decreases with increasing shear rates.

2. Plastic - viscosity decreases with increasing shear rates following the appearance of an initial yield stress.

TABLE 1. SAMPLES SELECTED FOR LOW-RANK COAL VISCOSITY STUDIES

Sample	Rank	Location (State)
1. Indian Head	Lignite	North Dakota
2. Gascoyne	Lignite	North Dakota
3. Baukol-Noonan	Lignite	North Dakota
4. Beulah	Lignite	North Dakota
5. Colstrip	Sub-bituminous	Montana
6. Decker	Sub-bituminous	Montana
7. Sarpy Creek	Sub-bituminous	Montana
8. Naughton	Sub-bituminous	Montana
9. Big Horn	Sub-bituminous	Wyoming
10. Kemmerer	Sub-bituminous	Wyoming
11. Black Butte	Sub-bituminous	Wyoming
12. Emery	Bituminous (low rank)	Colorado
13. Rockdale	Lignite	Texas
14. Martin Lake	Lignite	Texas
15. Big Brown	Lignite	Texas
16. Atlantic Richfield	Lignite	Texas
17. Burns & McDonnell	Lignite	Alabama

3. Thixotropic - viscosity decreases with increasing shear rates and with the duration of the applied shear stress.

In each of these cases, the viscosity varies with shear rate and/or with the period of shear, and the ratio of shear stress to shear rate is customarily designated as "apparent viscosity."

Plots of log η vs. T (°F) for three representative low-rank coal slags are shown in Figure 1. Curve A for the Black Butte sample illustrates the behavior of a

---

* From purely physico-chemical considerations, log η is proportional to 1/T where T is in °K. In practice, however, it is often more convenient to plot log η directly vs. temperature in °C, or (as in these studies where engineering conventions were employed in the design and operation of the coal gasifier) in °F.

glassy, siliceous-type slag that exhibits Newtonian properties over a wide temperature range. In addition, the viscosity behavior is reversible in that viscosities measured during reheating of the slag (solid circles) are essentially the same as those determined during the cooling cycle. The type of behavior represented by Curves B and C is more commonly observed for low-rank coal slags; log η is a linear function of temperature down to some point, designated as the temperature of critical viscosity, T_{cv} (as shown for Curve B). Below T_{cv}, the viscosity can increase quite abruptly (Curve B), or the increase may be somewhat more gradual (Curve C). Moreover, a "hysteresis" effect appears in the viscosity/temperature curve as the slag is reheated. This phenomenon is supposedly related to the slow redissolution of crystals, formed on cooling the slag below T_{cv}.(1) In theory, the viscosity of the slag on reheating should eventually return to the linear portion of the curve representing the fully liquid condition. However, as shown by Figure 1, this is not necessarily achieved experimentally, and the extent of the deviation is believed to be due to small compositional changes occurring in the melt during the viscosity determination (to be discussed later). Curve C in Figure 1 includes data points for two separate viscosity tests with Baukol-Noonan, approximately 6 months apart. As shown, the repeatability for the cooling curve is quite good; on the other hand, there is a marked difference in the two curves obtained on reheating the slags, and subsequent analytical data showed subtle differences in the compositions of the slags from the two tests.

The straight-line portion of the viscosity/temperature curve is traditionally designated as the "Newtonian" region of slag behavior, while the area below T_{cv}, where solid species are crystallizing from the melt, is designated as the "plastic" region. Strictly speaking, a slag can retain Newtonian properties below T_{cv}, and transition to a non-Newtonian state can be detected only by a change in the shape of the shear-stress vs. shear-rate curve. As a matter of fact, most of the slags included in this study actually did show pseudoplastic or thixotropic behavior at the higher viscosities.

Of the 17 coals listed in Table 1, 13 were tested in carbon crucibles and the remaining four were tested using alumina crucibles. In addition, the carbon-crucible test with Baukol-Noonan was repeated, and six of the coals from the carbon-crucible tests (Big Horn, Decker, Emery, Colstrip, Rockdale, and Burns & McDonnell) were also selected for alumina-crucible tests. Thus, a total of 24 slag-viscosity tests provided the data discussed in this paper.

The compositions of the slags from these viscosity tests are listed in Table 2 (compositional data are normalized to 100 percent). Also included are several other parameters that traditionally have been employed to characterize coal-ash slags. It should be emphasized that, unless otherwise noted, all calculations discussed herein were based on <u>slag</u> composition data (as opposed to <u>ash</u> composition data). This was done primarily for two reasons:

1) As previously noted, reactions with the sample crucible tended to result in depletion of Fe_2O_3 (carbon-crucible tests) and/or enrichment in Al_2O_3 (alumina-crucible tests), so that in some cases the composition of the slag was significantly different from that of the original coal ash. This effect can be seen by comparing the slag composition data in Table 2 for the carbon- and alumina-crucible tests with Colstrip, Decker, Big Horn, Emery, Rockdale, and Burns & McDonnell.

2) Results of an independent study, comparing high-temperature ash and slag compositions for 18 of the 24 viscosity tests, showed that from 80 to 100 percent of the SO_3 and usually all of the P_2O_5 (if present in the ash) were volatilized during melting of the ash. Admittedly, P_2O_5 is a minor constituent, and losses of SO_3 could be compensated for by normalizing the analytical data to a sulfur-free basis. On the other hand, in 11 out of 15 instances (73 percent) where Na_2O was present in the high-temperature ash, it was volatilized in amounts ranging from 10 to 50 percent of the amount available in the ash. Since the Na_2O content of some ashes

TABLE 2. ANALYSIS OF LOW-RANK-COAL SLAGS PRODUCED IN SLAG VISCOSITY TESTS

Carbon Crucible Tests:	Slag Composition, Weight Percent										Base/ Acid Ratio (1)	Silica Ratio (2)	SiO_2/ Al_2O_3 Ratio	Lignite Factor (3)
Sample	SiO_2	Al_2O_3	Fe_2O_3	TiO_2	P_2O_5	CaO	MgO	Na_2O	K_2O	SO_3				
Gascoyne	42.4	14.8	3.1	1.4	0.0	25.7	8.2	3.7	0.1	0.2	0.70	53.4	2.86	10.9
Baukol-Noonan 1	41.4	19.2	1.0	2.3	0.0	21.8	4.3	7.7	0.6	1.2	0.56	60.4	2.16	26.1
Baukol-Noonan 2	39.3	19.7	4.5	1.7	0.0	18.3	4.4	9.9	0.6	1.1	0.62	59.1	1.99	5.0
Colstrip	45.0	23.9	2.1	1.8	0.0	20.6	5.9	0.1	0.1	0.4	0.41	61.1	1.88	12.6
Decker	38.4	20.0	6.5	2.1	0.0	18.7	4.2	8.6	0.3	0.9	0.63	56.6	1.92	3.5
Sarpy Creek	44.2	27.4	1.9	1.1	0.0	18.3	4.0	1.2	1.2	0.3	0.37	64.6	1.61	11.7
Naughton	63.5	17.8	5.5	0.8	0.2	6.7	3.6	0.0	1.6	0.1	0.21	80.1	3.57	1.9
Big Horn	27.1	28.6	11.4	1.5	0.7	16.3	6.9	5.0	0.5	1.8	0.70	43.9	0.95	2.0
Kemmerer	59.6	13.3	0.9	0.9	0.0	15.5	7.7	0.8	0.6	0.1	0.35	71.2	4.48	25.8
Black Butte	53.9	18.3	6.0	1.3	0.0	11.7	4.2	4.0	0.3	0.0	0.36	71.1	2.94	2.6
Emery	40.2	21.4	9.1	1.1	0.1	16.9	5.5	2.9	0.2	2.0	0.55	56.1	1.88	2.5
Rockdale	42.9	24.0	2.4	2.0	0.0	23.8	3.9	0.0	0.5	0.3	0.44	58.8	1.79	11.5
Atlantic Richfield	40.6	15.8	2.7	2.0	0.1	29.4	6.7	2.0	0.3	0.2	0.70	51.1	2.57	13.4
Burns&McDonnell	47.0	26.1	12.7	0.8	0.0	6.6	3.7	0.0	2.2	0.5	0.34	67.1	1.80	0.8

TABLE 2. ANALYSIS OF LOW-RANK-COAL SLAGS PRODUCED IN SLAG VISCOSITY TESTS (Continued)

Alumina Crucible Tests:	Slag Composition, Weight Percent										Base/ Acid Ratio (1)	Silica Ratio (2)	SiO_2/ Al_2O_3 Ratio	Lignite Factor (3)
Sample	SiO_2	Al_2O_3	Fe_2O_3	TiO_2	P_2O_5	CaO	MgO	Na_2O	K_2O	SO_3				
Indian Head	20.0	36.7	12.5	0.6	0.0	17.0	7.1	5.4	0.1	0.0	0.73	35.3	0.54	1.9
Beulah (high sodium)	24.2	33.6	14.0	0.9	0.0	14.4	4.3	8.1	0.2	0.3	0.70	42.5	0.72	1.3
Colstrip	38.0	28.1	11.2	1.5	0.0	17.1	3.9	0.0	0.1	0.0	0.48	54.1	1.35	1.9
Decker	36.1	23.0	8.8	2.1	0.0	18.2	3.8	7.5	0.2	0.0	0.63	54.0	1.57	2.5
Big Horn	30.2	24.7	13.6	1.8	0.8	18.1	5.5	4.5	0.5	0.1	0.74	44.8	1.22	1.7
Emery	44.2	24.7	7.4	1.4	0.0	15.1	4.1	2.6	0.2	0.0	0.42	62.4	1.79	2.6
Rockdale	38.5	27.5	8.9	1.7	0.0	20.0	2.7	0.0	0.4	0.0	0.47	54.9	1.40	2.6
Martin Lake	39.0	22.4	11.6	1.1	0.0	22.4	2.5	0.0	1.0	0.1	0.60	51.6	1.74	2.1
Big Brown	(analytical data for slag not yet available)													
Burns&McDonnell	45.7	23.1	18.9	0.8	0.0	6.0	2.8	0.0	2.0	0.2	0.43	62.3	1.98	0.5

(1) Base/Acid Ratio = $(Fe_2O_3 + CaO + MgO + Na_2O + K_2O)/(SiO_2 + Al_2O_3 + TiO_2)$ (Ref. 2)

(2) Silica Ratio = $100\ SiO_2/(SiO_2 + \text{"}Fe_2O_3\text{"} + CaO + MgO)$ where "Fe_2O_3" = $(Fe_2O_3 + 1.11\ FeO + 1.43\ Fe)$ (Ref. 3)

(3) Lignite Factor = $(CaO + MgO)/Fe_2O_3$ (Ref. 2). Theoretically, $\Sigma(CaO + MgO + Fe_2O_3)$ must be greater than 20% and the lignite factor must be greater than 1.0 for the ash (slag) to be considered a low-rank-coal type; the Burns&McDonnell sample is an obvious exception to this rule.

ranged up to 10 percent, it is probable that volatilization of this constituent would have an effect on the slag viscosity.

The data in Table 2 illustrate the wide variability in concentrations of low-rank-coal slag constituents. This variability is reflected further by Table 3, where the ranges in slag compositions encountered during these studies (Table 2) are compared with the ash composition of an "average" bituminous coal (SO_3-free basis).(4) Especially noteworthy are the higher concentrations of alkaline-earth and alkali metal oxides in the low-rank coal slags.

The experimental viscosity data from these studies are summarized in Table 4. The two viscosity values shown for each sample, corresponding to specific melt temperatures, are sufficient to approximate the linear ("Newtonian") portion of the log η vs. T curve obtained during the cooling cycle. In addition, values for T_{cv} (when observable) and ash fusibility (reducing atmosphere) for the high-temperature ash (HTA) are included for comparison.

Slag Viscosity/Composition Correlations

Several attempts have been made in the past to define the linear portion of the viscosity/temperature curve based on the composition of the coal ash. In the mid-1960's, workers at the British Coal Utilization Research Association (BCURA) developed two such correlations based on work with British (bituminous) coals, now generally referred to as the Watt-Fereday(5) and "S^{2}"(3) correlations.* The Watt-Fereday correlation is based on results of 276 determinations of slag viscosity using 113 different ash compositions prepared by blending British coal ashes. Unfortunately, attempts to apply this correlation to low-rank coal slags, using either ash- or slag-composition data, have been generally unsuccessful. This is illustrated by Figure 2, in which the viscosity/temperature cooling curves for two Texas lignites, Big Brown and Martin Lake, are plotted. The corresponding Watt-Fereday correlation lines are based on the (750 C ASTM) ash-composition data. As indicated by Figure 2, the ash compositions and ash fusion temperatures of these two coals are very similar. However, the viscosity predicted by the Watt-Fereday correlation for Big Brown was higher than that observed experimentally, while for Martin Lake the Watt-Fereday equation under-predicted the actual viscosity.

Among the possible reasons why these predictive equations fail for low-rank coals are the following:

1. Ash constituents may fall outside the range of those in most bituminous coals (Table 3).

2. The BCURA predictive equations are based on ash analyses. As discussed earlier, significant losses of certain elements may occur as the ash from low-rank coals is heated to the melting point.

3. Sulfur retention is more prevalent in low-rank coal ashes, due to the generally higher calcium contents. Some of the slags from these viscosity studies retained up to 2 percent SO_3 (Table 2), even after being heated above 2600 F (1427 C).

4. In lignites, some 30 to 50 percent of the ash-forming constituents can consist of cations attached to the organic matter in ion-exchangeable form on carboxyl groups or as chelate complexes, rather than being present as distinct mineralogical species.(6)

---

* Details of the viscosity/composition correlations are presented in Appendix 1.

TABLE 3. COMPARISON OF "AVERAGE" BITUMINOUS COAL ASH COMPOSITION WITH LOW-RANK-COAL SLAG COMPOSITIONS

Constituent	Range in Low-Rank-Coal Slags from Viscosity Studies, Wt. Percent*	"Average" Bituminous Coal Ash (SO_3-free), Wt. Percent
SiO_2	20.0 - 63.5	48.1
Al_2O_3	13.3 - 36.7	24.9
Fe_2O_3	0.9 - 18.9	14.9
TiO_2	0.6 - 2.3	1.1
CaO	6.0 - 29.4	6.6
MgO	2.5 - 8.2	1.7
Na_2O	0.0 - 9.9	1.2
K_2O	0.1 - 2.0	1.5

* From data in Table 2.

TABLE 4. EXPERIMENTAL DATA FROM LOW-RANK-COAL SLAG VISCOSITY STUDIES

Carbon Crucible Tests: Sample	Temperature Range of Viscosity Measurements (Melt Temp., °F)	Measured Viscosity at Indicated Temperature η, poises	T, °F	T_{cv}, °F (Approx.)	HTA Fusion Temperatures, °F Initial Deformation	Softening (Spherical)	Fluid
Gascoyne	2510 - 2145	25	2458	2180	2000	2080	2120
		102	2237				
Baukol-Noonan 1	2480 - 2090	41	2480	2125	2000	2040	2100
		482	2133				
Baukol-Noonan 2	2340 - 2100	93	2343	2125	2000	2040	2100
		548	2128				
Colstrip	2560 - 2320	39	2557	2450	2100	2180	2280
		102	2463				
Decker	2350 - 2110	50	2346	2145	2020	2060	2120
		289	2147				
Sarpy Creek	2700 - 2460	56	2697	2490	2000	2080	2140
		220	2491				
Naughton	2730 - 2550	979	2731	none	2100	2200	2320
		3375	2553				
Big Horn	2490 - 2225	93	2407	2270	2060	2100	2140
		325	2272				
Kemmerer	2640 - 2340	88	2637	2375*	2100	2160	2300
		589	2413				
Black Butte	2690 - 2290	140	2688	none	2080	2120	2200
		3375	2294				
Emery	2620 - 2270	98	2548	2325*	2060	2120	2260
		422	2354				
Rockdale	2680 - 2440	26	2681	2475	2080	2160	2220
		105	2481				
Atlantic Richfield	2400 - 2125	27	2396	2175	2040	2100	2140
		172	2183				
Burns & McDonnell	2690 - 2370	94	2690	2500*	2000	2080	2260
		272	2535				

TABLE 4. EXPERIMENTAL DATA FROM LOW-RANK-COAL SLAG VISCOSITY STUDIES (Continued)

Alumina Crucible Tests: Sample	Temperature Range of Viscosity Measurements (Melt Temp., °F)	Measured Viscosity at Indicated Temperature: η, poises	T, °F	T_{cv}, °F (Approx.)	HTA Fusion Temperatures, °F: Initial Deformation	Softening (Spherical)	Fluid
Indian Head	2650 - 2350	48	2594	2500*	2100	2200	2320
		82	2508				
Beulah (high sodium)	2640 - 2270	38	2597	2330*	2060	2140	2220
		340	2380				
Colstrip	2650 - 2360	18	2653	2470*	2100	2180	2280
		34	2520				
Decker	2290 - 2090	69	2286	2145	2020	2060	2120
		237	2146				
Big Horn	2390 - 2110	90	2331	2175	2060	2100	2140
		289	2177				
Emery	2560 - 2280	53	2564	2420	2060	2120	2260
		114	2441				
Rockdale	2620 - 2440	25	2617	2525	2080	2160	2220
		36	2553				
Martin Lake	2680 - 2260	43	2679	2320	2100	2140	2200
		635	2322				
Big Brown	2530 - 2300	24	2530	2350	2080	2120	2180
		59	2385				
Burns & McDonnell	2700 - 2150	40	2698	2300*	2000	2080	2260
		242	2402				

*T_{cv} not well defined.

The Watt-Fereday equation is approximately a linear equation of the form

$$\log \eta = m \cdot f(T) + c \qquad (1)$$

where m is normally positive and c is negative. Revised values for the slope (m') and intercept (c') can be calculated based on the experimental data for the low-rank coals to obtain a good fit to the Watt-Fereday equation. However, for 20 of 23 tests (87 percent) the value of m' was larger than that predicted by the conventional Watt-Fereday equation; similarly, absolute values of c' were also larger for 16 of 23 tests (70 percent). Since the intercept is negative, these two effects should tend to offset each other, resulting in little change in the value of log η. In reality, the net result tended to be a larger value for log η, such that observed viscosities were higher than predicted viscosities in 18 of the 23 tests (78 percent). Thus, these studies indicate that the viscosities of low-rank coal slags are generally higher than those of slags derived from bituminous coals.

Attempts were made to correlate the experimental values of m' and c' with slag composition data (Table 2) using multiple linear regression analysis. These attempts were generally unsuccessful, although for the carbon-crucible tests, the correlation of m' with Na_2O content was significant at the 99.5 percent confidence level, and for the alumina-crucible tests, Na_2O was ranked second in correlations for both m' and c' (even though not statistically significant). These findings suggest that the role of Na_2O in low-rank-coal slags may be more important than previously realized.

Other combinations of variables, including those listed in Table 2, were employed in efforts to derive empirical correlations with slag viscosity, but again without much success. In addition, the BCURA S^2 correlation(3) and a modified form of the Watt-Fereday correlation developed at the National Bureau of Standards(7) were tested. Of the 23 viscosity tests for which slag composition data are available, the NBS correlation gave a good fit to the experimental data in only two cases, while the S^2 correlation applied in only one case. Generally, the NBS and S^2 calculations gave higher viscosities than those predicted from the conventional Watt-Fereday treatment; the S^2 values were larger for 22 (96 percent) of the 23 tests, and the NBS values were larger for 19 (83 percent) of the tests. On the other hand, all three correlations had a tendency to underestimate the slag viscosity, as observed viscosities were greater than those estimated by any of the three predictive methods in 14 (61 percent) of the tests. Consequently, we conclude that the BCURA methods (or the NBS modification thereof) are generally unsatisfactory for estimating the viscosities of low-rank coal slags.

More recently, two correlations have appeared in the literature that were developed in France in studies with metallurgical (steel making) slags: the IRSID correlation, published by Riboud et al.,(8) and the Urbain correlation.(9) These two correlations are conceptually more appealing because:

- Unlike the BCURA correlations, which are based on the Arrhenius form of the viscosity equation

$$\eta = A \exp(E/RT), \qquad (2)$$

the IRSID and Urbain correlations are based on the Frenkel relation

$$\eta = AT \exp(B/T) \qquad (3)$$

which, according to the authors, is the preferred form.

- All slag constituents are included, rather than just the five major oxides.

- Slag constituents are expressed as mole fractions instead of weight percentages.

- The Urbain correlation is based on the SiO_2-Al_2O_3-CaO pseudo ternary phase diagram, and these three constituents usually predominate in low-rank coal slags.

However, there is a slight complication in that these correlations assume the oxidation state of iron in the slag is known. Since this information is not currently available for the low-rank-coal slags, and because all tests were in a reducing atmosphere, for computational purposes it was tentatively assumed that all iron was in the form of FeO.*

On this basis, the IRSID correlation gave a reasonably good fit to the experimental data (within 20 percent) for three of the 23 viscosity tests. Unlike the BCURA correlations, which tended to give consistently low results, the error in the IRSID correlation tended to be random; predicted viscosities were too high in 11 cases and too low in nine cases.

The Urbain correlation was acceptable for six tests, too high in seven instances, and too low in 10 instances. Furthermore, even though the Urbain correlation was unsatisfactory for 17 tests, compared with the IRSID correlation, the predicted viscosities were closer to the actual values in 10 instances. Of all the correlations tested (including the BCURA correlations), the Urbain correlation was judged to give the closest agreement to the actual viscosities in seven of the 23 tests; among the remaining 16 tests, the Urbain correlation was judged second-best for nine.

Since the Urbain method appeared to give a fair-to-good correlation for nearly two-thirds of the viscosity tests, efforts were directed toward modifying this procedure with the goal of optimizing the fit to the experimental data. The logarithmic form of the Urbain equation is

$$\ln \eta = \ln A + \ln T + 10^3 B/T \quad (T \text{ in } ^\circ K) \tag{4}$$

where B is a parameter defined by the composition of the slag and A is a function of B. The equation can be "forced" to fit the experimental data by adding a fourth term

$$\ln \eta = \ln A + \ln T + 10^3 B/T + \Delta \tag{5}$$

where Δ is the difference (either positive or negative) between the actual and computed (by equation 4) values of $\ln \eta$. Since $\ln \eta$ is a linear function of temperature above T_{cv}, Δ will also be a linear function of temperature:

$$\Delta = mT\ (^\circ K) + b \tag{6}$$

Thus, for each slag, values for m and b can be derived from the experimental viscosity data which uniquely define the linear portion of the viscosity/temperature curve by means of equation 5. The process then becomes one of correlating the variables m and b with some particular property of the slag.

It was found that, to a first approximation, b could be correlated with m by means of the expression

$$b = -1.6870(10^3 m) + 0.2343 \tag{7}$$

---

* Some very limited data from Mössbauer spectroscopy analysis indicate the presence of ferrous silicate phases in the slags. In cases where metallic iron was formed as a separate phase, it was normally removed before the slag sample was subjected to X-ray analysis.

with a correlation coefficient R = -0.988 for all 23 viscosity tests. The process was then reduced to finding a correlation for the variable m. Unfortunately, however, although a number of such correlations were attempted based on individual slag constituents and combinations thereof, no single correlation was found that satisfied the data from all the viscosity tests.

As a further refinement, the slags were subdivided into three groups based on the magnitude of the parameter B in the Urbain equation (equation 4). The magnitude of this parameter is related to the location of the slag composition in the SiO_2-Al_2O_3-CaO ternary phase diagram, and it is proportional to the silica content of the slag. Thus, with certain borderline cases, the three subgroups correspond roughly to "high-silica," "intermediate-silica," and "low-silica" slags.

The "high-silica" group included the five tests with Naughton, Burns & McDonnell, Black Butte, and Kemmerer (B>28), and a fair correlation (R = -0.971) was found for m of the form

$$10^3 m = -1.7264F + 8.4404 \qquad (8)$$

where $F = SiO_2/(CaO + MgO + Na_2O + K_2O)$ and slag components are in mole fractions. With this correlation, calculated viscosities were within 10 percent (very good) of actual viscosities for one test, within 30 percent (acceptable) for two other tests, and within 60 percent (marginally acceptable) for the 4th of five tests. Similarly, for the "intermediate-silica" slags (Colstrip, Rockdale, Emery, Sarpy Creek, and Martin Lake; B = 24 to 28), an expression similar to equation 8 was found. In this case, however, the correlating variable (F) appeared to be the product of the Urbain parameter B times the sum of the mole fractions of Al_2O_3 and FeO. For the eight viscosity tests in this group, the modified correlation was very good for two, acceptable for two others, and marginally acceptable for two more. For the "low-silica" slags (Gascoyne, Baukol-Noonan, Indian Head, Big Horn, Decker, Atlantic Richfield, and Beulah; B <24), the correlating variable chosen was $CaO/(CaO + MgO + Na_2O + K_2O)$ (mole fractions), although the correlation was less satisfactory, being very good for two tests, acceptable for two others, and marginally acceptable for two more, out of 10 tests. The equations developed for the modified Urbain correlations are summarized below, and viscosities calculated using the various correlations are compared with measured viscosities in Table 5.

High-Silica Slags:

$$b = -1.7137(10^3 m) + 0.0509 \quad (R = -0.990 \text{ for 5 of 5 data points})$$

$$10^3 m = -1.7264F + 8.4404 \quad (R = -0.971 \text{ for 5 of 5 data points})$$

where $F = SiO_2/(CaO + MgO + Na_2O + K_2O)$, mole fractions.

Intermediate-Silica Slags:

$$b = -2.0356(10^3 m) + 1.1094 \quad (R = -0.998 \text{ for 7 of 8 data points})$$

$$10^3 m = -1.3101F' + 9.9279 \quad (R = -0.982 \text{ for 5 of 8 data points})$$

where $F' = B(\text{eqn. } 4) \times (Al_2O_3 + FeO)$

TABLE 5. OBSERVED AND CALCULATED VISCOSITIES FOR LOW-RANK-COAL SLAGS

Carbon Crucible Tests: Sample	Temp., °F	Observed Viscosity, poises	Viscosity (poises) Calculated from Predictive Correlations: Modified Urbain	Conventional Urbain	IRSID	Watt-Fereday	NBS-Modified Watt-Fereday	BCURA S^2
Gascoyne	2458	25	25	33	31	20	44	44
	2237	102	105	93	103	80	157	190
Baukol-Noonan 1	2480	41	40	48	56	54	101	87
	2133	482	524	296	500	822	1523	945
Baukol-Noonan 2	2343	93	273	83	91	119	197	176
	2128	548	2276	269	371	738	1220	833
Colstrip	2557	39	117	80	133	37	67	60
	2463	102	233	128	242	64	118	105
Decker	2346	50	158	78	94	84	134	129
	2147	289	911	228	346	414	651	536
Sarpy Creek	2697	56	45	60	83	27	43	44
	2491	220	177	169	318	86	144	139
Naughton	2731	979	611	667	264	262	180	365
	2553	3375	2018	2110	777	817	587	963
Big Horn	2407	93	130	44	67	10	22	23
	2272	325	477	85	172	22	48	57
Kemmerer	2637	88	118	121	98	116	149	151
	2413	589	753	415	341	514	649	566
Black Butte	2688	140	94	109	90	94	91	113
	2294	3375	2385	1059	1023	1494	1544	1227
Emery	2548	98	44	42	61	24	37	34
	2354	422	157	107	201	74	113	114
Rockdale	2681	26	41	38	55	16	29	23
	2481	105	165	97	185	44	82	70
Atlantic Richfield	2396	27	12	42	47	20	46	50
	2183	172	28	120	163	82	165	222
Burns & McDonnell	2690	94	105	119	160	54	47	64
	2535	272	304	272	448	129	118	151

TABLE 5. OBSERVED AND CALCULATED VISCOSITIES FOR LOW-RANK-COAL SLAGS (Continued)

Alumina Crucible Tests: Sample	Temp., °F	Observed Viscosity, poises	Viscosity (poises) Calculated from Predictive Correlations: Modified Urbain	Conventional Urbain	IRSID	Watt-Fereday	NBS-Modified Watt-Fereday	BCURA S^2
Indian Head	2594	48	24	21	19	2	5	4
	2508	82	52	30	34	3	7	6
Beulah (high sodium)	2597	38	31	24	24	5	8	7
	2380	340	249	65	103	13	25	24
Colstrip	2653	18	16	43	70	12	18	15
	2520	34	30	80	166	23	35	32
Decker	2286	69	214	124	180	91	145	143
	2146	237	690	273	488	283	451	399
Big Horn	2331	90	101	67	91	17	31	41
	2177	289	344	150	268	48	81	124
Emery	2564	53	66	96	138	51	68	68
	2441	114	145	183	309	107	146	142
Rockdale	2617	25	24	50	87	16	24	20
	2553	36	34	68	131	21	33	29
Martin Lake	2679	43	16	27	31	9	13	10
	2322	635	135	148	274	54	77	87
Burns & McDonnell	2698	40	73	82	97	38	28	32
	2402	242	491	401	670	202	156	178

Low-Silica Slags:

$$b = -1.8244(10^3 m) + 0.9416 \quad (R = -0.999 \text{ for 6 of 10 data points})$$

$$10^3 m = -55.3649F'' + 37.9186 \quad (R = -0.970 \text{ for 7 of 10 data points})$$

where $F'' = CaO/(CaO + MgO + Na_2O + K_2O)$, mole fractions.

The nature of the "F" terms in the modified Urbain correlations is of interest. Urbain categorizes the constituents of silicate melts as "glass formers" (SiO_2, P_2O_5), "modifiers" (CaO, MgO, Na_2O, K_2O) and "amphoterics" (Al_2O_3, Fe_2O_3) which can act either as glass formers or modifiers. The correlating term for high-silica slags is the ratio of SiO_2 to modifiers, suggesting that, for these slags, the silica content of the slag is the dominating factor. On the other hand, for low-silica slags the correlating term is the ratio of CaO to modifiers, which implies that the amount of CaO relative to total modifiers in the slag is a critical factor. For intermediate-silica slags, the correlating term involves the "amphoterics," suggesting that the role of these constituents becomes more important when the nature of the slag cannot be well defined by its silica content.

SUMMARY AND FUTURE WORK

Data from 23 low-rank coal slag viscosity determinations have been employed in attempts to correlate the linear portion of the log viscosity vs. temperature curve with five published empirical correlations for silicate slags. Of these five correlations, one developed by Urbain for metallurgical slags appeared to give a reasonable fit to the experimental data for nearly two-thirds of the viscosity tests. When the slags were subdivided into three groups, based on a parameter of the Urbain equation that is roughly proportional to silica content, it was possible to derive modified forms of the Urbain equation that gave acceptable correlations (within 30 percent) for 11 of the viscosity tests. Of the remaining 12 tests, the modified correlations were marginally acceptable (within 60 percent) in five cases.

Efforts are still being made to refine these empirical correlations and, in particular, to understand the reasons why certain slags fail to fit the correlations. The ultimate objective is to interpret slag rheological behavior in terms of specific phases present in the slag, to the extent that such phases can be identified and quantified.

ACKNOWLEDGMENTS

This work was conducted with the sponsorship of the U. S. Department of Energy under Contract No. DE-AC18-80FC10159. The authors wish to acknowledge the valuable assistance of S. Benson, D. Rindt, and A. Severson (GFETC) in obtaining the analytical data, and of L. Delaney, T. Kuhlman, and C. Matone (BCR) in conducting the slag viscosity measurements. Thanks are also due to J. Waldron of Commonwealth Edison for providing the Black Butte coal sample, and to Dr. K. Mills of the British National Physical Laboratory for furnishing information on the IRSID and Urbain correlations.

REFERENCES

1. Watt, J. D. and F. Fereday, "The flow properties of slags formed from the ashes of British coals: Part 2. The crystallizing behaviour of the slags," J. Inst. Fuel 42, 131-4 (1969).

2. Barrick, S. M. and G. F. Moore, "Empirical correlation of coal ash viscosity with ash chemical composition," ASME Paper No. 76-Wa/Fu-3 (1976).

3. Hoy, H. R., A. G. Roberts, and D. M. Wilkins, "Behavior of mineral matter in slagging gasification processes," Publication 672, Instn. Gas Engrs., Nov. 1964. 24 pp.

4. Diehl, E. K., "Viscosity of low-rank coal slags," Proc. Low Rank Coal Technology Development Workshop, San Antonio, TX, June 1981. pp. 5-29 to 5-32.

5. Watt, J. D. and F. Fereday, "The flow properties of slags formed from the ashes of British coals: Part 1. Viscosity of homogeneous liquid slags in relation to slag composition," J. Inst. Fuel 42, 99-103 (1969).

6. Given, P. H., D. Weldon and N. Suhr, "Investigation of the distribution of minerals in coals by normative analysis," The Pennsylvania State University; U. S. DOE Report FE-2494-TR-2, Jan. 1980.

7. Frederikse, H. P. R., T. Negas, and S. J. Schneider, "Development, testing, and evaluation of MHD materials," Contract No. E(49-18)-1230, NBS Quarterly Reports, Nos. 1, 2, 3, 4 (1974) and 5 (1975).

8. Riboud, P. V., Y. Roux, L.-D. Lucas, and H. Gaye, "Improvement of continuous casting powders," Fachberichte Hüttenpraxis Metallweiterverarbeitung 19 (10), 859-66 (1981).

9. Urbain, G., F. Cambier, M. Deletter, and M. R. Anseau, "Viscosity of silicate melts," Trans. J. Br. Ceram. Soc. 80, 139-41 (1981).

Appendix 1. Slag Viscosity/Composition Correlations

A. Watt-Fereday Correlation

$$\log \eta = [10^7 m/(t - 150)^2] + c$$

where η = viscosity in poises

t = temperature, °C

$m = 0.00835\ SiO_2 + 0.00601\ Al_2O_3 - 0.109$

$c = 0.0415\ SiO_2 + 0.0192\ Al_2O_3 + 0.0276\ \text{eq. } Fe_2O_3 + 0.0160\ CaO - 3.92$

eq. $Fe_2O_3 = Fe_2O_3 + 1.11\ FeO + 1.43\ Fe$

where slag components are expressed in weight percentages and, on a weight basis,

$$\Sigma\ SiO_2 + Al_2O_3 + Fe_2O_3 + CaO + MgO = 100\%$$

B. NBS-Modified Watt-Fereday Correlation

The equation for log η and units are identical to those above, except that

$$m = 0.0104291\ SiO_2 + 0.0100297\ Al_2O_3 - 0.296285$$

and $c = -0.0154148\ SiO_2 - 0.0388047\ Al_2O_3 - 0.016167\ Fe_2O_3 - 0.0089096\ CaO - 0.012932\ MgO + 1.04678$

C. BCURA S^2 Correlation

$$\log \eta = 4.468\ (S/100)^2 + 1.265\ (10^4/T) - 7.44$$

where η = viscosity in poises

T = temperature, °K

and S = silica ratio = $100\ SiO_2/(SiO_2 + \text{eq. } Fe_2O_3 + CaO + MgO)$

(slag components expressed in weight percentages)

D. IRSID Correlation

$$\eta = AT \exp(B/T)$$

or $\ln \eta = \ln A + \ln T + B/T$

where η = viscosity in Pa·s (multiply by 10 to convert to poises)

T = temperature, °K

$$\ln A = -19.81 + 1.73\ (CaO + MnO + MgO + FeO) + 5.82\ CaF_2 + 7.02\ (Na_2O + K_2O) - 35.76\ Al_2O_3$$

$$\text{and } B = 31{,}140 - 23{,}896\ (CaO + MnO + MgO + FeO) - 46{,}356\ CaF_2 - 39{,}519\ (Na_2O + K_2O) + 68{,}833\ Al_2O_3$$

Slag components are expressed as mole fractions; for coal ash slags, CaF_2 and MnO can be considered as zero.

E. Urbain Correlation

$$\eta = AT \exp(10^3 B/T)$$

$$\text{or } \ln \eta = \ln A + \ln T + 10^3 B/T$$

where η = viscosity in poises

T = temperature, °K

$$\ln A = -(0.2693\ B + 11.6725)$$

$$\text{and } B = B_0 + B_1 N + B_2 N^2 + B_3 N^3$$

where N = mole fraction of SiO_2

$$\text{and } B_0 = 13.8 + 39.9355\alpha - 44.049\alpha^2$$

$$B_1 = 30.481 - 117.1505\alpha + 129.9978\alpha^2$$

$$B_2 = -40.9429 + 234.0486\alpha - 300.04\alpha^2$$

$$B_3 = 60.7619 - 153.9276\alpha + 211.1616\alpha^2$$

where $\alpha = CaO/(CaO + Al_2O_3)$

Slag components are expressed as mole fractions. When other minor slag components (modifiers) are present, these are included by redefining α:

$$\alpha' = M/(M + Al_2O_3)$$

where M represents the modifiers as a single mole fraction and is defined as $M = \Sigma M_i L_i$ where M_i's are the individual mole fractions and L_i is the number of oxygen atoms in the molecule. Thus, for the slags considered in these studies containing CaO, MgO, Na_2O, K_2O, FeO, TiO_2, and (occasionally) SO_3,

$$M = CaO + MgO + Na_2O + K_2O + FeO + 2\ TiO_2 + 3\ SO_3$$

(again, all components expressed as mole fractions).

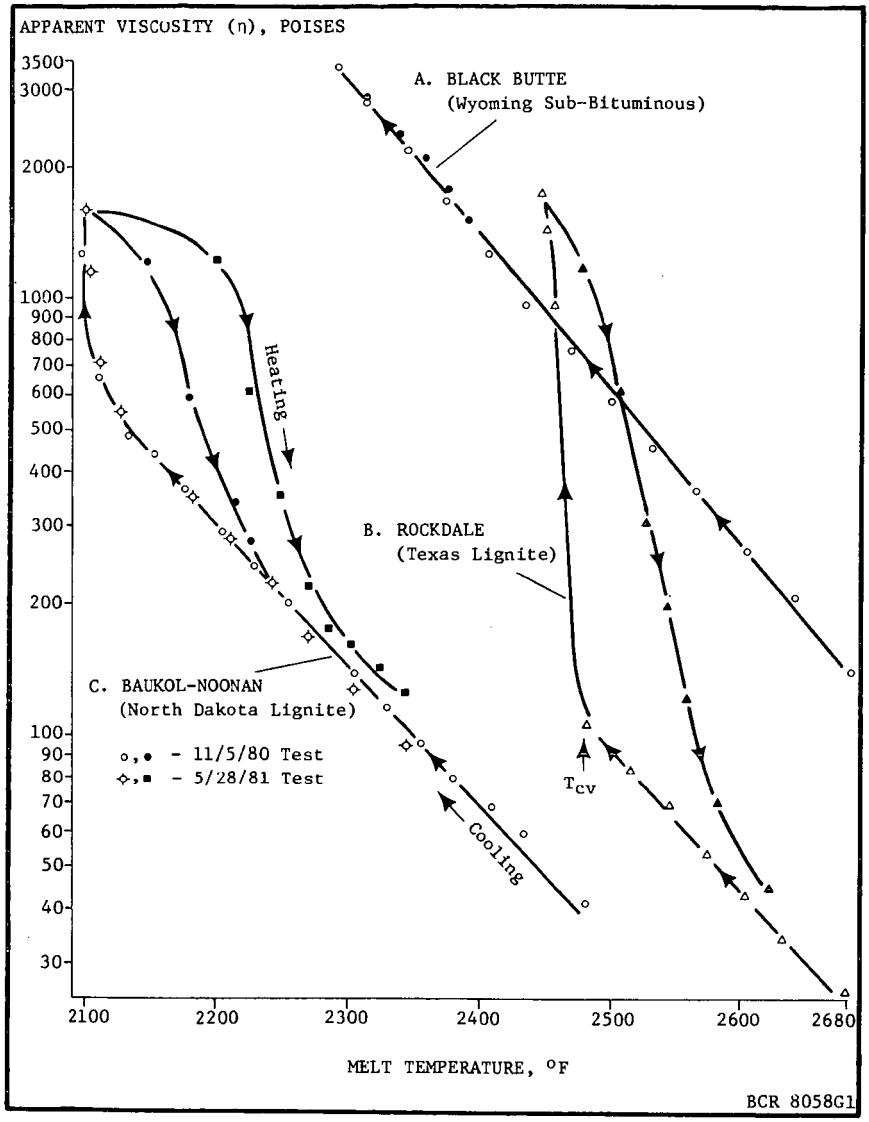

Figure 1. Representative Slag Viscosity Curves for Three Western U.S. Low-Rank Coals

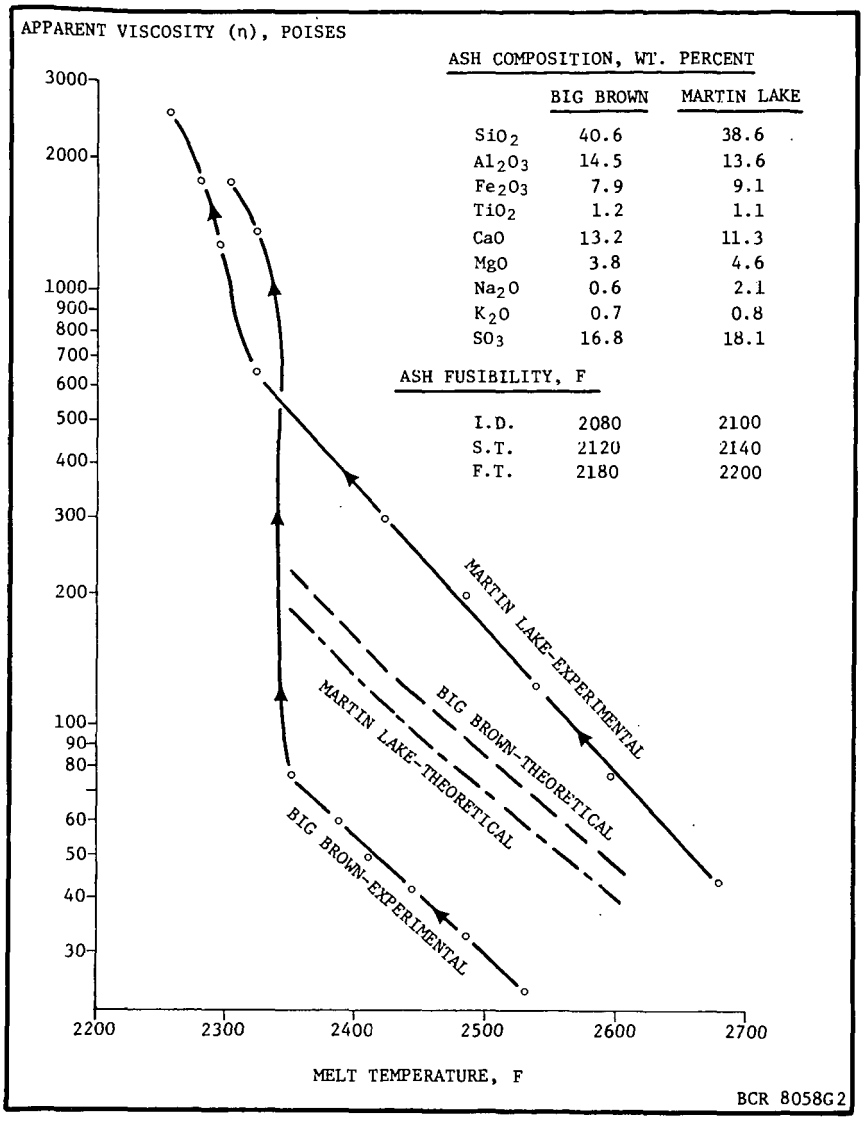

Figure 2. Comparison of Predicted (Watt-Fereday) and Actual Slag Viscosity Curves for Two Texas Lignites

MECHANISTIC STUDIES ON THE HYDROLIQUEFACTION OF VICTORIAN BROWN COAL AND OF COAL DERIVED PRODUCTS

F.P. Larkins*, W.R. Jackson, P.A. Hertan, P.J. Cassidy, M. Marshall and D. Rash

Department of Chemistry, Monash University, Clayton, Victoria, Australia 3168.

Introduction

The overall aim of our recent studies has been to obtain a more complete understanding of the mechanisms for the principal reactions which occur during the catalysed hydroliquefaction of low rank, high oxygen containing (ca. 25 wt% db) coals. The results of 70 ml batch autoclave studies with and without added catalysts on Victorian brown coal, on a number of different coal derived products and on related model ether compounds are discussed herein. More complete details of various aspects of this work may be found elsewhere (1-6). On the basis of these investigations a mechanism is proposed for the hydroliquefaction process which emphasises the role of catalysts in inhibiting repolymerisation reactions, the significance of interconvertibility of coal derived products and the importance of hydrogen donation from molecular hydrogen and the vehicle tetralin.

Experimental

Coals: Two samples of dried (105°C, under N_2) Victorian brown coals from the Morwell seam were used in these experiments viz., Drum 66 (1976 100t bulk sample) and Drum 289 (1979 100t bulk sample). The chemical characteristics of the coals on a weight per cent dmmf basis are as follows: Drum 66, C 69.3, H 5.0, O (by diff.) 24.5, N 0.6, S 0.6. Acidic O 9.7 mol kg^{-1} dmmf coal non-acidic O 5.6 mol kg^{-1} dmmf coal. Drum 289, C 69.2, H 4.8, O (by diff.) 25.2, N 0.52, S 0.25. Acidic O 9.6 mol kg^{-1} dmmf coal, non-acidic O 5.3 mol kg^{-1} dmmf coal. The elemental composition is therefore similar to that of a North Dakota lignite.

The coals (< 250 μm) were hydrogenated in a 70 ml rocking autoclave using a 1:1 slurry of tetralin: coal at initial hydrogen pressures of 1-10 mPa for 1 hour at a reaction temperature of 385°C. In related studies temperatures in the range 345 - 460°C were used at 6 mPa pressure. Both iron and tin-based catalyst systems were examined.

For the work reported herein the catalysts were incorporated by the ion exchange technique (1). In other studies we have shown that impregnation using soluble metal salts is as effective in achieving a comparable level of catalytic activity.

The products from these hydrogenations were separated into gases (analysed by g.c.), water (analysed by azeotropic distillation), insolubles (CH_2Cl_2 insolubles), asphaltene (CH_2Cl_2 soluble/X4 insoluble), oils (CH_2Cl_2 soluble/X4 soluble). Hydrogen transferred from the donor solvent was determined by g.l.c. analysis of the ratio of tetralin to naphthalene in the total hydrocarbon liquid product.

Coal derived materials: These products were obtained from our 1 kg h^{-1} continuous reactor unit (7) as oils (X4 soluble) asphaltenes (tetralin soluble/X4 insoluble) asphaltols (tetralin insolubles/tetrahydrofuran (THF) solubles) and THF insoluble materials for subsequent reactivity studies. Methylene chloride was not used in

*Now at Department of Chemistry, the University of Tasmania, Hobart, Tasmania, Australia 7001.

the separation because of concern for its potential catalyst deactivation role in the subsequent series of experiments to be undertaken. Experimental continuous reactor conditions were a 3:1 slurry of tetralin:coal to which an iron (278 ± 30 mmol kg^{-1} dc from $FeSO_4.7H_2O$) and tin (20 mmol kg^{-1} dc from $SnCl_2.2H_2O$) catalyst had been added. The reaction temperature was 400°C with a developed pressure of 10 MPa and a residence time from 15 to 40 minutes.

Samples of each of the coal derived materials were reacted separately in the presence of several catalysts in a 70 ml batch autoclave using a 1:1 slurry of tetralin:material at 425°C with an initial hydrogen pressure of 6 mPa for 1 h at reaction temperature. The products from these reactions were separated into oils, asphaltenes, asphaltols and THF insolubles.

Model ether systems: A series of ethers have been examined to assist in the elucidation of the role of the iron and tin catalyst systems investigated. Hydrogenation conditions were 1-2 g ether, initial hydrogen pressure 6 mPa, reaction time 1 h with catalyst loadings similar to those used for coal hydroliquefaction studies. Full details are outlined elsewhere (2,5).

Results

Reactions with coal

Total conversion yields for the temperature range 345-460°C at 6 mPa hydrogen are summarized in figure 1. Absolute conversions are lower than for work with 1 ℓ autoclaves and the continuous reactor unit because of different reactor temperature profiles and residence time; however, the qualitative conclusions are consistent. The effect of increasing the reaction temperature was to increase the total conversion of all reactions irrespective of the catalyst system.

The iron-tin catalyst system was the most temperature sensitive of the four coal-catalyst systems studied. Unlike the iron and tin treated coals which were only sensitive to temperature in the range 365-405°C, the iron-tin treated coal was also sensitive to temperature in the range 385°-425°C where the conversion rapidly increased from 66% to 85% (daf coal). Thus the iron-tin system was most efficient at the higher reaction temperatures up to 425°C while the iron and tin treated coals were most effective up to 405°C (see Table 1, reference 2).

The initial hydrogen pressure dependent conversion results in the range 1-10 mPa are given in figure 2 for studies at 385°C. The tin catalysed reactions show most pressure dependence, consistent with previous findings that tin facilitates molecular hydrogen transfer during hydrogenation (4). For the untreated coal and for other catalyst systems there is only a small pressure dependence of product yields beyond 4 mPa.

A detailed study of the chemical constitution of the products revealed that their composition is influenced by temperature but not by pressure or the nature of the catalyst. With increased reaction temperature there was a decrease in total and acidic oxygen concentrations in the asphaltenes and a corresponding increase in both aromatic content and C/H ratio. This observation is consistent with the loss of aliphatic side chains from the polycondensed ring systems

Reactions with coal derived products

Hydrogenation studies were undertaken on the parent iron-tin treated coal (Drum 289) as well as the THF insolubles, asphaltol, asphaltene and oil derived from a continuous reactor run as previously discussed. Studies with no additional catalyst added (case A) and with the addition of a sulphided nickel molybdate catalyst supported on alumina (case B) were performed. The results are presented in table 1. The Ni/Mo catalyst in case B did not increase the conversion of the coal or the THF insolubles beyond that for case A because sufficient amounts of

iron and tin materials were already associated with these reactants to catalyse the reaction. The iron-tin treated coal has of course a much greater reactivity than untreated coal as shown in table 1. It is noteworthy that once isolated the THF insolubles showed a similar reactivity (∿ 75 wt% daf) to the coal (∿ 80 wt% daf).

The results in table 1 show that for reactions at 425°C significant conversion of the asphaltols and the asphaltenes produced at 400°C to other products was possible. In particular for the asphaltol > 95% interconversion occurred, while for the asphaltene the interconversion was > 65%. A complete range of products was formed from high oil yields to repolymerised THF insoluble material. This reactivity underlines the inherent instability of these intermediate products. The addition of a sulphided Ni/Mo catalyst led to ∿ 50% improvement in oil yields, however addition of the traditional first stage catalysts iron, tin or the iron-tin mixture did not significantly improve the conversion of asphaltene or asphaltol to oil as compared to the reactions without additive (results not presented here). Tin, and to a lesser extent, iron were successful in reducing the amount of repolymerisation of asphaltols to THF insolubles.

Hydrogenation of the oil fraction resulted in the formation of a small amount of the higher molecular weight products (< 4 wt%), but the recovered oil contained a higher proportion of lower boiling point material.

Reactions with model ether compounds

The reactions of a series of lignin related model ether compounds with iron II acetate and tin metal have been investigated (2,5). The models selected contain phenoxy groups ($PhO-(CH_2)_nPh$ n = 1,2,3), benzyl groups ($PhCH_2-OCH_2Ph$) and alkoxy groups ($PhCH_2CH_2-OCH_2CH_2Ph$). Conversion results for the reactions of 2-phenylethyl phenyl ether ($PhO-CH_2CH_2Ph$) and dibenzyl ether ($PhCH_2OCH_2Ph$) are shown in figures 3 and 4 respectively. For the phenylethyl phenyl ether the extent of conversion is significantly reduced in the presence of both metal additives with iron being more effective than tin in suppressing the decomposition. For example at 325°C there was only 13% conversion in the presence of an iron based additive compared with 33% with tin and 43% without additive. In contrast, addition of an iron-based catalyst to a reaction of dibenzyl ether (figure 4) was found to promote the conversion while the tin-based catalyst suppressed it relative to no additive being present. At 300°C the conversion was 96% with iron, 12% with tin and 19% without additive. The thermal decomposition of these ethers is believed to be via a radical chain mechanism. (9) It is postulated that while iron catalysts may facilitate carbon-oxygen bond cleavage, as evidenced by the increased reactivity of benzyl and aliphatic ethers, when phenoxy radicals are produced they are strongly adsorbed on the catalyst surface. They are not therefore readily available to propogate the radical chain reactions. This effect is restricted to the phenoxy radical and not observed for a species such as $PhCH_2CH_2O$ in the reaction of $PhCH_2CH_2OCH_2CH_2Ph$ because the resonance stabilisation energy associated with the PhO would result in it having a longer half-life and hence time to diffuse to the catalyst surface without being stabilized by hydrogen. The iron catalyst does not show the same affinity for the benzylic radical even though it is also a long-lived species.

The tin additive is present in the liquid state under the conditions of the present experiments. It has a smaller inhibiting effect than iron on the reactivity of the phenoxy and benzyl ethers. Two explanations are plausible. Hydrogen dissolved in the tin may react with the benzyl and phenoxy radicals which are the chain propogators and remove them from the system. The rate of bond cleavage is therefore lowered. Alternatively, tin may promote radical recombination reactions. By either route the tin would be acting to inhibit propogation reactions.

Mechanistic considerations

Many reaction schemes have been proposed to interpret the results of hydroliquefaction experiments following the pioneering work of Weller et al. in 1951 (8). Factors to be taken into account when considering the complex liquefaction process include

1. Coal-solvent interactions leading to swelling and dissolution of the coal. (10,11)

2. The radical production resulting from thermal degradation of coal molecules. (12,13)

3. Capping of radicals by molecular hydrogen and by hydrogen abstraction from the solvent inhibiting polymerisation of intermediate radical species.

4. Thermal instability of coal derived materials leading to interconvertibility between products including retrograd reactions and the establishment of steady state conditions. The principle of reversibility is of importance in these processes.

5. The role of the catalyst at various stages of the process. Principally in coal dissolution reactions, in stabilisation of reactive radical intermediates against polymerisation, in promotion of bond cleavage reactions and in facilitating the transfer of hydrogen to coal derived materials. It is most unlikely that any single catalyst will have significant activity in all of these steps.

On the basis of our present knowledge of the role of iron- and tin-based catalysts and of the role of the sulphided nickel molybdate catalyst the mechanism shown in figure 5 is proposed to summarize the essential steps in the hydroliquefaction of low rank coals.

At temperatures > 360°C brown coal is rapidly dissolved in the vehicle without significant chemical reaction forming coal (reaction 1) which corresponds to the pyridine soluble material observed by Neavel. (10) At increasing reaction time coal[1] is thermally converted into reactive radical intermediates (reaction 2) which in the absence of a suitable hydrogen donor, either molecular hydrogen or the vehicle, rapidly repolymerises (reactions 3,4,5). In the presence of a good hydrogen donor, hydrogen abstraction reactions (reactions 6,7) compete with polymerisation reactions leading to the formation of oils and asphaltenes. The important concept of reversibility is included in this scheme by the two way arrows between the radical pool and the respective products. It is possible therefore for polymerised material to re-react (reactions 2,8,9) and form lower molecular weight oils and asphaltenes. Thus the system reaches a dynamic equilibrium after a period of time which is primarily dependent on the reaction temperature, the concentration of available hydrogen, and the metal catalyst.

At temperatures greater than 400°C, the asphaltenes rapidly degrade (reaction 10) and can either repolymerise or in the presence of hydrogen, form oil. At higher temperatures (> 425°C) thermal cracking of oils, asphaltenes and repolymerised products leads to increasing yields of hydrocarbon gases (reaction 12).

In the presence of a high pressure of hydrogen, tin metal facilitates the stabilisation of radicals formed by initial coal depolymerisation leading to the formation of asphaltols and asphaltenes (reactions 5 and 6). The stronger pressure dependence of the tin catalysed reactions compared with other systems investigated here may be linked to the fact that the amount of hydrogen dissolved in liquid tin is also pressure dependent.

In the absence of tin less asphaltene is produced which manifests itself as increased yields of THF insolbules and asphaltols. At this time the activity of iron is not completely certain as no effects have been observed on the reactions of the coal derived products. However the proven ability of iron to both catalyse the reactions of some ethers while suppressing propogation reactions of phenoxy radicals suggest that its major activity is probably restricted to the first minutes of reaction (reactions 1,2) and to the slow catalytic degradation of polymerised material. The iron-tin synergism can be interpreted as a co-operative action between the catalytic and radical stabilisation activities of iron with the hydrogen utilisation and radical stabilisation activities of tin which allows the radical intermediates to be stabilised as oil and asphaltene.

The conversion of asphaltene to oil is not catalysed by either iron or tin but it is facilitated by increased reaction temperature and the availability of a good H-donor solvent. The resulting oil formed at high temperatures (> 400°C) contains much less oxygen (especially acidic oxygen) and the conversion probably is the result of the loss of polar phenolic groups as well as cleavage of carbon-carbon bonds joining aromatic clusters together. Vernon (14) has shown that dibenzyl thermally decomposes above 400°C.

Formation of hydrocarbon gases principally results from thermal cracking although tin catalyses the formation of methane at temperatures > 425°C. Weller (15) has also shown that tin II chloride catalyses the formation of methane in the reaction of 1-methylnaphthalene with hydrogen.

The action of sulphided Ni/Mo catalyst was to dramatically increase the yield of oil from the reactions of asphaltol and asphaltenes. It is believed that the mechanism of the Ni/Mo catalyst involves a more conventional dissociative adsorption of both hydrogen and reactant molecule to the catalyst surface followed by hydrogenolysis and hydrogenation reactions. The mechanistic pathway thus differs from both iron and tin and is shown in figure 5 by reactions 13 and 14.

Acknowledgements

Financial support for this work was provided by the Victorian Brown Coal Council and the Australian Government Department of National Development and Energy under the National Energy, Research, Development and Demonstration Program. The view expressed herein are entirely those of the authors.

REFERENCES

1. Marshall, M., Jackson, W.R., Larkins, F.P., Hatswell, M.R., and Rash, D. Fuel 61, 121 (1982).

2. Cassidy, P.J., Hertan, P.A., Jackson, W.R., Larkins, F.P., and Rash, D. Fuel 61, 939 (1982).

3. Hatswell, M.R., Jackson, W.R., Larkins, F.P., Marshall, M., Rash, D., and Rogers, D.E. Fuel 62 (in press) (1983).

4. Cochran, S.J., Hatswell, M., Jackson, W.R., and Larkins, F.P. Fuel 61, 831 (1982).

5. Cassidy, P.J., Jackson, W.R., and Larkins, F.P. submitted to Fuel (1983).

6. Hertan, P.A., Jackson, W.R., and Larkins, F.P. submitted to Fuel (1983).

7. Agnew, J.B., Hoad, W.G., Prasad, G.N., Rash, D. and Rogers, D.E., submitted to Fuel (1983); Agnew, J.B., Jackson, W.R., Larkins, F.P., Rash, D., Rogers, D.E., Thewlis, P., and White, R. submitted to Fuel (1983).

8. Weller, S., Clark, E.L., and Pelipetz, M.G., Ind. Eng. Chem. 42, 334 (1950).

9. Schlosberg, R.H., Ashe, T.R., Pariciroie, R.J., and Donaldson, M., Fuel 60, 155 (1981).

10. Neavel, R.C., Coal Science 1, 1 (1982).

11. Whitehurst, D.D. and Mitchell, T.O., Am. Chem. Soc. (Div. Fuel Chem.) Preprints 26(2), 173 (1981).

12. Curran, G.P., Struck, R.T. and Goun, F., Ind. Eng. Chem. Proc. Des. Dev. 6, 166 (1967).

13. Grandey, D.W., and Petrakis, Fuel 58, 239 (1979).

14. Vernon, L.W., Fuel 59, 102 (1980).

15. Weller, S., personal communication.

Table 1: Product distribution from the catalysed and uncatalysed reactions of Victorian Morwell coal and coal derived reactants.

Reactant		PRODUCT DISTRIBUTION (wt.% reactant)						
		Oil	Asphaltene	Asphaltol	THF Insoluble	H_2O	CO/CO_2	Hydrocarbon Gases
Untreated coal	A	26	7	1[c]	36[c]	9	13.0	8.0
Iron-tin treated coal[a]	A	42	14	1	17	9	12.6	6.6
Iron-tin treated coal	B	40	10	2	20	13	12.5	7.1
THF[a] insolubles	A	39	13	2	25	11	5.7	6.0
	B	39	14	3	26	12	5.0	6.3
Asphaltol[a]	A	44	28	5	13	4	2.2	5.5
	B	63	19	3	5	6	1.5	6.0
Asphaltene[a]	A	37	41	7	6	3	1.4	5.3
	B	67	22	1	3	5	0.5	4.5
Oil[b]	A	96	4	tr.	1	0	0.1	1.2
	B	97	tr.	1	3	0	0.1	1.0

A No catalyst added. B Sulphided Ni/Mo catalyst (10% by weight reactant)

[a] Reactions at 425°C for 1 h using 3 g reactant and 3 g tetralin with initial hydrogen pressure of 6 mPa.

[b] Reactions as for a except 1 g oil and 5 g tetralin.

[c] Estimated values (asphaltol + THF insoluble = 37).

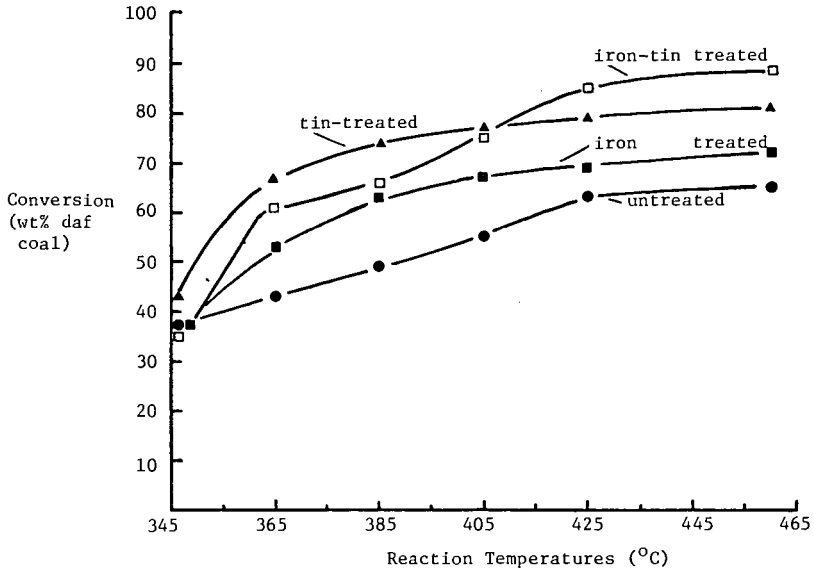

Figure 1: Total conversion versus reaction temperature. Reaction conditions: 6 mPa initial H_2 pressure, 1 h at temperature 1:1 tetralin to coal ratio.

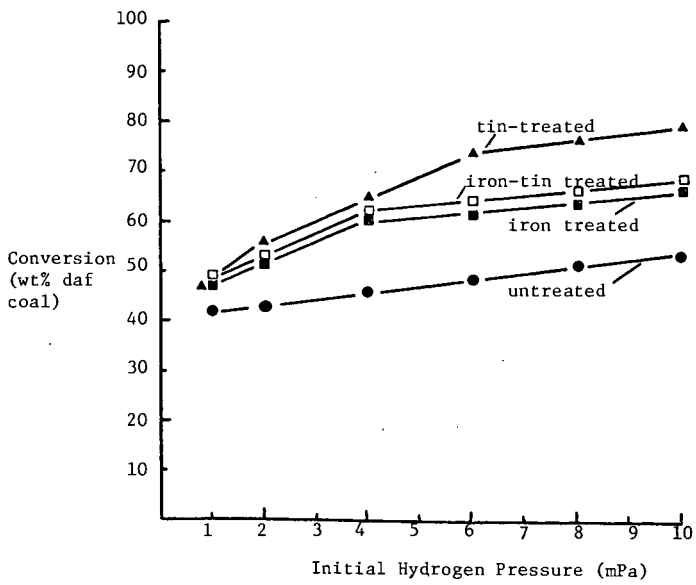

Figure 2: Total conversion versus initial hydrogen pressure. Reaction conditions: 385°C, 1 h at temperature, 1:1 tetralin to coal ratio.

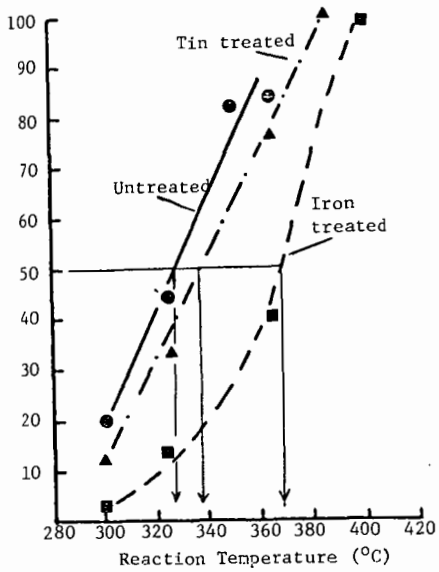

Figure 3: The conversion of 2-phenylethyl phenyl ether versus reaction temperature. Reaction conditions 6 mPa initial H_2 pressure, 1 h at temperature.

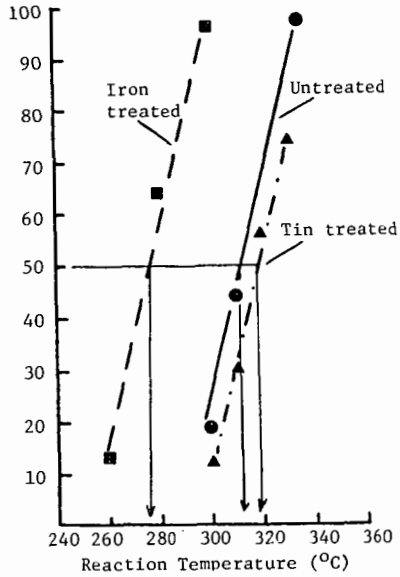

Figure 4: The conversion of dibenzyl ether versus reaction temperature. Reaction conditions 6 mPa initial H_2 pressure, 1 h at temperature.

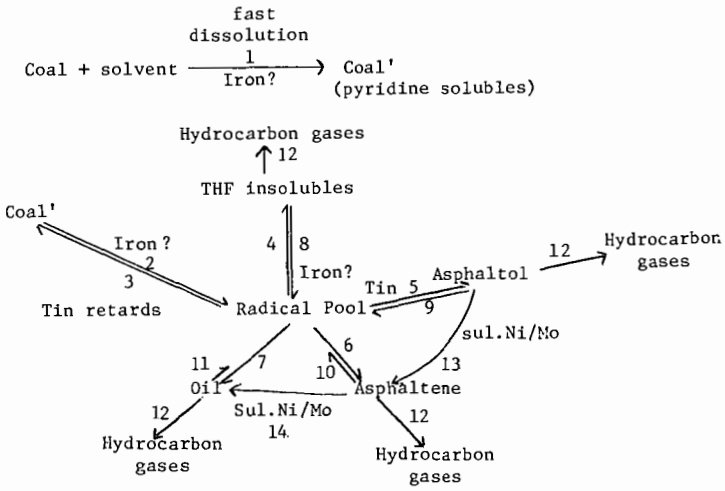

Figure 5: The proposed reaction mechanism of the catalytic hydroliquefaction of Victorian brown coal.

Note: The length of the arrows in reactions 8,9,10,11 indicate the relative reactivities of the respective fractions.

SUPERCRITICAL GAS EXTRACTION OF OIL SHALE

L. E. Compton

Jet Propulsion Laboratory
California Institute of Technology
4800 Oak Grove Drive
Mail Stop: 125/159
Pasadena, California 91109

INTRODUCTION

Green River oil shale in the western United States is considered by many as second only to coal as the largest potential source of fuel in the energy future of the United States. In addition, because of its high indigenous hydrogen content, it is considered superior to coal as a potential feedstock for conversion into liquid fuels. The organic matter in oil shale is conventionally separated by retorting from the inorganics with which it is associated. Temperatures sufficient to crack the organics are used, and a very-high-nitrogen, unstable "petroleum" is produced. It is forecasted by some strategic planners that such oil shale syncrude could enter into the domestic market during the next decade and result in reduction in the nation's dependency on overseas fuel supplies. However, retorting has not yet proven capable of producing a fuel that is truly cost competitive, and present decreases in the price of crude petroleum have reduced at least the short term commerical potential of all synfuels.

Oil shale retorting centers around heating the material, which is typically 85% rock, to about 480°C (900°F) or higher in a low oxygen environment (1). The kerogen and bitumen in the rock are decomposed into oil, gas, and a residual char which remains within the rock. Under favorable circumstances (laboratory analysis by modified Fischer assay) 70 wt% of the organic matter is converted to oil upon heating to 500°C, and the remainder is converted to about 15% gas and 15% char (1,2). These yields change when oil shale is processed in prototype commercial retorts. Oil yield is reduced from 10% to 30% below modified Fischer assay yields, depending on the process (1,3), and char and gas yields are correspondingly increased.

The energy content of the organic matter not converted to oil exceeds net process heat requirements for oil shale retorting. The excess depends on the organic content of the shale and the process design, but for well developed processes using a medium grade of shale (roughly 11 to 15 wt% organic matter) the excess can be 100% greater than heat requirements. For instance, the TOSCO II process is based on discarding 100% of the char produced from 11% organic matter shale (1). The excess can be double or triple this amount when richer material is processed.

The energy contained in the char and gas by-products typically cannot be used efficiently. The gas produced is often greatly diluted with nitrogen and carbon dioxide (1), and the heat content and its efficiency of usage are greatly reduced. In addition, the energy generated by combustion of the residual char in the rock is considerably less than might be anticipated, because of high temperature endothermic mineral carbonate decompositions (4) which occur when the char is burned. In short, the fuels are in dilute forms and the energy contents have low thermodynamic availability. This severly reduces or eliminates their commercial value. Areas in which western oil shale would be developed contain little or no nearby industrial base which could use such fuel, and the gas and char would require prohibitively costly transport. This, combined with very low value, causes char and gas in excess of process fuel requirements to be waste disposal problems, rather than salable byproducts.

The above characteristics of retorting are drawbacks, since energy in salable form is the only product. Requirements for heating rock to high temperature, excessive conversion of organic matter to char and gas, and the low value of the diluted energy content of these by-products combine to reduce the net salable energy to 1/3 to 1/2 below that contained in the raw oil shale. This is a technical problem contributing to an uncertain future for present schemes, and new technology could be useful.

Supercritical gas (SCG) extraction has the potential to make the energy in oil shale available in more concentrated form, because of the high solvent extraction ability of supercritical gases. SCG extraction has been the subject of a number of papers and reviews (5-8), and extensive study has been made of applications to coal (7-12). In the case of coal, simultaneous pyrolysis and extraction of pyrolysis products is effected at temperatures of around 350°C to 450°C. Extract yields in excess of 50% of the organic matter in coal and well in excess of volatile matter contents have been reported (12) when chemically inert SCG solvents are used. The SCG extraction ability is due to near-liquid-density solvent power combined with gas phase mass transfer and penetration properties which inhibit coking reactions that produce char and gas (8). An outstanding characteristic of the extracts is the high molecular weight (11), a property not characteristic of matter which is simply volatilized from coal. These results suggest that SCG extraction might be successfully applied to oil shale. In spite of the drawbacks associated with conventional oil shale retorting and the high SCG coal extraction results, description or discussion of SCG oil shale extraction is apparently absent from the literature, with the exception of a recent patent (13).

EXPERIMENTAL

Experimentation was performed with an apparatus similar to that described elsewhere (10). The apparatus is a 300 cc stainless steel reactor with attendant gauging and controls. The oil shale, 8 grams of material with particle diameters ranging between 50 and 188 microns, was enclosed in a fine mesh stainless steel basket located near the top of the reactor and under a fluid circulating stirrer. This location eliminated any contact between liquid solvent and the oil shale. Experimentation was performed by placing liquid solvent (approximately 150 grams) in the reactor bottom, inserting the extraction basket at the top of the reactor, and then heating reactor and contents to the chosen experimental temperature. The reactor was maintained at constant temperature for four hours and subsequently allowed to cool. Heat-up and cool-down times were both approximately 1 hour. Selected extracts were separated from the condensed SCG by vacuum distillation at 10 torr with a nitrogen flow assist. Raw and extracted shale were analyzed for carbon, hydrogen, and Kjeldahl nitrogen, and results were compared with analyses of raw shale (Table 1) to derive values of the extraction efficiency of organic matter and the H/C ratios of the extracts. It was assumed in these calculations that elemental constituents of oil shale organic matter other than C, H and Kjeldahl N [i.e., oxygen and sulfur at a total of about 6 wt% (1)] were extracted with the same efficiency as the total efficiency in extracting C, H plus N. Extract molecular weights were determined by gel permeation liquid chromatography using detection by differential refractometry and with methylene chloride as solvent. Separate refractive indices of the bulk extracts were determined by dissolving the bitumens in carbon tetrachloride and extrapolating results to zero solvent content or by direct determination for the oil.

RESULTS

This work shows that up to 92% of the organic matter in oil shale can be extracted using a supercritical gas. Results (Figure 1 and Table 1) show for toluene an essentially linear temperature dependence for the percent of total

organic matter extracted (extraction efficiency) in the range 330° to 393°C. A blank experiment at 385°C using pure nitrogen at 0.21MPa shows the difference between extraction with a dense gaseous solvent and a simple volatilization without solvent effects. Toluene extracts at all temperatures except 450°C are bitumens with molecular weights ranging up to about two thousand. At 450°C the toluene extract is a shale oil with an average molecular weight of about 300. The H/C atom ratio of these extracts averages 1.65.

TABLE 1

Extraction Conditions and Results*

Solvent	Temperature (°C)	Pressure (MPa)**	SCG Density (gm/cc)	TOM† Removed (wt%)
Toluene††	330	6.9	0.53	33.8
	340	7.2	0.53	40.5
	357	8.3	0.53	54.7
	385	13.8	0.53	80.1
	393	15.2	0.53	87.5
	450	22.4	0.53	92.5
Pyridine††	363	7.6	0.55	63.3
Nitrogen	385	0.21	0.0013	16.9

* Material Extracted: 12.9 wt% organic matter raw oil shale (21 gallon/ton) produced at Anvil Points, Colorado. Organic carbon and hydrogen contents: 10.3 and 1.53 wt%. Kjeldahl nitrogen content: 0.27 wt%.

** 0.101 MPa/Atm

† Total organic matter

†† Critical parameters: toluene - 319°C, 4.11 MPa; pyridine - 347°C, 5.63 MPa

DISCUSSION

The results demonstrate the powerful solvent properties of supercritical gases and provide incentive for further investigation of SCG oil shale extraction. Residual organic matter after extracting at 450°C is one-half that left by modified Fischer assay, and it is probably one-quarter or less of that which would be generated during prototype commercial retorting. In addition, the data shows organic matter removal occuring below 450°C can be greater than that found with prototype retorting. Certain process advantages associated with the results could occur, namely those associated with near quantitative removal of organic matter and with the presumably lower gas generation associated with lower temperatures and reduced char formation.

The results are not optimized. Questions regarding temperature, solvent power, solute-solvent ratio, pressure, particle size, and the kinetics associated with reactions in the non-gaseous and SCG phases are open. A question of immediate interest involves the temperature dependence of the data in the 330° to 393°C range. Several descriptions of the kinetics describing oil shale decomposition in inert atmospheres without solvent effects have been published (2,14,15). The work indicates oil shale organic matter can be characterized as two materials, kerogen and bitumen, the latter being benzene soluble. Thermal decomposition of the materials can be described by a kinetic mechanism involving two consecutive first order reactions:

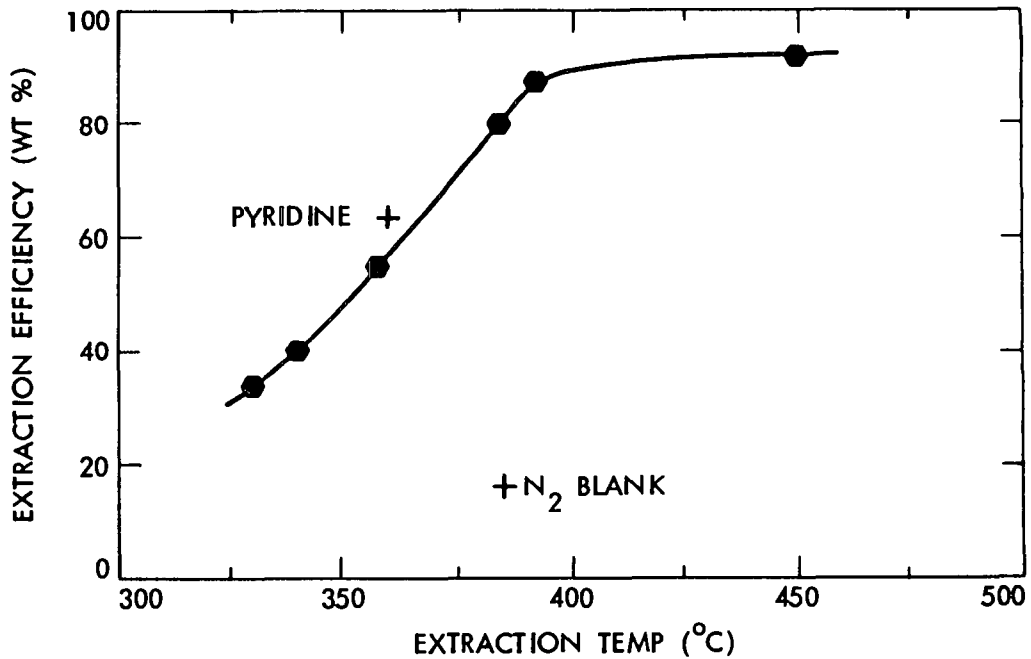

Figure 1. Extraction Efficiency vs. Temperature for Toluene, Compared with Single Temperature Results for Pyridine and Low Density Nitrogen.

$$\text{Kerogen} \xrightarrow{k_1} \text{Bitumen} + \text{Gas} + \text{Char} \qquad 1)$$

$$\text{Bitumen} \xrightarrow{k_2} \text{Oil} + \text{Gas} + \text{Char} \qquad 2)$$

The temperature dependence of both rate constants is available for the 400°C to 525°C range (15). Extrapolation of the very linear ln k versus 1/T (°K) dependence of k_1 into the 330° to 393°C range of interest should yield reasonably accurate k_1 values unless a change in the pyrolysis mechanism occurs over the range of the extrapolation. At 350°, k_1 then equals 3×10^{-3} sec^{-1}, and the corresponding first order half life of kerogen during conversion to bitumen would be 230 sec. Extraction times in this work were approximately 10^4 sec at constant temperature, and the observed temperature dependent extraction yield is not predictable if the indicated kinetics are applicable to these SCG experiments. A temperature dependent SCG extraction mechanism could be present.

Solvent theory is useful in examining this possibility. The theory of SCG extraction is currently approached by treating the dense gas either as a highly compressed gas or as an expanded liquid. The subject has been reviewed recently (5), and it is clear that some success has occurred in predicting single-component solubilities in supercritical gases. However, application has not been made to highly complex hydrocarbon mixtures, such as oil and coal extracts. A useful alternative has been to extend the concept of solubility parameter, which is regularly used in understanding liquid solutions, to supercritical gases.

The solubility parameter concept, developed by Hildebrand (17) and Scatchard (18), is based on the concept of cohesive energy density and the well-tested precept that a correlation exists between cohesive energy density and the mutual solubility of substances. The solubility parameter is defined as:

$$\delta = (E/V)^{1/2} \qquad 3)$$

where δ is in $(cal/cm^3)^{1/2}$, E is the energy required to convert one mole of a given substance from the state of interest to an infinitely expanded gas, the cohesive energy, and V is the molar volume of the substance in the state of interest. It has been shown that the free energy of mixing is minimized and complete miscibility occurs for non-polar liquids when the δ of both solvent and solute are equal. Limited solubility occurs when δ values diverge sufficiently. The concept has also been extended to solids and polar liquids. In addition, the theoretical evaluation of solubilities based on solubility parameters is developing (19).

The Van der Waals constant "a" from the equation of state for gases has been used to estimate solubility parameters for liquids (17), and the success has led to the derivation of the following relation for estimating δ values for supercritical gases (20):

$$\delta_g \cong \delta_l (d_g/d_l) \qquad 4)$$

where δ_g and δ_l are the solubility parameters of the gas and the room temperature liquid, and d_g and d_l are the densities of the gas and the room temperature liquid. The equation indicates the solubility parameter of a SCG varies directly with density, and there is no provision for temperature. This is a direct result of the use of the Van der Waals equation in the derivation.

The solubility parameter of materials for which values of the cohesive energy and/or molar volume are unavailable, such as oil shale bitumen, can be estimated by using correlations between δ and the refractive index (21). The following estimation is used:

$$\delta = \left[C \left(\frac{n^2 - 1}{n^2 + 2} \right) \right]^{0.5} \qquad 5)$$

where n is the refractive index and C is a constant representative of the chemical compound type. C ranges from a low of approximately 230 for branched aliphatic polymers to a high of 353 for aliphatic ester polymers. The average value of C over a broad range of compounds, including but not limited to polymers, is about 308. If it is assumed that the bitumen produced in this experimentation has about the same atomic makeup as oil shale kerogen, namely $C_{200}H_{300}SN_5O_{11}$ (22), then the material should contain a broad range of chemical functional groups, including large contributions from unsaturated and heteroatomic groups. This assumption is consistent with results from analyses of shale oil which show a rough distribution amounting to 11 wt% saturated hydrocarbons, 18% olefins, 10% aromatics, 36% nitrogen compounds, 6% sulfur compounds, and 19% oxygen compounds (23). The value of C used with Equation 5 for the oil shale bitumen is accordingly chosen as the broad range value of 308. The room temperature values for the refractive index of the bitumen and the oil extracted in this work are 1.62 and 1.59, and Equation 5 yields an average room temperature solubility parameter estimate for the compounds comprising the bitumen of 10.4. A somewhat higher value can be derived from a correlation based on the Lorentz-Lorenz function (21). The value of 10.4 has been temperature corrected with the following relationship derived for polymeric materials (24):

$$\delta_2 = \delta_1 \left[\frac{d_2}{d_1} \right]^{1.13} \qquad 6)$$

where δ_1 and δ_2 are the solubility parameters at the reference temperature and the temperature of interest and d_1 and d_2 are the respective densities. Basing the density change of the bitumen between room and experimentation temperatures on the volumetric expansion coefficient for petroleum at 100°C, namely 10^{-3}/°C, yields estimates of the solubility parameter of the bitumen ranging from 7.7 at 330°C to 7.3 at 393°C.

A comparison between the estimated solubility parameters of the bitumen and supercritical gas solvents can now be made to determine if a temperature dependent extraction could be expected. For SCG toluene at the 0.53 gm/cc density used, the estimated solubility parameter based on Equation 4 is 5.5, compared to the 7.3 to 7.7 estimated for the bitumen. In normal practice these δ values should be sufficiently different to allow prediction of a temperature-dependent, limited solubility for the bitumen in supercritical toluene. A higher δ SCG might be needed to eliminate temperature dependent extraction effects and increase the overall extraction efficiency at temperatures below 400°C.

Extraction with pyridine at 363°C was performed to test this possibility, and a comparison of results between extraction with toluene and pyridine is included in Figure 1 and Table 1. Extraction efficiency is increased by about 1/6 with pyridine, which has an Equation 4 δ of 6.0 under experimental conditions. This single result needs confirmation. However, both organic carbon and organic hydrogen extraction increase by the same amount with pyridine, and it is concluded that

experimentation with yet a higher solubility parameter SCG might result in additionally enhanced extraction at temperatures below 400°C. Results above 400°C might also be improved, but there is little practical incentive, because of the high extraction efficiency already found.

REFERENCES

1. Baughman, G. L. (Ed.), Synthetic Fuels Data Handbook, 2nd Ed., Cameron Engineers, Denver, 1978.
2. Hubbard, A. B. and Robinson, W. E., Bureau of Mines Report of Investigations 4744, 1950.
3. Brantley, F. E., et al., Ind. and Eng. Chem. 44, 2641 (1952).
4. Campbell, J. H., LLL Report UCRL-52089, Part 2, March 13, 1978.
5. Williams, D. F., Chem. Eng. Sci. 36, 1769 (1981).
6. Bott, T. R., Chem. and Ind., p. 228 (15 Mar., 1980).
7. Gangoli, N. and Thodos, G., Ind. Eng. Chem. Prod. Res. Dev. 16, 208 (1977).
8. Paul, P. F. M. and Wise, W. S., The Principles of Gas Extraction, Mills and Boon, London, 1971.
9. Maddocks, R. R., et al., Chem. Eng. Prog. p. 49 (June 1979).
10. Blessing, J. E. and Ross, D. R., ACS Symposium Series 71, Organic Chemistry of Coal, p. 15, 1978.
11. Bartle, K. D., et al., Fuel 58, 413 (1979).
12. Kershaw, J. R. and Jezko, J., Sep. Sci. and Tech. 17, 151 (1982).
13. Williams, D. F., U.S. Patent 4,108,760, 1978.
14. Allred, V. D., Chem. Eng. Prog. 62, 55 (1966).
15. Braun, R. L. and Rothman, A. J., Fuel 54, 129 (1975).
16. MacKay, M. E. and Paulaitis, M. E., Ind. Eng. Chem. Fund. 18, 149 (1979).
17. Hildebrand, J. H. and Scott, R. L., The Solubility of Nonelectrolytes, 3rd Ed., Reinhold, New York, 1950.
18. Scatchard, G., Chem. Rev. 8, 321 (1931).
19. Srebrenik, S. and Cohen, S., J. Phys. Chem. 80, 996 (1976).
20. Giddings, J. D., et al., J. Chromat. Sci. 7, 276 (1969).
21. Lawson, D. D. and Ingham, J. D., Nature 223, 615 (1969).
22. Weitkamp, A. W., and Gutberlet, L. C., Ind. Eng. Chem. Proc. Des. Dev. 9, 386 (1970).
23. Cady, W. E. and Seelig, H. S., Ind. and Eng. Chem. 44, 2636 (1952).
24. Fedors, R. F., Polymer Sci. and Eng. 14, 472 (1974).

ACKNOWLEDGMENT

The research described in this paper was carried out by the Jet Propulsion Laboratory, California Institute of Technology, under contract with the National Aeronautics and Space Administration.